The Hydrogeological Significance of Lithostatic Unloading and Geomechanical Response to Mineral Extraction at Open Pit Workings

Stephen Mark Foster

Submitted in accordance with the requirements for the degree of
Doctor of Philosophy

The University of Leeds

School of Earth and Environment

September 2022

The candidate confirms that the work submitted is his own, except where work which has formed part of jointly-authored publications has been included (a). The contribution of the candidate and other authors to this work has been explicitly indicated below (b). The candidate confirms that appropriate credit has been given within the thesis where reference has been made to the work of others.

(a) Foster, S.M., West, L.J., Bottrell, S.H., and Hildyard, M.W., 2018. A DFN Approach to Evaluating the Hydrogeological Significance of Lithostatic Unloading in Fractured Strata Around Open-Pit Workings. ARMA *Proceedings 2nd International Discrete Fracture Network Engineering Conference*. Seattle: ARMA.

(b) The above-mentioned publication is composed of material that comprises parts of Chapters 2 and 3. The scientific work contained in the above mentioned publication is directly attributed to the candidate. The other authors contributed solely to the format and language of the publication.

Acknowledgements

Abstract

This thesis presents a study into the effect of rock mass stress change, resulting from open pit mineral extraction, on the hydrogeological characteristics of the host rock, with particular focus on hydraulic conductivity change in fracture-dominated groundwater flow systems. The study investigates the potential significance of hydrogeological change and whether such effects should be considered during environmental impact assessment for new mineral workings.

Stress change resulting from lithostatic unloading due to mineral extraction results in the development of a near field excavation damage zone (EDZ) and an excavation disturbed zone (EdZ) that extends further into the host rock. In this study the boundary of the EdZ is defined as the point at which rock mass horizontal and vertical stresses are within 5% of pre-excavation gravitational stress. The majority of open pit mineral workings are established in formations where groundwater flow predominantly occurs via discontinuity networks consisting of interconnected fractures, joints and faults. Stress change, and associated extensional strain, may result in rock mass displacement and discontinuity dilation with effect on groundwater flow and contaminant transport capacity. The lateral and vertical boundaries of EdZ development around open pit excavations have not previously been well-defined and previous investigations into discontinuity dilation due to stress change have tended to focus on individual discontinuities rather than discrete fracture networks at field scale.

The EDZ extents around open pit excavations tend to be highly localised with limited hydrogeological significance. Investigation of EdZ extents and associated discontinuity dilation has been undertaken through development of a series of discrete fracture network (DFN) models with progressively increasing DFN complexity. Geomechanical modelling is undertaken in two and three dimensions using Rockfield's Elfen code. Open pit excavation is simulated at three successively increased depths and under two different in-situ stress conditions. The DFN configurations are designed to be generally representative of discontinuity networks observed at multiple excavations in northern England. The results of the geomechanical modelling programme are reported as vertical and lateral EdZ extents and discontinuity dilation -v-distance relationships. Discontinuity dilation has been translated into

equivalent porous media (EPM) hydraulic conductivity change through application of the cubic law and then applied to hydrogeological case studies through development of groundwater flow and contaminant transport models.

Modelling results indicate that the EdZ around open pit excavations extends for several hundred metres behind an excavation face and below an excavation floor. The EdZ extent increases with increasing depth of excavation. The presence of pre-existing discontinuities reduces EdZ extents with the magnitude of reduction influenced by discontinuity intensity, orientation and interaction with excavation surfaces. A normalised approach to EdZ estimation has been developed by reference to excavation dimensions. Rock mass displacements of up to 10cm occur at the excavation face and floor with discontinuity dilation of up to 1cm. Cumulative discontinuity dilation accounts for between 30%-50% of total vertical or lateral rock mass displacement. Discontinuity dilation magnitude -v- distance from the excavation floor or face has been described by an inverse power law function that captures the effect of discontinuity intensity variation. Discontinuity dilation occurs over a shorter distance than rock mass displacement, resulting in the separation of a dilation zone from a displacement zone, within the EdZ boundary. The dilation zone is defined in this study as the hydrogeological significant excavation disturbed zone (HS-EdZ).

Groundwater flow and contaminant transport modelling demonstrates that the effects of lithostatic unloading can result in a reduction in hydraulic gradient around open pit excavations with potential change in groundwater inflow to the excavations. The development of enhanced permeability zones behind excavation floor and face establishes preferential flowpaths for contaminant migration from open or restored mineral workings with implications for the after use of open pit excavations. The study concludes with recommendations regarding conditions in which consideration of lithostatic unloading effects should form part of hydrological impact assessments for new open pit mineral workings.

Table of Contents

Appendix A: List of models developed and applied during this study

Appendix B: Discontinuity log: Borehole 2 Blaxter Quarry, Northumberland

Appendix C: Conceptual models for geomechanical modelling

List of Tables

List of Figures

Abbreviations

BGS	British Geological Survey
DEM	Discrete Element Method
DFN	Discrete Fracture Network
EAL	Environmental Assessment Level
EDZ	Excavation Damage Zone
EdZ	Excavation Disturbed Zone
EPM	Equivalent Porous Media
FDEM	Finite Discrete Element Method
FOS	Factor of Safety
HRA	Hydrogeological Risk Assessment
HS-EdZ	Hydrogeologically Significant Excavation Disturbed Zone
JRC	Joint Roughness Coefficient
LML	Lower Magnesian Limestone
LOP	Large Open Pit
MPM	Middle Permian Marl
NLC	Non-Linear Compliance
REV	Representative Elementary Volume
TBM	Tunnel Boring Machine
UML	Upper Magnesian Limestone
WHR	Woodhead Hill Rock

List of Symbols

ρ	Density	(Kg/m^3)
g	Gravitational acceleration	(m^2/s)
σ	Stress	(Pa)
v	Poisson's Ratio	
k	Lateral confining stress ratio	
K	Hydraulic conductivity	(m/s)
E	Youngs Modulus	(Pa)
G	Shear Modulus	(Pa)
k_n	Normal stiffness	(Pa/m)
k_s	Shear stiffness	(Pa/m)
μ	Dynamic viscosity	(p.s)
q	Flow per unit length	(m^3/m)
ε	Strain	
$k\theta$	Unsaturated hydraulic conductivity	(m/s)
U_r	Radial displacement	(m)
V	Velocity	(m/s)
i	Hydraulic gradient	

CHAPTER 1: INTRODUCTION

This chapter provides an introduction to the research presented in this thesis and an overview of the research context, aims and objectives and potential application of research findings.

1.1 Research context and description

1.1.1 Research Context

This study has been designed to investigate the effect of lithostatic unloading associated with open pit mineral extraction on the hydrogeology of the surrounding host rock formations. Open pit mineral extraction, involving the removal of large volumes of rock and overburden, results in a reduction in loading on excavation surfaces and redistribution of stress within surrounding ground (Terzaghi, 1948, Goodman, 1989). Stress reduction, and any associated extensional strain, may result in damage to the rock mass in proximity to the excavation surfaces and disturbance of the host rock at greater distance.

The majority of hard rock mineral extraction occurs in consolidated geological formations that have low primary porosity and contain discontinuities that may include fractures, joints, bedding planes and faults (Jones et al, 2000, Beale, 2014). In such environments, groundwater flow through saturated and unsaturated strata tends to be dominated by flow through discontinuities that form secondary porosity.

Redistribution of stress in the host rock surrounding open pit mineral extraction has the potential to change the configuration of pre-existing discontinuity systems around the excavation, and in some cases, to induce new discontinuity development and connectivity. Where discontinuity networks convey groundwater, changes to network configuration may have an effect on the groundwater flow regime in the vicinity of mineral workings. Whether such effects are hydrogeologically significant depends on the magnitude of change to the groundwater regime and the sensitivity of the host environment.

Change to the groundwater regime around open pit mineral workings has the potential to influence both the internal management of water within the workings and the external effect of mineral extraction on receptors remote from the workings. Proposals for new mineral development, or extensions to existing development, are normally subject to detailed hydrological and hydrogeological impact assessment to establish potential risks to external surface water and groundwater dependent features. Impact assessment is typically based on data obtained from pre-development investigation and analysis and hence does not usually take account of development effects on ground conditions. The situation is summarised (Foster, 1998), as follows.

'It remains standard practice for mine environmental management programmes to be developed from environmental analysis undertaken at project feasibility and prefeasibility stage. It has also become standard practice for closure plans to be developed before mine development. Predictive assessment undertaken on the basis of data collected during environmental baseline studies can only provide an indication of the potential impacts that will result from mine development. For some environmental aspects of mining, the potential consequences of mine development may vary considerably over the lifetime of the operation.'

A general review of the accuracy of pre-development environmental impact assessment across the energy and minerals sector in Australia was published by (Buckley, 1991). The review concluded that impact assessment based on pre-development data had around 50% accuracy, as follows.

'The study showed that the average accuracy of quantified, critical, testable predictions in environmental impact statements in Australia to date is 44% +/- 5%; and that predictions where actual impacts proved more severe than expected were on average significantly less accurate (33% +/-9%) than those where they proved as or less severe (53%+/-6%).'

Where a development may change the environment within which it is situated, those changes should, where possible, be considered during pre-development impact assessment studies. This study is designed to investigate whether the potential effect of excavation unloading is likely to have a significant effect on

local hydrogeology. It is recognised that lithostatic unloading impacts, and any consequent hydrogeological effects, will be highly site-specific. As a consequence, this study is not aimed at quantification of effects at any specific site or under any specific hydrogeological conditions. The study incorporates analysis of unloading effects for a range of generic geological environments that could be considered representative of the majority of geological environments encountered during open pit mine and quarry development.

Research on the effect of lithostatic unloading on groundwater systems surrounding open pit mineral excavations is largely absent from the literature. The few studies that are available have tended to focus on the role of changing pore pressure on the stability of excavation slopes. Prior to this study, there was only anecdotal case study evidence of the potential extent of the damaged and disturbed zones around open pit mineral workings, with some corroborating evidence from analysis of unloading effects in natural environments i.e. deglaciation, erosion, etc.

There is a need for improved understanding of the potential vertical and lateral extent of the damaged (EDZ) and disturbed zones (EdZ) around open pit mineral workings and the factors that influence or control these deformation processes. The effect of lithostatic unloading on discontinuity-based groundwater systems is not well-defined and hence there is currently no reliable basis for accounting for such change in pre-development impact assessment. This study aims to progress understanding in this regard.

1.1.2 Research Description

To establish improved understanding of the potential hydrogeological significance of lithostatic unloading it has first been necessary to investigate the geomechanical response to unloading to define excavation disturbed zone extents and the potential influence of pre-existing discontinuity networks. This research study has therefore incorporated an extensive geomechanical modelling programme, incorporating discrete fracture network (DFN) modelling of a range of discontinuity network configurations. To date, DFN modelling of open pit excavations has not been widely applied. Geomechanical modelling has been undertaken using the hybrid finite element

method/discrete element method (FDEM) code, Elfen (Rockfield International).

Although the geomechanical modelling work included in this study is not based on simulation of conditions at any specific site, the DFN configurations used in the study have been derived from field survey of discontinuity systems in consolidated sedimentary rocks at several UK mineral workings. Reference data related to discontinuity orientation, intensity and persistence was obtained from survey of exposed faces at Blaxter Quarry in Northumberland. Blaxter Quarry, operated by Northumberland Stone Limited, is established in sandstone and limestone strata of the Carboniferous Tyne Limestone Formation. Additional data related to discontinuity system configuration was derived from survey of sandstone and limestone quarries in Yorkshire, Lancashire and Shropshire. Further details are provided in Chapter 3.

Geomechanical models have been developed in both 2D and 3D formats to represent a range of discontinuity configurations and intensity. Open pit mineral excavation has been simulated at three successive depths and under two different in-situ stress conditions. The study includes simulation of excavation to a maximum depth of 100m below ground level. Excluding Large Open Pits (LOPs), the majority of open pit mineral excavations in the UK, Europe and worldwide do not extend to greater depth than 100m.

Geomechanical models have been developed to reliably represent lithostatic unloading processes and the response of discontinuities to stress redistribution. Modelling outputs have supported analysis of the stress/strain response in the surrounding host rock, excavation disturbed zone extents, rock mass displacement characteristics and pre-existing discontinuity dilation magnitudes for the range of DFN configurations modelled.

Outputs from the geomechanical modelling programme have been used to define input data for subsequent assessment of potential hydrogeological significance. Assessment of potential hydrogeological change arising from the effects of lithostatic unloading has been undertaken through adaptation of a number of case study groundwater flow and contaminant transport models of

mineral sites across the UK. The results are discussed in relation to potential significance for mineral site operation and effects on external receptors.

The study concludes with discussion on geological environments in which lithostatic unloading around open pit mineral workings may be hydrogeologically significant and where such effects should be considered as part of pre-development hydrological and hydrogeological impact assessment. Recommendations are made regarding further research objectives and the development of guidance for industry application.

1.2 Aims and objectives

The primary aim of this study has been to establish an improved understanding of the hydrogeological significance of the geomechanical response to excavation induced stress change in the host rock mass around open pit mineral workings. Specific aims of the study are summarised as follows:

1.2.1 Research aims

o To establish improved understanding of the geomechanical response to lithostatic unloading at open pit mineral workings and whether the response of pre-existing discontinuity networks, or the formation of new discontinuities, has the potential for significant impact on groundwater flow and contaminant transport in the surrounding host rock;

o To improve understanding of whether the potential effects of lithostatic unloading on hydrogeological systems around open pit mineral workings should be considered during pre-development environmental impact assessment studies for new or extended mineral development;

o To improve understanding of the influence of variation in discontinuity network configuration and properties with regard to both the geomechanical response to lithostatic unloading and hydraulic performance of DFN systems;

o Improve potential to predict and anticipate operational aspects and external effects of groundwater management at open pit mineral workings; and,

o To advance general understanding of the linkage between geomechanical response and hydrogeological processes in fractured hard rock formations around open pit mineral workings.

1.2.2 Research objectives

o To investigate and quantify the excavation-induced stress/strain response in the host rock surrounding open pit mineral workings through a programme of geomechanical modelling designed to simulate excavation at multiple depth and under two alternative in-situ stress conditions;

o To review definitions of EdZ development in the literature and to examine their applicability to open pit excavations;

o To investigate and quantify the vertical and lateral extent of the excavation disturbed zone (EdZ) beneath an excavation floor and behind an excavation face and the effect of pre-existing or newly formed discontinuities on EdZ development;

o To investigate and quantify the magnitude of discontinuity dilation in response to stress reduction and the variation in dilation with increasing distance from the excavation floor and face for multiple excavation depths and alternative in-situ stress conditions;

o To translate the results of the geomechanical modelling programme, with respect to EdZ extents and discontinuity dilation magnitude, to hydraulic parameters using an equivalent porous media (EPM) approach to support investigation of potential hydrological and hydrogeological change in response to lithostatic unloading;

o To investigate and quantify the potential impact of lithostatic unloading on the following:

- Groundwater flow rates, levels and hydraulic gradients into and around mineral workings;
- Fate of contaminants migrating from mineral workings; and
- Unsaturated zone drainage effects on water resources.

o To provide guidance of the potential hydrogeological significance of the effects of lithostatic unloading at open pit mineral sites and the inclusion of such effects in hydrogeological impact assessment for new mineral workings.

1.3 Thesis structure

This thesis is presented in seven chapters with three appendices. A summary of the content of each chapter is provided below.

Chapter 1: Introduction

This chapter presents an overview of the context for this research study and a summary description of works undertaken. The research aims and objectives are defined and the structure of the thesis is presented.

Chapter 2: Literature Review

Presents a detailed review of the literature related to key components of this study. The review is separated into three parts. Part 1 examines current understanding of lithostatic unloading processes and effects, associated with both natural processes and man-made structures. Part 2 reviews current approaches to DFN modelling and the application to a range of surface and underground developments. Part 3 is a review of the hydraulic properties of fracture networks and current understanding of the relationships between geomechanical change and groundwater flow through fractured rock aquifers.

Chapter 3: Geomechanical Modelling – Investigation Design and Methodology

Chapter 3 details the approach adopted to the design and implementation of the geomechanical modelling programme. The approach to DFN modelling

and a review of alternative modelling systems is presented. Critical geomechanical processes associated with the stress response to lithostatic unloading are defined and the potential to represent such processes in DFN models is considered. The design of the geomechanical modelling programme is presented and assumptions and limitations of the proposed approach are discussed.

Chapter 4: Geomechanical Modelling Results

This chapter presents the results of both 2D and 3D geomechanical modelling for four separate model configurations and two in-situ stress conditions. The results for each model are presented to provide information on the stress response; excavation disturbed zone extents; rock mass displacement and, discontinuity dilation. Modelling programme outputs incorporate sensitivity analysis with regard to variation in discontinuity stiffness and rock mass material properties.

Chapter 5: Discussion – Geomechanical Response, Excavation Disturbed Zone Extents and Discontinuity Dilation Magnitude

The results of the geomechanical modelling programme are interpreted and discussed in Chapter 5. Results from multiple models are presented in combined format to support review of trends and DFN variation effects. Results for the extent of vertical and lateral EdZs for all models are combined and discussed leading to development of normalisation approaches to predict EdZ extent from excavation dimensions. Modelled EdZ extents are compared to stress response results determined through application of the Boussinesq approach to predict stresses from strip-loads in an elastic half-space. The effect of pre-existing discontinuities on rock mass displacement magnitude is discussed and discontinuity dilation magnitude data is presented. Formula are developed to describe the relationship between discontinuity normal dilation with distance from the excavation floor and face for all of the models developed for this study. The chapter concludes with a summary of the geomechanical modelling programme outputs that provide the basis for consideration of hydrological significance.

Chapter 6: Evaluation of Hydrological Significance

Chapter 6 presents the methodology and results of an assessment of whether the effects of excavation-induced stress redistribution have the potential to change hydrological and hydrogeological conditions in the surrounding host rock and whether such changes would be considered significant. The chapter presents a methodology for application of the cubic law to establish changes in baseline values of EPM hydraulic conductivity from geomechanical model results. Assessment of the potential impact of hydrogeological change is undertaken through amendment of several existing groundwater flow and contaminant transport models and results are presented, interpreted and discussed in this chapter.

Chapter 7: Conclusions and Recommendations

Chapter 7 presents the conclusions from all stages of this research study with particular reference to the extents of the EdZ, discontinuity dilation/displacement relationships and the potential hydrological significance of lithostatic unloading around open pit mineral workings. The chapter identifies areas in which further research would be beneficial and discusses options to integrate consideration of lithostatic unloading effects into pre-development hydrological and hydrogeological impact assessment.

A list of models developed and applied throughout this study is included at Appendix A.

CHAPTER 2: LITERATURE REVIEW

This chapter comprises a review of the literature related to the scope of this study. The review has been undertaken to establish the current state of research and application related to the following areas.

o Geomechanical response to lithostatic unloading around open pit excavations;

o Discrete fracture network (DFN) modelling approaches and limitations; and

o Hydraulic properties of fracture networks.

2.1 Geomechanical response to lithostatic unloading around open pit excavations

2.1.1 Lithostatic unloading process and occurrence

Concepts of stress change due to lithostatic unloading, either natural or man-made have been established for many years (Terzaghi, 1948, Goodman, 1989). Natural unloading processes including erosion and deglaciation, have long been recognised as the probable origin of regional scale deformation and discontinuity development that is not attributable to more dynamic tectonic action (Gross and Engelder, 1991, Nichols, 1980). Lateral stress relaxation due to fluvial erosion and loss of lateral constraint in deep river valleys has resulted in valley side deformation and discontinuity development. Many previous studies have demonstrated processes associated with stress relaxation around engineered underground structures such as tunnels, deep mine workings, waste repositories and oil and gas fields (Seager, 1963, Kelsell et al., 1984). Studies related to lithostatic unloading effects at open pit excavations have tended to focus on the stability of excavation slopes and the potential for basal heave (Kalkani, 1977, Nie, 2015).

Geological strata around open pit excavations are not usually subject to any form of loading other than the effects of gravity and any residual lateral confining stress. The in-situ state of stress is influenced by topography, tectonic forces, rock mass properties and geological history (Jaeger et al., 2007). The process of lithostatic unloading by removal of rock results in both a reduction in the load applied at excavation free-surfaces due to a reduction in 'self weight' and loss of lateral confinement. As observed at both naturally formed and man-made structures, the physical response to such change is typically uplift of horizontal surfaces and lateral expansion of previously confined sub-vertical surfaces. Re-distribution of stress within the host rock mass and at excavation surfaces is therefore a response to changes in loading and confinement.

On the basis that, in areas of subdued topographic variation, it can be assumed that one of the principal stress directions is vertical, Jaeger et al (2009), set out three alternative models for determination of in-situ stresses, all assuming that vertical stress = ρgz, where ρ = rock mass density, g = gravitational acceleration and z = depth below ground surface. The three models are:

(i) Lithostatic stress state (Heim's Rule): assumes that the other two lateral principal stresses are equal to the vertical overburden stress. Based on the concept that over a sufficiently long time period rock would behave in a viscoelastic manner, mimicking fluid behaviour and hydrostatic conditions. This model takes no account of tectonic forces or brittle behaviour of rock.

$$\sigma_z = \sigma_x = \sigma_y = \rho g z \qquad [2.1]$$

(ii) Uniaxial strain: assumes that rock is laterally constrained and therefore vertical strain results in lateral principal stresses related to the Poisson effect as follows.

$$\sigma_z = \rho g z, \ \sigma_x = \sigma_y = v/(1-v) * \sigma_z \qquad [2.2]$$

(iii) Uniaxial stress: assumes there are no lateral stresses and that only vertical gravitational stress is active, but that lateral strain could occur.

$$\sigma_z = \rho g z, \sigma_x = \sigma_y = 0 \hspace{4cm} [2.3]$$

In all three cases the relationship between the vertical principal stress can be defined in the form,

$$\sigma_z = \rho g z, \sigma_x = \sigma_y = k\sigma_z, \hspace{3.5cm} [2.4]$$

where, k = 1 under Heims Rule, v/(1-v) under the uniaxial strain model and 0 under the unconstrained lateral deformation model.

Brown and Hoek (Brown, 1978) present an overview of measured stress values within the earth's crust at multiple locations and depth of measurement, concluding that vertical stress (σ_v) can be defined by,

$$\sigma_v \text{ (MPa)} = 0.027 \text{ Z, where Z = depth (m).} \hspace{2cm} [2.5]$$

Comparison of vertical and horizontal stress ratios at a range of depths resulted in the finding that the horizontal to vertical stress ration (k) generally lies within the limits defined by,

$$100/Z + 0.30 \leq k \geq 1500/Z + 0.050$$

Data presented by Brown and Hoek (1978) indicates that measurements at depths below 500 m are more closely associated with the lower limit with k = 100/Z + 0.30. On this basis, at a depth of 100 m, k would equal 1.30.

Vertical and horizontal stress measurements reported by Ma, et al (Ma, 2013) at depths of 75 m to 420 m in the Sanshandao mining area, China, produced k values within the range 1.12 – 1.87 at 100 m depth. Recent ground

investigation (Solexperts, 2022) in a borehole constructed to a depth of 378 m in Jurassic sandstone and mudstone strata in northern England resulted in the in-situ stress measurements as summarised in Table 2.1.

Depth (m)	$\sigma_{vertical}$ (MPa)	$\sigma_{horizontal\ (min)}$ (MPa)	$\sigma_{horizontal\ (max)}$ (MPa)	k
220	5.5	3.4	6.1	0.62 – 1.11
231	5.8	3.5	4.2	0.60 – 0.72
271	6.7	4.4	7.0	0.66 – 1.04
361	9.0	6.3	10.3	0.70 – 1.14
378	9.4	5.6	8.2	0.60 – 0.87

Table 2.1: Vertical and horizontal stress measurements at increasing depth from location in North Yorkshire, UK.

In an overview of rock mass response to lithostatic unloading due to natural and man-made causes, Nichols (1980) considered a range of rock types and unloading processes. Evidence was cited for erosional unloading processes in clays and shales, interbedded hard rock sedimentary sequences and igneous and metamorphic terrains for which the following unloading characteristics were identified.

Clay and shale formations: evidence from valleys formed by river action at sites in the United States and Canada demonstrated a total vertical uplift or rebound in valley sides of up to 10% of the valley depth with unloading effects manifest as raised valley rims, lateral inward movement of valley walls and brittle fracturing.

Interbedded sandstone, limestone and shale formations: both brittle and ductile response to unloading by natural erosion processes was recognised. Thrust faulting, shearing and folding were identified in valley bottoms with extensional fracture development in valley walls.

Igneous and metamorphic formations: evidence of sheeting fractures in granite and metamorphic rocks with shallow fracture development sub-parallel to local topography.

Nichols discusses evidence for variation in unloading response in relation to variation in measured lateral confining stress and concludes that lateral tectonic stress does not fully explain observed extensional features e.g. faults and fracture zones, and that, in shallow rocks, horizontal tensile stresses in valley walls are inferred. Whilst the unloading response is considered to be generally due to elastic release of stored strain energy, acquired during the loading processes, Nichols argues that in addition to an immediate elastic response there is also a time-dependent release of stored strain energy associated with microscopic characteristics of loading at grain scale with residual strain 'locked in' through processes of cementation and chemical change.

Nichols suggests that fracturing that develops as a consequence of lithostatic unloading is dominantly present as extensional fracturing, together with shearing. In considering discontinuity development during unloading processes, Nichols refers to the work on shales and limestones that found unloading fractures were often specific to individual lithological units and that individual rock types responded differently to stress relaxation. Extensional fracture orientations were found to have developed generally parallel to the nearest free-surface i.e. parallel to an open valley wall or valley floor.

Analysis of natural unloading effects was undertaken by Lee (Lee, 1978) in relation stress relief at the Niagara Gorge in Ontario, Canada. The study looked at the effects of stress relief in the cliff faces of the Niagara Gorge in response to fluvial erosion over several hundred years, leading to characterisation of the consequences of strain energy release in specific lithologies. Lee reports that in-situ stresses in the Niagara Gorge have been measured in the region of 7-14 MPa and cutting of the gorge has resulted in release of horizontal stresses. The analysis demonstrates lateral displacement of the cliff face towards the gorge, with extensional strain and progressive stress relief. A tension zone is developed in the cliff face with the horizontal stress gradually changing from compressive to tensile towards the face.

Comparison of tensile stresses with the tensile strength of some of the weaker mudstone and limestone lithologies suggested the potential for tensile failure. The study suggests development of a tension zone extending approximately 50 m back from the cliff face for a gorge depth of approximately 60 m. Lee found that, as the horizontal tension zone was concentrated near the cliff face, vertical tension joints in the rock were closer together nearest to the face with increasing spacing with increasing distance from the face. Horizontal tensile stresses were measured, indicating variation with lithology/rock tensile strength and maximum tensile stress of -2.5 MPa as indicated in Table 2.2.

Formation	Depth (m)	Vertical stress (MPa)	Horizontal Stress (MPa)	Tensile Strength (MPa)
Goat Island Dolomitic chert	7.7	9.0	1.5	6.9
Goat Island Dolomitic chert	11.2	11.2	-0.3	6.9
Gasport Dolomitic limestone	19.9	2.5	-2.5	4.7
Decew Mudstone	24.0	1.6	-1.3	4.6

Table 2.2: Tensile strengths and tensile stress at Niagara Gorge (after Lee 1978)

The development of a tensile zone in the cliff face resulted in tensile failure close to the face and the formation of sub-vertical tension joints. Evidence from drilling investigations at the site indicated the presence of tension joints for a distance of up to 24 m from the valley face with increasing joint spacing with increasing distance. Although not covered explicitly, Lee indicates that the redistribution of stresses around a newly formed tension joint affects the lateral extent of tensile zone development.

Further work on the unloading effects at the Niagara Escarpment was reported by Gross & Engelder (1991). Analysis of tensile joint orientation in the

escarpment face demonstrated that joints tended to be orientated parallel to the direction of maximum horizontal stress i.e. parallel to the strike of the cliff face. Field investigation of post-glacial uplift and nearby quarry excavations demonstrated the presence of quarry floor buckling to create ridges that were orientated perpendicular to the direction of maximum horizontal stress, indicating the influence of high lateral stress on relaxation of vertical loading. Gross and Engelder investigated the frequency of jointing in the Niagara gorge cliff face in relation height above the valley floor and distance from the escarpment. They found reasonable correlation between joint frequency and height/distance when taken together but poor correlation with either height or distance separately. The implication of this result is that tensile joint development is linked to both height and distance. In common with Lee (1978), Gross and Engelder concluded that relaxation of confining pressure due to progressive retreat of the Niagara escarpment results in the development of horizontal tensile stresses normal to the escarpment face.

Analysis of the geomechanical effects of natural unloading processes, as summarised above, resulted in identification of the following common characteristics:

(i) Stress relaxation due to unloading or loss of confinement results in uplift of newly formed free surfaces;

(ii) The development of a tensile stress zone with associated extensional strain is influenced by lithological variation and pre-unloading in-situ stress conditions;

(iii) Tensile stress near the newly created free surface can be high enough to support rock mass failure and extensional joint development parallel to the strike of the free surface i.e. parallel to the direction of maximum horizontal stress;

(iv) The lateral extent of the tensile zone may be constrained by stress redistribution around successive joint development;

(v) Extensional joint frequency reduces with increasing distance from the free surface.

With regard to man-made structures, the majority of existing research into the geomechanical response to unloading or stress relaxation has tended to focus on investigations of tunnels or underground mine workings and deep underground repositories for hazardous waste. Whilst these areas of research have many differences with the current study i.e. depth of development, maintenance of high boundary stresses, scale of effect, etc., there are several common factors relevant to this work and therefore worthy of review.

Goodman (1989) provided an overview of the effects of underground openings on stresses in surrounding rock mass for a range of rock types and geometries. It is recognised that all underground workings will cause a change in pre-development stress regimes. Goodman suggests that when tangential stresses around underground openings become greater than approximately half the unconfined compressive strength of the rock mass, fractures will form, creating 'slabs' orientated approximately parallel to the opening periphery. Goodman draws distinction between a purely elastic response and a plastic response to stress relaxation, indicating that for an elastic response, excess stress at the opening periphery is expected to fall to around 10% above the initial stress at a distance of 3.5 radii from the opening face. Where plastic deformation occurs, the extent of influence may be much greater with a distance of up to 10 radii required to achieve the same conditions. In discussion on 'block theory', Goodman refers to the role of pre-existing discontinuities in competent rock and the role they may have in defining rock blocks that have potential to move by sliding or rotation in response to stress relaxation.

Whilst the effects of lithostatic unloading at open pit excavations and engineered slopes has been recognised for many years (Goodman, 1989), the vast majority of research in this area has focussed on the implications of unloading on the stability of excavated slopes. Studies have therefore tended to focus on examination of stress change at slope surfaces and the implications for risk of slope failure under a wide range of configurations and environmental conditions. Early studies recognised the importance of variation in in-situ stress conditions as a critical factor in the stress response to lithostatic unloading. Kalkani (1976) investigated the effects of slope unloading on the stability of a rock wedge where a range of lateral stress values were introduced to represent the possible range of in-situ stresses that would

become effective at the slope surface following excavation. Ambient in-situ stress ratios were represented as principal stress ratios (k) in the range 0.0 to 2.0. The results were expressed in terms of the slope factor of safety (FOS) which varied from 1.85 for a k=0.0, i.e. no lateral stress, to 0.16 for a k=2.0 with a FOS falling below 1.0 at k values above 0.33. The concept being examined in Kalkani's work is that loss of lateral constraint by excavation creates a requirement to incorporate in-situ stress into slope stability assessment.

Nichols (1980) discusses the unloading effects of engineered excavations, including open-pit mines and quarries, in relation to specific rock types. Reference is made to excavation slope failures associated with unloading effects in over consolidated clays and shales in the United States, Canada and Western Europe. Nichols cites references to unloading effects in limestone quarries where buckling of the quarry floor has occurred, and rock failures in metamorphic and igneous excavations due to removal of overburden load.

In a study on the stability of slopes in deep open pit mines, Stacey (Stacey et al., 2003) presented the results of numerical modelling of stress and strain conditions in deep mine slopes of between 400 m and 1200 m height. The study reported, on the basis of previous work by Stacy during the early 1970's, (Stacey, 1973) evidence for the development of tensile stress zones in responses to stress relaxation at high excavation slopes under a range of in-situ stress conditions. Two conclusions from this early work were:

o *That opposite slopes of an open pit do not interact when the floor width of the pit exceeds about 0.8 times the slope height, and*

o *A large horizontal in situ stress field has a major influence on the stress distributions in slopes and overrides the effect of any variation in Poisson's ratio.*

Stacy noted that field evidence of fracturing or slope failure under tensile stress conditions corresponded with the locations of tensile stress zones calculated by theoretical analysis, but that there had been no significant investigation of the role of extensional strain in slope failure. The results of finite element

analysis of stress and strain variation in slopes of various heights and angles, on the basis of elastic response to lithostatic unloading and stress relaxation, are reported. The analysis were undertaken in two-dimensions on the basis that plane strain conditions could be applied. With regard to stress distributions, the study found that under low in situ stress ratio (k=0.5) a localised tensile stress zone develops beneath the pit floor. During higher in situ stress ratio (k>1.0) there is no tensile stress zone in the pit floor but a localised tensile stress zone develops at the crest of slope. The magnitude and extent of the tensile stress zone was found to increase with increasing lateral confining stress.

Stacy defines extension strain as the minimum principal strain defined as follows:

$$\varepsilon_3 = [\sigma_3 - v(\sigma_1 + \sigma_2)]/E \qquad\qquad [2.6]$$

where,

$\sigma_2, \sigma_2, \sigma_3$ are the three principal stresses

v is Poisson's ratio, E is Youngs modulus

It is apparent therefore that the magnitude of extension strain would increase with reducing E and increasing v.

Modelling results reported by Stacey demonstrate that the maximum extensional strain occurs around the toe of the pit slope, either at the base of the slope or in the adjacent excavation floor with development of an extensional strain zone at the crest of the slope with higher lateral stress conditions. Modelling studies were carried out with a single lithology and a single modulus of elasticity of 80 Gpa. This is representative of particularly stiff rock types and approximately double the average values used in the current research. As indicated above, lower E values would result in higher a magnitude extensional strain. Stacey reported extensional strain magnitudes of 0.00001 to 0.0001, depending on prevailing in situ stress conditions, and concluded that the extensional strain values derived from finite element

modelling were large enough to cause fracturing of intact rock. Previous work by Stacey (Stacey, 1981) had indicated fracturing potential at extensional strains of 0.0001 to 0.0003. It was therefore suggested that modelled stress/strain conditions were sufficient to cause the extensional fracturing observed in pit floor and faces for slope heights of over 400 m.

Finite element modelling investigations presented by Stacey provided an indication of the potential lateral extent of extensional strain zones for deep excavations. For an excavation slope of 800 m the extensional strain zone extended up to 50 m behind the toe of the slope and up to 100 m up the slope face from the toe. These distances increased to 100 m and 400 m respectively for a deeper excavation with an excavation face of 1200 m. These distances relate to the lateral extent of a potential extensional disturbed zone behind deep excavations in competent, brittle rock with no pre-existing discontinuities.

In a study into the depressurisation behaviour of mudstones at a large open pit coal mine in Indonesia, Marchand (Marchand et al., 2010) concluded that depressurisation due to lithostatic unloading or stress relaxation had a greater effect on pore pressure reduction in a series of thick mudstones than depressurisation by engineered drainage. Lithostatic unloading, and associated extensional strain, resulted in an increase in total mudstone porosity with consequent pore pressure reduction. Extensive pore pressure monitoring around the excavation demonstrated pore pressure reduction compared to pre-mining values. Field data demonstrated that depressurisation due to lithostatic unloading was identifiable at distances of up to 200 m laterally from excavation faces.

Investigations into landslide mechanisms at West Open Pit Mine in Fushun, China (Nie, 2015), the largest open pit mine in Asia, concluded that lithostatic unloading was the dominant cause of pit slope deformation, observed as both lateral displacement and vertical settlement. The investigation also identified the development of new fracturing around the toe of the slope resulting in a factor of safety of less than 1. Analysis of the effects of surface excavations on underlying rail tunnels in China, reported by Liang (Liang, 2017) demonstrated the effect of lithostatic unloading on structures at depth. Analysis considered case studies with tunnels at a depth of 15 m - 20 m below

ground level, beneath open excavations of approximately 10 m depth and found evidence of heave at the tunnel crest due to the effects of excavation unloading. Measured heave at one location exceed 20 mm. The analysis demonstrates that, for relatively shallow open excavations, there is definable upward displacement extending several metres below the excavation floor.

Reduction in ground load due to removal of material at open pit excavations results in a redistribution of stress. Vertical stress beneath the floor of an excavation and on sloping excavation faces is reduced in response to reduction in vertical load and lateral stress behind an excavation face is reduced due to loss of lateral load on a sloping face and loss of lateral confinement. As a consequence, stress is redistributed in the surrounding rock mass.

The stress response to vertical unloading can be considered analogous to the stress response to vertical loading as defined through Boussinesq analysis for a uniform load on a 2D strip with infinite length. For vertical stress below the strip foundation, the relevant equation is as follows:

$$\sigma_z = q/\pi(\alpha + \sin \alpha \cos (\alpha + 2\beta)) \hspace{3cm} [2.7]$$

where,

σ_z = vertical stress

q = load

α = angle between edge of excavation and point of interest

β = angle between centre of excavation and point of interest

Boussinesq analysis indicates that below a linear strip subject to uniform load, the subsurface stress can be related to the width of the loaded surface with residual stress equal to approximately 20% of the applied load at a depth of approximately 3 times the width of loading (Craig, 1987). For an unloading situation this would translate to an expectation that subsurface stress would equate to 80% of the pre-unloading stress at a depth of 3 times the width of the excavation. Hencher (Hencher, 2015) refers to stress beneath foundations

and suggests that in practice, vertical stress is reduced by about 90% of the surface load at a depth of approximately 1.5 x foundation width.

Barton (Barton and Shen, 2017) presented analysis on extension failure mechanisms in intact rock around deep tunnels, demonstrating that failure of brittle rock can occur by extension strain, even when all stresses are compressive. Barton discusses stress distribution around deep tunnels with stress relaxation at the tunnel 'free surface' resulting in potential peripheral fracture development and rock mass deformation. For intact rock with no pre-existing discontinuities, linear elastic theory is applied to demonstrate that vertical compression is accompanied by lateral expansion due to the Poisson effect. Radial deformation at the free surface is attributed to tangential strain as the radial stress is reduced to almost zero. Barton indicates that initial fracturing in tunnel walls is extension strain controlled and occurs at a critical value of tangential stress defined by the ratio of tensile strength and Poisson's ratio as lateral extension exceeds the critical lateral tensile strain.

A major international research and technology transfer project on the stability of slopes in large open pits (LOP) was undertaken during the period 2005 to 2009, resulting in publication of the Guidelines for Open Pit Slope Design (Read, 2009). Following from the initial LOP work on stability, a second publication Guidelines for Evaluating Water in Pit Slope Stability (Beale and Read, 2014) drawing together research and case studies on hydrogeological aspects of pit slope design was published in 2013. The project involved leading scientists and engineers from the mining industry worldwide and produced detailed guidance on the technical basis of slope drainage and depressurisation at large open pit mines. The reference to multiple case studies allowed analysis of 'real world' data sets for comparison with theoretical and simulated results. The study is focussed on defining pit slope pore pressure reduction techniques and effects but incorporates an overview of the effects of lithostatic unloading around large open pit excavations. Studies of pore pressure response include both the rock matrix porosity and fracture network porosity. The main conclusions of the study that are of relevance to the current research are as follows.

o The deformation zone, defined by changes in rock mass total porosity including matrix porosity and fracture porosity, as evidenced by changes in pore pressure post excavation, may extend 200 m to 300 m behind the slope face for large open pits. The study indicates that the relative importance of lithostatic unloading as a depressurisation agent, when compared to drainage by dewatering, probably increases with increasing depth of excavation;

o Case study analysis of large open pits, with evidence drawn largely from field pore pressure measurement, demonstrates that lithostatic unloading and loss of constraint at the slope face leads to development of tensile stress and lateral deformation resulting in rock mass lateral displacement towards the face. The extensional strain response, with or without fracturing or effect on pre-existing discontinuities, results in expansion of the rock mass and an increase in matrix, and/or fracture porosity. The study suggests that dilatancy also results in an increase in rock mass permeability or transmissivity related to the degree of hydraulic connectivity associated with discontinuity connectivity;

o The study proposes a simple multi-stage network conceptual model for fracture network development and hydraulic functioning based on fracture scale and connectivity variation from higher capacity preferential flowpaths to progressively reduced scale fractures that allow connectivity with the rock matrix and hence connect to matrix storage. This drainage configuration is used to describe one model of the hydraulic processes involved in fractured rock drainage and depressurisation.

o Conceptual drainage models are based on the concept of hydraulic diffusivity which is described as the rate at which fluid can flow between the rock matrix and the fracture network. The model is based on the assumption that storage within a fracture network is low compared to the matrix storage and therefore pressure responses in the fracture network can propagate rapidly.

o Much of the analysis in the study covers depressurisation of saturated strata, leading to consideration of effective stress conditions and groundwater flow regimes. It is concluded that changes in effective stress

due to pore pressure reduction are likely to be insignificant when compared to the effect of fracture dilation due to lithostatic unloading. It is suggested that in saturated systems, whilst unloading leads to an increase in porosity and associated reduction in pore pressure, where there is adequate hydraulic connectivity (effective porosity) groundwater would enter the increased storage volume with no significant change in groundwater level unless well-connected to a fracture-based drainage system.

The LOP study findings are drawn from evidence at the world's largest and deepest open pit mines. The scale and magnitude of effects described in the study are likely to be significantly greater than would be experienced at open pits with a maximum depth of 100 m, however, the enhanced effects in large pits helps to identify critical processes and responses that may still be relevant to shallower excavations. Case study evidence of rock mass expansion, and associated porosity increase, is consistent with the concept of extensional strain described by others, regardless of the presence of pre-existing discontinuities.

Large open pit conceptual models of hydraulic diffusivity and fracture network hydraulics are designed specifically to inform understanding of slope drainage and depressurisation processes. As discussed further at section 2.2, such models do not necessarily adequately describe fracture flow hydraulics in either saturated or unsaturated conditions for the purpose of defining the hydrogeological response to lithostatic unloading.

2.1.2 Definition of damaged and disturbed zones

The physical response to mineral extraction and lithostatic unloading at open pit excavations results in the development of damage and disturbed zones around the perimeter of the pit. As discussed above, the damage zone typically incorporates rock mass deformation under extensional strain conditions and the formation of new discontinuities or the deformation of existing discontinuities, subject to a wide range of geomechanical and environmental variables. Attempts to better define the perimeter damage zone around excavations have been undertaken since the 1980's (Kelsall,1984), although almost all research studies have been focussed on investigation of damage

zone development around deep underground waste repositories and not open pit workings.

Early studies (Kelsall, 1984) referenced a single 'disturbed zone' to describe the zone around underground excavations affected by development. More recently, more detailed definition of deformation has been developed to distinguish damage resulting from the excavation process from wider disturbance. The most commonly used definitions were presented at the 2003 European Union Nuclear Science and Technology Cluster Conference: *Impact of the excavation or disturbed zone (EDZ) on the performance of radioactive waste geological repositories*, as follows:

Excavation Damage Zone (EDZ) – Region of irreversible deformation with fracture propagation and/or the development of new fractures.

Excavation Disturbed Zone (EdZ) – Region where only reversible (recoverable) elastic deformation has occurred.

In a paper on excavation induced damage in crystalline rocks, Siren et al (Siren, 2015) defined the EdZ as the 'Stress-induced excavation disturbed zone' associated with reversible property changes, and resulting in hydromechanical and geochemical changes with minor changes in flow and transport properties.

More detailed models of damage and disturbed zones have been developed (Perras and Diederichs, 2016), but the additional detail relates to separation of the EDZ into discrete damage zone more applicable to deep tunnel development in high stress environments. The above definitions for the EDZ and EdZ have been applied throughout the current research.

Geomechanical processes within the EDZ incorporate damage caused by the excavation processes and non-reversible damage resulting from stress redistribution around the excavation perimeter. In open pit excavations this is typically considered to be the narrow zone behind the excavation face in which

damage occurs due to blasting. It is apparent from case studies summarised above, that near slope environments also often exhibit extensional strain and associated fracturing which would also constitute irreversible damage and therefore form part of the EDZ. Evidence from stress field modelling and pore pressure monitoring at field sites, as described above, has indicated that the lateral extent of the EdZ around large open pit excavations can be 200 m – 300 m. The lateral extent of the EDZ at open pit excavations is typically limited to a few metres from the face and floor (Tsang et al., 2005) and (Perras and Diederichs, 2016) and may be much more localised in deep underground tunnels and waste repositories. Although there does not appear to have been any previous attempts to more formally define the extents of the EdZ around open pit workings there have been many studies into EDZ characteristics and extents around deep underground excavations.

Kelsall (1984) presented research into potential permeability change in the 'disturbed zone' around deep shafts and tunnels used to access nuclear waste repositories. The work considered both blast induced damage and stress relief, through application of analytical approaches to evaluation of stress change. Kelsall defined three processes that were considered to contribute to formation of the disturbed zone as follows:

(i)   Stress redistribution;
(ii) Damage by the excavation process; and
(iii) Interaction between rock and groundwater

The analysis related to fractured, high strength rock such as basalt or granite. Kelsall concluded that stress redistribution could affect rock mass permeability in three ways, as follows:

(i)   Fracturing of intact rock due to compressive or tensile stresses;
(ii) Opening or closing of pre-existing fractures in normal or shear stress; and
(iii) By loosening of the crystal structure of the rock due to reduced confining stress.

Kelsall concluded, on the basis of comparison of intact rock compressive strength with compressive or tensile stresses, that fracturing of intact rock in

high strength materials was unlikely to occur above a depth of c.1000 m. Analysis of potential hydraulic conductivity change in pre-existing fractures orientated parallel or tangential to the tunnel or shaft axis where estimated by application of the cubic rule in relation to the normal stress at the fracture for a depth of 1000 m and an assumed stress of 28 MPa. The results indicated an increase in the hydraulic conductivity of fractures tangential to the tunnel axis by 2-3 orders of magnitude, and a reduction in the hydraulic conductivity of fractures radial to the structure. The increased hydraulic conductivity zone extended a distance of 1-2 radii from the excavation wall. The analysis is based on a 3 m diameter shaft in basalt. Kelsall attempts to distinguish the effects of blasting from the effects of stress relaxation, reporting that case studies of the blast damage zone indicate blast damage depths of 0.3 m - 0.6 m, subject to blasting technique.

Several studies presented at the EU 2003 Workshop demonstrated further progress in the evaluation of the EDZ and EdZ. Tsang (Tsang, 2003) provided an overview of the potential stress/strain/deformation response in the EDZ around deep tunnels, reporting that in hard rock environments with tunnels constructed by drill and blast techniques, the EDZ could extend 0.1 m to 0.75 m into the surrounding rock, reducing to around 1 cm if the tunnel is constructed by a tunnel boring machine (TBM). Tangential permeability within the EDZ increased by one to two orders of magnitude due to the effect of radial tensile stresses but the radial permeability is found to reduce by a factor of five due to tangential compression near the tunnel wall. The analysis is restricted to the EDZ and hence less than 1 m radial distance from the tunnel wall and does not extend to consideration of the EdZ and disturbance further from the tunnel.

Several authors (Tsang, 2003) and (McEwen, 2003) conclude that whilst radial compression acts to reduce radial hydraulic conductivities around tunnels and mitigate risk of enhanced groundwater inflow into the tunnel, the presence of an enhanced hydraulic conductivity zone tangential to tunnel axis creates the potential for enhanced groundwater flow around the perimetry of tunnels and hence a transmissive pathway through the surrounding rock. Autio et al (Autio, 2003), concluded, on the basis of field investigations at the Aspo Hard Rock laboratory in Sweden, that the high hydraulic conductivity zone around the external surface of tunnels is restricted to a zone of intense microfracturing a

few millimetres in thickness. The same studies concluded that, subject to variation in in-situ stress conditions, the EDZ in the excavation floor is generally larger than in the excavation roof and walls.

A summary of EDZ characteristics for deep underground tunnels and drifts was presented by Tsang (2005) as summarised in Table 2.3:

Excavation damage	Hydraulic conductivity change	Depth of influence
Drill & blast	Increase 2-3 orders of mag.	10 cm -150 cm
TBM	Increase 1 order of mag.	1 cm
Stress redistribution		
Axial	Increase 1 order of mag.	2 m – 3 m
Radial	Decrease by factor of 5	2 m - 3 m

Table 2.3: Hydraulic conductivity change due to excavation damage around deep underground tunnels (after Tsang, 2005).

Analysis of whether new fractures develop around deep underground excavations in intact rock due to stress relaxation is dependent on excavation depth, in situ stress conditions and the properties of the host rock. Aoyagi et al (Aoyagi et al., 2014) describes the results of seismic tomography surveys of rock external to a 250m deep tunnel at an underground research laboratory at Horonobe, Japan, concluding that new tangential fracturing parallel to the tunnel axis results in a decrease in rock strength and an increases in tangential permeability.

New analytical procedures for determination of the lateral extent of the EDZ around deep tunnels and drifts in brittle rock were presented by Perras & Diedrichs (2016), through a combination of laboratory analysis of rock cores and numerical analysis of stress conditions with distance from the excavation surface. The analysis included determination of the transition from the EDZ to the EdZ but did not attempt to quantify the lateral extent of the EdZ. The boundary between the EdZ and the EDZ is defined as the start of plastic

yielding i.e. the point at which disturbance becomes non-reversible, in accordance with previous definitions of the EdZ. The study resulted in the depths of the EDZ as summarised in Table 2.4.

Rock type	In plane stress ratio	EDZ lateral extent (m)		
		Min	Mean	Max
Granite	1.5	0.0	1.2	3.5
	2.0	0.4	1.6	3.1
Limestone	1.5	0.3	1.9	3.2
	2.0	0.4	1.9	3.4
Mudstone	1.5	0.7	2.4	8.6
	2.0	0.8	2.4	6.3

Table 2.4: Lateral extent of excavation damage zone (EDZ) around deep tunnels and drifts (after Perras & Diedrichs, 2016)

A similar approach to determination of EDZ extents based on stress analysis, originally developed by Lame was re-stated by Hedayat & Weems (Hedayat, 2019) with development of a formula for estimation of radial displacement at the EDZ (plastic zone) and EdZ (elastic zone) interface around an underground tunnel, as follows.

$$u_r = \sigma_o - \sigma_{cr}/2G \cdot (R_p^2/r), \qquad\qquad\qquad [2.8]$$

where u_r = radial displacement, σ_o = far field hydrostatic stress, σ_{cr} = critical stress at elasto-plastic interface, G = shear modulus of rock, R_p = radius of plastic zone and r = tunnel radius.

All attempts to quantify the lateral extent of the EDZ, whether analytical or field-based, are associated with deep underground tunnel, shaft or drift excavation. Available data for the lateral extent of the EDZ and the EdZ at open pit excavations are limited to purely theoretical numerical modelling studies or

anecdotal evidence from case study LOP's. Further work is therefore required to characterise and quantify the EDZ and EdZ around open pit workings, particularly at depths of less than 400 m.

2.1.3 Significance and effect of pre-existing discontinuities

The majority of previous theoretical investigations into the effects of lithostatic unloading on host rock stress distribution have been based on analysis of intact rock without pre-existing discontinuities. Analysis of case studies, either natural or man-made structures, make reference to both new fracture development and the presence of pre-existing discontinuities at a range of scales, but primarily as conduits for groundwater flow and not in relation to effect on the stress response.

Most recent studies related to the effect of lithostatic unloading at open pits have focussed solely on analysis of potential rock mass porosity change, and hence pore pressure change, as a consequence of stress relaxation and do not include evaluation of discrete discontinuity systems.

The majority of mined and quarried materials have low intergranular porosity and therefore groundwater drainage systems tend to be dominated by the presence of discontinuities in the rock mass. Reference to the comprehensive British Geological Survey (BGS) research output on major and minor aquifers in England and Wales provides further detail on the role of discontinuities in groundwater flow in each of the geological formations exploited for minerals (Allen et al., 1997, Jones et al., 2000) and indicates that groundwater flow through geological formations that dominate open-pit mineral development in the UK occurs predominantly via flow through discontinuity systems. A similar conclusion was reached on an international basis in hydrogeological studies that formed part of the international research and technology transfer Large Open Pit (LOP) project completed in 2009 (Beale and Read, 2014). With regard to consolidated materials encountered during open pit mining operations the study concluded '*Fracture flow conditions usually occur within most competent (consolidated) rock types, such as igneous, metamorphic, cemented clastic and carbonate rocks, and in consolidated coal formations. Although the unfractured rock may contain some pore space, this is mostly*

unconnected and much of the groundwater within these rocks occurs within fractures in the rock mass. Groundwater movement in these materials therefore occurs mostly by fracture flow and drainage from unfractured blocks will be effectively non-existent.'

Rock mass pre-existing discontinuities exist at a wide range of scales from microscopic features at granular scale through to large scale joints, faults and bedding planes. Hencher (2015) discusses the presence of small-scale 'incipient geological weaknesses' consisting of stress related fracture networks that can have a significant bearing on the strength, deformability and permeability of a rock mass. Such features develop as a consequence of rock mass over-stressing resulting in brittle failure. Changes to the local stress regime, loading or unloading, may lead to further fracture development through fracture propagation or coalescence. The extent to which small-scale incipient discontinuities influence rock mass permeability is dependent on whether such features are open and connected. For the purpose of the current research it is assumed that small-scale incipient discontinuities can be considered part of rock mass structure and permeability and that any change due to stress change would be incorporated as a change in bulk rock mass properties i.e. porosity increase due to elastic strain response.

Whilst discontinuities can occur at any scale, the focus of the current research is on discontinuities with the potential to transmit water as part of a discrete flow network separate from the rock mass. Such systems may develop due to the opening and connection of small-scale incipient discontinuities or larger-scale features such as persistent joints and bedding planes. The simple fracture diffusivity model referenced by the LOP study incorporates discontinuity networks at a range of scales with small-scale fracture systems draining to increasing larger-scale structures that form the dominant drainage conduits.

Goodman (1989) introduces concepts of unloading in relation to rock elasticity and loading/unloading cycles to demonstrate the significance of discontinuities on the elastic response to load variation, concluding that fractured rocks are rarely entirely elastic as discontinuity deformation may lead to irrecoverability of a component of strain during loading cycles. Concepts of recovery of elastic

strain energy during unloading must also be influenced by the presence of pre-existing discontinuities as discontinuities with typically lower stiffness than the surrounding host rock will tend to respond preferentially prior to a rock mass strain response. Conceptually it would seem reasonable to assume that the distance over which an elastic strain response is observed would be attenuated as a consequence of the presence of pre-existing discontinuities, with the degree of attenuation related to discontinuity stiffness, spacing, orientation, connectivity and persistence.

Jaeger et al (2009) discusses the mechanics of linear elastic failure during new fracture generation demonstrating that:

- o *If far field stress remains constant – energy required for fracturing is supplied from a decrease in the potential energy of the loading system; and*

- o *If far field displacement remains constant – energy required for fracturing is supplied by a decrease in the stored elastic strain energy of the rock mass.*

In the open pit simulations that form part of the current research, the only external loading is gravity and it is the far field displacement that is held constant. New fracture development may therefore lead to a reduction in stored elastic strain energy. For pre-existing discontinuities there is no energy required for the formation of new fracture surfaces and consideration of elastic strain energy use relates solely to linear elastic deformation.

Considering a strain response to loading using the classic spring analogy, the majority of displacement would occur during deformation or closure of discontinuities that have a lower stiffness than the host rock. As discontinuities close or reach a stiffness comparable to the surrounding rock mass, intact rock strain would be expected. This model infers that, for a given stress change, displacement resulting from the applied load would be preferentially accommodated in discontinuity deformation. The frequency, orientation, stiffness and initial aperture of pre-existing discontinuities would therefore

influence the residual energy available for rock mass strain and the lateral extent of deformation.

Goodman (1989) considers the effect of pre-existing discontinuities on the host rock mass concluding that *'the rock mass becomes weaker, more deformable and highly anisotropic because there is reduced shear strength and higher permeability parallel to discontinuities and increased compressibility as well as reduced tensile strength (essentially zero) perpendicular to them.'* Goodman considers that the most important property of a discontinuity, with regard to effect on rock mass properties, is the discontinuity orientation.

The significance of pre-existing discontinuities in rock mass deformation is re-stated by Bandis et al (Bandis et al., 1983) in relation to shallow excavations *'At relatively low stress levels encountered in near surface excavations, the deformation of joints dominates the elastic deflection of the intact rock'.* Reference is made to the work of Goodman (1968) in which the definitions of normal and tangential joint stiffness are introduced and applied to analysis of the contribution of joints to total displacement.
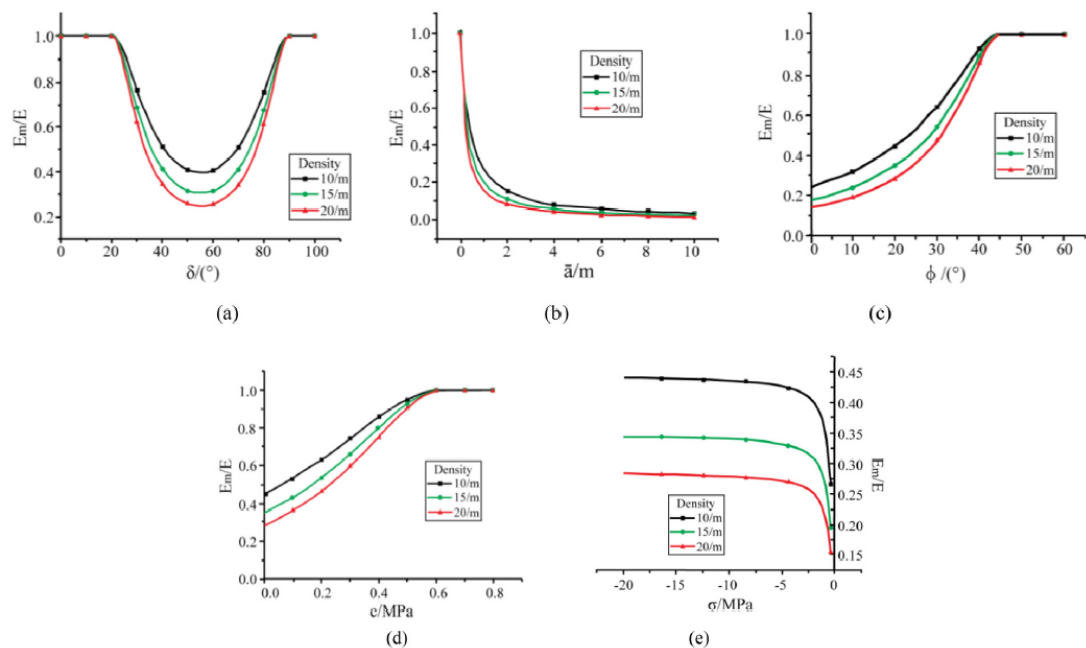
Figure 2.1: Effects of joint parameters on the elastic modulus of a rock mass: (a) internal angle, (b) average radius, (c) friction angle, (d) cohesion, and (e) stress state. (Source: Wu et al, 2020)

The effect of discontinuities on the stress-strain relationship of fractured rock was investigated by Wu et al (Wu, 2020) through analysis of fracture mechanics, rock mass structure theory and strain energy theory. Wu demonstrated that the presence of discontinuities in a rock mass result in a weakening of the elastic modulus with variability associated with discontinuity orientation, discontinuity length, friction angle, cohesion and stress state. As shown in Figure 2.1, prepared by Wu, the ratio of the elastic modulus of fractured rock (Em) to the elastic modulus of intact rock (E) varies significantly in relation to variation in all five parameters.

The analysis undertaken by Wu demonstrates that the presence of discontinuities increases the deformability of a rock mass where discontinuities are orientated at high angle to the direction of loading or where the discontinuity friction angle is low.

It is apparent, on the basis of previous studies, that the presence of pre-existing discontinuities act to increase the deformability of a rock mass with deformation of the discontinuities potentially accounting for the majority of rock mass displacement, subject to discontinuity frequency, stiffness and orientation. On this basis, under loading conditions, both the residual rock mass strain and the lateral extent of deformation would be influenced by the number and frequency of discontinuities with more localised effects associated with higher discontinuity frequency.

2.1.4 Discontinuity stiffness and deformation processes

Discontinuity deformation, as part of the rock mass response to unloading, can be described by discontinuity stress-deformation relationships used to define normal and shear stiffness. Bandis et al (1983) presented a benchmark study into discontinuity stress-deformation processes, following work by Goodman (1968). Goodman established that discontinuity closure under normal stress is non-linear and that with increasing stress, discontinuity surface normal displacement approximates a hyperbolic trend, tending towards a limiting value representing maximum closure. Bandis demonstrated that stress-displacement non-linearity also applied to shear displacement which could also be represented by hyperbolic functions. Discontinuity stiffness, as initially

defined by Goodman, describes the rate of change of stress to discontinuity closure or opening. Normal stiffness (k_n) is defined as the change in normal stress in relation to the change in normal displacement and shear stiffness (k_s) is defined as the rate of change of shear stress in relation to change in shear displacement. Goodman (1989) investigated joint stress-displacement relationships for interlocking and unmatched joints and established that with unmatched surfaces the joints exhibited much lower stiffness and greater joint closure when compared to interlocking surfaces. The variation was attributed to deformation of asperities in the unmatched joints.

Li et al (Li, 2014) investigated the effect of excavation induced unloading on previously closed joints reconfirming that the results of stress-displacement experiments undertaken by other in relation to joint closure also held true during stress reduction and joint opening. Experiments undertaken by Li demonstrated the effect of normal joint dilation on both normal stiffness and shear stiffness of joints, concluding that joint normal dilation reduces joint shear stiffness and hence shear deformability. It is apparent that as a joint opens, resistance to shearing associated with the presence of asperities in non-planer joints, is reduced and hence shear stiffness is correspondingly reduced. Li proposed that when evaluating joint dilation in relation to underground excavation, stress related change to both normal and shear stiffness should be considered.

Homburg et al, (Homburg et al., 2018) undertook experiments to test the stress-displacement relationship of naturally cemented joints in fractured carbonate rocks with natural fracture apertures within the range 0.1 mm to 1.4 mm. The study demonstrated that with the presence of natural cements between joint surfaces, the cements did not prevent joint closure under stress, although both cements and joint surfaces experienced damage. Homburg concluded that joint cements did not strongly modify fracture stress-dependent behaviour. Hillis (Hillis, 1998) investigated the role of variation in in-situ stress conditions on the closure of natural fractures and concluded that when the lateral confining stress is high, natural fracture closure is highly sensitive to fracture alignment, but that sensitivity drops markedly at lower lateral stress ratios of ≤ 2.

The scaling relationship between fracture size , fracture stiffness and in-situ stress conditions was investigated and reported by Morris et al, (Morris et al., 2017). Through a series of numerical analyses, stress and scale relationships where developed for fractures with a length of up to 0.512 m. Morris demonstrated a power law fitting to fracture specific stiffness -v- length data with the following examples for normal stress of 1 MPa and 10 MPa.

$$k_n \ (\sigma_n = 1 \ MPa) = 1200L^{-0.847} \hspace{3cm} [2.9]$$

$$k_n \ (\sigma_n = 10 \ MPa) = 7240L^{-0631} \hspace{3cm} [2.10]$$

where, k_n = normal specific stiffness (MPa/mm), σ_n = normal stress and L = fracture length (mm).

Simulation data was shown to be generally consistent with fracture normal compliance -v- length data collected by Hobday and Worthington (Hobday, 2012) for a data set that incorporated fractures up to a length of 100 m. Fracture length-specific stiffness fittings derived by Morris are shown in Figure 2.2.
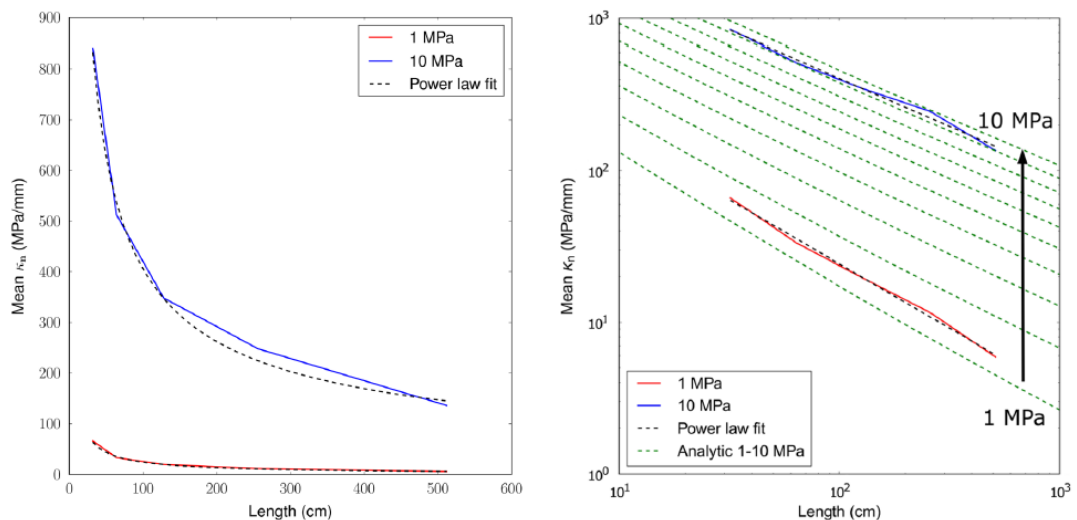
Figure 2.2: Fracture length-specific stiffness relationships for normal stress of 1MPa and 10MPa. (Source: Morris et al, 2017)

Bandis (1983) demonstrated the significance of joint surface roughness in relation to shear dilation for joints sheared under normal stress. Joint dilation curves presented by Bandis for both horizontal and vertical dilation indicated increase in dilation magnitude with increasing joint roughness, consistent with the general observation that in order to achieve shear displacement joint surfaces with asperities must pass over each other resulting in normal dilation and resultant reduction in shear stiffness.

Whilst discontinuity aperture can be related to both normal and shear stiffness, in-situ stress conditions, discontinuity length and discontinuity orientation, several studies (Bisdom, 2016, Pyrak-Nolte and Nolte, 2016, Crawford et al., 2018, Jiang, 2009) have investigated variation in the hydraulic properties of discontinuities in response to variation in geomechanical properties. Studies undertaken by Bisdom et al (2016), demonstrated that, due to the heterogeneity of fracture shear dilation, fracture network hydraulic connectivity could be low with only a small proportion of the network contributing to equivalent permeability. Through work on oil and gas reservoirs, Crawford et al, established procedures to relate fracture compressibility and fluid transmissibility to fracture porosity.

Through investigation of a case study of Xiaolangdi Reservoir on the Yellow River, China, Jiang (2009) et al, recognised that, as the permeability of rock masses decrease with depth due to rock mass and discontinuity compression, consideration of depth-dependent permeability may provide a basis for assessment of discontinuity normal stiffness. Hydraulic testing in the form of packer tests to a depth of 134 m were undertaken in calcareous sandstone, siltstone and mudstone. Discontinuity normal stiffness values where derived through development of an empirical formula relating normal stiffness to discontinuity transmissivity, in-situ stress and hydraulic head. Analytical results produced fracture normal stiffness values of 2.4 GPa/m to 35 GPa/m for a range of stress values of 0.26 MPa to 3.6 MPa, respectively.

Detailed analysis of relationships between discontinuity stiffness and fluid flow was presented by Pyrak-Nolte et al (2016). Statistical analysis demonstrated that a scaling relationship exists between fracture flow and stiffness, with potential for application to prediction of fracture behaviour as a function of

stress or depth. The approach is based on the conclusions that change to fracture topology (void geometry) is related to fracture stiffness and that the same changes control fluid flow through the fracture. The study investigated fracture flow and stiffness scaling relationships for fracture lengths of 0.0625 m – 1 m and demonstrated strong scale dependency of both parameters.

2.2   Discrete fracture network (DFN) modelling approaches and limitations

Discrete fracture network (DFN) modelling allows the explicit modelling of geomechanical and hydraulic processes in discrete discontinuity networks that can be defined as separate entities from the host rock mass through specification of discontinuity-specific contact properties. DFN modelling is a developing science that is increasingly applied to complex geomechanical problems with particular application in the design and analysis of underground hazardous waste repositories and evaluation of unconventional gas deposits. There has been much less extensive application to open pit mining projects where the complexity and resource demand of DFN modelling may not always be justified by the potential benefits that are achieved and the potentially low operational sensitivity to hydrogeological variability.

The current study is focussed on evaluation of excavation induced effects on discontinuity networks around open pit excavations, requiring a means to investigate the response of discontinuities explicitly and separately from the bulk rock mass response. Current approaches to the design and implementation of discrete fracture modelling of large-scale features are briefly discussed below.

Lisjak and Grasselli (Lisjak, 2014) provide a comprehensive overview of the difference between continuum and discontinuous (discrete) modelling techniques. The paper notes that discontinuous modelling systems have advanced rapidly since 2014, and that in continuum modelling there is no explicit representation of discontinuities. Such features are generally represented by adjustment of rock mass properties to reflect variation in deformation modulus and strength parameters. In discrete element methods

(DEM) of modelling, rock mass materials are treated as a group of separate blocks or grains separated by discontinuities that are discretely represented.

Application of the DFN approach to mining and mineral projects is illustrated by Digges La Touch and Cottrell (Digges La Touche and Cottrell, 2017) where stochastically generated complex fracture networks were developed, on the basis of both measured and assumed fracture configurations, and linked groundwater seepage analysis using Golder Associates FracMan software. Flow modelling in the DFN systems generated by FracMan was undertaken to investigate mine water inflows, to derive hydraulic properties of the rock mass at an underground polymetallic mine and to investigate fracture system heterogeneity in fractured limestone strata.

Elmo et al, (Elmo, 2014) applied DFN modelling techniques to characterise rock block fragmentation in block cave mining environments and in the early stage development of Rockfield International's ELFEN modelling system. Pine et al, (Pine, 2006) used DFN modelling techniques to investigate the effects of normal loading on fractured mine pillars. In both cases, the importance of accurately defining fracture length, orientation and intensity was recognised as critical to DFN model performance. During relatively early studies into the use of DFN modelling techniques to investigate hydraulic fracturing results in preconditioning works for underground cave mining Rogers et al (Rogers, 2011) demonstrated that damage resulting from hydraulic fracturing may extend beyond the design fracture configuration to interconnected fractures, opening of incipient fractures and damage to the adjacent rock mass.

In more recent studies (Obeysekara et al., 2017, Bisdom, 2017, Pham, 2021) DFN modelling approaches have been applied to analysis of the coupled geomechanical and hydraulic response to stress change associated with development in sub-surface environments where groundwater seepage rates are influenced by change to discontinuity network configuration. Obeysekara et al, investigated the evolution of fracture systems in the EDZ around a sub-surface tunnel in response to excavation induced stress change using a combination of a DEM approach (Solidity Model) and a separate flow solver to simulate pore pressure change and fracture flow response to tunnel excavation under a range of pre-excavation hydrostatic pressures.

The extent to which DFN modelling is representative of real environments is dependent on the quality of input data. Bisdom et al, discusses derivation of fracture configuration data from outcrop studies and proposes a detailed workflow for translation of field data to discrete fracture models, with particular focus on stress-aperture relationships and associated matrix and fracture permeabilities. Bisdom identifies difficulties in assigning aperture values on the basis of outcrop measurement if stress relief effects are not accounted for and notes that in many situations the complexity of fully integrating geomechanical and hydraulic processes results in simplifications achieved by upscaling fracture characteristics at model grid scale rather than discrete fracture response simulation. Bisdom notes that outcrop studies have demonstrated that variation in both fracture length and aperture tend to follow a power law scaling relationship.

Discrete fracture network modelling was applied by Pham et al, to estimate fracture aperture distribution in fractured aquifers for which bulk hydrogeological test data was available. The DFN models of the fracture system were calibrated against the hydrogeological response to pumping tests. A 3D open source DFN code (dfnWorks) was used to develop the DFN model for flow and contaminant transport. The integrated model was calibrated by gradually varying fracture apertures until an acceptable match was achieved with the observed hydrogeological response.

A brief review of previous applications of DFN modelling to discontinuity network response to geomechanical and hydrological variables demonstrates potential for application to evaluation of the potential hydrogeological significance of excavation induced unloading effects around open pit mineral workings. However, it is apparent that, with the exception of slope stability analysis and damage zone loading and fragmentation studies, examples of the application of DFN modelling approaches to the evaluation of external hydrological effects of open pit mineral extraction are largely absent from the literature.

Discontinuity response to excavation induced stress change is a complex process and not all aspects of discontinuity response are represented in current DFN modelling codes e.g. representation of shear dilation and the

linkage of shear dilation to normal dilation. The primary limitation on wider application of DFN modelling approaches is the high input data demand and the high resource use associated with running DFN models when compared to continuum modelling systems.

2.3 Hydraulic properties of fracture networks

Rock discontinuities capable of storage and transmission of groundwater include structural features such as faults and joints and lithological features such as bedding planes and solution cavities. Although rock discontinuities may have high permeability compared to the rock matrix, the potential for storage and transmission of groundwater is critically determined by the connectivity of the discontinuity network. Isolated fractures and joints have no significant potential to promote groundwater flow, other than as connections between formations with inherent matrix porosity. Work undertaken on pit slope depressurisation at large open pits, defined fracture networks as a multi-scale sequence with transient drainage of fractures occurring in a sequential manner depending on fracture scale and connectivity (Beale and Read, 2014).

In saturated systems, dual porosity flow can occur where groundwater is able to move through both intergranular pore space and connected fracture networks. Where downstream constraints prevent free drainage, fully saturated groundwater flow through both mechanisms may occur. At mineral excavations, the downstream boundary at the open pit face is a free surface with no head constraint on groundwater drainage. Under such conditions there is potential for more rapid groundwater flow through higher capacity fracture networks than through the rock matrix. If the capacity differential is large enough the fracture network acts as a drainage network with inflow from the surrounding matrix and a tendency towards fracture flow as the primary drainage mechanism, regardless of the porosity and permeability of the rock matrix. The distribution of flow between matrix flow and fracture flow is therefore influenced by the respective capacity of each system and the boundary head conditions.

A review of the literature related to the hydraulic properties of fracture networks has been focused on the following subject areas:

o   Discontinuity hydraulic change induced by lithostatic unloading;

o   Discontinuity network characteristics that influence hydraulic properties;

o   Linear and non-linear flow regimes; and

o   Application and estimation of equivalent porous media values.

2.3.1 Discontinuity hydraulic change induced by lithostatic unloading;

Price (Price, 2016) provides a comprehensive overview of hydraulic issues associated with open pit slope design and the potential effects of excavation induced unloading on groundwater behaviour. Although primarily related to development of an excavation damage zone (EDZ) rather than the excavation disturbed zone (EdZ), the role of discontinuity configuration, geometry and physical properties are identified as factors relevant to hydraulic response to loading and unloading. Price discusses the significance of hydromechanical coupling in relation to the hydraulic characteristics of a fractured rock mass and the role of effective stress in rock slope stability. Fluid flow in fracture systems is discussed in relation to fracture roughness and non-linear flow, fracture stiffness and aperture change and the role of capillary pressure in controlling drainage in small-scale fracture systems.

Earlier work undertaken by Bai and Elsworth (Bai and Elsworth, 1994) investigated hydraulic conductivity change in fractured strata around underground coal mine development, including variations in pore pressure. Analytical assessment demonstrated development of enhanced hydraulic conductivity around a longwall panel at a depth of approximately 220 mbgl. Hydraulic conductivity values around the underground excavation were estimated to increase by several orders of magnitude close to the panel and by a factor of 2 approximately 100 m above the panel. A summary of spatial results for a 10 m fracture spacing is presented as Figure 2.3. Bai and Elsworth

(1994) found that fracture spacing was one of the key controls on post-mining hydraulic conductivity.
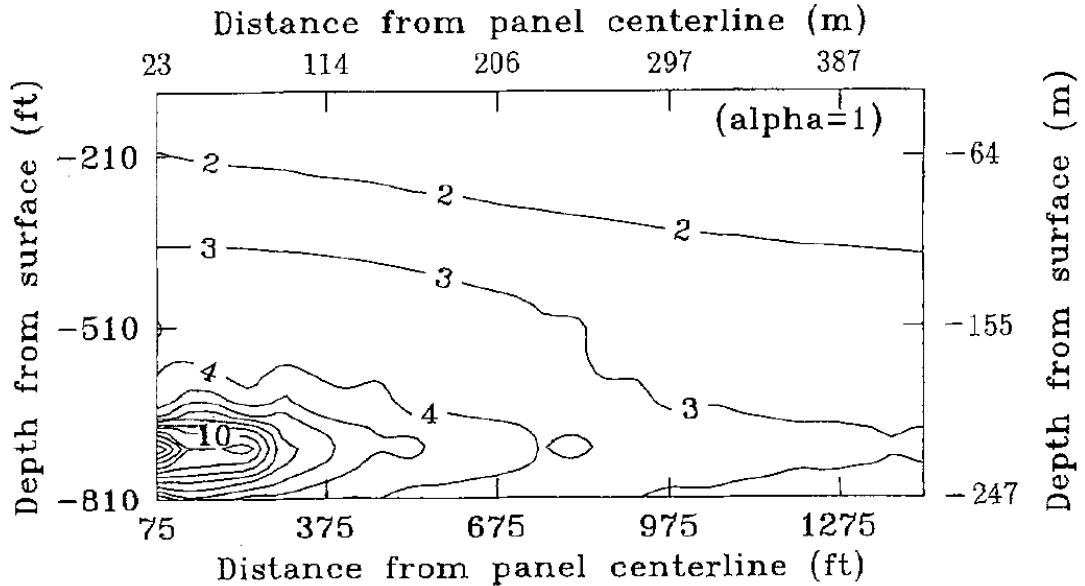
Figure 2.3: Results of stress related hydraulic conductivity variation around underground longwall mine panel showing ratio of conductivity (K/K$_o$) in fractured rocks with fracture spacing of 10m. K=post mining hydraulic conductivity, K$_o$=original hydraulic conductivity. (Source Bai & Elsworth 1994)

Indraratna et all (Indraratna et al., 1994) investigated water inflows to underground mining excavations and identified the significance of shear deformation resulting from mineral extraction on resultant hydraulic conductivity. It was demonstrated that, with increasing fracture length, fracture shear strength decreases and the magnitude of shear dilation increases. The resultant hydraulic conductivity of the fracture is increased as a combination of both normal and shear dilation.

2.3 2 Discontinuity network characteristics that influence hydraulic properties

Characteristics of discontinuity networks in relation to changes in discontinuity hydraulic conductivity have been extensively studied (Haagenson, 2018, Black, 2017, Zoorabadi, 2022, Leung, 2012, Pyrak-Nolte, 2000, Lei et al., 2017).`Haagenson et al (2018), investigated fluid diffusion characteristics

between matrix and fracture flow for a range of materials and geomechanical properties. Modelling demonstrated that where matrix and fracture permeability is similar, fluid pressure diffusion into the rock mass is homogeneous but where fractures are assigned a much higher permeability than the matrix, diffusion into the fracture network is enhanced with development of preferential flow paths through the fractures.

Lei et al (2017), demonstrated that the development of preferential flow paths in fracture flow systems can be influenced by the magnitude and orientation of in-situ stresses. Lei reported that flow localisation in discrete fractures tends to increase in fractures orientated preferentially for shearing and with increasing far-field stress. Finite discrete element modelling undertaken by Lei et al, supported conclusions by others that, in natural fracture flow systems, the majority of flow may be focussed in a small number of fractures with fracture hydraulic conductivity critically influenced by the local in-situ stress state.

Further work on flow localisation and the development of preferential flow paths was undertaken by Black et al (2017) in which the concept of long 'sparse networks' of flowing fracture systems was proposed. Based on retrospective analysis of data obtained from geomechanical and hydraulic monitoring at the Stripa Mine Underground Research Laboratory in Sweden, Black et al demonstrated that areas of low permeability in tunnel walls, defined as 'skin', within the laboratory could be better accounted for where fracture flow systems are represented by sparsely distributed flowing channels than by a more intensively distributed network of well-connected shorter channels. This concept was further extended by Black & Barker (Black and Barker, 2018) through investigation of the shape, size and organisation of fractures in flowing networks in relation to the equidimensional approach typically adopted in DFN modelling. The investigation indicated that observed flow could be related to lower fracture density when fracture length and shape is fully accounted for and that, for the data set referenced, less than 10% of the network formed part of the active flow path.

The significance of discontinuity density and aperture distribution on discontinuity network hydraulic conductivity was investigated by Leung &

Zimmerman (2012), resulting in the conclusion that fracture network hydraulic conductivity is linearly correlated with fracture density, defined by reference to fracture length and intensity. Zoorabadi et al, (2022) identified the difference between approaches to determination of fracture network hydraulic conductivity in joint sets with finite length compared to models representing joints as a plane of infinite dimensions. Based on analysis of data from Fabay-Augeres Mine in France, the study proposed new approaches to estimation of hydraulic conductivity around underground mine tunnels based on consideration of joints as finite planes with defined connectivity. Analytical results for the case study referenced demonstrated that hydraulic conductivity decreased with increasing joint spacing.

It is clear that discontinuity hydraulic conductivity is dependent on discontinuity aperture and that aperture can vary in relation to variation in local and far field stress, with the magnitude of aperture variation determined by aperture normal and tangential stiffness. Pyrak-Nolte & Morris (2000) investigated the relationship between fracture specific stiffness and fluid flow for a single fracture and found that flow characteristics are dependent on the aperture void space distribution in relation to void space variation under normal stress. The work demonstrated that fractures in which asperities form multiple peaks (referred to as correlated aperture distributions), rather than more equitably distributed heights (referred to as uncorrelated aperture distributions) show greater effect on aperture void space and fluid flow capacity under normal stress.

2.3.3 Linear and non-linear flow regimes

Groundwater flow through discontinuity systems may be either (linear) laminar or (nonlinear) turbulent depending on system permeability and hydraulic gradient (Singhal, 2010). In laminar flow the flow velocity is proportional to the hydraulic gradient (Darcy's Law), as;

$$V = Ki, \qquad\qquad\qquad [2.11]$$

where V = velocity, K = constant, i = hydraulic gradient

In turbulent flow the velocity is non-linear and can be expressed as,

$$V = Ki^{\alpha}, \qquad\qquad\qquad [2.12]$$

where V = velocity, K = constant, i = hydraulic gradient, α = non-linearity coefficient ($0.5 \leq \alpha \leq 1$).

The transition from laminar to turbulent flow is usually defined by the Reynolds number (R_e) which relates the ratio of inertial to viscous forces acting on the fluid, in the form,

$$R_e = \rho V d/\mu, \qquad\qquad\qquad [2.13]$$

where ρ = fluid density, V = mean velocity, d = conduit diameter, μ = dynamic viscosity of the fluid.

In general, the flow regime is laminar for $R_e < 2000$ and turbulent for $R_e > 2000$ (Singhal & Gupta, 2010)

Most analytical approaches to assessment of groundwater impacts around mineral workings are based on the assumption that Darcy's Law is applicable and that groundwater flow can be considered to be laminar. Work undertaken by Dudgeon (Dudgeon, 1985a, Dudgeon, 1985b) has demonstrated that as groundwater flowing towards open pit excavations reaches the increasingly fractured perimeter of the pit there is a tendency for flow conditions to become turbulent with significantly increased head losses when compared to laminar flow conditions. The point at which laminar flow becomes turbulent is directly related to fracture aperture size and roughness plus the magnitude of the driving head. Changes in fracture system configuration can therefore lead to changes from laminar to turbulent flow conditions.

Fracture flow studies based on the parallel-plate model with smooth fracture surfaces result in linear laminar flow and hence the applicability of Darcy's law and variations of the cubic law for derivation of fracture network hydraulic

conductivity. However, in real hydrogeological environments, fractures are typically characterised by rough walls and conditions for laminar flow may not apply. Flow through a fracture network may occur as a variable combination of laminar, non-laminar and transitional flow regimes related to variation in hydraulic resistance through different parts of the system. Zhou et al (Zhou, 2015) reports that, in laboratory studies, flow under a non-linear regime resulted in a 3-17% higher pressure drop when compared to the flow through the same system under laminar flow. Zhou reports that field study hydraulic conductivity test results for non-laminar flow may underestimate hydraulic conductivity by an order of magnitude if laminar flow conditions, and hence the applicability of Darcy's Law, is assumed.

Lui et al (Lui, 2021), undertook laboratory investigations to establish the effect of fracture roughness on the transition from laminar to turbulent flow in fractured rock. The study found that as fracture roughness was increased, the additional energy loss resulted in a higher degree of non-linearity in fluid flow. Lui reports that as joint roughness coefficients (JRC) were increased from 2 to 20, the Reynolds number at which transition to non-linear turbulent flow occurred was reduced from 566 to 67. Lui notes that use of Darcy linear flow equations may result in overprediction of water inflow into mine tunnels as additional head losses are neglected.

Allowance for the additional head loss that occurs under nonlinear flow conditions can be achieved by application of the widely used Forchheimer equation in the form,

$$i = aQ + bQ^2, \tag{2.14}$$

where i = hydraulic gradient, Q = flow rate, a & b or linear and nonlinear coefficients.

The second coefficient, b, is the non-Darcy flow coefficient that describes the role of inertial forces in nonlinear flow (Lui et al, 2021).

Evidence of the significance of nonlinear flow in real hydrogeological environments was reported by Altinors & Onder (Altinors, 2008) through development of dual porosity model of flow through a fractured aquifer in response to variable head conditions related to rapidly rising stream water levels. The model, based on linear flow through the matrix and nonlinear flow through the fracture network, demonstrated that as fracture flow nonlinearity increased, due to increasing fracture aperture, flow to the aquifer decreased and transfer of water between fractures and the matrix decreased. Flow in the fracture network was controlled by the Forchheimer *b* coefficient.

2.3.4 Translation to equivalent porous media (EPM) hydraulic conductivity

Whilst DFN modelling is increasingly used to simulate geomechanical and coupled geomechanical-hydraulic response in fractured rock, it is common practice to adopt a simplified approach to modelling of flow through fractured media where discrete fracture flow outputs are not required (Singhal & Gupta, 2010). Many studies have demonstrated that when a fracture system is represented at a large enough scale, it can be reasonably represented by flow through an equivalent porous media (EPM).

Early studies undertaken by Long et al (Long, 1982), proposed that a fractured rock can be reasonably represented by an EPM when,

'There is insignificant change in the value of the equivalent permeability with a small addition or subtraction to the test volume, and

An equivalent permeability tensor exists which predicts the correct flux when the direction of a constant gradient is changed.'

Translation of fracture-specific hydraulic conductivity values to EPM values is usually achieved through application of the cubic law in the following general form (Bear, 1993).

$$Q = \rho g / 12 \mu \left[\Sigma b_i{}^3 + \Sigma b_j{}^3 \right] . \; dh/dx \hspace{4cm} [2.15]$$

Where,

ρ = fluid density (kg/m^3)

g = gravitational acceleration (m/s^2)

Q = flow (m^3/s)

μ = dynamic viscosity (p.s)

b_i = joint aperture normal dimension (m)

b_j = bedding plane aperture normal dimension (m)

dh/dx = hydraulic gradient

A comprehensive review of mathematical expressions for estimating EPM for a fractured rock mass was presented by Lui et al, (Liu and Liu, 2017), in which consideration was given to the significance of fracture length; aperture distribution; fracture surface roughness; fracture network connectivity; hydraulic gradient; boundary stress conditions, and scale. Lui concluded that '*The influence of surface roughness on the magnitude of permeability is much less than that of the length and aperture of fractures, which justifies the usage of parallel-plates in most models.*'

In a review of the performance of EPM's in relation to DFN modelling, Zareidarmiyan et al (Zareidarmiyan, 2021) undertook comparative analysis associated with simulation of fluid injection into a fractured rock mass. The analysis resulted in the conclusions that whilst EPM based models can accurately represent fluid flow rates, the pore pressure distribution in the two models was significantly different, with variance at up to 50%. The variation in pore pressure distribution was attributed to variation in hydraulic conductivity between the rock matrix and the fracture network.

CHAPTER 3: GEOMECHANICAL MODELLING – INVESTIGATION DESIGN AND METHODOLOGY

3.1 Introduction

Naturally high variability in the location, orientation, connectivity and configuration of hard rock fracture systems means that physical investigation of discontinuity response to unloading around open pit workings would require a high-density ground investigation programme incorporating multiple borehole construction and testing, together with a range of geophysical survey techniques. The high cost of such investigations is rarely justifiable and is a significant factor in the lack of site-specific data on the magnitude and extent of discontinuity deformation around mineral workings. Following ground investigation and testing at Blaxter Quarry in Northumberland to provide baseline geotechnical data to support representative discrete fracture network (DFN) configuration in this study, the response of pre-existing discontinuities to stress change resulting from lithostatic unloading around open pit excavations has been investigated through a programme of geomechanical modelling.

This study is focussed on assessment of unloading effects in hard rock environments. As the objective of this component of study is to provide input to evaluation of hydrogeological significance, and as groundwater flow through discontinuities is the dominant flow mechanism in the majority of open-pit mining environments (Beale et al, 2014), modelling has been focussed on evaluation of geomechanical effects on discontinuities rather than the host rock mass, resulting in a requirement for DFN modelling.

It is recognised that discontinuity response to stress change resulting from mineral excavation is likely to be highly site-specific and influenced by such factors as, host rock properties; lithological variation; depth of excavation; in-situ stress conditions; and discontinuity type, orientation, frequency, persistence, and stiffness, together with wider environmental influences such as weathering profiles, the presence of groundwater and discontinuity infill characteristics. It is not possible within the scope of this research to fully represent all possible combinations of variables and therefore it has been necessary to develop a small number of generic conceptual geomechanical

models that represent the majority of excavation environments and within which key parameters can be varied to encompass a wider range of potential site conditions.

Geotechnical model development has been based on the principle of increasing discontinuity network complexity and orientational variability from the simplest geometrical configuration to more complex configurations. Models have incorporated multi-layered bedding and simple lithological variation based primarily on two separate sets of rock properties. Based on site-specific review of discontinuity geometry in a range of open pit workings across the UK, the modelling sequence commences with a single orientation discontinuity configuration, consisting of just bedding planes, and progresses through simple orthogonally jointed systems to increasingly variable multi-set joint systems. Baseline modelling without discontinuities has also been undertaken to provide a reference for comparative analysis of the effects of discontinuity inclusion.

Hydrogeologically, discontinuity network characteristics of greatest interest are those that influence discontinuity permeability, rock mass transmissivity, fluid flow hydraulics and change in unsaturated or saturated flowpaths. Geomechanical modelling has therefore been designed to provide data in relation to the following.

(i) Variation in discontinuity aperture dimensions;
(ii) Discontinuity network connectivity; and
(iii) Excavation disturbed zone (EdZ) extent.

Whilst it is recognised that discontinuities occur at a range of scales from incipient micro-fractures to large scale bedding planes, due to the need to balance model domain dimensions with discontinuity resolution, this study is primarily concerned with large scale discontinuities in the form of bedding planes and large-scale jointing.

The study is aimed at investigation of effects that may be applicable to the majority of open pit excavations and not specifically to the relatively small

number of large open pits (LOP) around the world. All modelled excavations have therefore been limited to a maximum depth of 100 m below ground level. This depth encompasses the majority of open pit excavations for construction materials, energy minerals, industrial minerals and metals, worldwide.

Following a detailed review of several geomechanical modelling systems, Rockfield International's Elfen modelling system was selected for application to this research. All geomechanical modelling work has been undertaken with Elfen, although additional stochastic modelling to support development of a representative fracture network was undertaken with Golder Associates FracMan model. Further details regarding model selection are provided in subsequent sections of this chapter.

Figure 3.1: Exposed rock faces at Blaxter Quarry showing bedding planes and orthogonal jointing. Rock is extracted at the quarry by hydraulic excavator without requirement for blasting.

Although the modelling program has not been designed to simulate site-specific conditions at any particular site, the use of source data from Blaxter Quarry in Northumberland has ensured that the DFN configurations used in this study are representative of real world environments, providing a degree of

ground truthing for model outputs. As indicated in Figure 3.1, excavated faces at Blaxter Quarry are accessible, allowing detailed inspection of discontinuity characteristics. Discontinuity survey at Blaxter Quarry included wireline logging of Borehole 2 to increase understanding of discontinuity spacing and orientation. Both acoustic and optical logs were run. A copy of the discontinuity log for Borehole 2 is included at Appendix B.

Geomechanical modelling results for a range of parameters and model configurations are presented and discussed in Chapter 4. With regard to subsequent use of model data in hydraulic and hydrogeological analysis, the following two outputs were required.

(i)   The lateral extent of the excavation disturbed zone (EdZ) behind the excavation face and floor for a range of excavation depths, in-situ stress conditions and DFN configurations; and

(ii)   The magnitude of discontinuity dilation within the EdZ as a function of distance from the excavation face and floor.

EdZ extent has been determined by reference to a pre-defined stress threshold and reference to rock mass displacement direction and magnitude. Discontinuity dilation with distance from the excavation is expressed as a function of distance for each model and model configuration.

3.2   General approach to discrete fracture network modelling

3.2.1 Model selection and application

There are several well-established geomechanical modelling systems that have the potential to support investigation of unloading effects on pre-existing hard rock discontinuities. A search of web-based resources and reference to technical literature and conference proceedings led to the identification of ten commercially available modelling systems with potential application to this research. The majority of models adopt the discrete element method (DEM) to discretise the joint bounded blocks and allow explicit simulation of discontinuity response to stress change. More recently, a hybrid continuum-discontinuum

approach, the combined finite discrete element method (FDEM), has been developed with the potential to simulate deformation from a continuum state to a fully discontinuous state through initiation and propagation of discontinuities. FDEM models overcome problems with DEM models associated with new fracture initiation.

A detailed review of the specific requirements of this research provided the basis for model selection. The primary modelling objective of this study is to investigate potential change in the hydraulic characteristics of discontinuity systems in hard rock fracture flow environments due to evolution of system response to stress change arising from mineral extraction. In addition to realistic representation of the unloading stress response, a geomechanical model therefore needs the capability to deliver data on aspects of discontinuity development that could have an effect on host rock hydraulic characteristics. These include:

(i) Discontinuity location, orientation and length

(ii) Discontinuity aperture size and shape

(iii) Discontinuity connectivity

At project commencement it was anticipated that stress change in the surrounding rock mass due to unloading and relaxation of lateral confining stress, under elastic response conditions, may lead to a number of changes to discontinuity systems that could include the following:

(i) Propagation of existing discontinuities

(ii) Change in aperture size of existing discontinuities

(iii) Initiation of new discontinuities

(iv) Coalescence of existing and new discontinuities

Whilst ideally, modelling systems would have capability to incorporate discrete discontinuities and to simulate the above processes, it was recognised at an early stage in the investigation design process that, in practice, the stress

changes involved in relatively shallow open pit excavations are unlikely to lead to new fracture development. The capacity to simulate change to the existing discontinuity network is therefore the key requirement. Geomechanical modelling also needed to include assessment of several different conceptual configurations aimed at representing a range of lithological variations in open pit mines and quarries. An ability to develop models that include a number of separate layers with distinct geomechanical properties was therefore an essential requirement.

Careful consideration was given to the requirement for two-dimensional (2D) and/or three-dimensional (3D) modelling capability. Whilst ideally the capability to model discontinuity systems at 3D would provide the most representative basis for comparison with real world situations, account had to be taken of the project objectives, related to assessment of hydrogeological significance, and the time and resources required to investigate multiple DFN configurations in 3D. Research outputs are required to inform evaluation of hydrogeological significance, rather than replication of site-specific conditions. It was considered unlikely on the basis of that test that research results from 3D modelling would vary from conclusions derived from 2D modelling with regard to significance. It has been considered more important to investigate DFN response to unloading under a range of DFN configurations and stress conditions, which given study time constraints, was only possible in 2D. A commitment to model in 3D would have limited the potential to investigate such a wide range of variables.

Whilst modelling of a range of DFN configurations has been undertaken in 2D, baseline modelling of the unloading response in strata without discontinuities has been undertaken in both 2D and 3D. The 3D models allow evaluation of EdZ configuration in relation to excavation geometry. The bedding-only model developed early in the modelling sequence can be considered reliably representative of plane strain conditions under which a third modelling dimension is unlikely to influence results. Subsequent phases of modelling incorporate more variable joint distributions in which a third dimension could have an effect on discontinuity response to unloading, although with a relatively low level of discontinuity connectivity in these models it was concluded that such third dimension effects may be limited.

The hydrogeological objectives of this study creates a requirement to be able to investigate changes in groundwater flow patterns around mineral workings. Some geomechanical models allow simulation of groundwater seepage through discontinuity systems although the primary aim of such models is determination of pore pressures and, in some cases, coupled modelling of stress-flow regimes. Two-dimensional seepage analysis was not considered to be adequate for hydrogeological impact assessment which needs to incorporate a range of external boundary conditions and contaminant transport processes. A separate modelling system has been used for simulation of 3D groundwater flow and contaminant transport through discontinuity systems. The selected geomechanical model therefore needed to have the capability to present or export results in a format that could be translated to or accommodated within a suitable hydrogeological modelling system.

Capability	Essential	Preferred
2D capability	✓	
3D capability		✓
Automated discontinuity generation	✓	
DFN capability	✓	
Fracture aperture change	✓	
Fracture initiation	✓	
Multi -layer capability	✓	
Phased development	✓	
Results export options	✓	

Table 3.1: List of preferred DFM model capabilities.

Open pit mineral workings develop in a phased manner with increasing depth and decreasing lateral extent. The geomechanical response at different levels of open pit development was expected to vary as both loss of lateral containment and reduction in basal loading take effect with increasing development. Taking account of modelling system requirements discussed above, a listing of preferred model capabilities was prepared as indicated in Table 3.1.

No	Model	Source	Type	Capability limitations	Review Status
1	Rocscience (RS2)	Rocscience	2D	New fracture initiation	Reference technical literature
2	Rocscience (RS3)	Rocscience	3D	No explicit joint definition	Demo obtained for evaluation
3	UDEC	Itasca	2D	New fracture initiation	Demo obtained for evaluation
4	3DEC	Itasca	3D	New fracture initiation	Demo obtained for evaluation
5	Fracman	Golder	3D	New fracture initiation	Reference technical literature
6	Elfen	Rockfield	3D		Reference technical literature/telephone consultation
7	Irazu	Geomechanica	2D	New with limited application experience	Demo obtained for evaluation
8	Frac3D	Itasca	3D	Continuum modelling only	Reference technical literature
9	YADE	Open Source	2D	Limited pre & post processing	Reference technical literature
10	Y-GEO	Univ Toronto	2D	New with limited application experience	Reference technical literature

Table 3.2: Summary details of DFN modelling systems reviewed for application to this study. Details correct at December 2015.

A review of ten alternative modelling systems was undertaken to identify modelling systems that meet project requirements. Where possible, a demonstration version of the model was obtained or the model originator was consulted directly. Additional information was derived from commercial literature, internet references and technical papers. The models reviewed are listed in Table 3.2. Seven models were reviewed in detail through trial analysis with demonstration versions or case study review. Of the seven models reviewed in detail, three appeared to have the capability to best meet project modelling requirements. All three are FDEM based models as follows.

ELFEN (Rockfield International)

Irazu (Geomechanics Inc)

Y-Geo (Opensource code/University of Toronto)

Elfen is a FDEM model designed to allow simulation from a continuum state to a fully discontinuous state through the inclusion of fracture networks and the progressive development of new fracture systems. New fractures are automatically linked to the initial DFN allowing full DFN evolution. The model is fully 3D and incorporates capability for groundwater seepage analysis. Elfen has primarily been used in the oil & gas sector to investigate fracture system response to changes in hydraulic pressure at greater depth than the excavations included in this study.

Elfen includes capacity for development of a basic DFN within the model environment. For more complex DFN development, Elfen can accept input DFN data from external models such as Fracman (Golder Associates). The model includes capacity for layered and phased simulation and has fluid flow capacity to allow simulation of groundwater seepage through DFN systems.

At the time of project commencement, Irazu was a relatively new 2D geomechanical model developed and marketed by Geomechanica Inc. in Canada. A demonstration version of the model was obtained for evaluation. The model uses a finite-discrete element method to define and solve geomechanical problems. The software has particular capability to investigate damage around excavations, surface and sub-surface, through evolution of fracture systems following stress change due to extraction. Direct communication with Geomechanica allowed confirmation that the Irazu system incorporates capability to simulate phased development and open-pit excavation damage zones in response to stress change following mineral extraction. The model has full DFN capability although it did not appear to have a mechanism for automated DFN development.

Irazu has capability for coupled fluid flow – rock stress analysis and supports analysis of groundwater seepage and pore pressure analysis. The primary issue regarding the Irazu software was its limited application history due to its

very recent development. At the time of project commencement, software manuals had not been finalised and Geomechanica confirmed that some aspects of the model were still under development i.e. new fracture propagation. The model has capability for existing fracture change simulation in response to hydraulic pressure change, i.e. to simulate hydraulic fracturing processes, but it is unclear how effective the model would be without a positive driver such as increasing hydraulic pressure, under the stress relaxation conditions experienced during mineral extraction. On balance, it was considered that the lack of significant application history and unknown potential to interface with other geomechanical/hydrogeological models, would make use of the Irazu model more uncertain with regard to achievement of research objectives when compared to other geomechanical models.

Y-Geo is a FDEM based model developed at the University of Toronto for application to a range of geomechanical problems. The Y-Geo code is comparable to the Irazu code that was developed on the same basis. As with other FDEM based models Y-Geo allows simulation of new fracture development and propagation to capture progressive damage and failure processes. Limited information was available regarding Y-Geo and it was unclear whether the model includes any fluid flow capacity. Y-Geo is focussed primarily on improved representation of micro-mechanical behaviour as part of the failure process in brittle rocks. No evidence was found to confirm that it would provide all the capabilities required for modelling in this project.

Following further review it was concluded that residual uncertainty regarding the full capability of Irazu and Y-Geo combined with limited application experience would introduce additional unnecessary research risk. As the geomechanical modelling component of this research is a means of defining parameters/constraints for subsequent hydrogeological modelling and not the focus of primary research, a more developed and commercially proven modelling system was preferred. Rockfield International's Elfen modelling system was therefore selected for application throughout this project.

Elfen is described by Rockfield International as a '*comprehensive finite element and discrete element software tool*' containing a '*wide range of features for solving multi-physics, multi-scale, highly non-linear problems for*

both continuum and discontinuum domains.' Features of Elfen that are particularly relevant to this research include a capacity for discrete multi-body interaction, potential for use of non-linear compliance and the wide-ranging capacity for results abstraction and processing.

Rockfield International provided a license to run Elfen version 4.7.1 (27) at project commencement. Technical support for Elfen was provided in the form of a detailed training manual and additional guidance papers. During the early stages of model development further direct technical guidance was provided during a visit to Rockfield International offices in Swansea.

Elfen can be operated in both implicit and explicit modes with regard to solution of the dynamic equilibrium equation (Equation 3.1). Implicit techniques enforce global equilibrium at the end of each model timestep. Explicit techniques are based on progressive convergence towards an equilibrium solution through use of a forward time integration scheme (Rockfield-International, 2019). However, for models that incorporate discontinuities the explicit form is required. The explicit approach offers improved performance for transient problems as the solution is iteratively advanced in time without a pre-specified equilibrium condition. All Elfen modelling undertaken as part of this study has been undertaken with a dynamic rather than steady state approach. This has allowed investigation of transient conditions throughout the modelling programme. Care has been taken to set model durations at a timescale that allows achievement of equilibrium conditions at each stage.

Dynamic explicit modelling in Elfen is based on iterative solution of the general approach for determining the response of a body to loading as follows,

$$Ma + ku = f^{ext} \qquad\qquad [3.1]$$

where,

M = mass, a = acceleration, k = stiffness, u = displacement and f^{ext} = external force.

For non-rigid bodies, as included throughout this study, the consequence of external loading can be both displacement and deformation. Transient dynamic modelling is progressed using a central differencing approach which is applied in the following order:

1. Evaluate force at time t

2. Evaluate acceleration at time t

3. Evaluate velocity at time t + Δt/2

4. Evaluate displacement at t + Δt

5. Evaluate coordinates at t + Δt

An understanding of the sequencing of the central differencing process becomes important when interpreting discontinuity deformation effects. The model focusses on evaluating nodal displacement in response to an applied force, as regulated by material stiffness. When using non-linear compliance for contact surface interaction, the process allows for contact surface stiffness to be re-evaluated on an iterative basis following calculation of displacement with reference to stiffness -v- displacement (penetration) relationships.

3.2.2 Model scales and dimensions

Development of an appropriate approach to DFN modelling required early consideration of the distance scale of potential excavation effects. All models are based on a 'half-space' representation of an open pit profile, excavated in three phases. The decision to restrict excavation depth to 100 m, and application of an average excavation face slope of 70º to the horizontal, defines both the dimensions of the simulated excavation and provides the basis for determination of the dimensions of the model domain. As discussed at Section 3.3.3, the model domain was established with dimensions of 1000 m horizontally x 600 m vertically.

Within the main area of interest, around the simulated excavation, bedding planes have a 10 m - 20 m separation and joints have a 10 m separation. Whilst bedding planes extend across the entire model domain, joint length

varies from approximately 20 m to several tens of metres. In the orthogonally jointed model (Model 4), joints extend across the full model domain. It is apparent therefore that within a model domain of 600 000 m^2 there is a need to investigate discontinuity response at a scale of a few tens of metres. Model domain and discontinuity configuration scales are indicated in Figure 3.2.
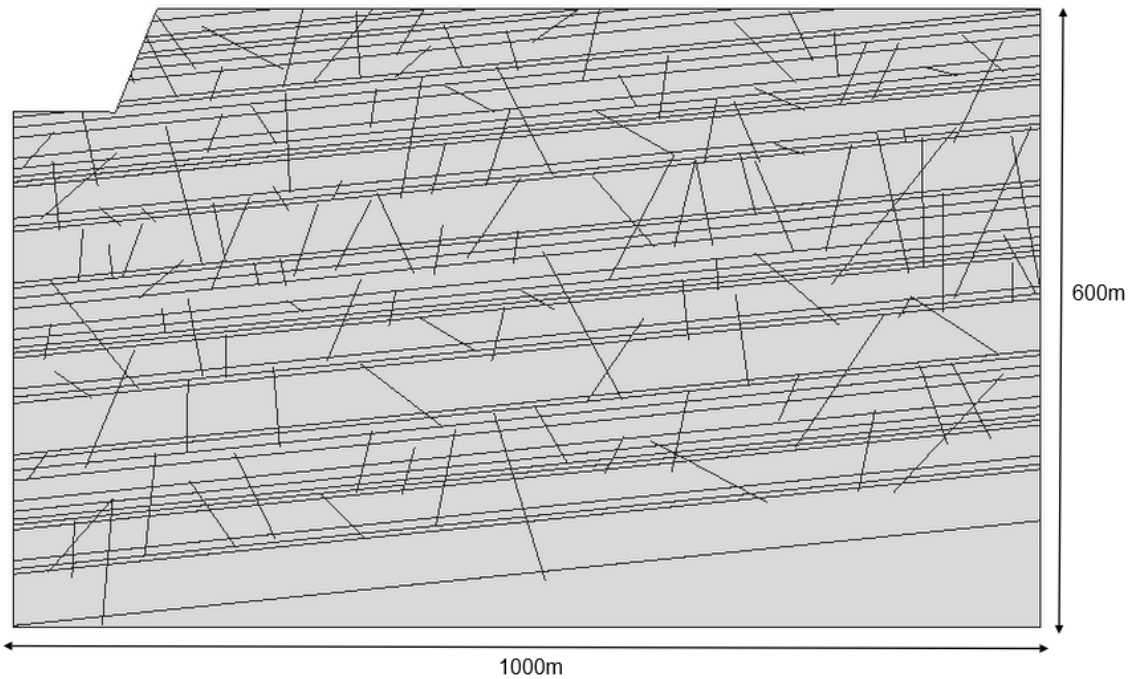
Figure 3.2: Example model domain showing the domain size (1000 m x 600 m) and representation of the excavation area (100 m deep excavation shown). Model shown is Model 3 – Variably jointed model.

Model results demonstrate that discontinuity aperture dilation or closure occurs over distances ranging from a few microns to a few millimetres. Adequate model resolution is required to be able to evaluate small-scale aperture response in response to large scale simulated excavation. The 'particulate' nature of model development in Elfen provides a basis for response evaluation at a range of scales. However, a degree of balance is required when setting finite element mesh dimensions. In all models developed for this study the finite element mesh size has been set at a nominal 5 m. This results in a minimum of 24,000 elements. To allow for potential new fracture development or fracture propagation, the minimum element size is defined at 1 m. Experience has demonstrated that these mesh dimensions

provide adequate resolution at joint aperture scale without overly onerous processing time.

3.2.3 Model outputs and options

Whilst the primary objective of geomechanical modelling is to investigate potential change to discontinuity aperture dimensions and discontinuity network connectivity, it has also been important to establish that the models are responding appropriately to lithostatic unloading by evaluation of bulk rock displacements and stress/strain response. Multiple parameter outputs from the model have therefore been required. Model results have been derived in the following forms

o Contoured graphics;
o Vector plots;
o Tabular data; and
o Time series graphs.

Elfen allows access to a large number of output variables that are specified during the model parameterisation stage. The multi-plotting 'results visualisation application' in Elfen allows parameter variation graphics to be plotted with vector plots and for comparative analysis of multiple data sets to be undertaken directly. Elfen output data files can be formatted for input to a range of external processing systems. Direct transfer of model results to MS Excel has allowed efficient analysis of output variables.

3.3   Process definition

Lithostatic unloading due to open pit mineral extraction is numerically simulated by progressive removal of a representative area (volume in three dimensions) from the model domain to create a free surface (excavation face) that increases in length with increasing depth of excavation. Changed stress conditions within the model domain result in changes to the stress conditions of rock blocks and discontinuities within the domain. Elfen has capacity for simulation of multiple geomechanical processes in response to changes in stress distribution. Analysis of critical geomechanical processes and their

representation within the model has therefore been undertaken to ensure that all processes are adequately accounted for in each model.

3.3.1 In-situ stress conditions and lithostatic unloading

Previous research (Stacey, 2003) demonstrated that the geomechanical response to unloading at excavation faces is influenced by the pre-excavation in-situ stress regime. It has therefore been assumed that consideration of a range of pre-existing stress conditions would be important in relation to analysis of discontinuity response to unloading. The geomechanical models developed through this project have incorporated gravity loading as part of a 'pre-excavation' geostatic initialisation process. The process leads to development of stresses within the rock mass in relation to increased loading with increasing depth of overburden as defined by the standard ρgh definition of gravity loading in which ρ is the average rock density, g is the gravitational acceleration and h is the depth below ground surface.

Development of pre-existing lateral stresses, with increasing depth, occur as a consequence of lateral confinement within the rock mass. Jaeger et al. (2007), report that, assuming uniform and isotropic rock properties, the natural lateral stress magnitude can be related to the vertical stress by reference to Poisson's ratio as follows:

k = v/(1-v), where,   [3.2]

k = lateral in-situ stress ratio (i.e. ratio $\sigma_{horizontal}/\sigma_{vertical}$)

v = Poisson's ratio

The Poisson's ratio values used in models within this project range from 0.200 to 0.211 resulting in a gravity loading induced k of 0.25 to 0.27. These values represent the natural lateral stress ratio as a multiplier of vertical gravitational loading in tectonically benign environments. Higher lateral stress ratios may develop in areas that have a more active tectonic history. Hoek and Brown (1978) produced a compilation of measured or inferred sub-surface stresses

from locations worldwide. The results indicate that, at depths below 300 m, k is found to be within the range 1.0 – 4.0, whilst at a depth of 600 m k varies between 0.5 – 2.8. Below a depth of approximately 2000 m, k is generally less than 1.0.

As detailed in subsequent sections of this report, all models have been developed with a domain depth of 600 m. On the basis of the above analysis, it was concluded that the modelling program should incorporate in-situ stress conditions within the range k=0.27 – k=2.0 as representative of the range of conditions that may be appropriate for simulation of open pit excavations in a 600m deep model domain.

Vertical and lateral gravitational loads are the only loads applied throughout the modelling program. Changes to the local stress regime occur in response to lithostatic unloading as a consequence of open pit development and the removal of rock mass. Removal of rock, by mineral excavation, results in a reduction in the vertical loading at the excavation floor and face. The local stress regime is influenced by the following:

1. Reduction in load at the excavation floor and face, and

2. Removal of lateral constraint at the excavation face.

As discussed at Chapter 2, physical deformation of both the excavation floor and face in response to lithostatic unloading is a widely recognized and reported process. A number of theoretical studies have demonstrated that the effects of unloading are likely to extend beyond the excavation floor and face, into the host rock and the concept of excavation damaged zones (EDZ) and excavation disturbed zone (EdZ) are well established.

The vertical and lateral extent of geomechanical response to mineral extraction in open pit environments is not well established and there have been only a limited number of empirical studies aimed at estimating the extent of the EdZ in particular (Marchmont et al, 2010, Beale et al, 2014). The role of pre-existing discontinuities in defining the stress response and consequent rock

mass deformation in the host rock around open pit excavations remains an unresolved issue. The current investigation aims to improve definition of the extent of EdZ development beneath and around open pit excavations and the impact of stress response on discontinuity configuration. Previous studies (Stacey 2003) have indicated that in low in-situ stress environments the majority of host rock deformation is likely to be observed in the excavation floor. Conversely, in high lateral stress environments the most significant effects may be observed in the excavation face.

The excavation process would normally occur over a period of several years, or tens of years, resulting in slow adjustment of excavation surfaces to stress change. The excavation process has been modelled throughout as a transient process to avoid the generation of unrealistically high stresses that would occur in response to instantaneous unloading.

3.3.2 Deformation processes

Deformation processes in rock with pre-existing discontinuities may incorporate the following:

1. Rock mass strain
2. Rock block failure
3. Rock block displacement
4. Discontinuity deformation

Throughout the modelling process the rock mass has been modelled as an elastic medium, subject to strain in response to stress change. Variation in the stress regime around the modelled excavation is therefore expected to result in a degree of rock mass strain. In general, strains registered in the models are likely to represent a partial return to pre-loading conditions prior to the assignment of compressive stresses during gravitational loading.

With the depth of excavation limited to 100mbgl, the expected change in the stress regime around the modelled excavation is expected to be relatively modest in comparison to rock strength and stiffness. As detailed at Chapter 4,

modelling indicates that the magnitude of stress reduction at a 100 m deep excavation floor is around 2 MPa. The Young's Modulus applied to the sandstone and limestone lithologies in the models is 32.7 GPa and 47.0 GPa respectively. Strains in the region of 5×10^{-5} might therefore be expected if the stress response where fully accounted for by variation in intact rock strain without the presence of discontinuities.

With maximum model compressive stress not exceeding around 10MPa, there is no expectation of intact rock failure. All models developed for this study incorporate two separate materials referred to as Blaxter Sandstone and Blaxter Limestone. The tensile strength assigned to the two materials is 6.5 MPa and 10.6 MPa respectively. As stated by Hencher (2016), most new rock fractures develop under tensile stress conditions. At most locations in each model, stresses remain compressive. In the few locations where tensile stresses develop, as discussed in Chapter 4, the stress magnitude does not exceed 0.147 MPa. Consequently, tensile development of new fractures was not expected.

The generic geomechanical models developed for this investigation incorporate discontinuity sets that separate the model domain into a series of intact rock blocks that are defined by discontinuity boundaries. The connectivity and contact properties of the discontinuity network define the degree of mobility within the rock mass with higher mobility associated with high levels of connectivity. Stress relaxation due to lithostatic unloading may therefore lead to displacement of mobile rock blocks by movement along discontinuity surfaces that are orientated parallel to the direction of maximum stress reduction 'sliding', or by dilation of discontinuity surfaces where discontinuities are orientated perpendicular or sub-perpendicular to the direction of maximum stress reduction.

In the orthogonally jointed model (Model 4) developed for this study, the model domain is separated into discrete rock blocks defined by a fully connected discontinuity network. This simple 'sugarcube' model allows a high level of rock block mobility in vertical and horizontal directions, subject to the contact properties of the discontinuity sets. In this configuration, a significant component of rock mass deformation, resulting from lithostatic unloading, may

occur due to sliding on advantageously orientated discontinuity surfaces, when discontinuity shear strength is exceeded. Given the magnitude of stress reduction at 100m excavation depth, the displacements are expected to be relatively small and highly dependent on discontinuity orientation.

The primary focus of this research is quantification of discontinuity dilation under a range of geomechanical configurations and conditions. In addition to a strain response, and potential rock mass displacement along planes of weakness represented by appropriately orientated discontinuities, it is anticipated that, subject to variation in contact conditions, rock mass deformation may also occur due to dilation of discontinuity surfaces and change in discontinuity aperture. In an unloading scenario, where there is reduction in compressive stress, the expectation is that any change in discontinuity aperture would occur as an increase in aperture magnitude through discontinuity dilation. Discontinuity response to a change in local stress is primarily dependent on the orientation of the discontinuity in relation to the direction of maximum and minimum compressive stress and the stiffness of the discontinuity surfaces. Where discontinuities are infilled, surface adhesion and increased tangential cohesion may also be relevant.

Discontinuity dilation may occur in response to changes in both normal and tangential stresses. Under unloading conditions, it is clear that reduction in normal stress may lead to opening of a discontinuity resulting in increase in aperture dimensions. As discussed further at Chapter 5, the potential for discontinuity dilation due to stress reduction is highly dependent on discontinuity orientation with respect to the principal stresses. Discontinuity dilation due to shear stress could occur in response to an increase in shear stress where contact surfaces move over each other and dilate due to the presence of asperities, or due to a reduction in normal stress leading to reduction in contact surface cohesion and/or stiffness. Elfen does not currently have facility to simulate shear dilation and therefore only normal dilation of discontinuities is included in this study.

The magnitude and extent of normal dilation of fractures, joints and bedding planes is determined by the magnitude of normal stress change and the stiffness of the discontinuity surfaces. For analytical and modelling purposes

it is assumed that, in the normal direction and to the point at which full closure is achieved, discontinuity surfaces deform on a fully elastic basis with increasing discontinuity closure or opening related to increase or reduction in normal stress. In cases where there is a well-connected discontinuity network and a high degree of rock block mobility, discontinuity dilation can be considered as the differential movement of rock blocks on either side of the discontinuity. More commonly, in cases where discontinuities are less well connected, and joints or fractures do not separate the rock mass into clearly defined blocks, discontinuity normal dilation is constrained at discontinuity ends resulting in differential dilation along the discontinuity length.

As discussed at Chapter 2, the normal response to stress change is governed by the normal stiffness, defined as normal displacement per unit stress change. Previous studies have demonstrated that discontinuity normal stiffness varies in relation to discontinuity length and stress state. Both parameters therefore need to be considered during analysis of discontinuity response to change in local stress conditions under lithostatic unloading. In the absence of site-specific discontinuity stiffness data, normal stiffness values applied in the current study have been derived from several previous studies, particularly work by Morris et al (2017), of normal stiffness variation for a range of discontinuity lengths and stress conditions. Geomechanical models developed for this research incorporate discontinuities at a range of scales and stiffness values. In general, discontinuity stiffness is expected to reduce with increasing discontinuity length and increase with increasing normal stress.

All discontinuities included in the current modelling studies are pre-existing and subject to loading during the geo-initialization phase of modelling. Whilst under such conditions, model discontinuities are assumed to be at maximum closure and therefore theoretically at maximum stiffness. The unloading response therefore results in stress relaxation and potential increase in discontinuity aperture with associated reduction in discontinuity stiffness. Full representation of this process therefore requires specification of the maximum stiffness at full closure and the stress/stiffness relationship associated with discontinuity dilation.

As discussed at Chapter 4, the maximum vertical stress change resulting from open pit excavation of 100 m depth is relatively low at around 2 MPa. Maximum stresses encountered in the model domains is up to 10 MPa, towards the domain base. Modelled discontinuity dilation arising from excavation is also likely to be relatively low, in the order of fractions of 1mm, which approximates to the magnitude of stress reduction divided by the normal stiffness, as expected. Although there is relatively low variation in model stress in response to unloading, and discontinuity dilation magnitude is relatively small, it is recognized that discontinuity stiffness is typically highly stress dependent and that the stress-stiffness relationship is highly non-linear (Jaeger et al 2007). All models have therefore been developed to incorporate non-linear stress – stiffness relationships.

In the absence of site-specific data and with a requirement to establish a relatively simple relationship between stress and discontinuity stiffness an approach to non-linear compliance was developed by reference to trial model results with fixed stiffness values and application of the work by Morris et al (2017) to define minimum and maximum stiffness values for respective discontinuity sets. As discussed at Section 3.3.4, Elfen allows use of non-linear compliance relationships that relate either stress or stiffness to discontinuity aperture, rather than stress -v- stiffness. Estimated maximum and minimum stiffness values were therefore related to maximum and minimum aperture values derived from trial model runs and assumed to be representative of minimum and maximum stress conditions. Stiffness values are calculated for the maximum and minimum model stresses of 2 MPa and 10 MPa for discontinuity lengths used in models developed during this study. Morris et al (2017) produced generic equations relating discontinuity length to stiffness for a range of stresses, as included as Equations 2.8 and 2.9.

As discussed further in section 3.3.3.4, application of the above equations to model discontinuity sets allowed determination of upper and lower boundary values for non-linear compliance curves for each discontinuity set used in the models. On this basis, discontinuity stiffness is varied in relation to aperture size, as a proxy for stress variation e.g., as a discontinuity dilates due to reduction in normal stress the discontinuity stiffness decreases.

Tangential discontinuity stiffness has been defined as the ratio of shear displacement to shear stress. In the absence of site-specific field data to quantify tangential stiffness, parameter values used in this study have been determined empirically on the basis of previous research. Discontinuity roughness is a key consideration in determination of discontinuity response to shear stress. As discussed by Jaeger et al (2004), joint or fracture surface roughness acts to resist shear displacement with the magnitude of resistance defined by the magnitude, frequency and distribution of asperities. In this context, surface roughness acts to provide a cohesion that resists shear displacement. In all the geomechanical models developed during this study, there is no explicit definition of discontinuity roughness. However, the effects of joint roughness are incorporated via the discontinuity cohesion term applied to each discontinuity set.

Rock mass response to stress is defined by the material properties applied to each model. Within the range of stresses experienced through the modelling programme, rock mass deformation and nodal displacements generally occur in response to elastic deformation or unloading as a strain response or sliding at continuous discontinuity surfaces. The model incorporates a standard Mohr-Coulomb failure model to define conditions under which intact rock failure would occur but it is recognised that with the specified material properties and maximum model stresses, failure is unlikely to occur under any model scenario.

Fracture propagation or new fracture generation simulation is based on application of a Rankine Rotating Crack failure model. Evidence from analysis of model results indicates that the energy generated within each model is generally insufficient to support either new fracture generation or pre-existing fracture propagation. Discontinuity cohesion values are set at relatively low values but joint penetration prevents loss of cohesion resulting in contact sliding due to elastic deformation in advance of the shear stress accumulation required to progress new fracture propagation.

3.3.3 Process representation in Elfen

The processes defined in Section 3.3.2 had to be incorporated into Elfen to ensure appropriate representation of geomechanical conditions in each of the models used in this study. The following general approach to process representation is set out below in relation to Elfen model input data.

3.3.3.1 Model geometry

Within a model domain of 1000 m x 600 m, a three-stage excavation area is included at the upper left corner of all models. The maximum depth of excavation is 100 m and the basal excavation width is 100 m, representing half the width of an excavation floor. The excavation volume is split into three stages with depths of 30 m, 60 m and 100 m. Stages of excavation are defined as discrete objects within Elfen to allow progressive removal from the model on a stage-by-stage basis. General arrangement of the excavation volume is shown in Figure 3.3.
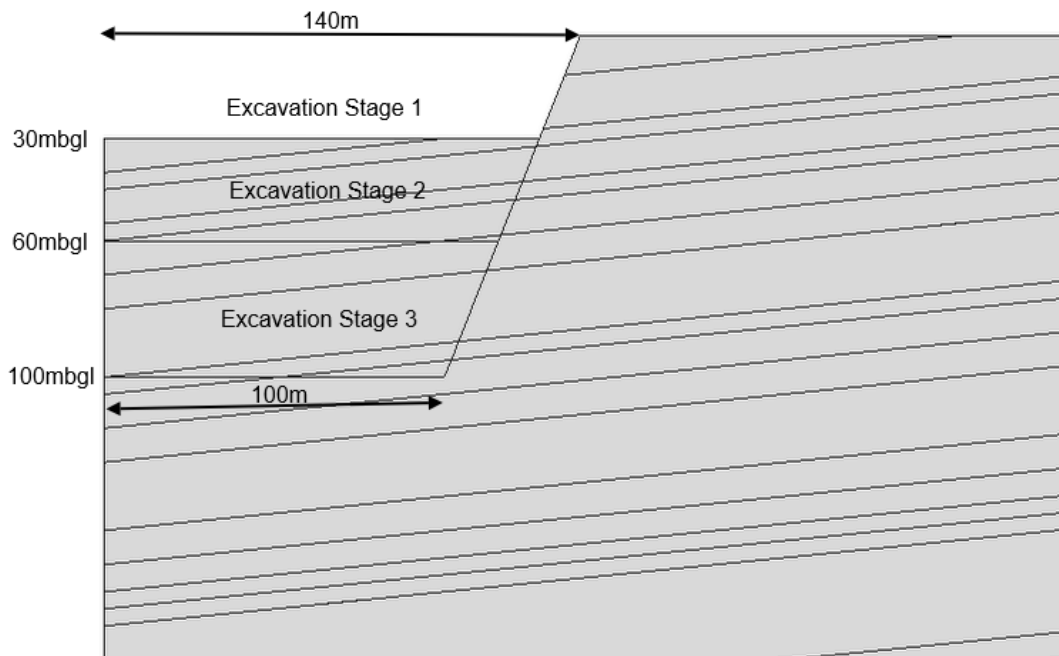
Figure 3.3: Configuration of excavation areas represented in all 2D models. Showing excavation depths of 30 m, 60 m and 100 m.

Bedding planes are included in the model as discontinuities and to provide the basis for specification of lithological variation. Where lithological variation is specified, the model surface is separated into a series of discrete surfaces to allow allocation of alternate material properties to each unit. All discontinuities, including bedding planes and joint sets are defined as 'joints' with specified joint properties. Full details are provided in Section 3.4 in relation to each model.

All 2D models included in this study are 'half space' models based on the assumption of symmetry either side of the excavation centerline. This approach is consistent with previous research (Stacey, 1973) that demonstrated *'That opposite slopes of an open pit do not interact when the floor width of the pit exceeds about 0.8 times the slope height.'*

3.3.3.2 Model loading

There is no external loading applied to any of the models developed through this study. The only model loading is the gravitational initialisation process discussed under initial conditions.

3.3.3.3 Initial conditions

All models are subject to initial gravitational loading 'initialization' which is applied throughout the model domain. Gravitational initialization leads to the development of internal model stresses and consequent deformation of both the rock mass and pre-existing discontinuities. Gravitational loading remains active throughout each modelling stage, for all three stages of excavation. Gravitational loading is applied through input parameters for gravitational acceleration, gravitational direction and magnitude. Lateral in-situ stress conditions are assigned as a multiplier of gravitational loading with lateral stress ratios of k=0.27 and k=2.0.

In homogeneous lithologies with no discontinuities, gravitational initialization is not expected to result in rock mass deformation or displacement. Deformation does, however, occur when, (i) there are differences in lithological

density i.e., sandstone/limestone beds, resulting in stress variation at lithological boundaries, and (ii) to account for discontinuity penetration/dilation where discontinuities are present.

Following advice from Rockfield, gravitational loading is applied as a 'drop load' throughout the modelling process. Drop loading is effectively instantaneous loading that is '*suitable for simple geometries where equilibrium stress fields can be easily established*.' Drop loading of the initial gravitational load is accompanied by contact relaxation by 'ramp load' to prevent the generation of large contact forces during gravitational initialization.

3.3.3.4 Model constraints

The constraints menu in Elfen is used to define structural constraints and discontinuity contact properties. The following constraints are applied.

- o Structural boundary constraints
- o Contact pairings and contact properties
- o Point and global damping

In all models, as shown in Figure 3.4, the model lower left and right boundaries are constrained to prevent displacement perpendicular to each boundary. All three boundaries are therefore defined as 'no displacement' boundaries. No other structural constraints are applied to the model.

Discontinuity contact properties are assigned individually to each discontinuity set. Contact properties define the way in which discontinuity surfaces interact with each other and with other objects. The following properties are specified.

- o Normal penalty (normal stiffness) (Pa)
- o Tangential penalty (tangential stiffness) (Pa)
- o Adhesion (Pa)
- o Cohesion (Pa)
- o Friction angle
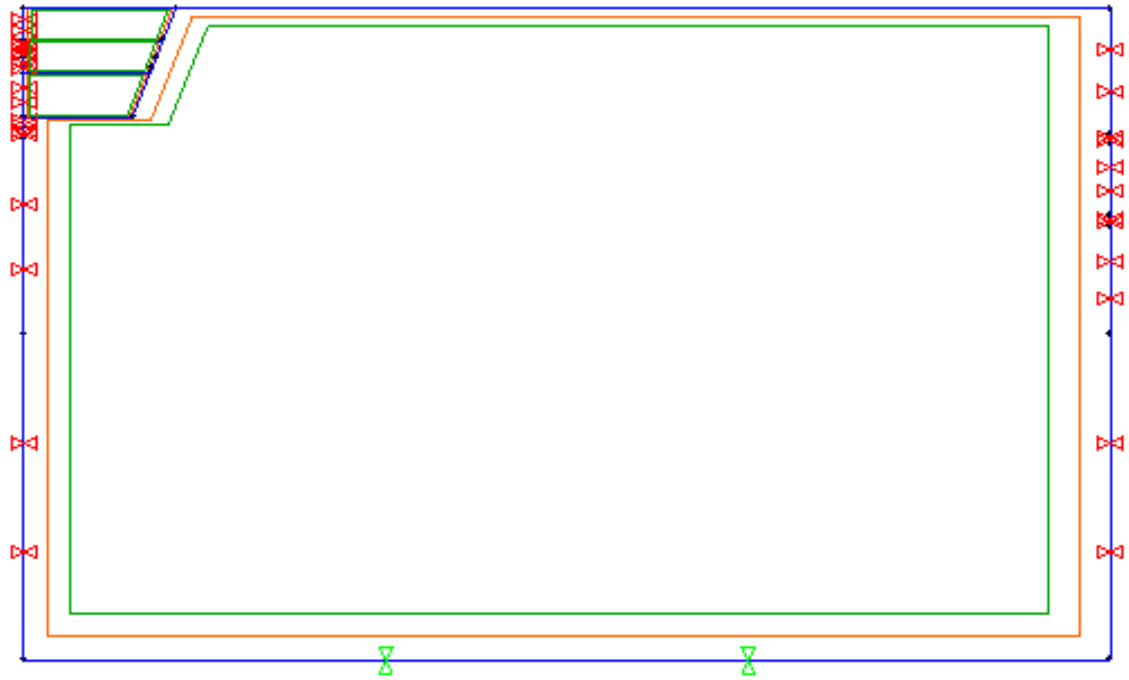
Figure 3.4: Model domain showing 'no-displacement' boundary conditions. Red markers represent horizontal displacement constraint. Green markers represent vertical displacement constraint.

Parameter values applied to each model are summarized in Table 3.3.

Parameter	Value	Units	Source
HOST ROCK PROPERTIES			
SANDSTONE			
Youngs modulus	32.7	GPa	(Bell, 1978)
Poisson ratio	0.211	-	(Bell, 1978)
Shear modulus	13.36	GPa	(Jaeger et al, 2007)
Density	2360	kg/m^3	(Hawkins, 1991)
Cohesion	27.2	MPa	(Goodman, 1989) p83
Friction angle	27.8	Degree	(Goodman, 1989) p83
Dilation angle	5	Degree	(Alejano, 2005)
Tensile strength	6.5	MPa	(Bell, 1978)
Fracture energy	27.29	J/m^2	(Whittaker, 1992, Zhang, 2014)
LIMESTONE			
Youngs modulus	49	GPa	(Bandis et al., 1983)

Poisson ratio	0.20	-	(Goodman, 1989) p186
Shear modulus	15	GPa	(Jaeger et al, 2007) p190
Density	2660	kg/m^3	(Hawkins, 1991)
Cohesion	6.7	MPa	(Goodman, 1989) p83
Friction angle	42	Degree	(Goodman, 1989) p83
Dilation angle	5	Degree	(Alejano, 2005)
Tensile strength	10.6	MPa	(Bandis et al., 1983)
Fracture energy	48.44	J/m^2	Whittaker, 1992, Zhang, 2014)
DISCONTINUITY PROPERTIES			
Joint normal stiffness	3.45	GPa/m	(Morris, 2017)
Joint tangential stiffness	0.345	GPa/m	(Rockfield-International, 2017)
Joint Adhesion	37	kPa	(Goodman, 1989) p374
Joint friction ratio (tan ϕ)	0.55	-	(Goodman, 1989) p164
Joint cohesion	2.0	MPa	(Goodman, 1989) p166
Bedding normal stiffness	0.50	GPa	(Morris, 2017)
Bedding tangential stiffness	0.10	GPa	(Rockfield International, 2017)
Adhesion	37	kPa	(Goodman, 1989) p374
Bedding friction ratio (tan ϕ)	0.55	-	(Goodman, 1989) p164
Bedding cohesion	2.0	MPa	(Goodman, 1989) p166
Basal Bedding normal stiffness	0.50	GPa	(Morris, 2017)
Basal Bedding tangential stiffness	0.10	GPa	(Rockfield International, 2017)
Basal Adhesion	37	kPa	(Goodman, 1989) p374
Basal Bedding friction ratio (tan ϕ)	0.55	-	(Goodman, 1989) p164
Basal Bedding cohesion	10.0	MPa	(Goodman, 1989) p166 amended

Table 3.3: Parameter values assigned to rock mass materials and discontinuities used in all models.

In geomechanical models in Elfen, penalty values are analogous to contact surface stiffness and defined in units of stress/distance. The adhesion value is used to define the tensile strength of the contact surface pairing. In practice this can be representative of any form of discontinuity cementation or similar effects of infill materials. Low values of adhesion have been assigned throughout the modelling programme. Contact surface cohesion defines the frictional resistance to shear deformation and sets the threshold above which, subject to the degree of freedom, differential contact surface sliding could occur at zero normal stress. Once surfaces separate all cohesion and adhesion is assumed to be lost.

Contact property input data also specifies the way in which the model applies contact data. The specified data sets are as follows:

o   Search zone (m)
o   Contact field (m)
o   Smallest element (m)
o   Contact type
o   Contact damping type
o   Contact damping

The contact search zone defines the distance from each node that is used to search for potential contacts and the contact field defines the maximum dimensions of the search area for establishing nodal contacts. The smallest element relates to the development of new fractures and defines the minimum dimensions of new finite elements that could be generated by splitting of pre-fracture model elements. The contact type and contact damping assignments specify the way in which contact surfaces interact. A default 'node-edge' contact type is applied throughout all the models. Contact damping is defined as velocity/momentum damping, specified as a dimensionless coefficient acting to modify the contact normal penalty relative to the velocity of impacting bodies, to prevent high frequency velocity oscillation in contact interaction.

Discontinuity dilation is not explicitly defined or calculated in Elfen and therefore has to be calculated from other parameters. Discontinuity surfaces are represented by elements on opposing faces and therefore differential

movement of model nodes on opposing faces defines the magnitude of respective movement towards each other (closure) or away from each other (dilation). Nodal movement is defined as a displacement with respect to the post-gravity initialization location of each model node. However, nodal displacement can occur due to one or more of several processes and not just closure or dilation. The dominant influences on discontinuity surface displacement are as follows:

(i) Rock block normal or shear strain
(ii) Contact sliding
(iii) Dilation/closure

Discontinuity surface dilation can be calculated by deduction of directional strain and perpendicular contact slide distance from the total displacement value. For multiple joint orientations this process is complicated by the requirement to adjust non-dilation displacement for joint orientation.

In Elfen, discontinuities are assumed to be fully closed prior to gravitational initialization. The application of gravitational loading results in definable normal penetration of discontinuity surfaces based on the following relationship.

$$\text{Stress}_n = \text{stiffness}_n \times \text{penetration}_n \qquad\qquad [3.3]$$

where,

Stress_n = normal stress at the discontinuity surface (Pa)

Stiffness_n = normal discontinuity stiffness (Pa/m)

Penetration_n = distance between respective joint surfaces (m)

With stiffness (penalty) values defined in the model input data, penetration values are directly related to applied stress at the joint surface. An increase in penetration, which is defined as a negative aperture, due to increased loading or a decrease in penetration due to load relaxation is comparable to joint normal closure or dilation in response to stress change. When penetration of joint surfaces occurs, the change in penetration due to stress change can be

used as a proxy to define joint closure or dilation. It is therefore assumed that reduction in penetration equates to the generation of positive aperture. In reality, it can be considered that penetration is analogous to elastic deformation of asperities, with aperture increasing as stress is reduced and joint surfaces dilate. Once joint surfaces lose contact the model returns zero penetration. The penetration parameter can therefore be used to define joint normal dilation, independent of any other cause of displacement.

The non-linearity of stress-stiffness relationships has been incorporated in the models by use of the non-linear compliance function in Elfen. Non-linear compliance allows assignment of a function to define the relationship between stiffness and penetration. Initial model runs with fixed stiffness values were undertaken to investigate minimum and maximum penetration values that were used as bounding values for development of a non-linear compliance curve.
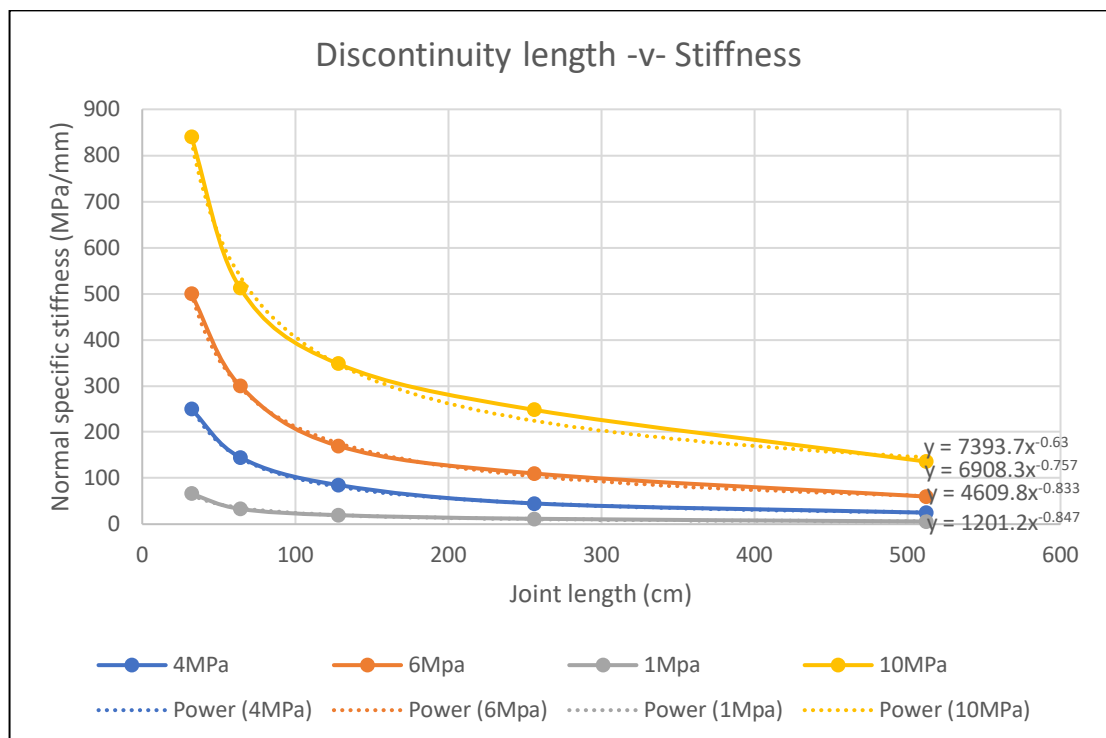
Figure 3.5: Discontinuity length -v- stiffness curves for normal stress of 1 MPa, 4 MPa, 6 MPa and 10 MPa. Data derived from data originally presented in Morris et al (2017). Power law fittings are applied to all four curves as indicated. Length units of the original analysis undertaken by Morris et al, are retained for consistency.

It was first necessary to relate discontinuity normal stiffness to normal stress, taking account of average discontinuity length. Reference was made to the work by Morris et al (2017) and the derivation of Equations 2.9 and 2.10 which are used to estimate discontinuity stiffness in relation to length, for stresses of 1 MPa and 10 MPa. Further analysis of the original data presented graphically by Morris et al was undertaken to establish further equations for different stress magnitudes. The results of this analysis have been applied in this study to prepare Figure 3.5 which shows the relationship between discontinuity stiffness and joint length for four stress magnitudes. The analysis demonstrates how, for a given length, discontinuity normal stiffness is higher under higher normal stress.

The non-linear compliance function in Elfen requires specification of a relationship between normal stiffness and penetration. Representative penetration values were calculated by application of Equation 3.3. The resultant stiffness -v- penetration curve for bedding planes used in all discontinuity models is presented as Figure 3.6. The curve demonstrates that as penetration distance reduces in response to decrease in normal stress, the bedding plane stiffness also reduces. Non-linear compliance parameters have been assigned to all discontinuity sets in all models.
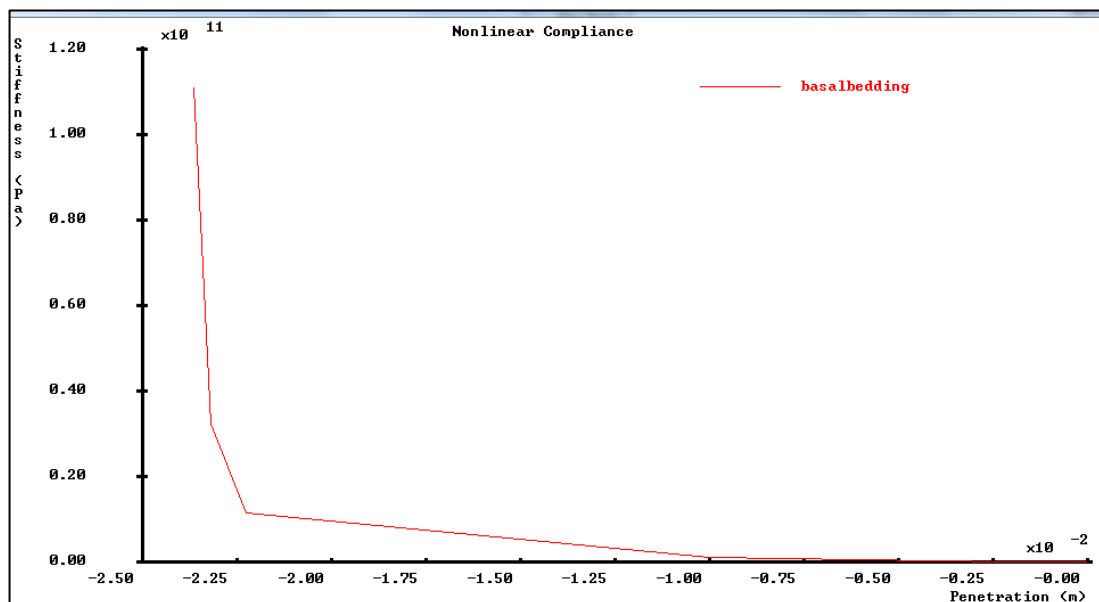
Figure 3.6: Non-linear compliance curve for bedding planes indicating decreasing bedding plane stiffness with decreasing penetration (positive aperture).

The models respond to variation in contact surface penetration by corresponding variation in contact stiffness which then affects subsequent calculation of contact force on an iterative basis. As discussed at Chapter 4, the relatively small variation in contact surface penetration throughout all stages of simulation results in relatively modest variation in discontinuity stiffness.

All model components were subject to point damping to reduce oscillation in stress wave velocity and support model convergence. Damping has been applied to all model surfaces at a rate of 0.05 or 5%.

3.3.3.5 Material models

Material properties for each lithology are specified in the materials database used by the model. Only two lithologies (sandstone and limestone) have been used throughout the modelling programme. Material properties for each are as summarised in Table 3.3. Material properties are defined for the bulk rock mass. Allowance is included for specification of linear properties and non-linear properties associated with a range of deformation/failure models.

3.3.3.6 Model mesh design

The design of the finite element mesh is largely constrained by the model configuration. Unstructured meshing is a requirement for models involving discrete contact. For projects that may include fracture propagation the mesh must be defined with triangular elements. All models use an advancing front approach to mesh generation.

The primary options for unstructured mesh design with discrete contact models is the mesh size and the mesh density. A balance has to be achieved between model resolution and processing time when setting mesh size. With a minimum model discontinuity spacing of 10 m, a mesh size of 5 m has been specified throughout. Trials with smaller mesh sizes resulted in excessive model processing time with no improvement in results resolution.

All models have been developed with a constant mesh size. Experimentation with higher mesh density regions around the extraction areas resulted in excessively high processing demand and no significant variation in the quality of model outputs in the areas of interest.

3.3.3.7 Modelling controls

Model specific controls are used to define the way in which the models are implemented at all stages. The most significant parameters are those related to:

- o Definition of model components and stages
- o Definition of model duration
- o Definition of time step limits and model termination criteria
- o Definition of require output data sets including time series data

The model control settings provide the basis for progressive removal of excavations and the reinitialization of model displacements following gravitational initialization.

3.4 Investigation design

3.4.1 Model development and sequencing

The geomechanical modelling programme was designed to deliver data required for subsequent hydraulic and hydrogeological analysis. In addition to quantification of pre-existing discontinuity deformation magnitude and lateral extent, it was necessary to investigate response sensitivity to discontinuity orientation, discontinuity mechanical properties, discontinuity connectivity and lithological variation. A series of four separate 2D geomechanical models were developed in Elfen for this purpose. Models were designed to provide generic representation of discontinuity configurations that could be considered representative of configurations encountered in relatively shallow mineral excavation in hard rock environments.

Prior to the development of 2D models, a 3D model of the entire excavation, in two alternative configurations, was developed to investigate geometrical constraints on EdZ development for non-circular excavations. In a circular excavation it is reasonable to expect that the EdZ would develop around the perimeter of the excavation as a concentric zone equidistant from the floor and face around the full perimeter. Most open pit excavations are not circular. Most excavations consist of straight linear excavation faces arranged in quadrilateral or orthogonal configurations. Excavation faces are bounded at each end by perpendicular faces that constrain the lateral and vertical response to stress relaxation in both face and floor.

The 3D modelling programme was undertaken specifically to investigate EdZ geometrical constraints around non-circular open pits. The models do not incorporate discontinuities and were not used to investigate discontinuity response to unloading due to the extensive time and resources required for large scale 3D modelling of discontinuity systems.

The modelling programme was designed to first investigate the geomechanical response to unloading without discontinuities and then to progress to increasing discontinuity intensity. All discontinuity models contain lithological bedding and therefore are generally representative of a range of sedimentary systems. The four baseline geomechanical models are listed below and shown in Table 3.4. A conceptual basis for the development of each model is included at Appendix C.

- o Model 1 - No discontinuity validation model
- o Model 2 - Bedding only model
- o Model 3 - Variably jointed model with bedding
- o Model 4 - Orthogonally jointed model with bedding

The 2D modelling programme was preceded by the no-discontinuity 3D modelling to investigate EdZ constraints. The four 2D models were run under two alternative lateral confining stress ratios (k=0.27 and k=2.0).
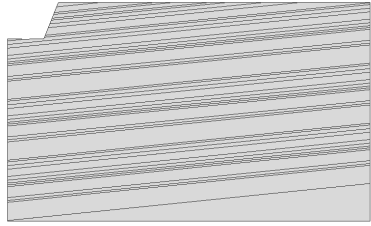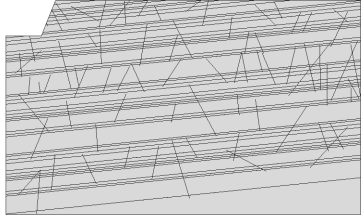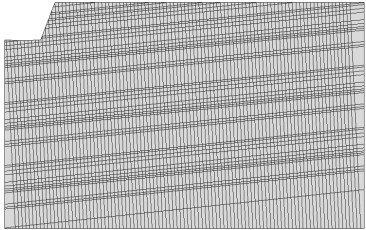
Model No.	Base configuration	Comments	Configuration
1	No discontinuities	Validation model to test key processes and compare to 3D model results	
2	Bedding only	Laterally continuous bedding planes only	
3	Variable jointing	Laterally persistent bedding planes and variably persistent and orientated joints	
4	Orthogonal jointing	Laterally persistent bedding planes and orthogonal joints resulting in high rock mass connectivity	

Table 3.4: Summary of the four model configurations used in the 2D geomechanical programme.

3.4.2 Model design and configuration

All models have been developed as 2D 'half space' models consisting of a planar cross section through a half width excavation void. Excavations have been represented as an excavated void 100 m deep with a half floor width of 100 m at the base. The excavated face is established at an angle of 70° to the horizontal. The excavated void is separated into three phases of excavation with basal depths of 30 mbgl, 60 mbgl and 100 mbgl.

In all models, it has been necessary to design the model domain with boundary conditions that have minimum potential to influence model results in the areas of interest. In Elfen, as in most geomechanical modelling systems, there are three types of boundary condition available as follows:

(i)   Stress boundary condition: a defined stress is applied at the boundary;

(ii)   Displacement boundary condition: displacement at the boundary is defined as a known value which can be zero i.e. constraint; and

(iii)   Mixed boundary condition: where both boundary stress is specified in some directions and displacement is specified in other directions.

With the exception of the excavation face and floor, all model boundaries in all models developed during this study are defined as displacement boundaries where displacement is fully constrained in either the vertical or horizontal direction. The excavation face and floor act as free surfaces with no external constraints.

Design of a suitable model domain for the issues under investigation has been based on the aim of establishing zero displacement boundaries at an adequate distance from the excavation areas. With large domains, a balance has to be achieved between data resolution and the computational resource required to run the model. Geomechanical unloading analysis is primarily concerned with the redistribution of stresses within the model domain. Consideration of model domain extents has therefore been referenced to consideration of the potential stress change at increasing distance from the excavation. Analysis of potential

stress change beneath an excavation floor as a consequence of unloading has been undertaken using the approach developed by Boussinesq applying Equation 2.7 (σ_z = q/π(α + sin α cos (α + 2β) in the configuration shown in Figure 3.7.
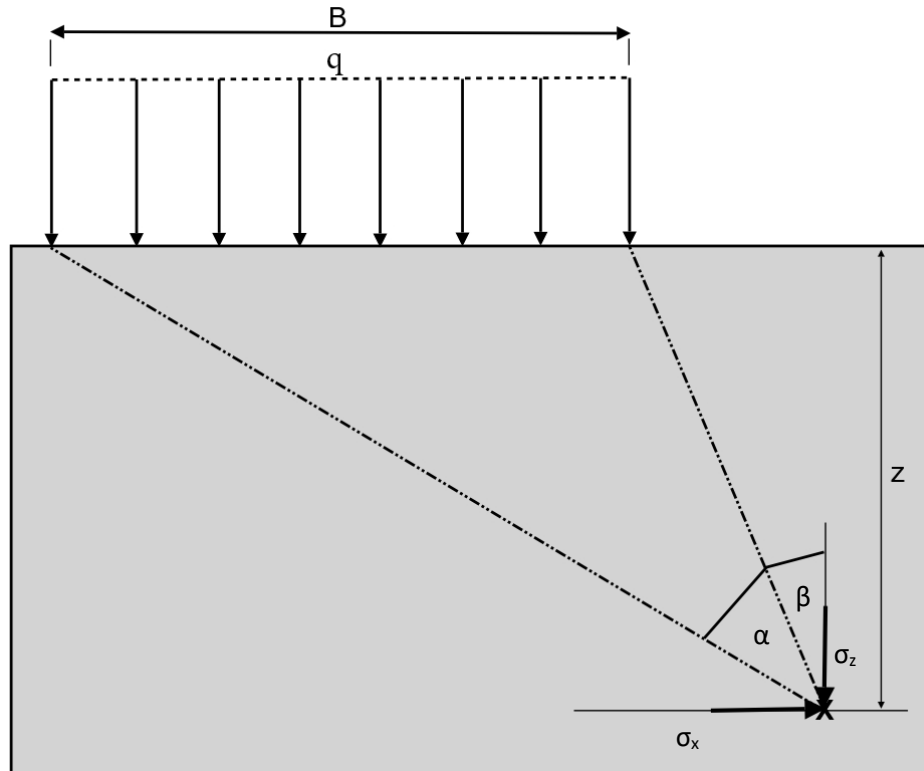
Figure 3.7: Showing general configuration of loading in relation to point of residual stress calculation for loading on a linear strip with uniform pressure (Craig, 1987).

Analysis has been undertaken for an intermediate excavation depth of 60 mbgl. Unloading is defined as the removal of modelled overburden stress at 60 m depth pre-excavation. The model value is 1.434 MPa which approximates to the manually calculated self weight of the excavated rock. For a location immediately below the excavation face, β= 0 and can be ignored. Calculated stresses at increasing depth below the excavation floor are shown graphically in Figure 3.8.
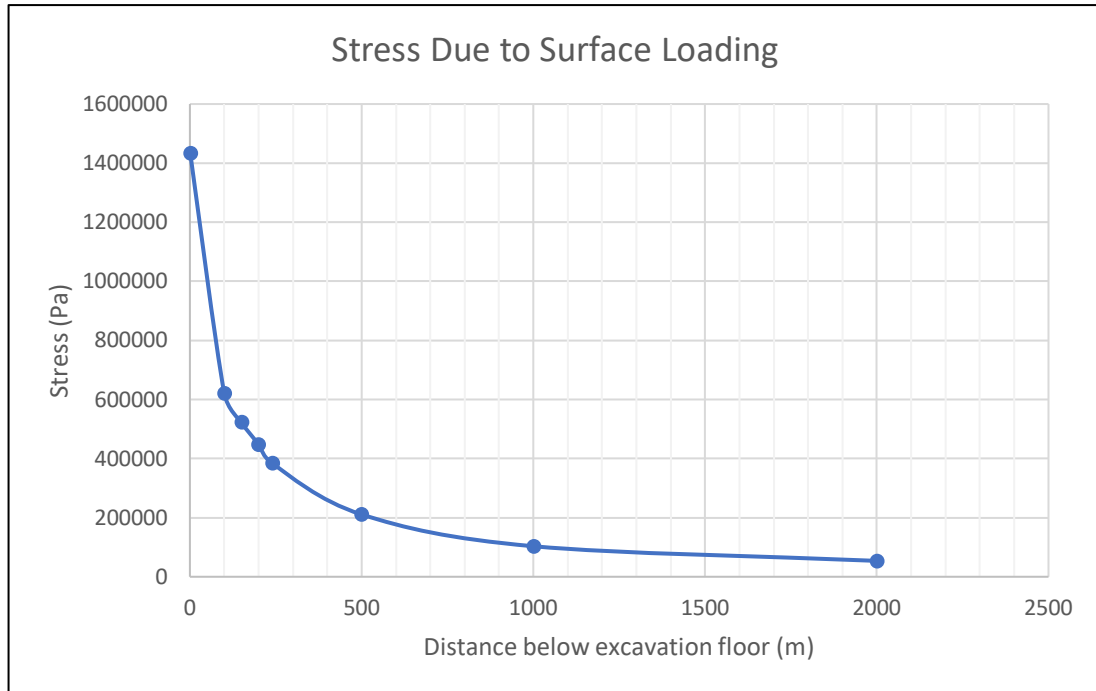
Figure 3.8: Graph showing variation in vertical stress (Pa) with increasing distance below the excavation floor, based on Boussinesq analysis and indicating that the majority of stress change due to unloading occurs above a depth of 500 m below the unloaded surface.

Manual calculation indicates that the effects of unloading could be definable at a significant distance, in excess of 2000 m, below the excavation floor but that the most significant change in the rate of stress reduction occurs above around 500 m below the floor. At this depth the calculated reduction in stress is approximately 10% of the surface unloading. Analysis of actual stress magnitudes in preliminary model development work at a depth of 500 m below the excavation floor indicates that the manually calculated stress change due to loading or unloading at 60 mbgl constitutes approximately 1% of the total stress at this depth; so at greater depths the change would be smaller and probably have negligible practical impact.

It was therefore concluded that fixed model boundaries below the floor of the excavation should be set at a depth of 500 m i.e. a model domain depth of 600 m. At this distance model boundaries are unlikely to have significant effect on model results around the excavation areas. Boundary effects described above relate to homogeneous and isotropic geological environments. In practice

structural and lithological variations have significantly greater effect on model domain stress distribution.

All geomechanical simulations have been undertaken on a 'dry' basis without allowance for groundwater. Many open pit excavations are predominantly developed within the unsaturated zone. Research undertaken as part of the Large Open Pit (LOP) project (Beale et al, 2014) concluded that pore pressure arising from saturated conditions was unlikely to be a significant factor in the geomechanical response of discontinuities to unloading.

Each 2D model has incorporated four phases. Lithostatic unloading has been undertaken in three phases after an initial phase during which pre-excavation in-situ stresses are assigned to the model through gravitational initialisation. The gravity induced stress distribution remains throughout the modelling process. All model displacements are reinitialised to zero after the completion of the gravitational initialisation phase so that modelled displacements in Phases 2-4 are representative of the effects of extraction.

3.4.3 Model outputs, presentation and processing

Model results have been extracted in both graphical and numerical formats. Elfen visualisation functions allow visualisation of many selected data types and the contouring of variables where appropriate. Vector outputs allow visualisation of directional parameters. Although the primary objective of geomechanical modelling was to establish EdZ extents and aperture dilations, reference was also made to other data outputs to confirm model functioning and validity and to support associated data processing. Relevant data sets are as follows:

o   Principal and directional stress
o   Directional host rock strain
o   Host rock directional displacement
o   Discontinuity surface directional displacement
o   Discontinuity normal penetration
o   Discontinuity shear stress
o   Discontinuity sliding distance

o   Discontinuity cohesion
o   External loading
o   Nodal velocity
o   Nodal energy

Model outputs have primarily been evaluated in relation to stress change, displacement and discontinuity dilation at increasing vertical distance beneath the excavation floor and with increasing lateral distance from the excavation face. Results have been considered at several heights in the excavation face to reflect the three stages of excavation. Analysis of stress/strain/displacement results throughout the models has provided the basis to evaluate unloading response throughout the model domains.

3.5   Modelling assumptions and limitations

As indicated in preceding sections of this chapter, a number of critical assumptions or decisions have been made throughout the model development, configuration and parameterisation process. Some of these assumptions are tested as part of the sensitivity analysis undertaken with each model. Other assumptions need to be acknowledged during discussion and interpretation of modelling outputs. A summary of key modelling assumptions and potential implications is presented as Table 3.5.

Assumption/decision	Application	Implications
1. Restriction to 2D	Discontinuity modelling has been undertaken in 2D to allow development of a larger number of separate models and support analysis of a larger number of variables than would have been possible with 3D modelling due to time constraints.	In the bedding only and orthogonally jointed models it is reasonable to assume that plane strain conditions apply and that 2D modelling can be considered representative of effects on the modelled DFN that would result from modelling in 3D. On the basis of 3D model results, it could be concluded that 2D model results represent the

		maximum magnitude of EdZ extent in an excavation face.
2. Domain size	Model domain dimensions have been designed to minimise the effect of boundary conditions on model results. A balance had to be achieved between an excessively large domain and an ability to focus on detail around the excavation areas.	Displacement boundaries in Elfen introduce a linear displacement distribution from the limit of excavation effects to the model boundary creating a need to try and separate boundary effects from excavation induced effects. Tests with much larger model domains just extended the linear boundary effect with no improvement on boundary effect separation.
3. Excavation representation	The excavations are represented as three excavation phases with a fixed 70° angle face. In practice, excavation faces are likely to be limited to a height of 10-15m and be separated by horizontal benches that increase face stability.	The excavated areas are idealistically represented in the model. The primary aim was to define an excavated volume, and hence load. The use of a generalised excavation profile is likely to have influenced the stability of excavation faces but have had limited impact on far field stress distribution, rock mass displacement or joint dilation.
4. Dry modelling	All geomechanical models have been run under dry conditions with no inclusion of pore pressure	As discussed at Section 3.4.2, LOP research indicates that pore pressure is unlikely to be a significant factor in the geomechanical response of discontinuities to unloading. Dry modelling is unlikely to have had adverse impact on model results.
5. Single mesh size	All models have been developed with a fixed mesh size of 5m. Investigation into use of	As the study has focussed on far field stress distribution and discontinuity dilation it was important to retain

	a finer mesh around the excavation area with gradation to model boundaries demonstrated that such an approach resulted in large increase in model run time with no improvement in result resolution.	adequate model resolution across the full model domain. With no observed resolution improvement with a graded mesh, a fixed mesh is unlikely to have influenced model results.

Table 3.5: Summary of geotechnical modelling assumptions and limitations

Geomechanical modelling results are presented in Chapter 4, for all models developed during this study. As included at Section 4.3.7, additional sensitivity analysis has been undertaken in relation to model sensitivity to variation in in-situ stress conditions, discontinuity normal stiffness and rock mass material properties.

CHAPTER 4: GEOMECHANICAL MODELLING RESULTS

4.1   Introduction

Geomechanical modelling results are presented sequentially in accordance with the methodology set out in Chapter 3. The sequence commences with simple 3-Dimensional modelling undertaken to investigate EdZ configuration and constraints in strata without discontinuities to provide a context for subsequent 2-Dimensional modelling of multiple discontinuity configurations. Whereas 3D modelling has been applied to support investigation of EdZ configuration, more detailed 2D modelling has been used to investigate EdZ extents, the response of pre-existing discontinues to excavation and to establish the role of discontinuities in the stress response. The results from both phases of modelling are presented in this chapter and discussed further in Chapter 5.

As detailed in Chapter 3, the EdZ is defined as the Excavation disturbed Zone, in contrast the much less extensive Excavation Damage Zone (EDZ). The EdZ represents the area around an excavation in which there is definable disturbance of the host strata. As discussed at Section 4.1.2, strata disturbance is defined in relation to both the stress and the displacement response to excavation.

Prior to presentation and analysis of model results, further information is provided regarding the development of pre-excavation stress conditions within the models and its significance with regard to interpretation of model results. Initial model results demonstrated the need to clarify procedures for definition of EdZ extents to take account of model boundary conditions and the effect of pre-existing discontinuities.

4.1.1 Gravity initialization and pre-excavation stress regime

Pre-excavation stress conditions in all 2D models are established by application of the gravity initialization process in Elfen. Gravity initialization

establishes stress conditions at each model node with the assumption that all compression or settlement of strata has already happened and therefore local stress magnitude is determined simply as density x gravitational acceleration x depth below datum (ρgh). Variations occur where there is a change in lithological density which creates a requirement for iterative development of stress values across lithological boundaries. Where discontinuities are present, a similar approach is required to account for stress variation around discontinuities and in response to discontinuity deformation.

The gravity initialization approach, in contrast to global gravity loading, does not therefore result in any significant displacement within the model at completion of the initialization phase. Subsequent model response to lithostatic unloading by progressive excavation development, is predominantly an elastic response controlled by the material properties of the rock type, plus any response at discontinuities. A similar response is achieved for both the gravitational initialization approach and the global gravity loading approach.

As discussed in Chapter 3, all 2D models have been run with two alternative in-situ stress conditions defined by variation in the pre-existing lateral confining stress ratio with respect to gravitational loading. All 2D models have been run with 'low' lateral confining stress with a horizontal stress/vertical stress ratio of 0.27 and 'high' lateral confining stress with a horizontal stress/vertical stress ratio of 2.00. The pre-existing lateral confining stress ratio is referred to as the 'lateral stress ratio - k' throughout this chapter.

4.1.2 Approach to determination of EdZ boundaries

All models produce data to define change in stress, strain, displacement and discontinuity dilation with increasing distance from the excavation face and floor. As one of the key modelling objectives is to establish an understanding of the vertical and lateral extent of the EdZ for a range of geomechanical conditions it is necessary to establish a consistent procedure for determination of EdZ limits.

For open-pit excavations there are several analytical methods with potential application to definition of EdZ limits. They are as follows:

o The point at which there is no change in stress magnitude when compared to the pre-excavation condition (**stress variant approach**);

o The point at which rock mass displacement towards the excavation face or floor is zero or an alternative threshold value (**threshold approach**); and

o The point at which displacement direction changes when compared to the minor pre-excavation displacement direction (**displacement direction approach**).

In common with previous studies related to EDZ and EdZ development around deep underground excavations (Tsang et al. 2005, Perras & Diedrichs 2016) the preferred approach to EdZ extent definition is the stress variant approach as the EdZ defined by this method encompasses the full stress response and is less affected by zero-displacement boundary conditions. However, vertical effects associated with excavation extend close to the lower model boundary, and lateral effects in the upper excavation face do not fully return to the pre-excavation stress magnitude in some models. It has therefore been necessary to check EdZ extents defined by model stress results with directional displacement results, leading to the development of a minimum threshold for variance from pre-excavation stress levels. The approach is illustrated by reference to some of the model outputs for the bedding only model (Model 2) with a lateral stress ratio of 2.0.

Vertical stress with increasing depth below the excavation floor for all three modelled excavation depths and the pre-excavation gravity initialization condition, are presented in Figure 4.1. Figure 4.1 shows that, in this model (Model 2), all excavations result in compressive stress reduction beneath the excavation floor with rock mass stress converging towards the pre-excavation gravity stress with increasing depth, although full convergence is not achieved. The effect is most clearly observed by reference to linear regression lines for each excavation depth, as shown. The residual stress variance occurs in response to displacement boundary conditions at the lower model boundary. Reference to displacement direction, as defined by vector plots of the entire

model domain provide general definition of the EdZ extents as the point at which there is a significant change in displacement magnitude and direction.
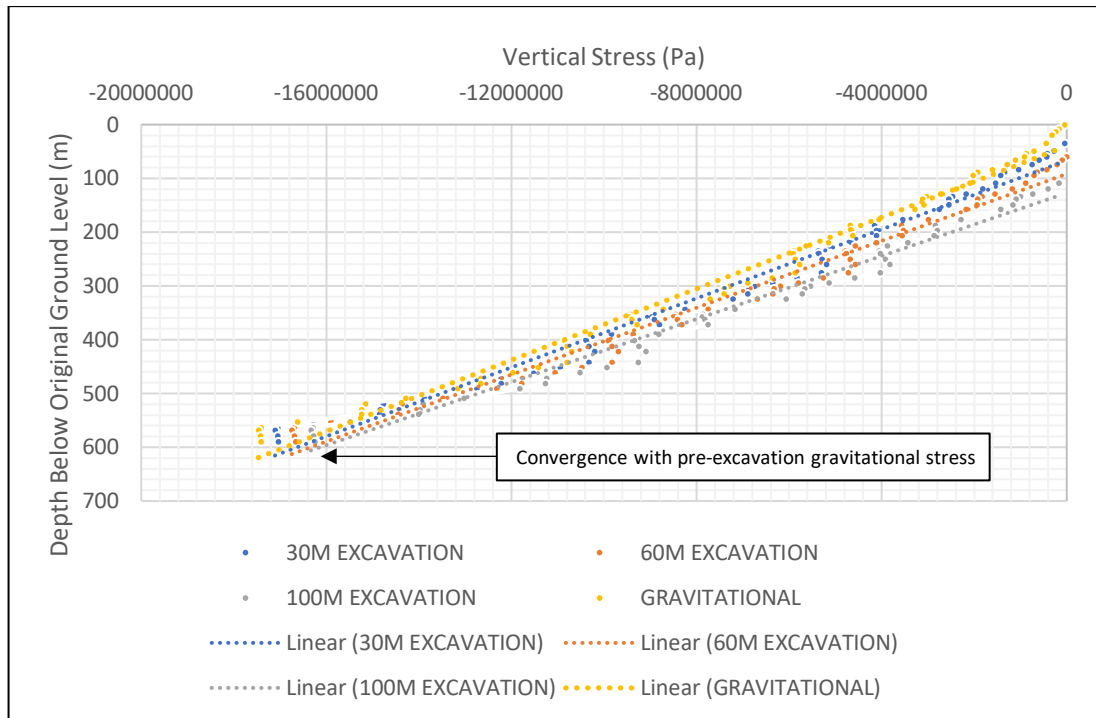
Figure 4.1: Model 2 Vertical stress variation data and linear trend line, with increasing distance below the excavation floor for excavation depths of 30m, 60m and 100m, compared to the pre-excavation gravitational stress profile. The results indicate reducing variance from gravitational stress with increasing distance below the excavation floor for all excavation depths.

The displacement plot for the same model (Model 2) at 100m depth of excavation is shown as a vector plot in Figure 4.2. The figure is not intended to show individual displacement values but the variation in vector direction and magnitude defining EdZ extents. Figures 4.3 and 4.4 are a close up of the vertical and horizontal EdZ boundaries defined in Figure 4.2 and show the variation in vector direction and scale that results in the visual representation of the EdZ boundary.

Figure 4.2 shows the limit of disturbed displacement extending close to the lower model boundary and the same zone extending laterally from the excavation face to almost the right-hand model boundary. Vertical displacement boundaries, as defined by vector plots, have been compared to

graphical output from model stress results for each of the three excavation depths. In this example the horizontal extent of the EdZ extends close to the right-side model boundary behind the excavation face but is limited to a distance of approximately 250 m beneath the excavation floor. The vertical extent of the EdZ does not vary significantly with depth of excavation with a limit of approximately 440 m below the excavation floor which is 540 m below pre-excavation ground level. Vertical stress magnitude at this depth is as follows.

Gravity initialization – 16.6 MPa

30 m deep excavation – 16.3 MPa (98.2% gravity initialization)

60 m deep excavation – 15.9 MPa (95.7% gravity initialization)

100 m deep excavation – 15.5 MPa (93.4% gravity initialization)
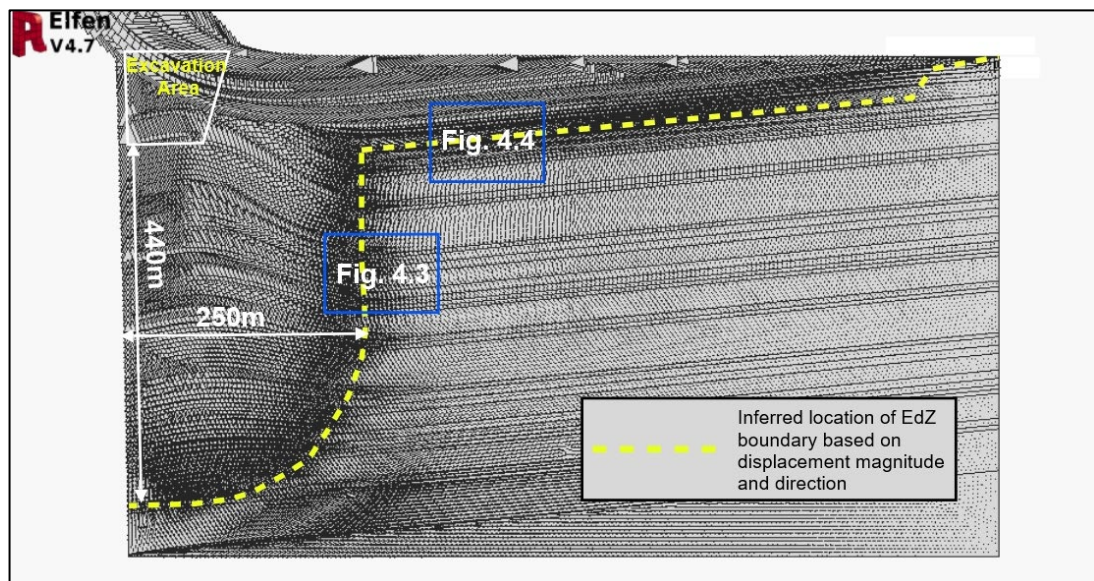
Figure 4.2: Model 2 Directional displacement plot for 100 m deep excavation in bedding-only model showing magnitude increase and directional change as darker bands (model domain 1000 m x 600 m). The figure shows the potential for use of vector displacement plotting to support definition of EdZ extents.

On the basis of combined analysis of model stress results and directional displacement data, it is apparent that the majority of the 'disturbance' occurs within the boundary defined by a post-extraction vertical stress that has returned to 95% of the pre-excavation stress magnitude. The post-excavation

lateral stress -v- gravitational initialisation lateral stress ratio at the horizontal boundary of the EdZ is less consistent due to the increasing length of the excavation face with successive stages of excavation. A return to full pre-excavation stress magnitude has been used to define the horizontal EdZ boundary, where possible.
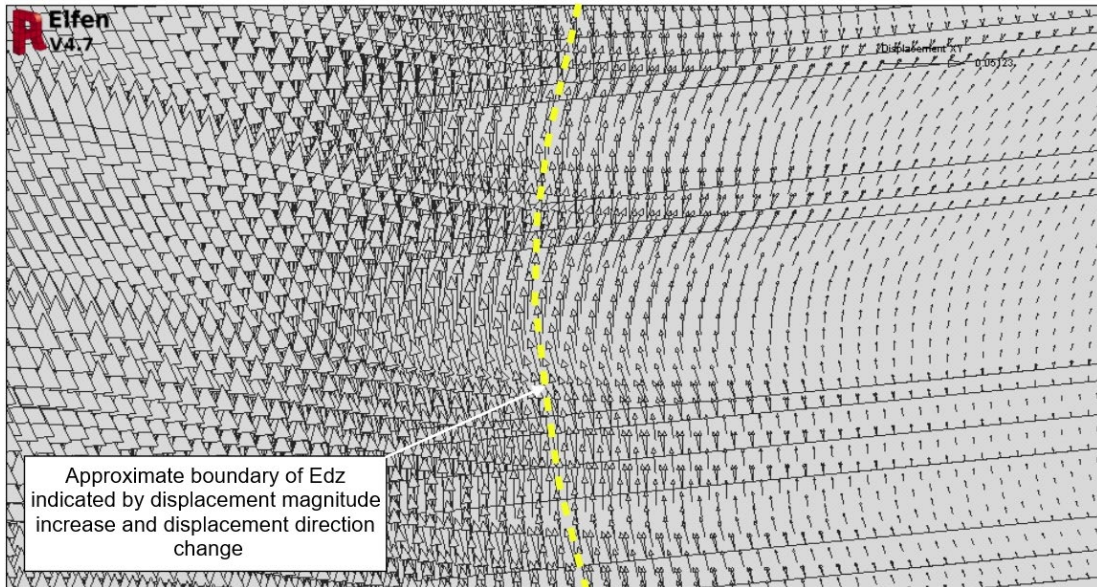
Figure 4.3: Model 2 Close-up from Figure 4.2 of directional displacement plot of vertical EdZ boundary with 100 m deep excavation in bedding-only model. Inferred EdZ boundary marked by an increase in displacement magnitude and minor directional change.

The approach adopted towards EdZ extent definition in this study is therefore to define the vertical and horizontal boundary at the point at which residual vertical and horizontal stress, respectively, is 95% of the initial gravity initialization stress magnitude in all situations where model stress magnitude does not return fully to pre-excavation values. A further example of the application of this approach is illustrated in Figure 4.5 for horizontal EdZ extents using the same bedding only model (Model 2) with a high lateral stress ratio of 2.0.
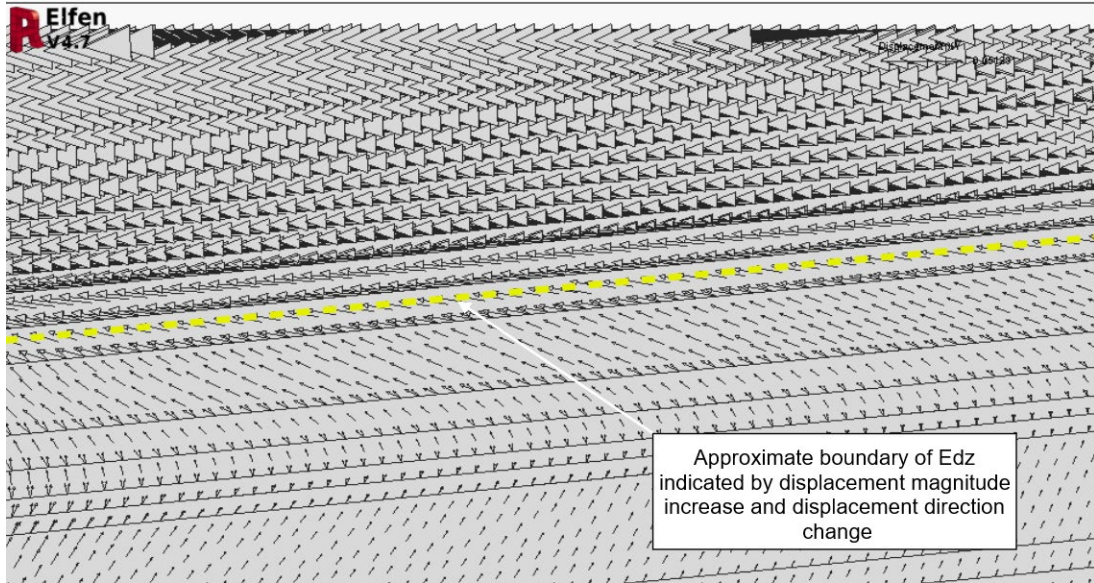
Figure 4.4: Model 2 Close-up from Figure 4.2 of directional displacement plot of horizontal EdZ boundary with 100 m deep excavation in bedding-only model. Inferred EdZ boundary marked by a change in displacement direction and increase in magnitude.
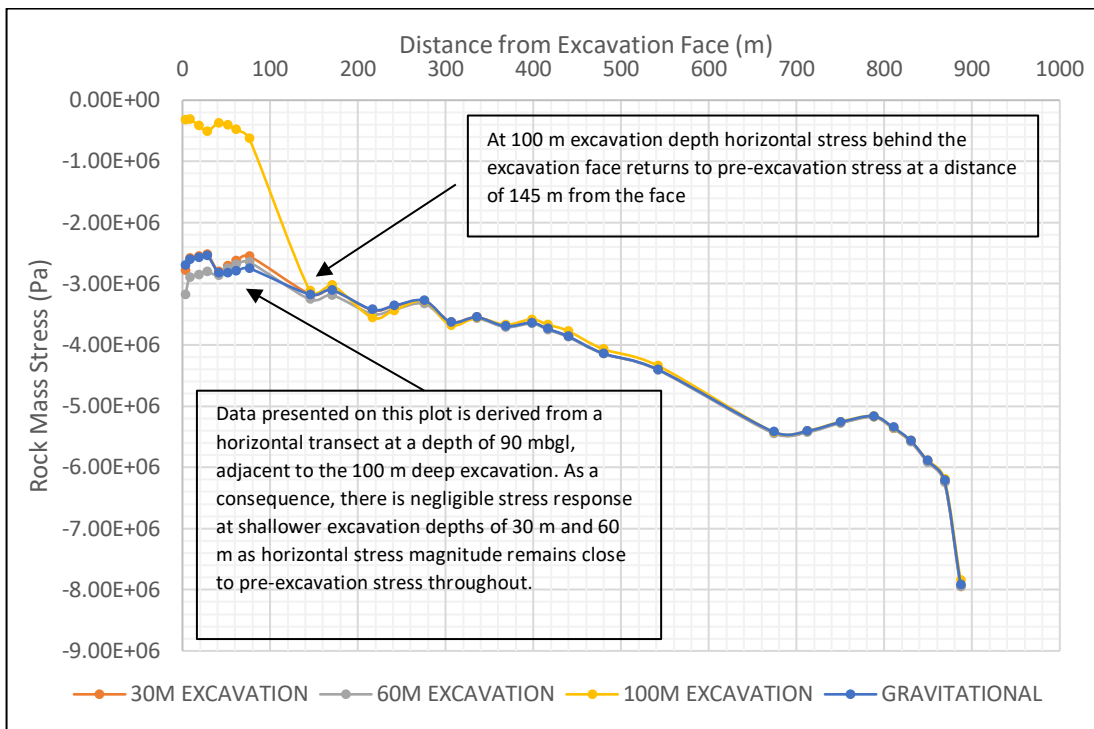
Figure 4.5: Model 2 Horizontal stress variation with increasing distance behind the lower excavation face in the bedding-only model indicating a return to at least 95% pre-excavation gravitational stress at a distance of 145 m from the face for a 100 m deep excavation.

Figure 4.5 presents results for a horizontal transect at a depth of 90 m below the top of the model and hence towards the base of open face adjacent to the 100 m deep excavation phase, and therefore, as shown, there is no significant response to shallower excavation at 30 m and 60 m depth which do not create a free face at this depth. The results show clearly that, in response to a 100 m deep excavation, horizontal compressive stress magnitude is reduced at the excavation face but returns to pre-excavation magnitude at a distance of approximately 145 m from the lower excavation face. As the excavation is 100 m wide at this depth this corresponds to a distance of 245 m from the left-hand model boundary and matches the displacement boundary defined by directional displacement plotting as shown on Figure 4.2.
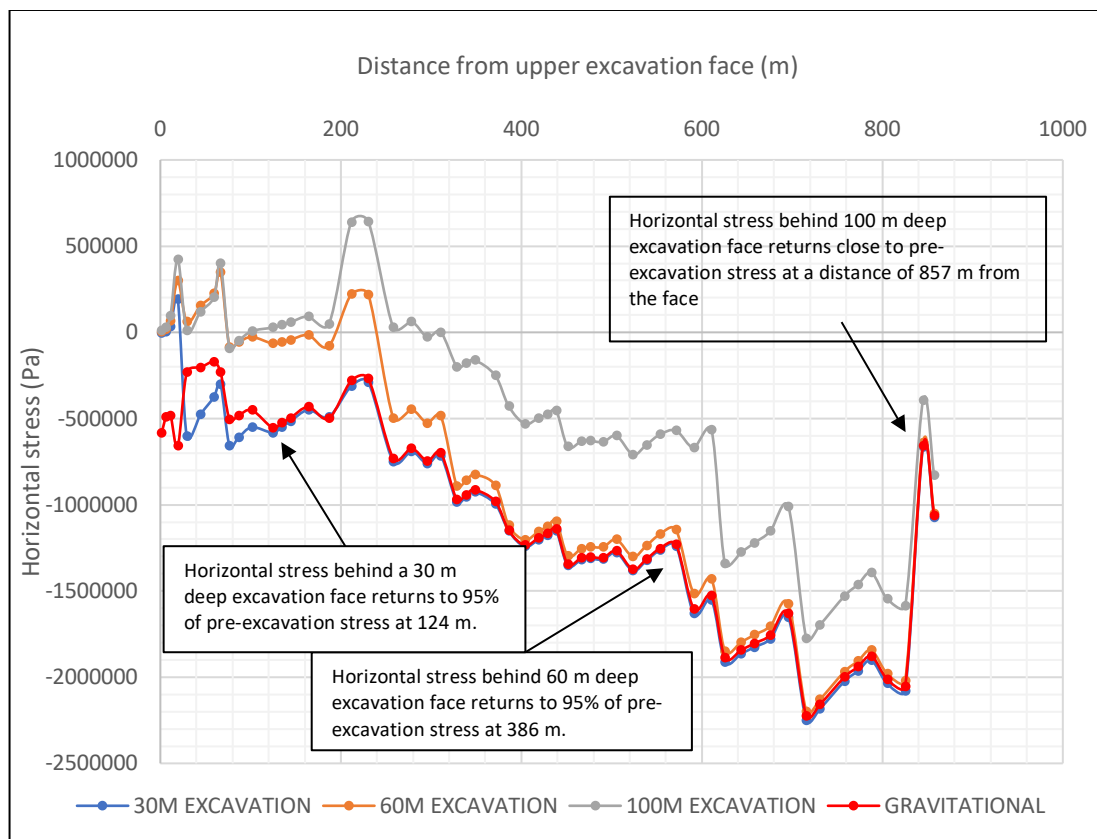
Figure 4.6: Model 2 Stress variation behind the upper excavation face with increasing distance for excavation depths of 30 m, 60 m and 100 m showing the distance at which rock mass stress equates to 95% of pre-excavation stress.

Figure 4.2 suggests that in response to a 100 m deep excavation, the EdZ may extend a significant distance behind the upper levels of the excavation face with indicated extents close to the right-hand model boundary which is

set at 1000 m. Variation in stress magnitude with increasing distance from the upper excavation face, defined by a horizontal transect at a depth of 20 m below the upper model boundary, is shown in Figure 4.6. For a 100m deep excavation the figure indicates that residual stress magnitude is close to the pre-excavation magnitude at a distance of approximately 845 m from the face. As discussed in detail at Section 4.3.2 in relation to Model 2 results, the stress displacement response to extraction in this example is influenced by bedding plane dip and intersection with the open face.

Results in Figure 4.6 demonstrate that post extraction stress magnitude, for a 100 m deep excavation, returns to a maximum of 78% of the pre-excavation magnitude at the model boundary, suggesting EdZ extents in excess of 850 m from the excavation face. For shallower excavation depths, application of the 95% threshold indicates return to pre-excavation stress magnitude at distances of 124 m and 386 m from the excavation face for excavation depths of 30 m and 60 m respectively.

The above analysis, based on the bedding-only model (Model 2) with high lateral stress, demonstrates that EdZ extents can be effectively defined through combined analysis of rock mass stress variance from pre-excavation magnitude, and directional displacement plotting. This approach has been applied throughout this study.

4.2   Three dimensional (3D) modelling results

A simple 3D block model was developed to investigate the effects of sequential excavation on rock mass stress response and the resultant strains exhibited in response to excavation. The primary objective of 3D modelling was to investigate how the excavation configuration, and specifically vertical and lateral constraints at the end of each open face, might influence the shape of the EdZ around the excavation. Two model designs were developed to represent alternative open pit configurations. These were;

(i) A fully enclosed vertical excavation, and
(ii) An open-sided lateral excavation.

Both model domains have dimensions of 2500 m x 2500 m x 600 m. The fully enclosed excavation model incorporates an excavation that is 500 m x 500 m at surface resulting in a minimum distance of 1000 m from the upper excavation face to the model boundary. The excavation is developed in three benches at depths of 30 m, 60 m and 100 m. In the open-sided lateral excavation the open excavation has dimensions at surface of 500 m x 1500 m with the same depth profile as the enclosed excavation model.
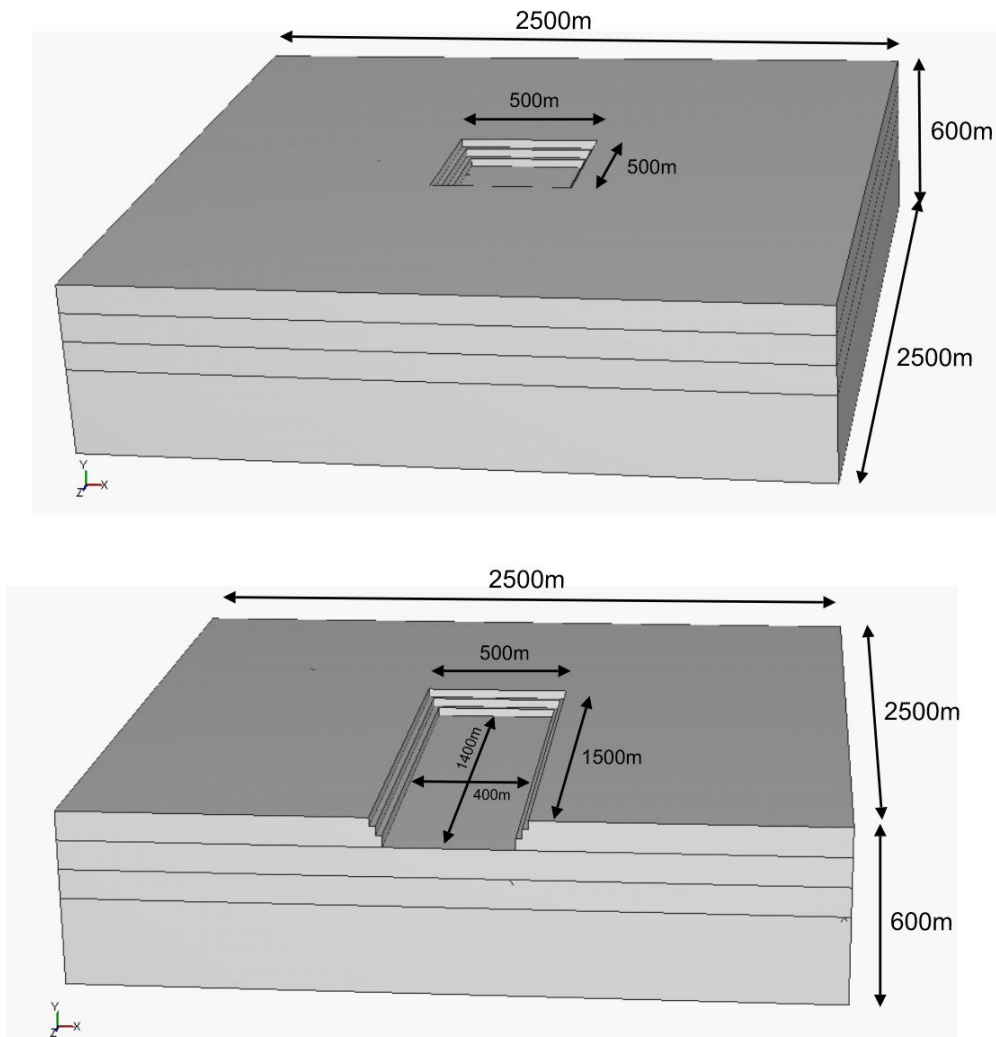
Figure 4.7: Three dimensional (3D) model configurations. Upper model - enclosed vertical excavation. Lower model – open-sided lateral excavation.

Model configurations are shown in Figure 4.7. The enclosed configuration is representative of open pit excavations that progress vertically downwards from an equivalent elevation on all sides. The open-sided excavation is

representative of open pit workings that extend laterally into a hillside or where there is significant topographic variation. The majority of open pit workings can be defined geometrically as a combination of enclosed and open-sided excavations.

Both models were assigned single material properties throughout using the 'Blaxter Sandstone' specification (see Table 3.3) with no lithological variation. The models do not include any discontinuities and therefore simply represent the bulk rock mass response the excavation induced stress change. The models are initially subject to global gravitational loading to establish initial in-situ stress conditions prior to excavation. In the case without discontinuities or lithological variation the gravitational initialisation function in Elfen builds internal stress without rock mass strain. As the object of this stage of research is to investigate the elastic strain response, the alternative approach of applying global gravity in Elfen was adopted following advice from Rockfield. Gravity loading was applied to the entire model domain with a gravitational acceleration of 9.81 m/s^2 in a basic ρgh form. In contrast to the gravitational initialisation function, the global gravity function does not incorporate provision for direct variation of pre-existing lateral stress.

Lateral stress variation is therefore achieved by adjustment of material Poisson's Ratio in accordance with the following.

k = v/(1-v), where   [4.1]

v = Poisson's Ratio

k = lateral stress ratio

This approach is valid for conditions in which there is loading of an elastic material and no significant horizontal strain (Goodman, 1989). Both 3D models were run with a lateral stress ratio of 0.27 i.e. with low lateral stress, and therefore the Blaxter Sandstone unconfined Poisson's Ratio of 0.23 was applied to both simulations.

Following initial gravitational loading, the models incorporated three stages of excavation to represent increasing excavation depth from 30 mbgl to 60 mbgl

and 100 mbgl, consistent with subsequent 2D modelling. The response to excavation is realised as a simple elastic strain response resulting from a reduction in vertical loading and lateral confinement at excavation floor and faces, respectively.

Gravitational loading results in the development of internal stresses with a maximum of 13.7 MPa at the model base, distributed linearly from top to bottom with highest stress at the base of the model, a depth of 600 m. Horizontal stress at the base of the model is 3.64 MPa, confirming the 0.27 lateral stress ratio, as discussed above. Rock mass strain due to compression of the sandstone under gravitational loading increases with increasing depth to -3.77×10^{-4} at the base of the model. Model stress and strain values are consistent with expected values derived from manual calculation.

In response to phased excavation, the models demonstrate local reduction in stress around the excavated surfaces resulting in an elastic strain response that occurs as uplift in the excavation floor and lateral displacement away from excavation faces. Examination of vertical displacements indicates vertical displacement beneath the excavation floor and faces that extend a significant distance from the excavated void. Horizontal profiles indicate lateral displacement extending for a significant distance behind the excavation face. In the case of these models with no discontinuities, nodal displacements can be considered representative of rock mass strain as there are no other processes active. Vertical and horizontal displacement results for the fully enclosed excavation are shown graphically in Figure 4.8.

With elastic strain response being the only process operating, the magnitude of rock mass displacement at excavation surfaces is small. As shown in Figure 4.8 for a 100 m deep excavation, the maximum vertical displacement occurs at the centre of the excavation floor with a magnitude of 0.01 m. At the boundary of the excavation, vertical displacement is reduced to approximately half the maximum value. Horizontal displacement in the X and Y axis directions occurs at lower magnitude. Results are shown for displacements greater than 1 mm.
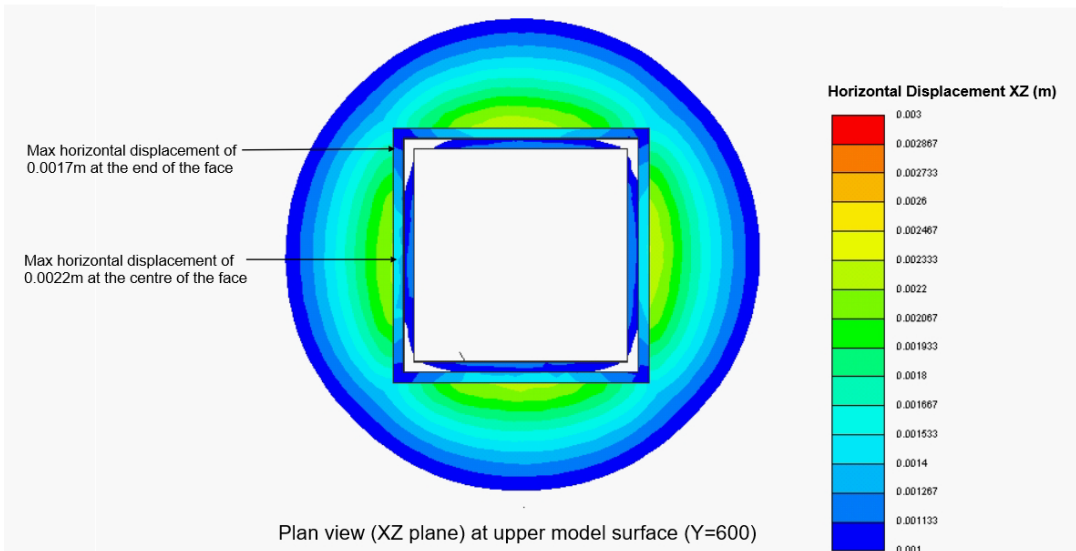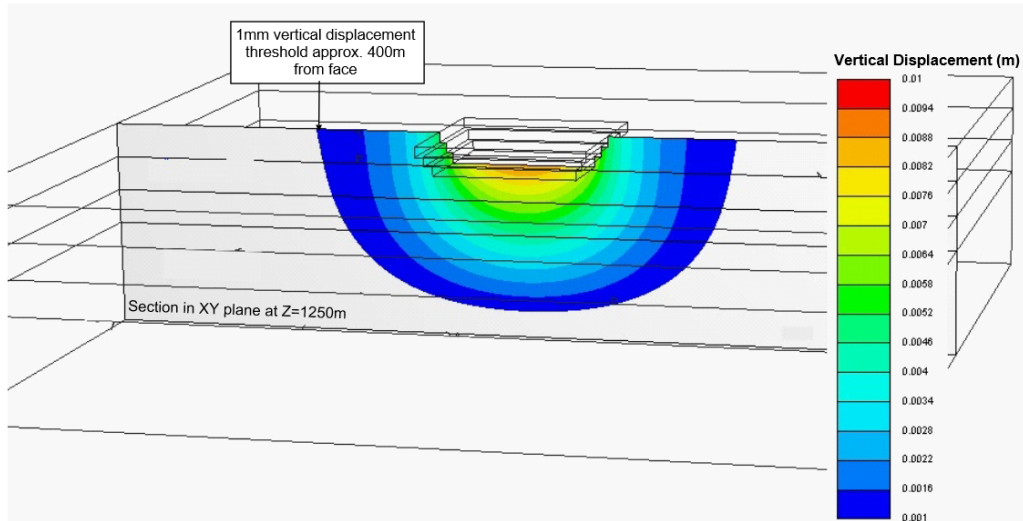
Figure 4.8: Modelled vertical and horizontal displacements in response to excavation at 100 mbgl. Upper diagram shows vertical displacment towards the excavation at a vertical plane through the centre of the excavation. The lower diagram shows the excavation in plan view with lateral displacment (x and z directions) at the upper model surface. Lateral displacement is outwards, away from the excavation faces.

As indicated in Figure 4.8, maximum lateral displacement, after excavation, is approximately 0.003 m at the centre of each face, reducing to approximately 0.0015 m at the end of each face. Modelled displacements in the horizontal direction are displacements away from the excavation face, referred to here as 'outward' displacement away from the excavation void, contrary to expected inward displacement, referred to here as 'inward' displacement towards the

excavation void, due to removal of lateral confinement. As discussed in relation to 2D modelling later in this chapter, this effect occurs as the small lateral outward displacement arising from uplift is greater than the inward lateral displacement due to loss of lateral containment at the face. However, although horizontal strain behind the excavation face remains compressive normal to the face, an extensional strain zone develops parallel to the face. Average lateral extensional strain is approximately 3×10^{-6} over the 1000 m distance to the model boundary which equates to the observed maximum lateral outward displacement of 0.003 m.
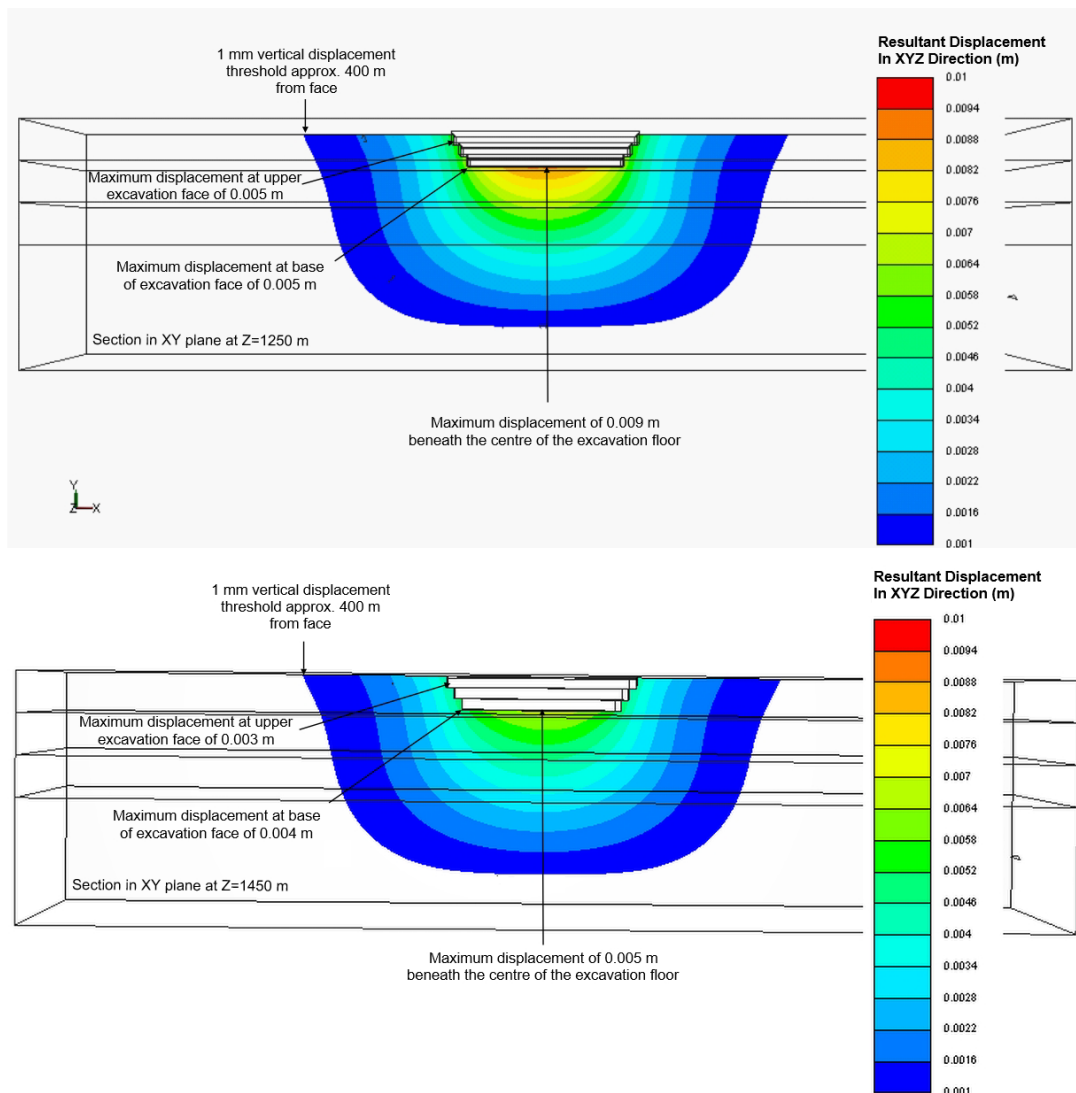
Figure 4.9: Displacement magnitude above a 1 mm displacement threshold in XYZ direction through central plane (upper diagram) indicating the dominance of vertical displacement by comparison with Figure 4.8. Lower diagram shows XYZ displacement at a plane intersecting the edge of the excavation indicating lower displacement magnitudes.

Model results plotted in the XYZ direction, as shown in Figure 4.9, on a single plane through the centre of the 3D model (plane orientated parallel to XY axis at 1250 m in Z axis direction) show displacement in all three directions indicating that lateral displacement in the X and Z directions have minor effect on resultant displacement magnitude or direction when compared to the vertical displacement only plot at Figure 4.8, suggesting that the dominant displacement direction is vertical. Displacements in all model outputs are shown for all displacements >1.0 mm. A nominal 1 mm threshold has been assumed as the magnitude below which displacement is considered likely to be insignificant.

Figure 4.9 also shows XYZ displacement magnitude at a second plane located close to the excavation boundary (plane orientated parallel to XY axis at 1450 m in Z axis direction). The results demonstrate a reduction in displacement magnitude at excavation corners when compared to displacement magnitude at the centre of the excavation.

Although the displacements are small, the model results allow analysis of constraints imposed by the excavation configuration. Reference to Figure 4.9 demonstrates that maximum vertical displacement occurs at the centre of the excavation floor, reducing towards the perimeter where vertical movement is influenced by the overlying excavation face.

Reference to Figure 4.8 demonstrates that lateral displacement at the excavation face varies along the face. Lateral displacement is greatest at the centre of each excavation face, decreasing towards each corner where the face is laterally constrained by each perpendicular face. As a consequence, the disturbed zone does not extend for the same distance behind all locations along the face and is not defined as equidistant from the face around the excavation. This is contrary to previous conceptual interpretations of lateral excavation EdZ's in which a homogeneous peripheral displacement or 'halo' around an excavation is often suggested. Where faces are constrained at both ends the maximum predicted displacement at the centre of the face is approximately twice the displacement at the end of each face for a fully enclosed excavation.
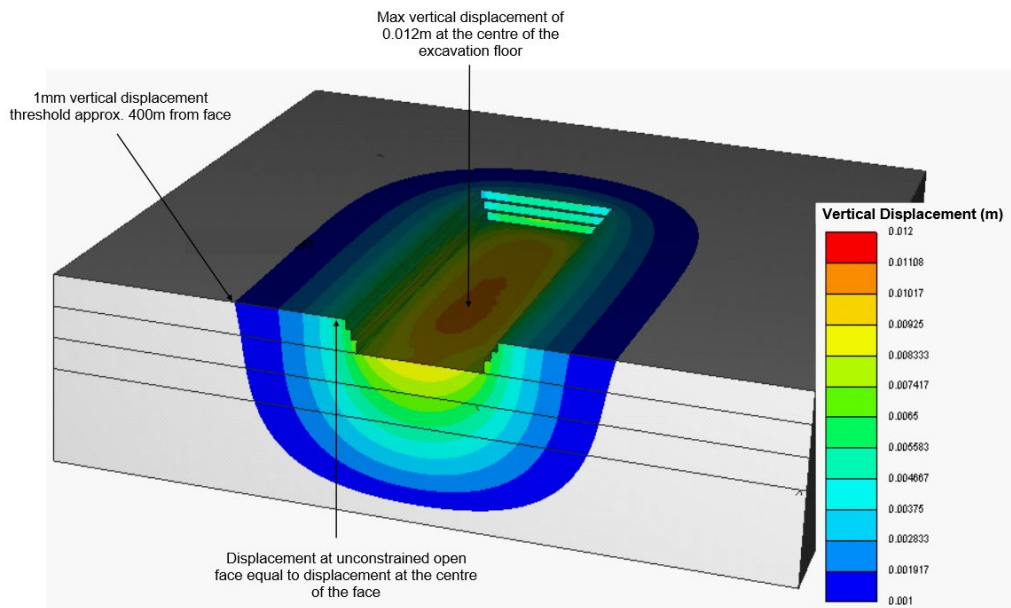
Figure 4.10: Displacement magnitude in the vertical direction for the opencut model showing greatest upward displacement at the centre of the excavation floor and increased vertical displacement at the open end of the excavation in comparison to the fully enclosed model.

The open-cut model demonstrates the effect of a loss of lateral constraint at the model boundary with increased displacement at the 'open' end of the excavation and larger resultant lateral outward displacement of up to 0.003 m at the model boundary. As indicated on Figure 4.10, which shows the resultant vertical displacement magnitude from all three directions, the largest displacement still occurs in the centre of the excavation floor and vertical displacement dominates with a maximum magnitude of 0.012 m.

The heterogeneity of the elastic strain response around the excavations provides a context for subsequent 2D modelling which has been undertaken on a plane strain basis assuming no constraint in the third dimension. In that context, the results of 2D modelling should be considered representative of the maximum strain/displacement values likely to be observed in excavation faces. As all 2D models are orientated within the XY plane there should be negligible variation between vertical displacements in 2D and 3D model configurations. This is demonstrated in subsequent discussions of the results of 2D modelling.

Three-dimensional modelling without discontinuities demonstrates reduction in compressive stress around an excavation, leading to differential uplift in the excavation floor and differential displacement of the excavation face. The development of an extensional strain zone parallel to the excavation face, but without significant extension behind the face, is identified in 3D models but would not be definable in 2D modelling restricted to plane strain conditions. In the analysis of 2D modelling results it is appropriate to recognise that any development of localised extensional strain conditions immediately behind the excavation face could extend parallel to the face.

4.2.1 Excavation disturbed Zone (EdZ) extents in 3D

Three-dimensional modelling provides an opportunity to investigate the extent of the disturbed zone beneath the excavation floor and behind the excavation face, without the presence of any discontinuities. Under such conditions, the magnitude of extensional strains and associated displacement are small, but the boundaries of disturbance have been defined as the point at which model stress values return to 95% of the pre-excavation gravitational stress, the defined boundary condition as set out at Section 4.1.2. Results for the enclosed and open-cut excavation are summarised in Table 4.1.

Model configuration	Excavation depth (mbgl)	Limit of EdZ – Vertical (m)	Limit of EdZ – Horizontal (m)
Enclosed excavation	30	202	299
	60	286	421
	100	329	770
Opencut excavation	30	223	356
	60	322	504
	100	438	798

Table 4.1: 3D models estimated EdZ extents without discontinuities (k=0.27). Results show increasing EdZ extents in both vertical (below the excavation floor) and horizontal (at the upper excavation face) directions with increasing depth of excavation. EdZ extents are greater for the opencut model in which there is lower lateral containment of the excavation face.

The results presented in Table 4.1 show that the vertical extent of the EdZ below the excavation floor increases with increased depth of excavation. EdZ depth is greater in the opencut excavation where there is reduced peripheral constraint. The vertical depths in Table 4.1 are depths below the excavation floor and not below the top of the model domain and therefore represent increasing depth below the model surface with increasing depth of excavation. Model results indicate that the horizontal extent of the disturbed zone increases significantly with increasing depth of excavation.

4.2.2 Displacement magnitudes with no discontinuities in 3D

Maximum displacements have been recorded for the excavation floor and face under all modelled scenarios. With no discontinuities, displacements occur solely in response to release of extensional strain energy and magnitudes are low, given the relatively high compressive modulus of the sandstone formation referenced for the simulation. Displacement magnitudes are summarised in Table 4.2.

Model configuration	Excavation depth (mbgl)	Maximum vertical displacement (m)	Maximum horizontal displacement (m)
Enclosed excavation	30	0.004091	0.001049
	60	0.006700	0.001649
	100	0.008800	0.002282
Opencut excavation	30	0.004806	0.001300
	60	0.008000	0.002100
	100	0.010470	0.003024

Table 4.2: 3D models estimated displacement magnitude with increasing excavation depth for both fully enclosed and opencut excavation models without discontinuities. Vertical displacement is recorded at the excavation floor and horizontal displacement is recorded at the upper excavation face.

Although all modelled displacements are small, with a maximum magnitude of approximately 1 cm, it is apparent that displacements in the open cut configuration are higher than those in the enclosed configuration by between 17% and 33% with higher variation at greater depth of excavation. Higher displacement in the open cut model reflects the lower degree of constraint imposed by connecting excavation faces and, consequently, the higher degree of freedom experienced when one side of the excavation is laterally unconstrained.

The primary significance of the above analysis is the provisional conclusion that, without discontinuities, the excavation configuration, and particularly the structural constraint imposed by connecting excavation faces, has an impact on the extent and magnitude of the geomechanical response to excavation. General conclusions from the 3D modelling work can be summarised as follows:

o   EdZ extents are not homogeneous around an excavation;

o   Strain-based displacement magnitudes are low (no-discontinuities);

o   Modelled EdZ extents are approximately 200 m to 400 m below the excavation floor and 300 m to 800 m behind the upper excavation face for excavation depths of 30 m to 100 m; and

o   An extensional strain zone is developed parallel to the excavation face.

This simplified 3D modelling programme was undertaken to investigate excavation configuration influences on the stress/strain response to excavation and to provide a provisional estimate of the potential magnitude of disturbed zone extents. The analysis provides a context for subsequent 2D modelling in which plane strain conditions are assumed. Subsequent modelling investigates the effect of pre-existing discontinuities on the stress/strain response for a range of discontinuity network configurations and in-situ stress conditions.

4.3   Two dimensional (2D) modelling results

As detailed at Chapter 3, the majority of geomechanical modelling has been undertaken in two dimensions due to the complexity and resource demand associated with discrete fracture network (DFN) modelling in three dimensions when multiple models and lateral stress conditions need to be considered. The 2D modelling programme has followed a sequence from no-discontinuity models through models incorporating a range of DFN configurations. The modelling sequence has been designed to incorporate progressively increasing DFN intensity and connectivity resulting in a progressively more mobile rock mass. The programme commences with a model without any discontinuities (Model 1) and progresses to a bedding planes only model (Model 2) and then to models that include the same bedding sequence plus the addition of increasingly connected joint or fracture systems (Models 3 and 4). Model results are primarily presented in relation to post extraction geometry, as displacements and discontinuity dilations, although analysis of respective model stress/strain relationships has been undertaken to support process interpretation and ensure that key processes are realistically represented.
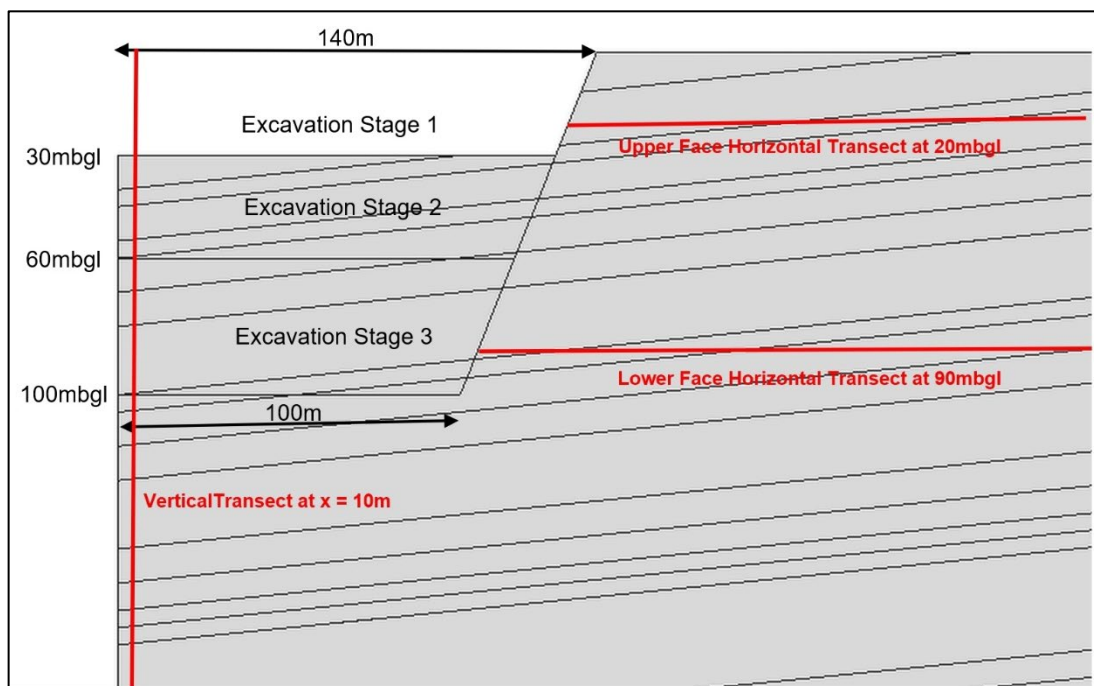
Figure 4.11: Simulated excavation dimensions used in all 2D models. The figure also shows vertical and horizontal transects used to extract data from all models.

As detailed at Section 3.3.3, all 2D model simulations incorporate simulated excavation to depths of 30 m, 60 m and 100 m below ground level. Excavation dimensions and the location of vertical and horizontal transects used for the extraction of data from all models are shown on Figure 4.11.

4.3.1 Model 1: Rock mass without discontinuities

The primary objective of 2D no-discontinuity modelling is to provide a basis for comparison with 3D no-discontinuity modelling results and to validate model performance with regard to the expected stress/strain response. The baseline model without discontinuities has been run with lateral stress ratios of 0.27 and 2.00 to represent low lateral stress and lateral stress equivalent to double the gravitational loading, respectively. The 2D low lateral stress ratio configuration is comparable to the 3D model configuration which was also based on lateral stress ratio of 0.27.

In common with all other models developed during this study, the no-discontinuity models incorporated four stages as follows:

(i) Stage 1: Gravity initialisation
(ii) Stage 2: 30 m deep excavation
(iii) Stage 3: 60 m deep excavation
(iv) Stage 4: 100 m deep excavation

To allow evaluation of the effect of variation in lateral stress and to maintain consistency with subsequent discontinuity modelling, loading was achieved with the gravity initialization function of Elfen which establishes a 'current day' stress state consistent with settlement under gravity over long timescales. Gravitational initialization generates stresses within the model domain on a ρgh basis but, for single material models or models without discontinuities, does not incorporate compaction as stresses are effectively lithostatic.

For all subsequent discontinuity-based models, loading has also been applied through the gravity initialization process which provides greater control over lateral stress variation than use of the global gravity function in Elfen. With low lateral stress conditions gravity initialization resulted in a highly regular stress

distribution with vertical stress ranging from zero at ground level to 13.8 MPa at a depth of 600 m and horizontal stress ranging from zero at ground surface to 3.7 MPa at 600 m depth.

4.3.1.1 Stress response

Under low lateral stress conditions, as excavation proceeds to increasing depth, stresses around the excavation reduce and stresses are influenced over an increasing distance from the excavation floor and face. Figure 4.12 Shows the vertical stress distribution for a 100 m deep excavation. The vertical stress just below the excavation floor decreases from 2.27 MPa pre-excavation to 0.041 MPa post-excavation. Stresses at the excavation floor remain compressive throughout. Vertical stress at the upper section of the excavation face (20 m below the upper model surface, adjacent to the 30 m excavation), for the same 100 m deep excavation, increases from 0.136 MPa pre-excavation to 0.148 MPa post excavation.
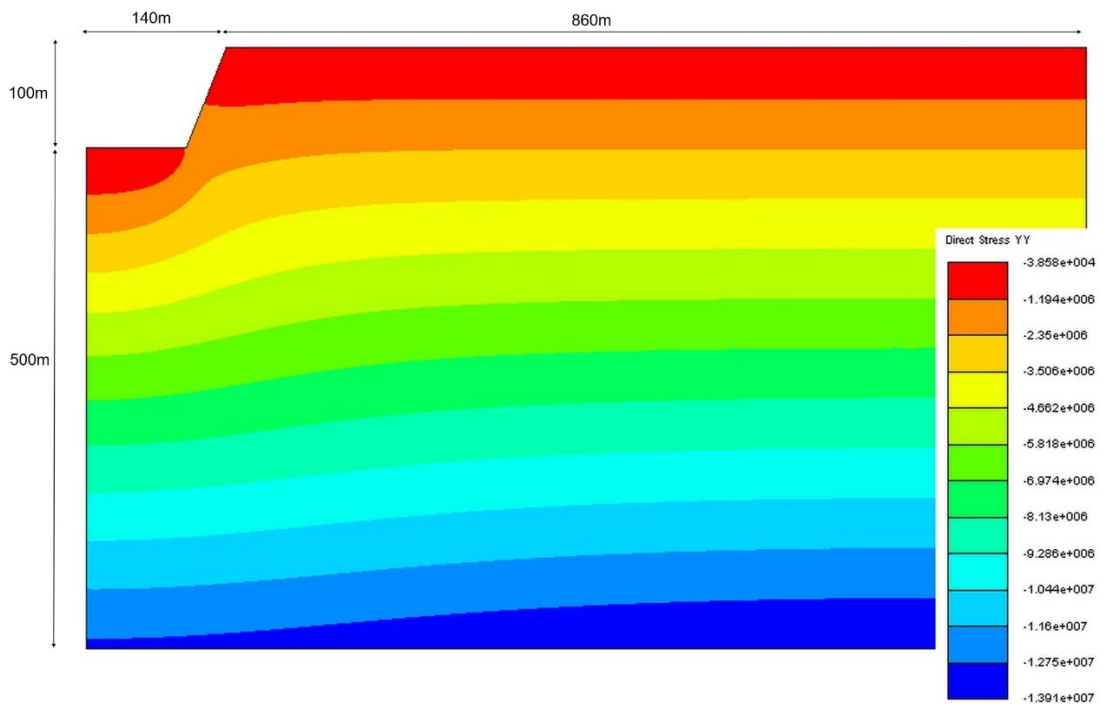
Figure 4.12: Model 1 Vertical stress distribution (Pa) with 100 m deep excavation indicating stress reduction beneath the excavation floor in response to excavation (k=0.27).

Horizontal stresses on the excavation floor at 100 m depth of excavation change from a compressive stress of 0.615 MPa pre-excavation, to a tensile stress of 0.755 MPa post excavation. The model indicates development of a tensile horizontal stress zone beneath the excavation floor for all depths of excavation. As indicated in Figure 4.13, the tensile stress zone does not extend behind the excavation face and the magnitude of horizontal tensile stress increases with increasing distance away from the excavation face. Model results indicate that the tensile stress zone below the excavation floor extends to a depth of 35 m - 40 m below the excavation floor with no significant depth increase with increasing depth of excavation. Model results indicate that horizontal stresses at the upper excavation face (upper transect as shown in Figure 4.11) remain compressive throughout all excavation simulations, increasing from a pre-excavation compressive stress of 0.0367 MPa to 0.0502 MPa for an excavation depth of 100 m.
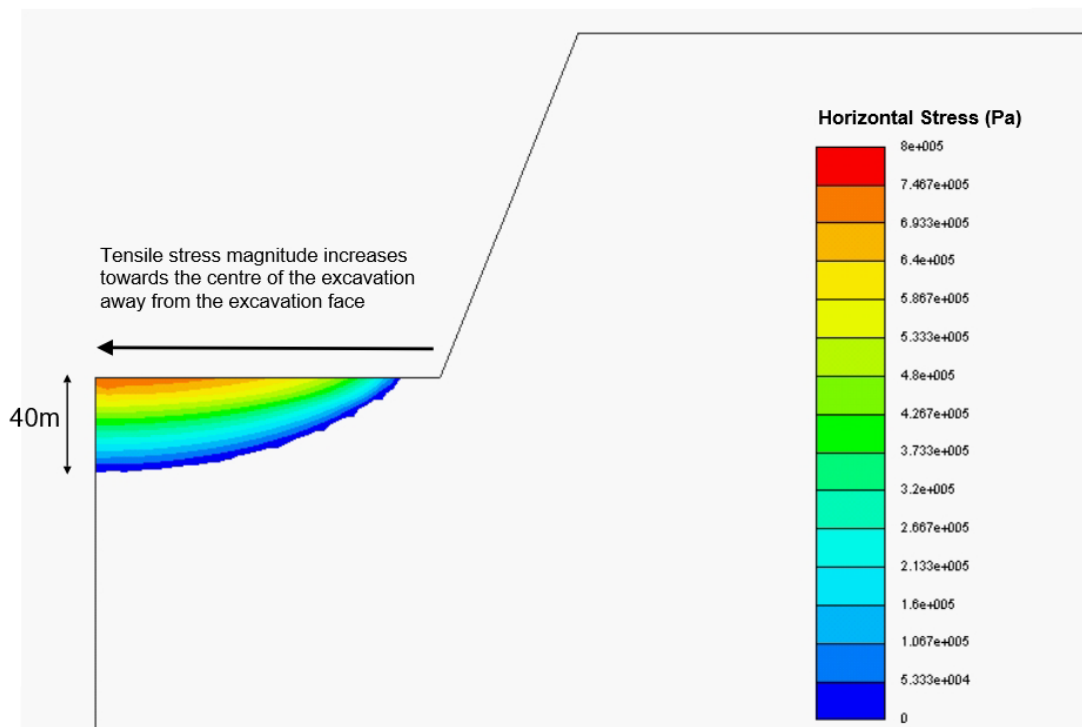
Figure 4.13: Model 1 Excavation floor horizontal tensile stress (Pa) zone at 100 m depth of excavation (k=0.27) showing increasing tensile stress away from the excavation face.

The development of a lateral tensile stress zone at the excavation floor is consistent with the results of previous studies of stress response behind

excavated faces. Stacey (2003) reported that '*relatively limited tensile stress zones occur behind the crest of slopes for in situ stress conditions with k ratios greater than 1.0, and in the floor of the pit for low k values*'.

At low lateral stress there is no tensile stress behind the excavation face. The apparent increase in compressive stress as a result of excavation occurs in response to uplift at the centre of the excavation floor and an associated increase in lateral compression that exceeds any reduction in stress occurring as a result of loss of lateral confinement. The model was re-run with the lateral stress ratio increased from 0.27 to 2.0. Model results for the high lateral stress case demonstrate maintenance of compressive vertical and horizontal stress conditions at the excavation floor but indicate the development of tensile stress conditions, both vertical and horizontal, at the upper elevations of the excavation face, as shown on Figure 4.14.
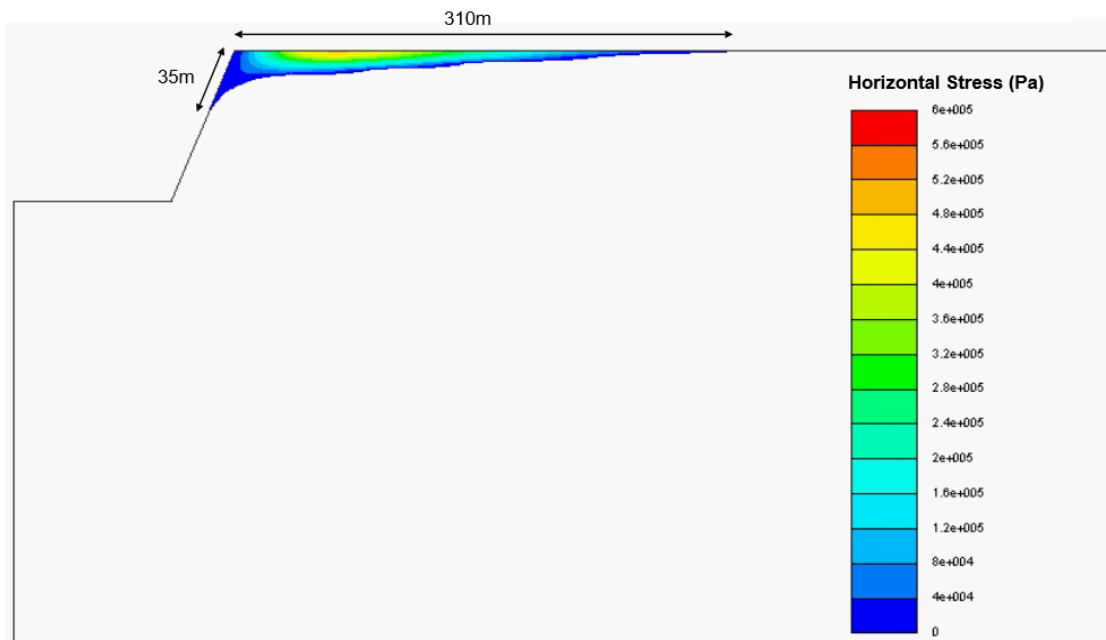
Figure 4.14: Model 1 Excavation face horizontal tensile stress (Pa) zone at 100 m depth of excavation with high lateral stress (k=2.0) showing development of a lateral tensile stress zone behind the excavation face.

Under high lateral stress conditions the vertical stress response at the excavation floor is unchanged. Vertical stress variation at the upper excavation face is reduced from a pre-excavation compressive stress of 0.0546 MPa to a compressive stress of 0.0418 MPa at 100 m depth of excavation. Under the

same high lateral stress conditions, horizontal stress at the excavation floor remained compressive throughout i.e. there is no development of a horizontal tensile stress zone, in contrast to observations at low lateral stress. Excavation floor horizontal stresses remain relatively unchanged with a pre-excavation value of 4.55 MPa and a post-excavation value of 4.59 MPa. As shown in Figure 4.14, horizontal stresses in the excavation face show more significant response with development of a tensile stress zone behind the upper elevations of the excavation face for all excavation depths. Pre-excavation compressive stress of 0.109 MPa in the upper excavation face changes to a tensile stress of 0.026 MPa for an excavation depth of 100 m.

Model results indicate that the lateral and vertical extent of the horizontal tensile stress zone varies with increasing depth of excavation. As summarised in Table 4.3, under high lateral stress conditions, although the tensile stress magnitude is low, tensile stress conditions in the upper sections of the excavation face can extend a significant distance behind the face.

Excavation depth (m)	Max. Tensile Stress (MPa)	Horizontal extent (m)	Vertical extent (m)
30	0.047	40	5
60	0.235	120	15
100	0.507	310	35

Table 4.3: Model 1 Horizontal tensile stress zone magnitude and extents in the excavation face under high lateral stress conditions (k=2.0).

Table 4.3 demonstrates that, under all in-situ stress conditions, the magnitude of the tensile stress that develops in the excavation face is much lower than the tensile strength of the sandstone formation included in the model and conditions for new fracture development do not occur. Tensile strength is specified as 3.8 MPa for the sandstone formation compared with maximum modelled tensile stress of 0.755 MPa for a 100 m deep excavation.

Extensional strains develop in the excavation floor and upper face. With relatively low reduction in vertical and lateral stress, extensional strain

magnitudes are low with a maximum value of 0.00001 at the excavation floor under low lateral stress conditions. Although investigation of rock strength is not the focus of this research, model results indicate an absence of new fracture development under unloading conditions. Stacey (2003) previously reported that critical extensional strain magnitudes at which fracturing might be expected are within the range 0.0001 to 0.0003. Extensional strains developed in the current models are an order of magnitude lower than the levels normally required for fracturing of the rock mass. As discussed in relation to subsequent discontinuity models, the effect of extensional strain is observed as the dilation of pre-existing discontinuities rather than new fracture development.

In common with 3D modelling results, the no-discontinuity models exhibit limited deformation during loading and unloading processes as deformation is dependent on the elastic strain response of a relatively high strength rock. 2D model displacements have been investigated primarily to demonstrate general consistency with 3D modelling results and to confirm that there is an appropriate strain response. With low lateral stress, maximum vertical displacement at the excavation floor is 0.0329 m upwards at an excavation depth of 100 m. Maximum vertical displacement in the upper levels of the excavation face is 0.0195 m. Horizontal displacement just below the excavation floor achieves a maximum magnitude of 0.0020 m at an excavation depth of 100 m with displacement towards the foot of the excavation face. Maximum horizontal displacement outwards away from the upper excavation face is 0.0059 m at an excavation depth of 100 m.

The modelled vertical displacement on the excavation floor is consistent with the development of a horizontal tensile stress zone beneath the floor as a consequence of excavation floor uplift. At low lateral stress, the dominant geomechanical response is uplift of the excavation floor as a consequence of the removal of vertical loading, resulting in differential vertical strain as uplift is greatest at the centre of the excavation and constrained at the base of the excavation face. This type of response creates the potential for tension cracking in the excavation floor as indicated in the limestone quarry example at Figure 4.15. As indicated in Figure 4.16, the combination of uplift at the base of the face and vertical gravitational load at the top of the face results in a minor rotational effect with low magnitude displacement into the upper face.

Figure 4.15: Tension cracking due to quarry floor heave at a 30 m deep quarry excavation in the Lincolnshire Limestone

As indicated schematically in Figure 4.16, at low lateral stress, horizontal tensile stress develops in the excavation floor whilst stresses within the face remain compressive. Uplift in the floor occurs due to reduction in lithostatic load, with differential vertical displacement resulting in the development of horizontal tensile strain and lateral displacement of up to 0.002 m. Displacement at the excavation face is outward, away from the excavation, although displacement magnitude is low.

At high lateral stress, all stresses below the excavation floor remain compressive and excavation floor uplift occurs as both a vertical elastic strain response to unloading plus a tangential strain response due to lateral compression, although the vertical displacement magnitude is consistent under both stress regimes. When compared to the low lateral stress model, there is a more significant change in horizontal displacement with the development of displacement in the excavation face towards the excavation with a maximum magnitude of 0.0140 m, consistent with the development of a tensile stress zone in this area.

LOW IN-SITU LATERAL STRESS (K=0.27)

Excavation floor width 200m

Excavation floor uplift due to elastic response to reduction in lithostatic loading

Tensile stress conditions

0.002m

Displacement away from face a response to uplift parallel to face

0.03m

0.002m 0.002m

Tensile stress zone depth = 20m

Tensile stress zone width =170m

Principal Stress Direction Prior to Excavation

HIGH IN-SITU LATERAL STRESS (K=2.00)

Tensile stress zone width =200m

Tensile stress zone depth = 22m

Excavation floor uplift due to elastic response to reduction in lithostatic loading and lateral compression

Compressive stress conditions

0.014m

Maximum horizontal displacement occurs one-third of face height

0.03m

0.001m 0.001m

All stresses compressive

Principal Stress Direction Prior to Excavation

KEY

0.001m — Displacement direction and magnitude

Compressive stress direction

Tensile stress direction

CONCEPTUAL INTERPRETATION OF EXCAVATION RESPONSE TO LITHOSTATIC UNLOADING FOR HIGH AND LOW IN-SITU STRESS CONDITIONS

Figure 4.16: Model 1 Conceptual interpretation of lateral confining stress influence on excavation response. Schematic illustration represents modelled geometry with excavation floor width of 200 m at an excavation depth of 100 m. The upper diagram shows development of tensile stress in the excavation floor with all stresses remaining compressive in the face. Under high lateral stress conditions, as shown in the lower diagram, stresses in the floor remain compressive whilst a tensile stress zone develops behind the face.

With high lateral stress, the small magnitude lateral displacement away from the excavation face is lower than the lateral displacement resulting from loss of lateral containment at the excavation face, resulting in a net inward displacement into the excavation.

The above analysis has significance when considering the potential effect of excavation unloading on pre-existing discontinuities below and behind an excavation. Under low lateral stress conditions, with a tensile stress response below the excavation floor there may be greater potential for dilation of sub-vertical discontinuities than would be observed under higher lateral stress conditions when sub-floor stresses remain compressive. Similarly, under higher lateral stress conditions there would be greater potential for dilation of discontinuities parallel to the excavation face than would be the case under low lateral stress conditions.

4.3.1.2   Excavation disturbed Zone (EdZ) extents

As discussed at Section 4.1.2, EdZ extents have been defined by reference to the model stress response in both the vertical and horizontal directions. EdZ limits are established at a distance at which post-excavation excavation stress returns to at least 95% of the pre-excavation gravitation stress, supported by analysis of directional displacement plots where necessary. EdZ limits for the no discontinuity model are presented in Table 4.4.

At greater excavation depth, model results indicate that the lateral extent of the EdZ is greater in the upper face (20 mbgl) than the lower face (90 mbgl). The vertical extent of the EdZ is greater under low lateral stress. Defined vertical EdZ extent at high lateral stress is approximately 70% of the magnitude of the vertical EdZ extent at low lateral stress. Under high lateral stress, lateral compression effectively results in potential for increased vertical strain response to unloading with the same total displacement achieved over a shorter distance.

Lateral Stress ratio (k)	Excavation depth (mbgl)	Limit of EdZ Below Exc. Floor Vertical (m)	Limit of EdZ Horizontal Upper Face (m)	Limit of EdZ Horizontal Lower Face (m)
k=0.27	30	290	299	n/a
	60	415	421	n/a
	100	491	770	120
k=2.0	30	265	290	300
	60	366	380	405
	100	440	785	450

Table 4.4: Model 1 EdZ vertical and horizontal extents defined at 95% gravitational stress. (n/a = no inward displacement – increase in horizontal compressive stress). Location of upper and lower face transects shown on Figure 4.11.

The 2D model results for the extent of the EdZ are comparable to the results obtained from 3D modelling, as presented in Table 4.1. Vertical EdZ extents derived from 2D modelling average approximately 70% of 3D model results for low lateral stress. The horizontal EdZ extents under low lateral stress conditions are the same in both 2D and 3D models, whilst under high lateral stress, the horizontal EdZ extents in the 2D model is 20% higher than in the 3D models. As with 3D modelling, the extent of the lateral disturbed zone behind the excavation face is significantly more sensitive to depth of excavation than the vertical extent of the disturbed zone beneath the excavation floor. At low lateral stress, the vertical extent of the EdZ is approximately 25% greater than under high lateral stress. The horizontal EdZ extent in the upper face is relatively insensitive to variation in lateral stress.

4.3.1.3 Rock mass displacement

Deformation magnitudes and extents in three-dimensions were derived from the 3D no-discontinuity model as detailed in Table 4.1. Analysis of 2D model outputs indicates the rate at which rock mass displacement reduces with increasing distance from the excavation floor and face, as shown in Figure 4.17 for a low lateral stress ratio of 0.27.

Maximum vertical displacement at 100 m depth of excavation is approximately 0.02 m, reducing to 0.007 m for a shallower 30 m deep excavation. Rock mass displacements reduce with increasing distance beneath the excavation floor towards the lower domain boundary condition which is defined as zero vertical displacement. Inflection in the plotted displacement lines could be considered indicative of the point at which boundary conditions exert dominant control over displacement magnitudes. 2D model vertical displacement magnitudes are up to twice the magnitude observed in the 3D model, although displacement magnitudes are low in both models. The difference is due to the higher degree of freedom available in the 2D 'plane strain' model, when there are no lateral constraints in the third dimension.
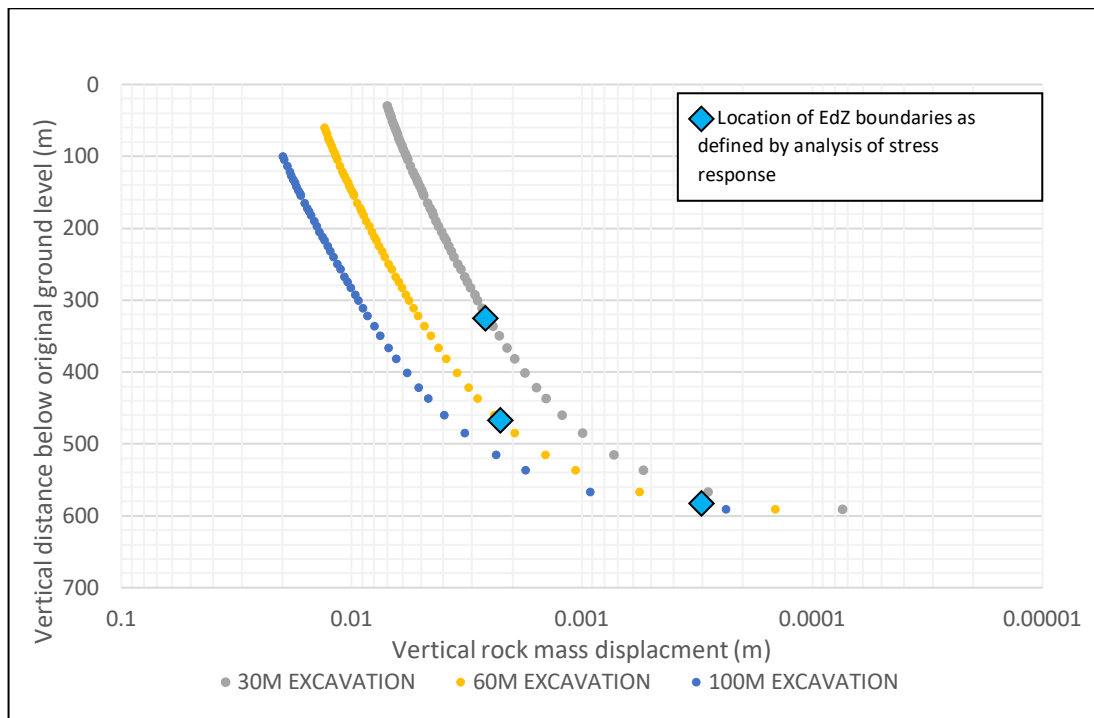
Figure 4.17: Model 1 Vertical rock mass displacement with increasing distance from the excavation floor for excavation depths of 30 m, 60 m and 100 m. EdZ extents shown as blue diamonds (k=0.27).

Analysis of vertical displacement variation with distance from the excavation floor demonstrates a good fit to an exponential function to a depth of approximately 400 m below original ground level, after which the trend becomes linear. The change from an exponential to a linear trend, which is clearly shown on a semi-log plot in Figure 4.17, is attributed to the effect of boundary conditions.
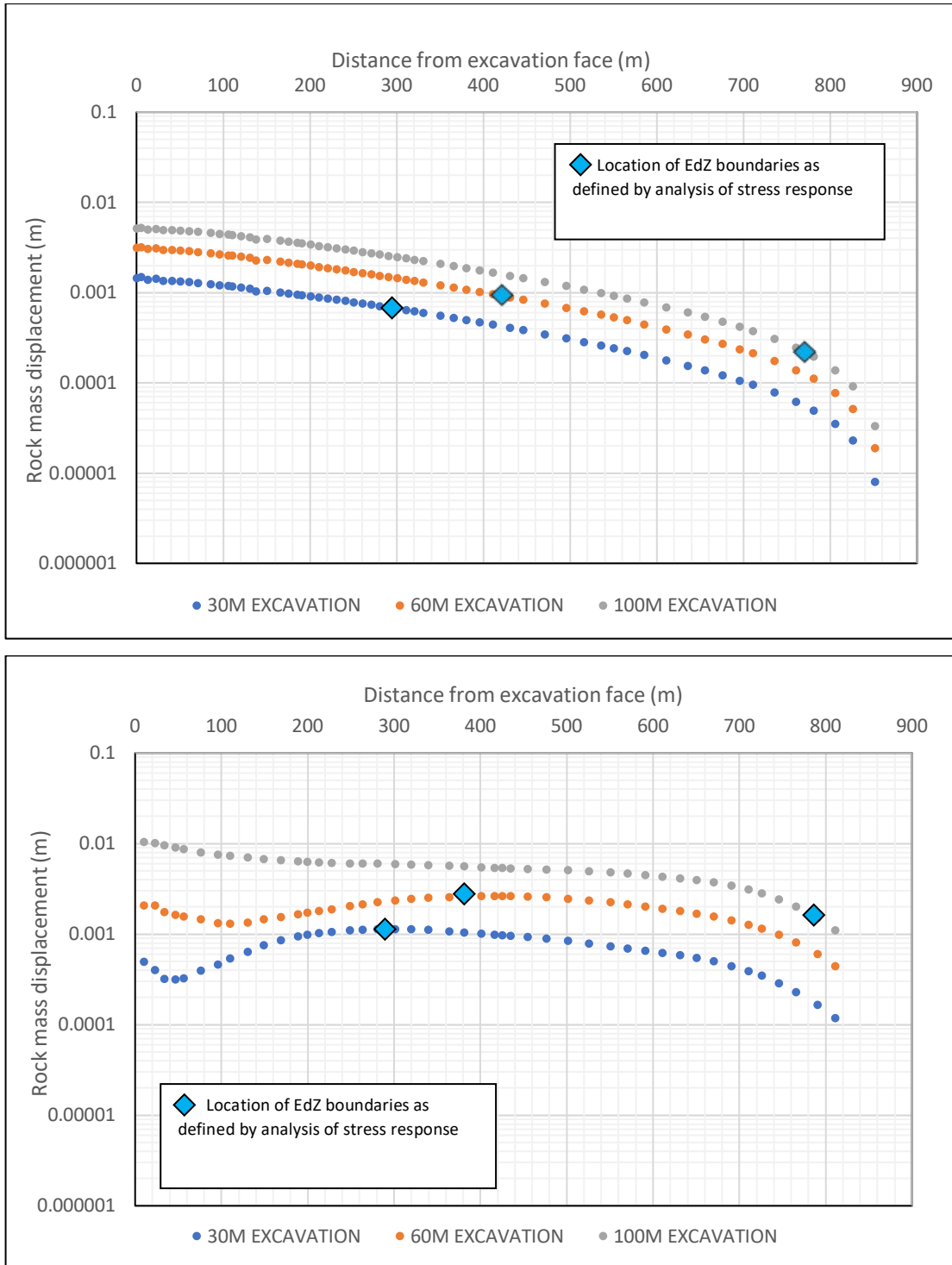
Figure 4.18: Model 1 Horizontal rock mass displacement behind excavation face. Upper plot shows displacement with lateral stress ratio of 0.27. Lower plot shows displacement with lateral stress ratio of 2.00. Displacement rate of change with distance from the face is generally consistent for all depths of excavation. Under high lateral stress conditions displacement magnitude shows lower change with increasing distance from the face.

For horizontal displacement, the potential influence of displacement boundary conditions is less clear but has generally been interpreted as the point at which the displacement -v- distance relationship becomes linear. In Figure 4.17, the stress-based limits of the EdZ are approximately coincident with a change in gradient in the displacement curves.

Model results for horizontal displacement behind the upper face are shown in Figure 4.18 for lateral stress ratios of 0.27 and 2.0. Under low lateral stress conditions the model results indicate net outward displacement away from the excavation face as the lateral component of excavation floor uplift exceeds the lateral strain resulting from loss of lateral constraint at the excavation face. The displacement magnitudes for a lateral stress ratio of 0.27, as shown in Figure 4.18, refer to outward displacement away from the open face.

The net lateral displacement away from the excavation face, with low lateral stress conditions, is shown more clearly in the XY displacement vector plot where a lateral component of displacement into the face is apparent. The vector plot is presented as Figure 4.19. Vector displacement for the high lateral stress condition is also shown in Figure 4.19. High lateral stress results in net displacement inwards into the excavation as shown.

Under high lateral stress conditions, there is net inward displacement towards the open excavation face at all excavation depths with an order of magnitude increase in displacement magnitude and a reversal of direction when compared to the low lateral stress case. Lateral EdZ extents for the high lateral stress situation are defined in Table 4.4 as distances of 290 m, 380 m and 785 m from the open excavation face. These distances approximately correspond with a change in gradient on respective graphs in Figure 4.18 representing the distances at which model boundary conditions begin to influence results.
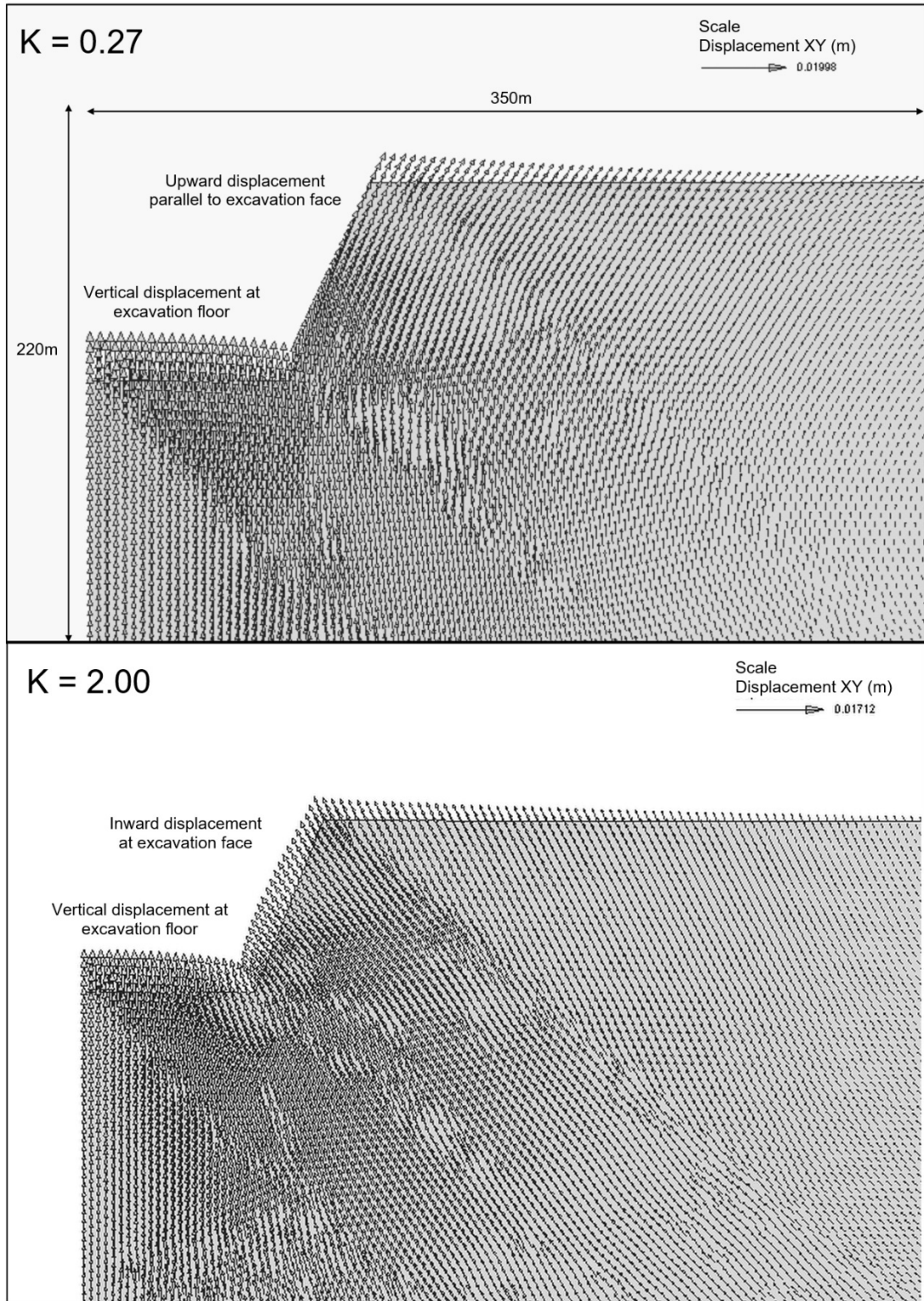
Figure 4.19: Model 1 Vector plot to show displacement direction and magnitude under low and high lateral stress conditions. The figure shows upward displacement at the excavation floor and at depth beneath the floor under both stress conditions. At the excavation face, displacement is parallel to the face with a horizontal component outward, away from the excavation under low lateral stress conditions but inward into the excavation under high lateral stress conditions.

Modelling results for models without discontinuities has demonstrated that the stress/strain response to excavation is consistent with expectations based on previous studies by others (Goodman 1989, Stacey 2003) and that at the relatively shallow depths modelled, the magnitude of the elastic strain response is consistently low. Although results indicate that a definable EdZ could extent for several hundred metres beneath the excavation floor and behind the excavation face, the magnitude of displacement is consistently low with a maximum vertical displacement at the excavation floor of just 2cm at maximum excavation depth of 100 mbgl. Model 1 (No-discontinuities) demonstrates that in the unrealistic situation of having no bedding, joints or fracturing to a depth of 100 mbgl, the geomechanical response of the rock mass to excavation is purely a function of low magnitude rock mass strain in response to unloading. Subsequent modelling investigates the effect of introducing pre-existing discontinuities into the model domain.

Conclusions from the excavation unloading model without discontinuities (Model 1) can be summarised as follows:

o   Lateral tensile stress zones develop in the excavation floor at low lateral stress and behind the excavation face at high lateral stress;

o   Lateral extensional strain develops in the excavation floor and upper face;

o   Vertical EdZ extents are greater under low lateral stress conditions;

o   Horizontal EdZ extent is relatively insensitive to variation in lateral stress;

o   Rock mass displacements result from extensional strain only.

4.3.2 Model 2: Model with sub-horizontal bedding planes

Model 2 introduces multiple sub-horizontal bedding planes into the model. Bedding planes reflect the sandstone bedding configuration at Blaxter Quarry with a dip angle of 5° to the horizontal with the dip direction corresponding to the modelled plane. Bedding planes are included at 10 m spacing in the upper

sections of the model, increasing to a maximum of 40 m spacing at depth. Model configuration is shown in Figure 4.20.
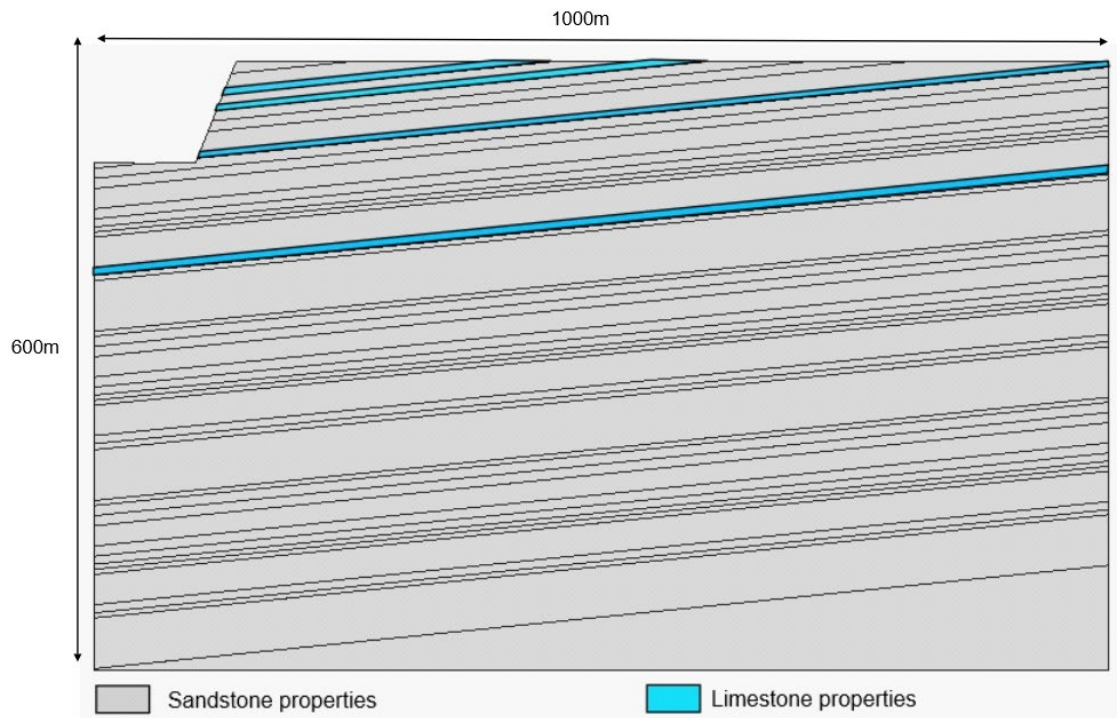
Figure 4.20: Model 2 Bedding plane model configuration showing the location of bedding planes and the location of limestone beds. Bedding planes dip at an angle of 5° towards the left model boundary with several bedding planes intersecting the excavation face and floor. The model domain dimensions remain 1000 m x 600 m.

The majority of the material within the model domain is designated 'Blaxter sandstone', but the model includes several interbedded limestone layers representing the generalized lithology of the geological sequence within which the Blaxter sandstone unit is located, as indicated in Figure 4.20. All bedding planes are designated as discontinuities and have discrete contact properties assigned as detailed in Chapter 3. In comparison to the 'no-discontinuities' model, the bedding plane model therefore incorporates two changes (i) inclusion of discontinuities, and (ii) lithological variation. Respective sandstone and limestone properties are detailed at Chapter 3.

4.3.2.1   Stress response

Model results with low lateral stress indicate that, with pre-existing bedding planes, the stress reduction observed at the excavation floor and face is slightly greater than without any discontinuities. However, in contrast to the no-discontinuity model, there is no development of lateral tensile stress beneath the excavation floor. As discussed below, vertical displacement in the bedding model (Model 2) occurs due to a combination of extensional strain and cumulative dilation of bedding planes, precluding the development of tensile stress conditions.

At an excavation depth of 100mbgl, the maximum stress reduction at the excavation floor is 2.37 MPa compared to 2.31 MPa without discontinuities. The horizontal stress at the excavation face decreases by 0.18 MPa compared to an increase of 0.135 MPa without discontinuities. The increase in stress reduction in the bedding plane model (Model 2) is attributed to the presence of higher density limestone units that are absent from the no-discontinuity model (Model 1). The introduction of limestone horizons with a slightly higher density increases pre-excavation load by approximately 2% at each excavation stage. This change approximates to the observed 2.5% increase in stress reduction at the excavation floor when compared to the no-discontinuity model (Model 1).

The effect on the stress response of introducing bedding plane discontinuities can be seen by comparison of the pre and post-excavation vertical stress profile for the no-discontinuity model (Model 1) and the bedding plane model (Model 2), as shown in Figure 4.21. The presence of dipping bedding planes results in an increase in shear stress in a down-dip direction with associated reduction in vertical compressive stress. This variation is enhanced in the stress response to a 100 m deep excavation as the vertical stress profile departs from the linear no-discontinuity (Model 1) response. The attenuated vertical stress response is consistent with the development of a shallower EdZ, as discussed at Section 4.3.2.2.
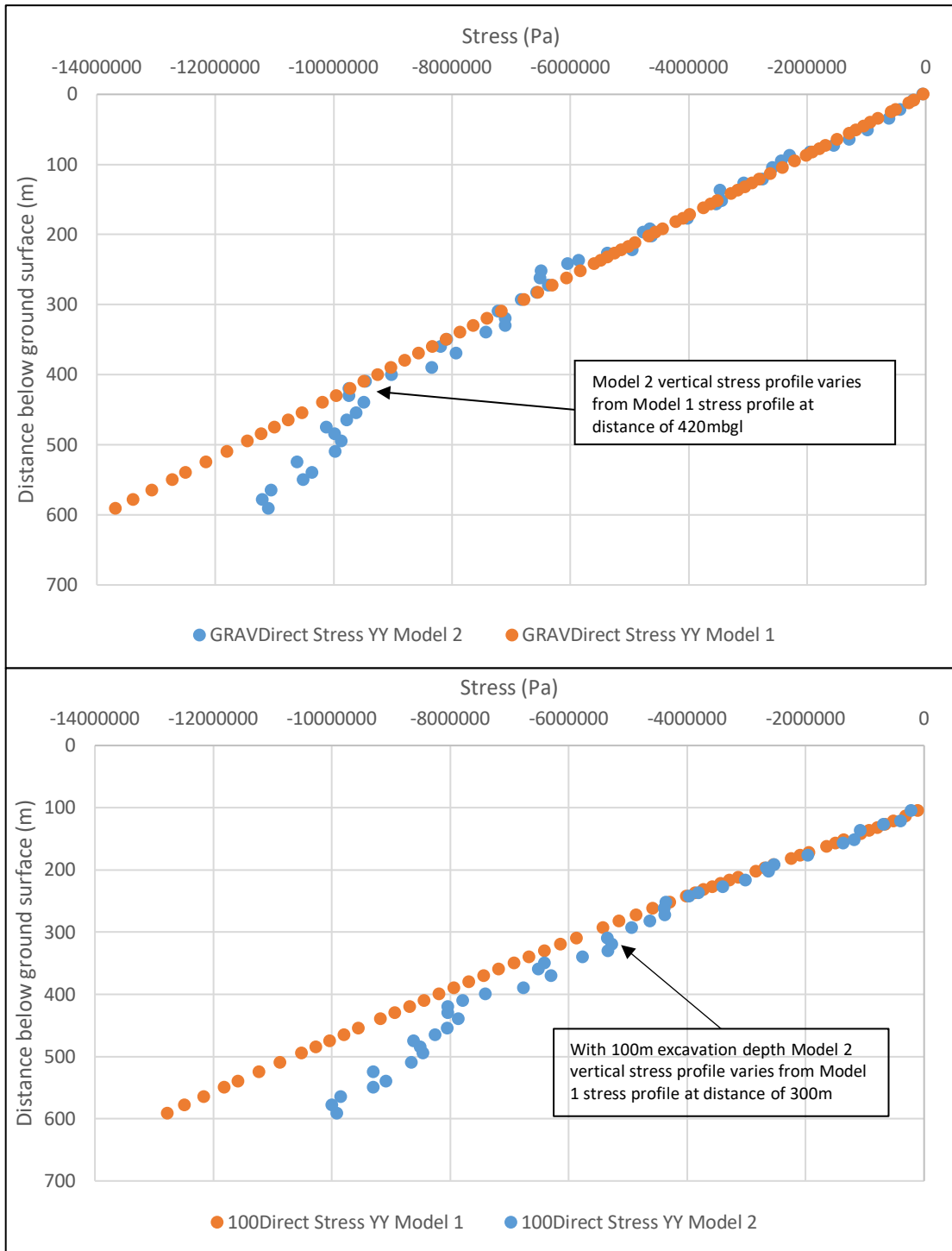
Figure 4.21: Vertical stress profile comparison between the no-discontinuity model (Model 1) and the bedding-only model (Model 2). Upper graph shows stress profile at the end of gravitational initialization indicating lower stress in Model 2 below 420 m depth. Lower graph shows stress profile for a 100 m deep excavation with variation from gravitational stress profile at a depth of approximately 200 m below the excavation floor.
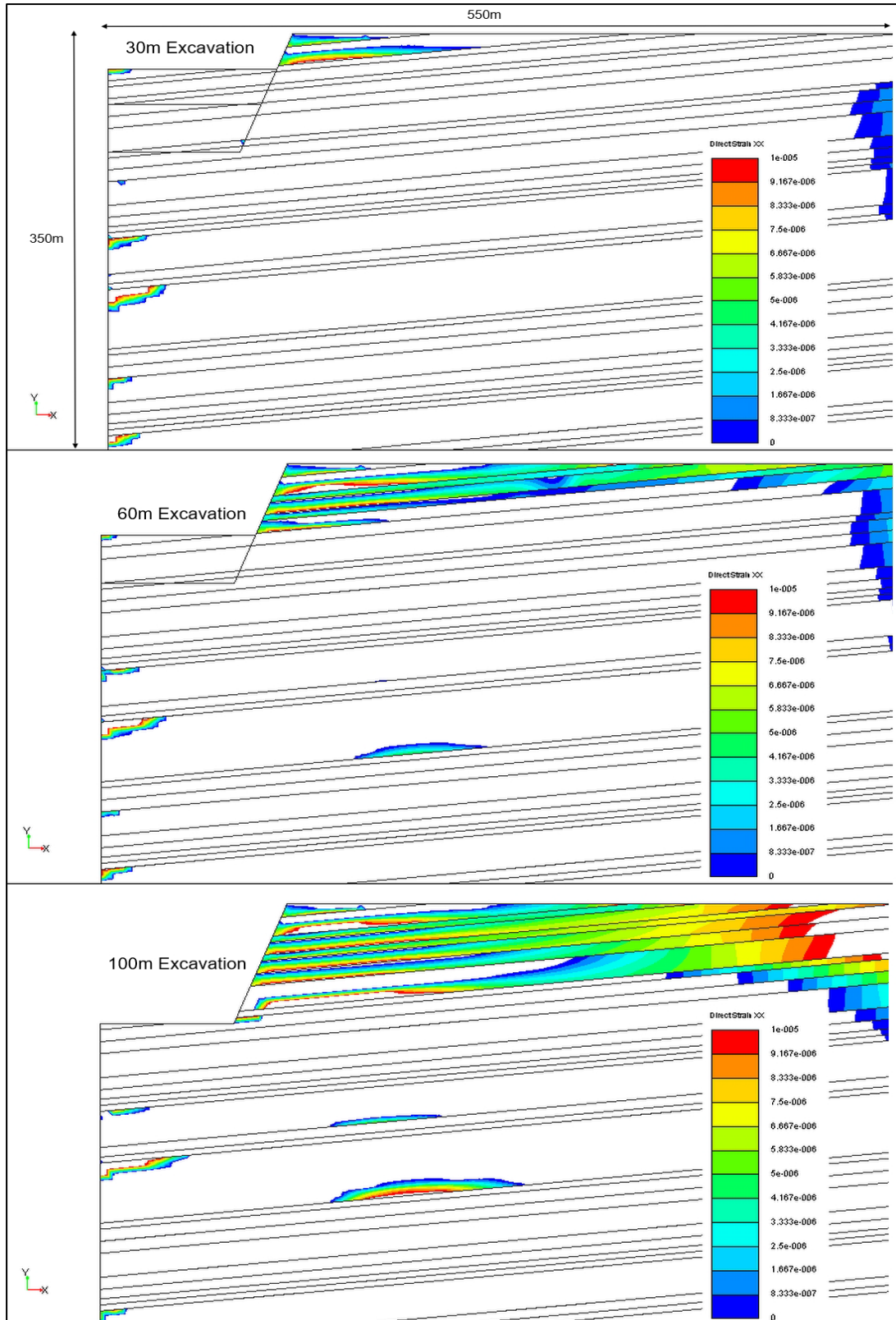
Figure 4.22: Model 2 Development of horizontal extensional strain zones behind the excavation face for increasing depth of excavation under low lateral stress conditions (k=0.27). Highest strain occurs at upper bedding plane surfaces.

Model results demonstrate the presence of lateral extensional strain in the lower section of each lithological unit extending from the open face across the model domain, although potentially influenced by no-displacement boundary conditions at the domain extremity. As shown in Figure 4.22 for the low lateral stress case, extensional strain zones are bounded by successive discontinuities. However, strain magnitude remains low, ranging from 1.92E-06 at the top of the excavation face to a maximum of 4.61E-05 at the base of the excavation face. There is no lateral extensional strain zone in the excavation floor. Low magnitude vertical extensional strain occurs below the floor and behind the face.

The lateral extensional strain zones are related to extension at upper bedding plane surfaces that daylight in the open excavation face where loss of lateral constraint occurs. Although in this model the lateral extent of extensional strain increases with depth, it is apparent that extensional strain extents will be influenced by bedding dip and direction. The highest lateral strain magnitude occurs above the bedding plane surface, indicating differential strain across individual lithological units.

Reference to Figure 4.22 demonstrates that lateral extensional strain conditions do not develop across the full thickness of each lithological unit behind the excavation face. The upper section of each lithological unit remains compressive (white areas on Figure 4.22). Extensional strain in the rock mass occurs in response to elastic shear strain at bedding plane surfaces with strain magnitude influenced by increasing vertical loading and frictional resistance in a down-dip direction.

The magnitude of vertical stress reduction at the excavation floor, at 100 m depth of excavation, decreases from 3.58 MPa under low lateral stress conditions to 1.93 MPa under high lateral stress conditions. However, horizontal stress reduction at the excavation face increases from 0.18 MPa under low lateral stress to 0.32 MPa under high lateral stress. As with Model 1, under high lateral stress conditions, a lateral tensile stress zone develops behind the upper excavation face. Tensile stress extents at 100 m depth of excavation are illustrated in Figure 4.23. As with the extensional strain zones in Figure 4.22, lateral stress remains compressive in the upper sections of

each lithological unit behind the excavation face away from the area of maximum elastic shear strain at bedding plane surfaces.
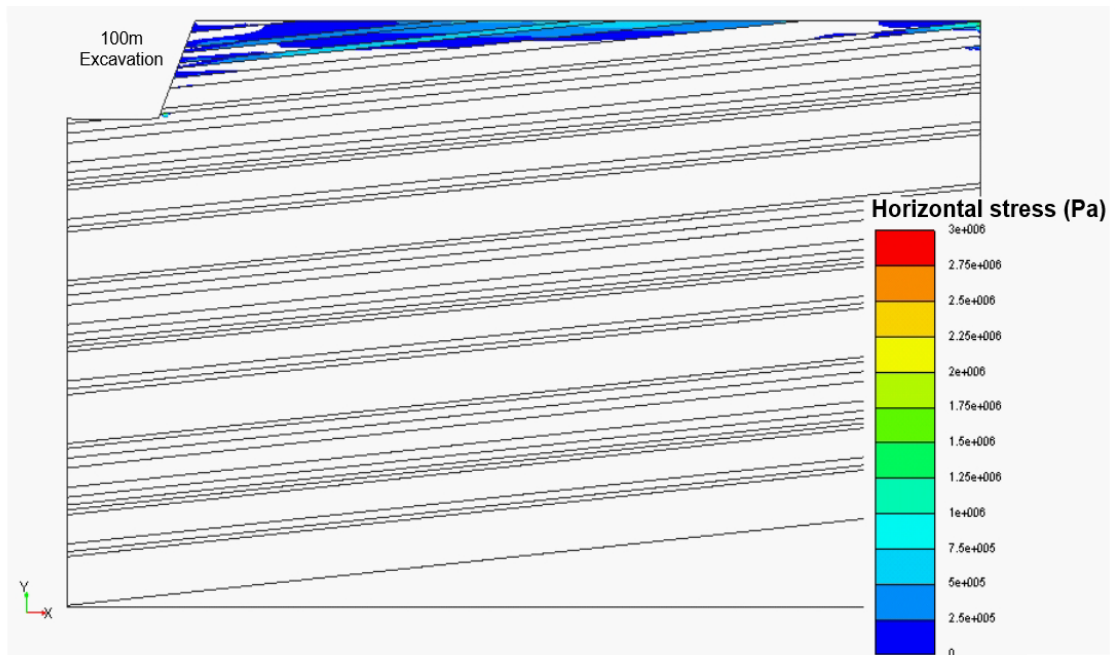
Figure 4.23: Model 2 Tensile stress development behind excavation face at 100m excavation depth under high lateral stress conditions (K=2.0). Horizontal tensile stress zone behind the excavation face primarily occurs behind the upper face and is less influenced by the presence of bedding planes than observed in relation to the extensional strain response (see Figure 4.22)

4.3.2.2   Excavation disturbed Zone (EdZ) extents

The vertical and lateral extents of the EdZ with bedding planes included in the model (Model 2) have been defined by reference to vertical and lateral stress change in relation to pre-excavation stress magnitude, as discussed in relation to Model 1. Summary results are presented in Table 4.5.

When compared to the no-discontinuity model (Model 1), the introduction of bedding plane discontinuities throughout the model has the effect of decreasing the vertical and lateral extent of the EdZ. Under low lateral stress, the vertical extent of the EdZ is decreased by an average of 20% and there is less extensive development of a horizontal disturbed zone than in the no-discontinuity model (Model 1). Under high lateral stress, the impact of bedding

plane discontinuities is significantly reduced and EdZ extents, both vertically and horizontally, tend towards the no-discontinuity extents.

Lateral Stress Ratio (k)	Excavation depth (mbgl)	Limit of EdZ Below Exc. Floor Vertical (m)	Limit of EdZ Horizontal Upper Face (m)
k=0.27	30	245	220
	60	390	375
	100	490	780
k=2.0	30	265	258
	60	337	386
	100	452	850

Table 4.5: Model 2 EdZ vertical and horizontal extents under high and low lateral stress conditions for excavation depths of 30 m, 60 m and 100 m.

The general reduction in EdZ extents with bedding plane discontinuities present can be attributed to the increased mobility of the rock mass and associated dissipation elastic strain over a shorter distance as discontinuity stiffness is lower than rock mass stiffness. Model 2 demonstrates that, in general, the introduction of discontinuities reduces the EdZ area around the excavation.

4.3.2.3 Rock mass displacement

With low lateral stress, rock mass displacement due to lithostatic unloading is dominantly vertical although there is a lateral component resulting from loss of containment at the excavation face. Vertical displacement occurs as an elastic strain response in the rock mass and associated dilation of bedding planes as normal compressive stress is reduced. Lateral displacement inwards towards the excavation occurs as an extensional strain response to loss of lateral containment plus a degree of movement on discontinuity surfaces that are dipping at 5° to the horizontal.

The potential for movement on bedding plane surfaces increases rock mass mobility, allowing lateral movement towards the excavation that exceeds the uplift related displacement away from the face that is observed in the no-discontinuity model (Model 1). The variation in vertical rock mass displacement beneath the excavation floor for each of the three simulated depths of excavation is shown graphically as Figure 4.24.
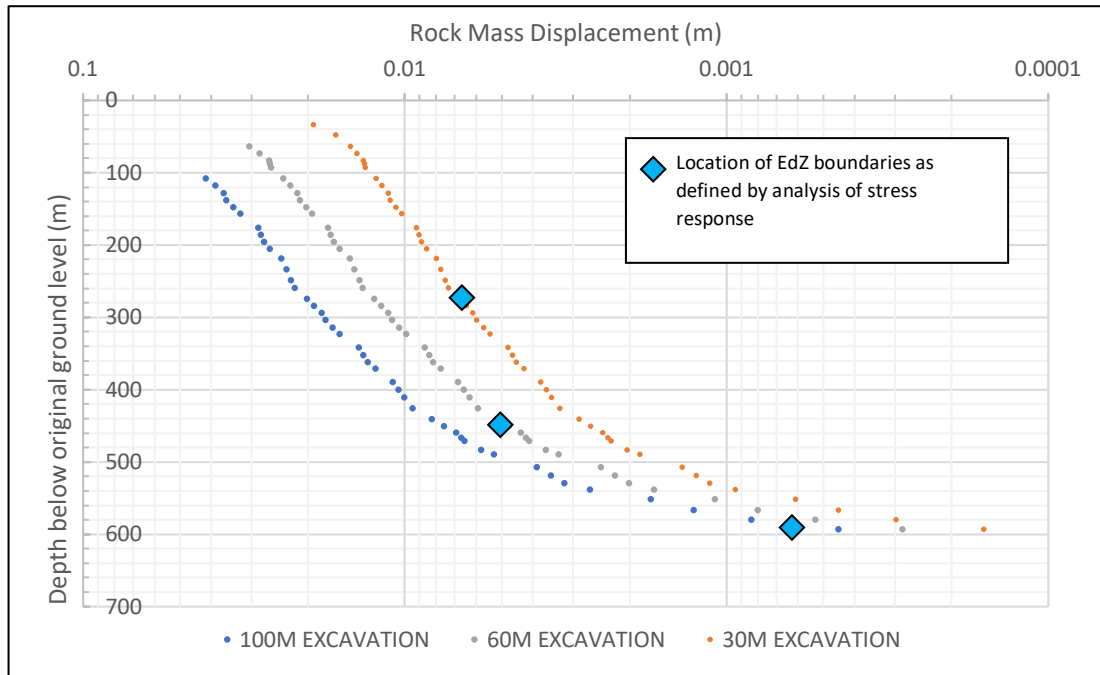
Figure 4.24: Model 2 Vertical rock mass displacement (k=0.27) for excavation depths of 30 m, 60 m and 100 m. Blue diamonds indicate the limits of the EdZ as defined by stress analysis.

Model results demonstrate that, under low lateral stress, vertical displacement at the excavation floor increases from 1.92 cm at a 30 m depth of excavation to 4.10 cm at 100 m depth of excavation. Figure 4.24 shows the stress based EdZ extents in relation to displacement variation with distance from original ground level. EdZ extents approximately coincide with a change in gradient on each displacement curve, indicating probable boundary influence, as discussed in relation to Model 1. The observed vertical displacement is approximately twice the displacement magnitude observed without discontinuities (Model 1).
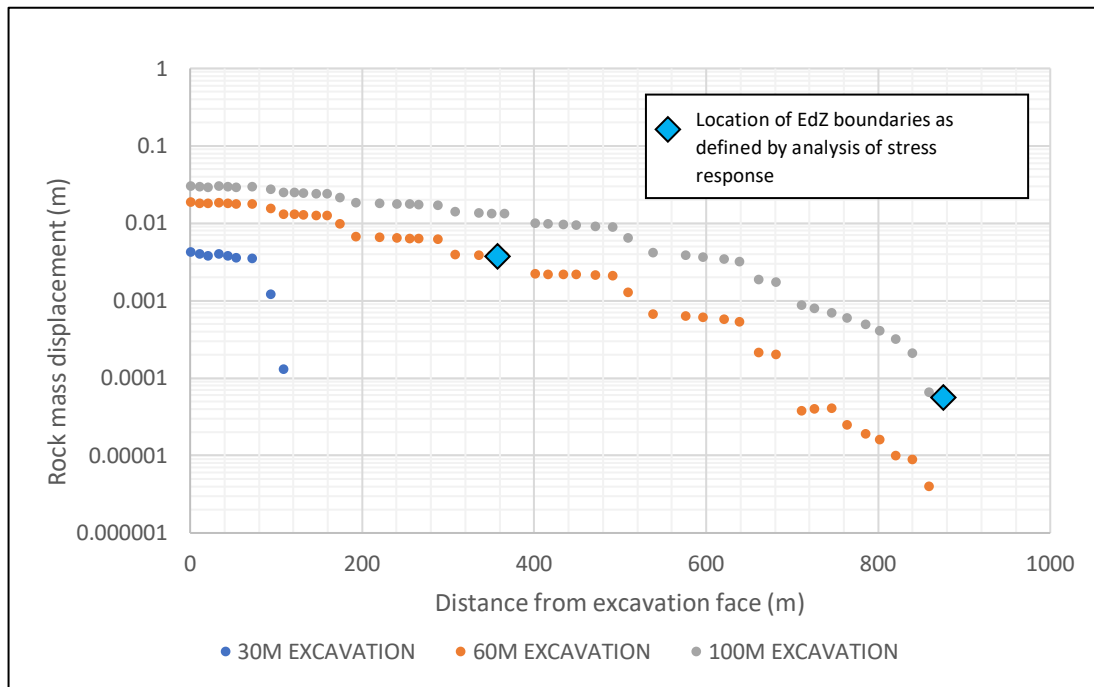
Figure 4.25: Model 2 Lateral rock mass displacement towards the upper excavation face (k=0.27) for excavation depths of 30 m, 60 m and 100 m. Displacement decreases from a maximum magnitude of 4 mm, 18 mm and 29 mm at the face for excavation depths of 30 m, 60 m and 100 m respectively. For the 30 m deep excavation there is no definable displacement beyond 108 m from the excavation face.

Lateral displacement in the upper excavation face, under both low and high lateral stress conditions, are shown graphically in Figure 4.25 and Figure 4.26 respectively. As indicated on Figure 4.26, lateral displacement behind the excavation face is influenced by the presence of bedding, with maximum displacement occurring in individual lithologic units by shear displacement or sliding at the unit base. Analysis of model results demonstrates that lateral displacement in the excavation face occurs through a combination of extensional rock mass strain and bedding plane contact sliding. In the 100 m depth example, contact plane sliding accounts for approximately 80% of modelled displacement at the bedding plane. Analysis of model results demonstrates that shear failure is occurring on bedding planes within approximately 50 m of the excavation face (100 m deep excavation), as shear stress exceeds discontinuity cohesion, with elastic shear displacement occurring at greater distance from the face.
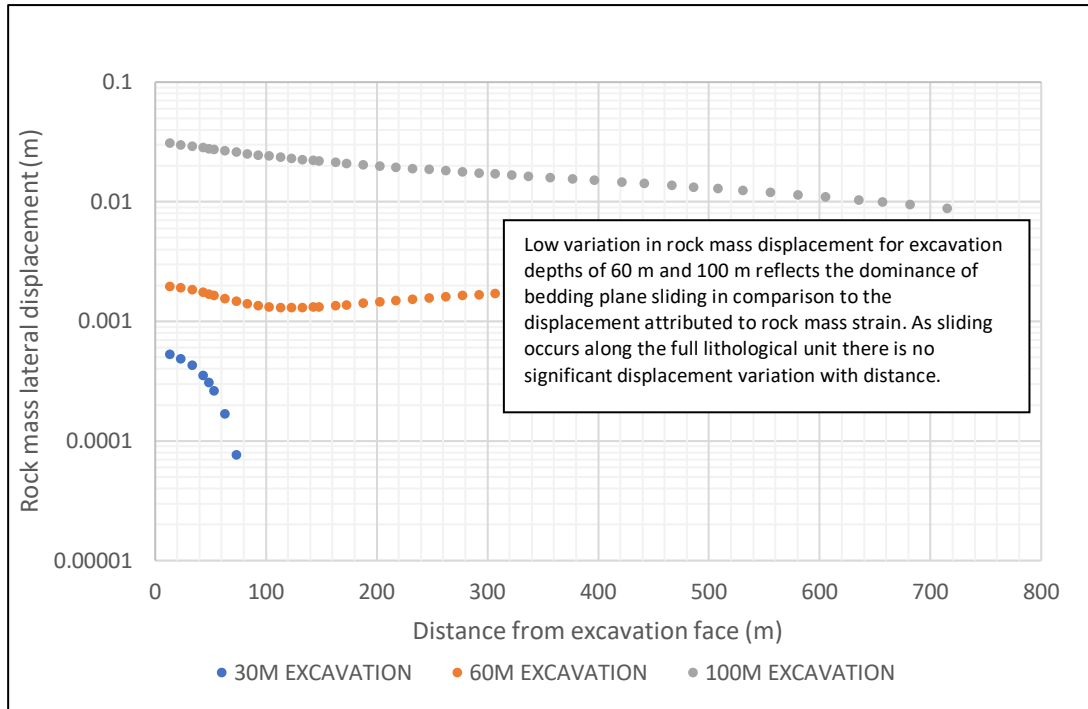
Figure 4.26: Model 2 Lateral rock mass displacement in upper face at high lateral stress (k=2.0). Compared to the low lateral stress results shown in Figure 4.24, this figure shows minor reduction in displacement magnitude with increasing distance from the face, confirming the dominance of bedding plane sliding under high lateral stress conditions.

Under high lateral stress, horizontal displacement towards the open excavation face decreases at a lower rate than under low lateral stress with increasing distance from the face, as expected. Lateral displacement extents, prior to potential boundary influence, are broadly consistent with EdZ extents defined by stress analysis, as summarized in Table 4.5, although there is no definable lateral displacement after a distance of 85 m from the face in response to a 30 m excavation depth, compared to a predicted EdZ extent of 258 m. Displacement at the excavation face increases from approximately 0.05 cm in response to a 30 m deep excavation to approximately 3 cm in response to a 100 m deep excavation. The maximum displacement magnitude at 30 m excavation depth is comparable to that observed in the no-discontinuity model (Model 1) but the displacement magnitude at 100 m excavation depth is approximately 3 x that observed without discontinuities. This variation is attributed to increasing magnitude of sliding on bedding plane surfaces with increasing depth of excavation.

Bedding planes that intersect the face are unconstrained at both ends with regard to displacement. Individual beds are therefore free to move in response to changes in the stress regime, once shear stress exceeds bedding plane cohesion, subject to frictional resistance. In the 100 m deep excavation case, shear stress at the base of the excavation face is 2.61 MPa compared to a bedding plane cohesion of 2 MPa. Lateral displacement is greatest at the base of each bed and differential displacement occurs across each bedding plane.

4.3.2.4 Discontinuity dilation

As discussed at Chapter 3, discontinuity dilation has been calculated for each bedding plane by reference to discontinuity normal penetration values. As all penetration directions remained constant throughout the four stages of modelling the difference between the penetration magnitude at the end of each phase, and the penetration achieved at gravity initialization, can be used as a proxy for discontinuity dilation. Vertical bedding plane discontinuity dilation results are presented as Figure 4.27 for each of the three stages of excavation.

The analysis indicates maximum bedding plane dilation of approximately 2.70 mm just below the excavation floor in response to a 100 m deep excavation. For shallower excavation depths of 30 m and 60 m the maximum dilation is approximately 1.50 mm and 2.00 mm respectively. Bedding plane dilation magnitude reduces in accordance with a power law function over a depth of up to 60 m below the excavation floor (100 m deep excavation) and then declines rapidly at greater depth. The results demonstrate that that the most significant bedding plane dilation occurs within a relatively short distance beneath the excavation floor, in contrast to rock mass displacement which decreases over much greater depth.

Under high lateral stress conditions bedding plane dilation magnitude beneath the excavation floor is slightly reduced with magnitudes of 1.4 mm, 1.7 mm and 2.3 mm for excavation depths of 30 m, 60 m and 100 m respectively. The high lateral stress results are presented as Figure 4.28. The high lateral stress dilation response can be defined by the same power law equations derived for the low lateral stress results. The curves are the same shape but are displaced slightly to the right, representing lower magnitude dilation values.
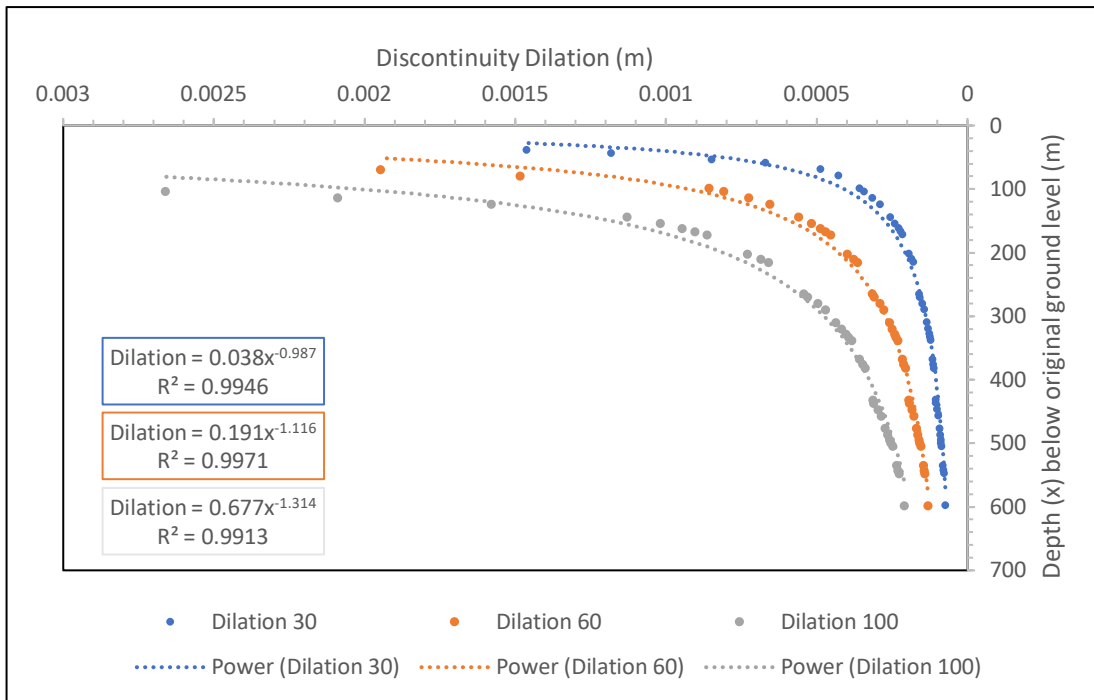
Figure 4.27: Model 2 Bedding plane dilation in response to excavation at depths of 30 m, 60 m and 100 m under low lateral stress conditions (k=0.27). The results, which approximate to a power law fitting as shown, demonstrate relatively small change in dilation magnitude below depths of 35 m, 40 m and 60 m for excavation depths of 30 m, 60 m and 100 m respectively.
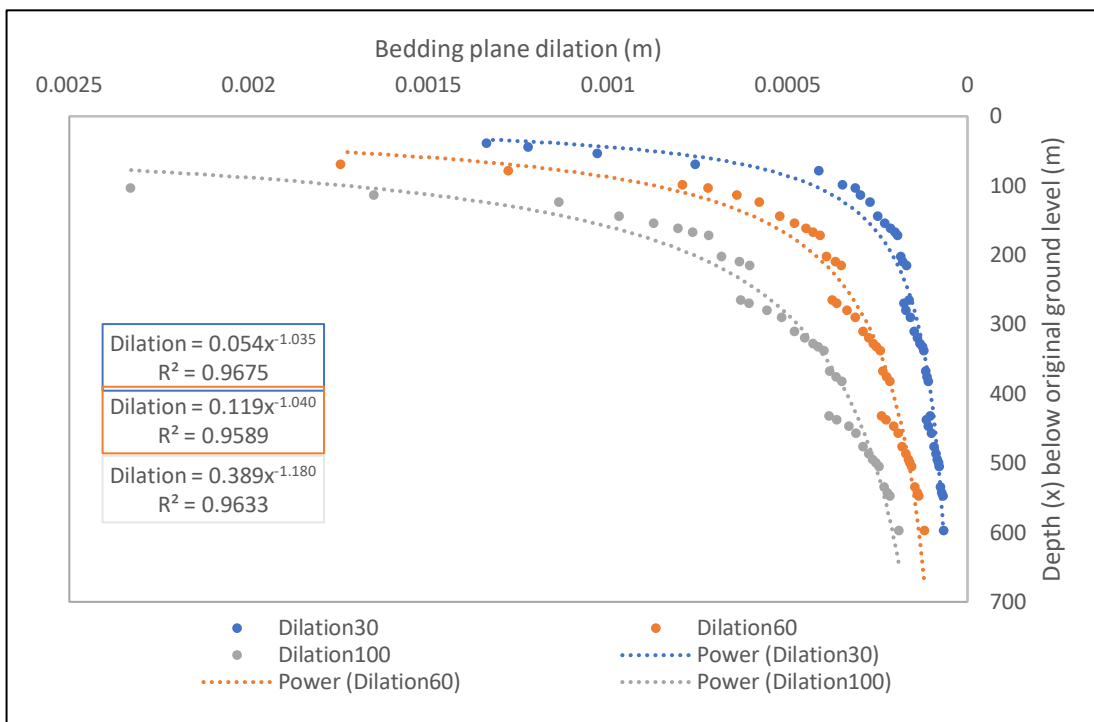
Figure 4.28: Model 2 Bedding plane dilation in response to excavation under high lateral stress conditions (k=2.0) showing power law fittings at excavation depths of 30 m, 60 m and 100 m.

Variation in dilation magnitude follows a clear power law trend in relation to distance below the excavation floor. Dilation variation equations for each excavation depth and in-situ stress condition have been derived as indicated below. Dilation magnitude is defined in relation to distance from the excavation floor or face (x). Dilation magnitude is proportional to the reciprocal of the distance (x) from the excavation floor.

Low in-situ stress (k=0.27)

30m excavation depth   -   Dilation = $0.038x^{-0.987}$

60m excavation depth   -   Dilation = $0.171x^{-1.116}$

100m excavation depth   -   Dilation = $0.677x^{-1.314}$

High in-situ stress (k=2.0)

30m excavation depth   -   Dilation = $0.054x^{-1.035}$

60m excavation depth   -   Dilation = $0.119x^{-1.040}$

100m excavation depth   -   Dilation = $0.389x^{-1.180}$

Analysis of total vertical displacement components is undertaken by reference to maximum rock mass displacement and cumulative dilation beneath the excavation floor. The results are presented in Table 4.6 for each depth of excavation.

Excavation depth (mbgl)	Modelled displacement (m)	Total cumulative dilation (m)	Dilation % displacement
30	0.01925	0.01088	57
60	0.03047	0.01531	50
100	0.04157	0.02184	53

Table 4.6: Bedding plane dilation % of total displacement

The cumulative dilation results in Table 4.6 suggest that the average rock mass strain component of displacement contributes approximately 50% of

total vertical displacement below the excavation floor. To achieve this, intact rock strains within the range 0.000015 to 0.000039 would be required. These values are consistent with vertical strain values predicted in the model.

The primary results from analysis of the bedding only model (Model 2) can be summarized as follows:

o Under low lateral stress conditions, the introduction of bedding planes results in a vertical and lateral decrease in the EdZ extent which is attributed to greater rock mass mobility and induced stress dissemination over a shorter distance. EdZ extents in the bedding plane model were approximately 20% lower than in the model without discontinuities;

o Under high lateral stress conditions, vertical and horizontal EdZ extents tend towards the no-discontinuity extents;

o Vertical rock mass displacement achieves a maximum of approximately 4 cm at the excavation floor, approximately twice the magnitude observed without discontinuities. Lateral displacement achieves a maximum of up to 3 cm which is three times the magnitude observed without discontinuities;

o Under low lateral stress conditions, bedding plane vertical dilation in response to excavation achieves a maximum magnitude of 2.7 mm at the excavation floor. Dilation magnitude decreases with decreasing depth of excavation. Under high lateral stress conditions, dilation magnitude is marginally lower with a maximum magnitude of 2.3 mm;

o Analysis of rock mass displacement mechanisms indicates that total cumulative discontinuity dilation accounts for approximately 50% of total vertical rock mass displacement beneath the excavation floor;

o Dilation -v- distance below the excavation floor can be defined by a power law relationship in the form;

$$\text{Dilation (D)} = c\, x^{b}, \hspace{6cm} [4.2]$$

where x is the distance below the excavation floor (m), c is a coefficient related to depth of excavation and b is the power value;

o   The limit of definable discontinuity dilation is significantly smaller than the limit of definable rock mass displacement.

4.3.3 Model 3: Model with variably orientated joints

Model 3 introduces additional DFN complexity with the addition of a series of predominantly stratabound sub-vertical variably orientated joints to the existing bedding planes. The lithological variation remains as in previous models. Joint configuration is generated stochastically by application of FracMan to a generalized joint set distribution. In accordance with the stated methodology to progressively increase DFN complexity, Model 3 incorporates a selection from the full stochastically generated DFN with smaller joints excluded to reduce model resource demand to a practical level. The representative section from the full FracMan generated DFN is illustrated in Figure 4.29 which shows the upper 300 m DFN sequence.
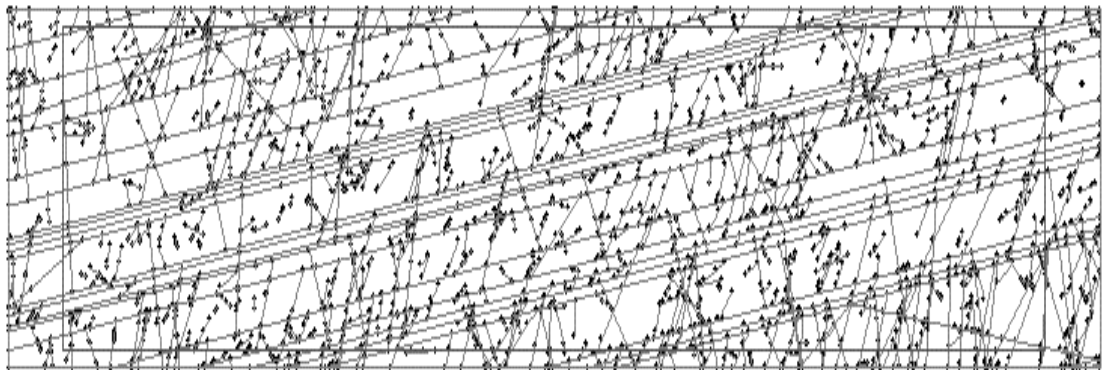
Figure 4.29: Stochastically generated DFN based on Blaxter Quarry joint geometry. DFN generated in FracMan from generalized Blaxter Quarry joint distribution data. The model domain equates to a two-dimensional area of 360,000 m^2 (1,200 m x 300 m).

All joints in the model are defined as discrete contact discontinuities with discrete contact properties that are different from those applied to the bedding planes. As discussed in detail at Chapter 3, the much shorter joints are modelled as significantly stiffer than the more laterally extensive bedding

planes. In contrast to the bedding planes, the joints do not extend across the full model domain and are therefore constrained at either end by the properties of the strata within which they terminate.
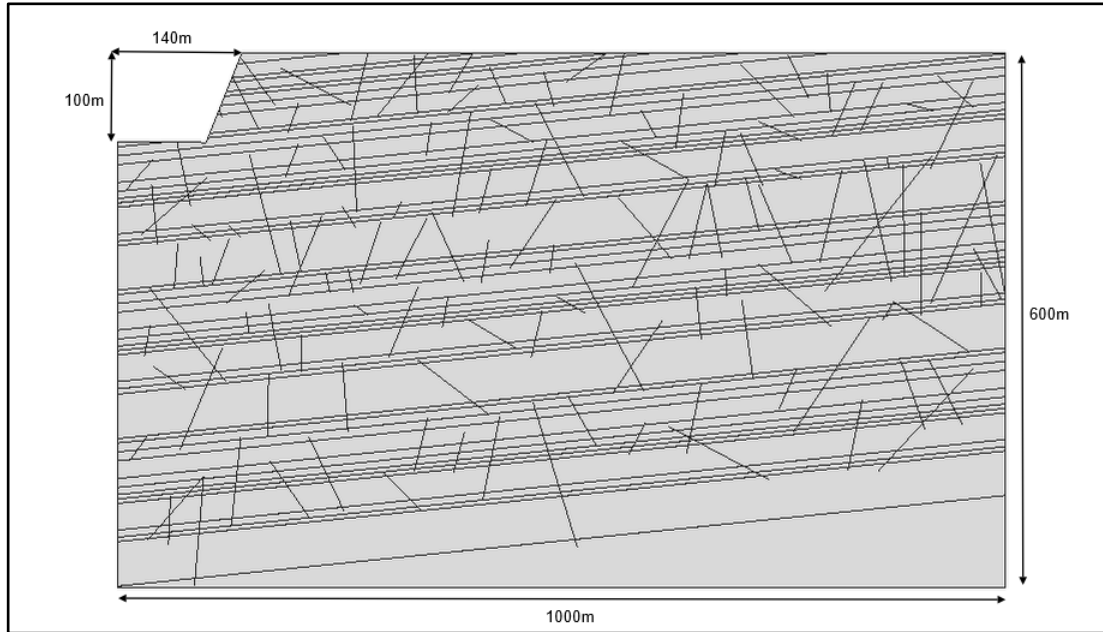
Figure 4.30: Model 3 configuration showing model domain dimensions and DFN configuration.

Due to data transfer compatibility issues between FracMan and Elfen, the Elfen Model 3 DFN was added manually by replication of joint location, length and orientation from the FracMan output, but excluding joints with a length of less than 10 m to reduce model processing time. The Elfen model domain has dimensions of 1000 m x 600 m. Joints included in the model are orientated at a range of angles from 30° to 87° from the horizontal to allow investigation of the effect of variably orientated joint sets on response to excavation induced stress change. The DFN configuration of Model 3 is shown in Figure 4.30. Increased DFN complexity leads to a significant increase in model run-time. Model mesh size is retained at 5m to preserve consistency across all models.

4.3.3.1   Stress response

In common with Model 2, the presence of discontinuities precludes the development of a lateral tensile stress zone in the excavation floor. Tensile stress conditions do, however, develop behind the excavation face. As shown in Figure 4.31, tensile stress conditions extend a significant distance from the

excavation face with highest magnitude stresses towards the upper elevations in the excavation face. It is apparent that in this model configuration, the tensile stress zone is generally restricted to areas of the model domain in which bedding planes daylight in the open excavation face. Figure 4.31 demonstrates that the highest tensile stresses occur at the intersection of sub-vertical joints with bedding planes.
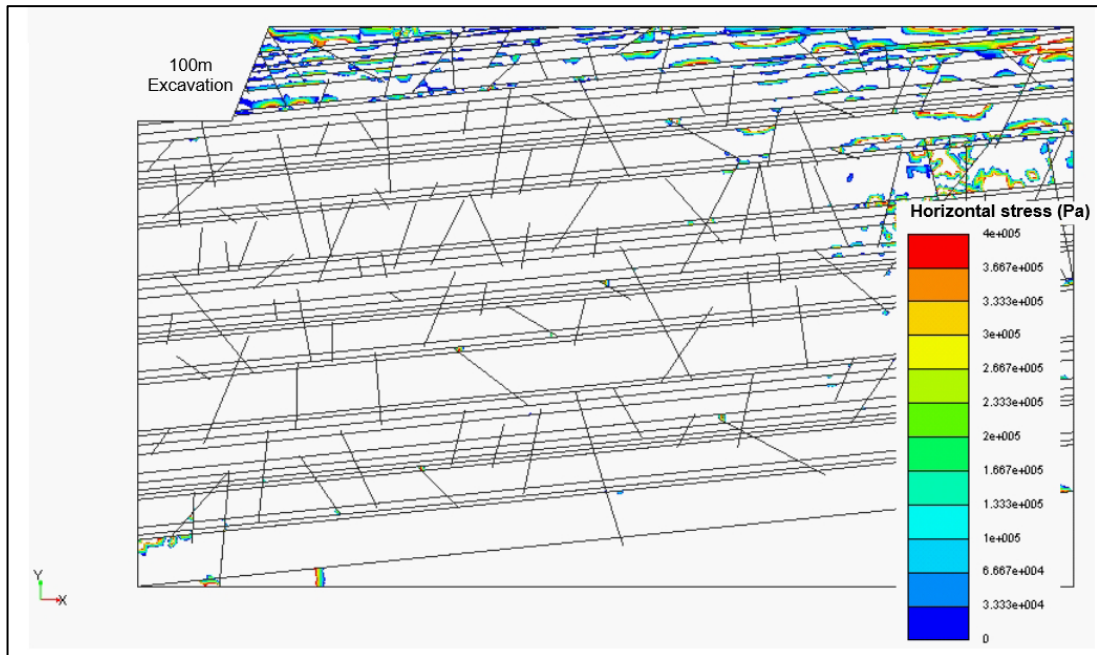
Figure 4.31: Model 3 Lateral tensile stress zone behind the excavation face with 100m deep excavation showing development of highest tensile stress (Pa) at discontinuity intersections (k=0.27)

Due to a combination of shallowly dipping bedding, loss of lateral containment at the excavation face and reduction in lateral stress, extensional strain conditions develop behind the excavation face and extend for a significant distance. As indicated in Figure 4.32, for a 100 m deep excavation under low lateral stress conditions, the extensional strain zone extends for a distance of approximately 320 m from the excavation face. At a 30 m depth of excavation the extent of the extensional strain zone behind the excavation face is reduced to approximately 150 m.
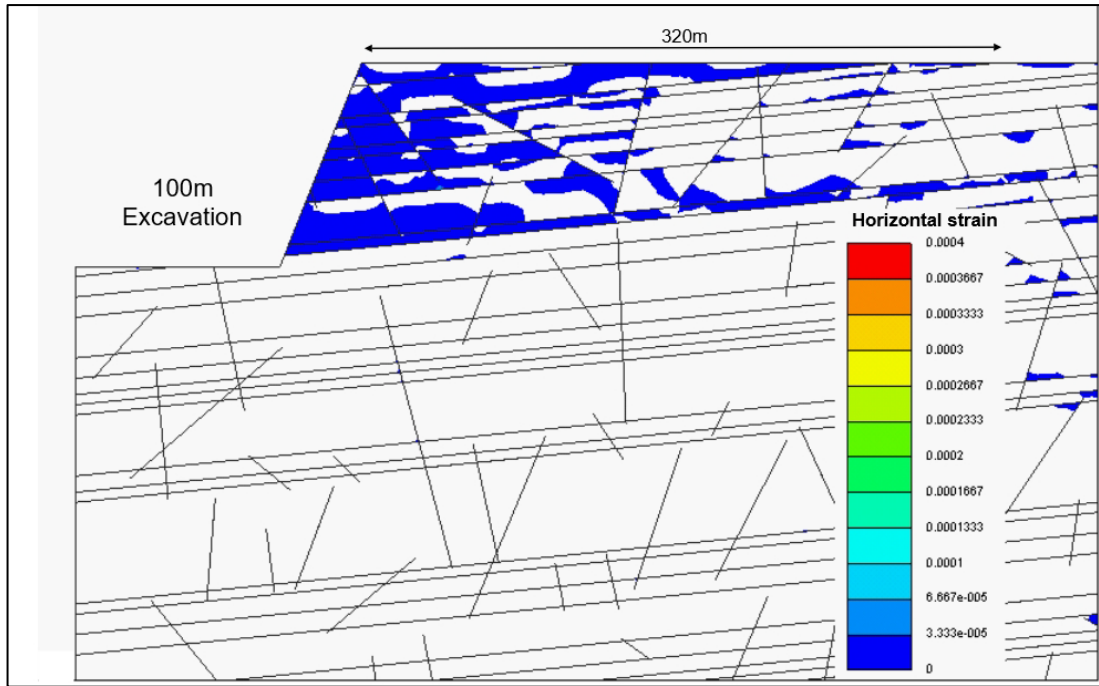
Figure 4.32: Model 3 Lateral extensional strain zone at 100 m excavation depth (k=0.27) showing development of extensional strain conditions at a distance of up to 320m behind the excavation face.
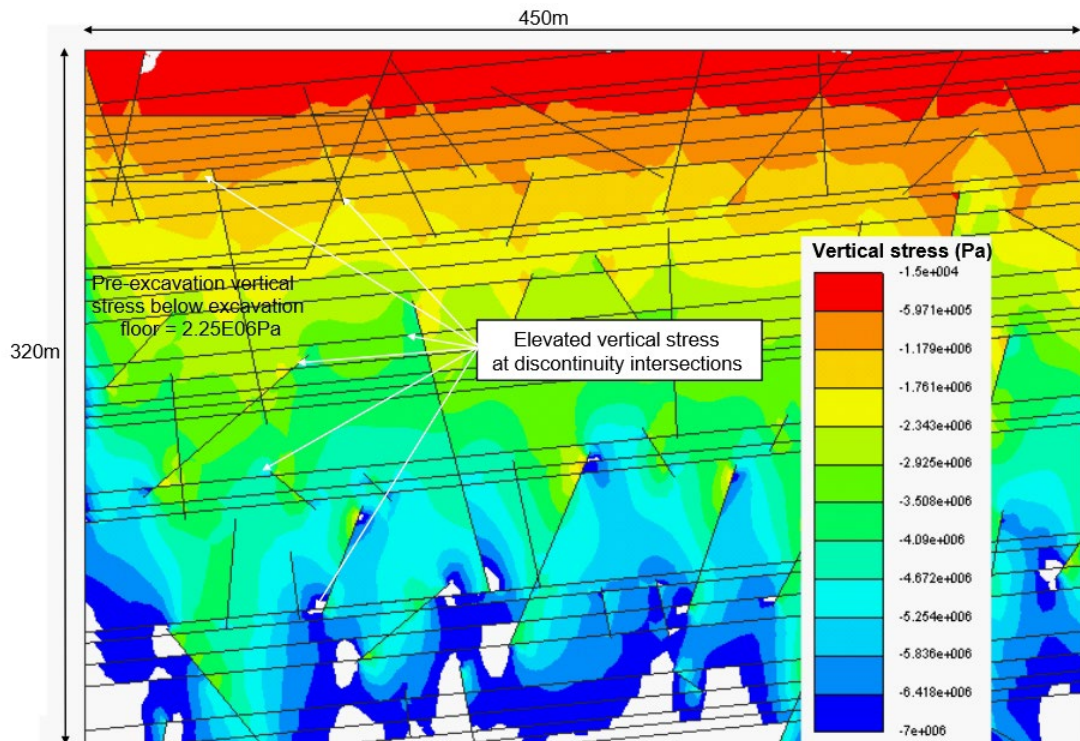
Figure 4.33: Model 3 Vertical stress distribution (Pa) around the excavation area under gravitational initialization showing peak stress concentration at joint/bedding intersections. Showing partial model domain with dimensions 500 m x 300 m.

Under low lateral stress conditions, where loading and unloading is dominantly vertical, the presence of sub-vertical jointing results in a change in the vertical stress distribution when compared to Model 2, the bedding only model. As shown in Figure 4.33, although stress increase is relatively low, gravitational initialisation results in variable vertical stress distribution across joint surfaces with a tendency to higher stress on the underside of each joint. The stress assignment process in Elfen involves initial calculation of nodal stress as ρgh (self weight) followed by adjustments to account for any lithological density differences and the presence of discontinuities.
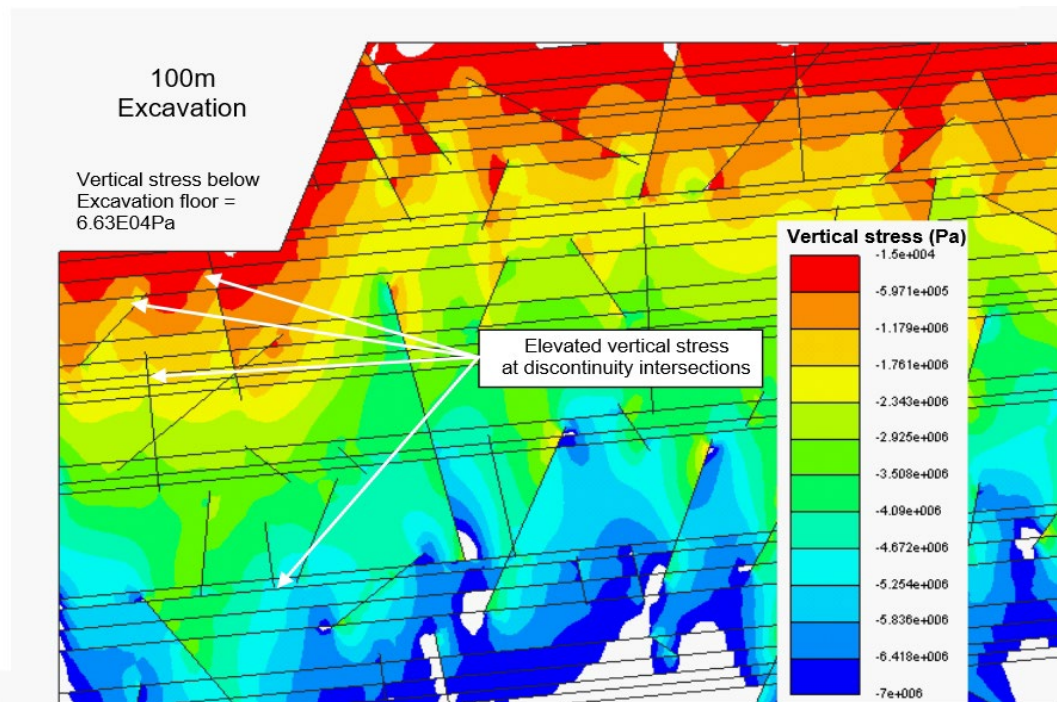
Figure 4.34: Model 3 Vertical stress distribution (Pa) with 100 m deep excavation showing peak stress concentration at joint/bedding intersections but with reduced stress magnitude compared to gravitational initialization. Showing partial model domain with dimensions 500 m x 300 m.

A small amount of rock mass compression can result at density change boundaries and as discontinuities achieve penetration in relation to the non-linear compliance conditions that are applied. With high joint stiffness, resisting compression can lead to elevated stress at joint surfaces/intersections. During Model 3 development, a range of joint stiffness values were investigated with the aim of reducing stress field perturbation to a minimum. Stress values used in the non-linear compliance function were adjusted during this process. Under high lateral stress conditions, where loading is dominantly horizontal, higher

stress zones are developed along bedding planes, particularly at joint intersections.

Although the presence of interconnected discontinuities influences the stress distribution during gravitational initialization, stress reduction due to excavation unloading occurs at both discontinuity surfaces and in the host rock. As shown in Figure 4.34, although following unloading, stress concentration at discontinuity intersections remains, stress magnitude is reduced by a comparable magnitude to stress reduction in the surrounding host rock.

A fixed value of joint cohesion is used for each group of joints in Elfen. Once the joints lose contact the cohesion reverts to zero. The stress field resulting from gravitational loading leads to the development of minor penetration across discontinuity surfaces. As stress magnitude is reduced, the magnitude of penetration reduces in accordance with the relationship stress = stiffness x penetration. As discussed at Chapter 3, for situations where loss of cohesion is not achieved, the change in penetration of discontinuity surfaces has been used to determine discontinuity dilation in the models applied during this study. Where cohesion is lost, respective joint surface displacements are calculated directly.

5.3.2.2 Excavation disturbed Zone (EdZ) extents

In common with other models, the vertical and lateral extents of the EdZ with both bedding planes and variably orientated joints included in the model, have been defined by reference to vertical and lateral stress change in relation to pre-excavation stress magnitude, as discussed in relation to Model 1. Summary results are presented in Table 4.7.

Under both low and high lateral stress conditions, the introduction of sub-vertical, non-pervasive, variably orientated jointing results in a decrease in the vertical and lateral extent of the EdZ when compared to the no discontinuity model (Model 1) and the bedding-only model (Model 2).

Lateral Stress Ratio (k)	Excavation depth (mbgl)	Limit of EdZ Vertical (m below excav. floor)	Limit of EdZ Horizontal Upper Face (m behind excav. face)
k=0.27	30	176	131
	60	264	299
	100	362	530
k=2.0	30	127	166
	60	214	264
	100	297	575

Table 4.7: Model 3 EdZ vertical and horizontal extents under low and high lateral stress conditions.

The reduction in EdZ extent in a vertical direction below the excavation floor, compared to EdZ extents associated with the no-discontinuity model (Model 1) and the bedding only model (Model 2), is attributed to an increase in rock mass mobility resulting in a more attenuated stress response due to an increase in the number of independent blocks and an increase in the number of discontinuity surfaces when compared to the bedding only model (Model 2). Comparison of rock mass stress variation with depth between Models 2 and 3 is shown in Figure 4.35. It is apparent that in Model 3, at a 100 m depth of excavation, stress below the excavation floor returns to near gravitational initialisation stress over a shorter distance than for Model 2, with variation occurring at approximately 100 m below the excavation floor.

In a horizontal direction, the presence of sub-vertical jointing behind the excavation face introduces multiple sub-vertical planes of lower stiffness than the rock mass, allowing greater extensional response than the bedding only model (Model 2) and hence attenuation of stress response over a shorter distance. EdZ extents defined on the basis of stress variation can be compared to lateral tensile stress and extensional strain zones discussed above. It is apparent that in the upper face, the lateral extent of the extensional strain zone is approximately 70% of the EdZ, whilst at the base of the face the lateral extent of the extensional strain zone is comparable to the EdZ. In the upper face other mechanisms i.e., bedding plane sliding, contribute to lateral stress dissipation.
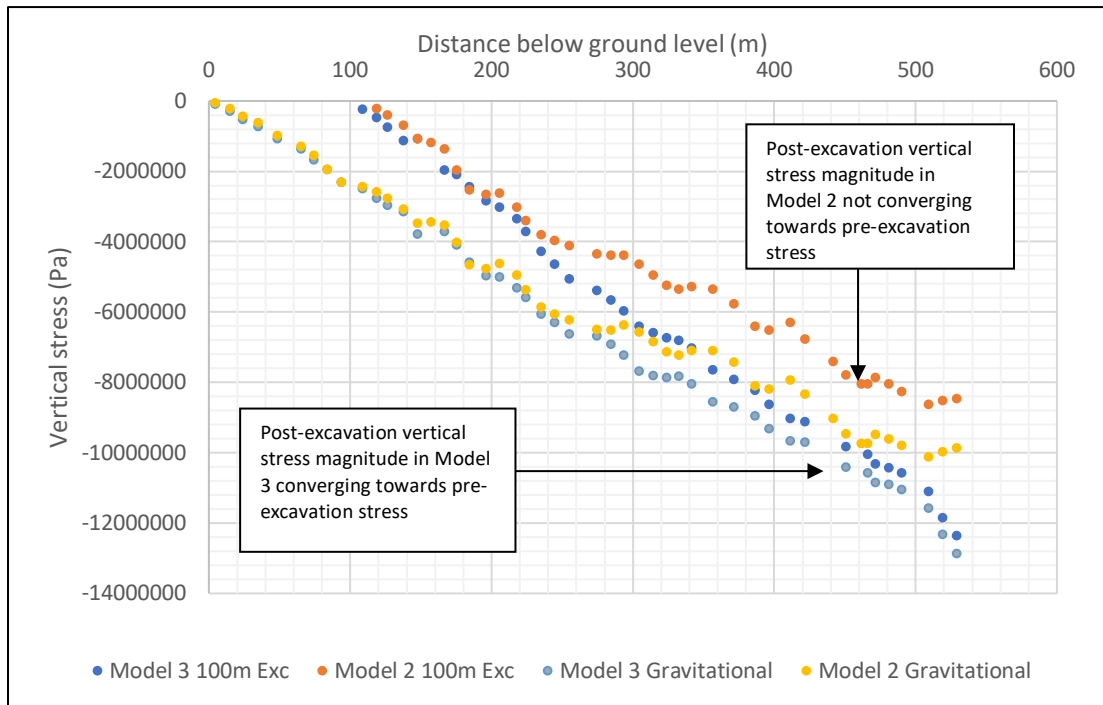
Figure 4.35: Model 3 Comparison of stress attenuation rates below the excavation floor for a 100 m deep excavation in Model 2 (Bedding only model) and Model 3 (variably jointed model). In Model 3, stress resulting from excavation returns to pre-excavation gravitational initialisation stress over shorter distance than in Model 2.

4.3.3.3   Rock mass displacement

Model 3 introduces relatively low vertical connectivity between successive bedding planes. However, the introduction of sub-vertical joints across several bedding planes tends to increase vertical rock mass mobility as bedding planes are split into shorter sections by cross-cutting joints. As shown in Figure 4.36, under low lateral stress, the maximum vertical displacement beneath the excavation floor during a 100 m deep excavation is 0.033 m compared with 0.051 m with the bedding only model (Model 2).

It is recognized that the vertical displacement result for Model 3, and the reduction in maximum vertical displacement magnitude when compared to Model 2, may be a consequence of increased bedding plane stiffness at joint intersections. The non-linear compliance function will increase bedding plane stiffness in response to higher stress at joint intersections, as shown in Figures 4.33 and 4.34. Locally increased bedding plane stiffness will tend to reduce vertical dilation when compared to the bedding only model (Model 2).
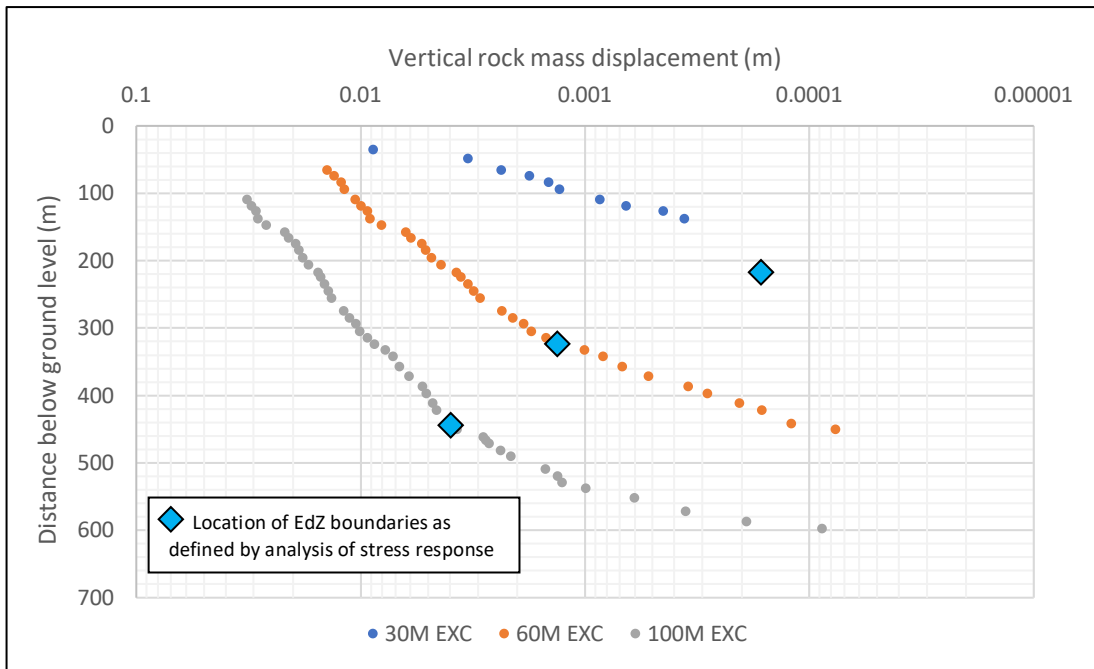
Figure 4.36: Model 3 Vertical displacement below the excavation floor for excavation depths of 30 m, 60 m and 100 m (k=0.27). Potential influence of boundary effects shown at change in gradient for 60 m and 100 m deep excavations.
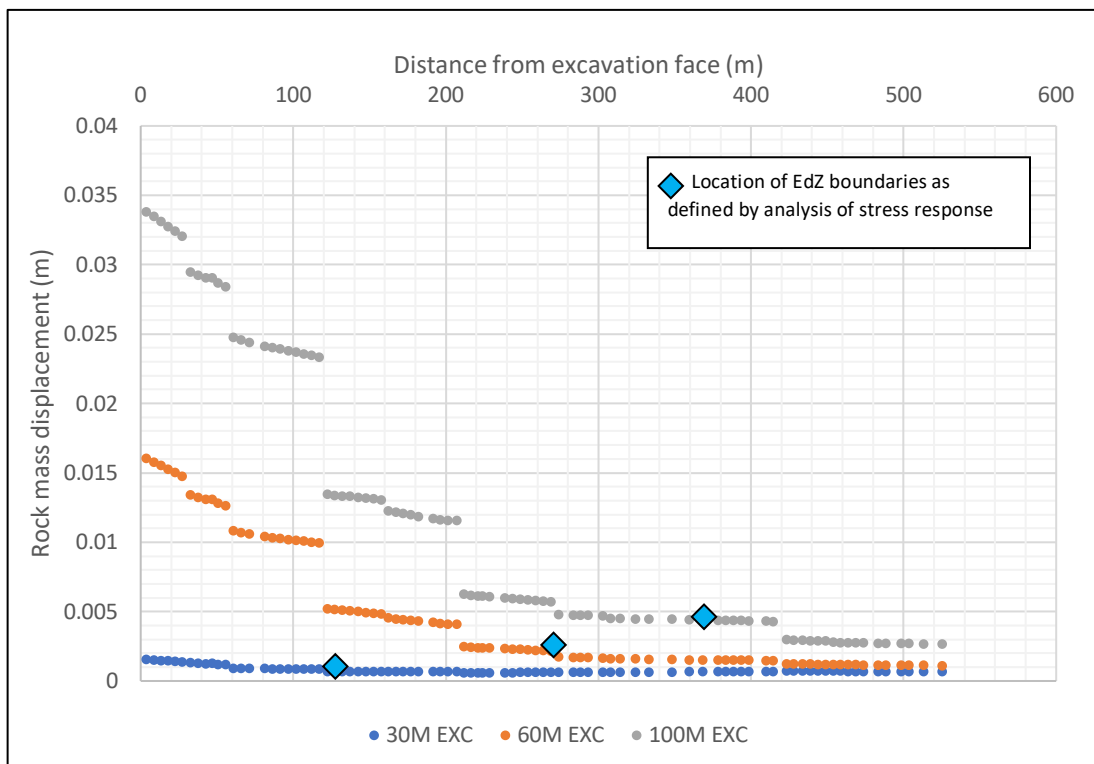
Figure 4.37: Model 3 Horizontal rock mass displacement behind the upper excavation face for excavation depths of 30 m, 60 m and 100 m (k=0.27). (Note: steps in plotted data relate to abrupt changes in the horizontal transect used to extract data where model nodes are not horizontally lineated).

The magnitude of horizontal displacement behind the excavation face for Model 3 is shown in Figure 4.37. The addition of subvertical jointing results in a maximum horizontal displacement at 100 m excavation depth of 0.034 m compared to 0.031 m for the bedding only model (Model 2) under the same in-situ stress conditions.

The slightly increased horizontal displacement at the excavation face, as a consequence of the inclusion of sub-vertical jointing is consistent with expectations, given that jointing introduces capacity for horizontal displacement by joint dilation, a process absent from the bedding only model (Model 2). However, given the reduced extent of the EdZ and the increase in rock mass mobility in Model 3, it would be reasonable to also expect an increase in vertical displacement beneath the excavation floor when compared to the bedding only model (Model 2). Model results indicate two reasons for reduced vertical displacement in Model 3, as follows:

1. Variation in displacement distribution across the excavation floor: and

2. Higher residual stress at sub-vertical joint surfaces.

As shown in Figure 4.38, displacement at the excavation floor in the bedding only model (Model 2) is greatest at the farthest distance from the excavation face, and progressively reduces towards the face. In the variably jointed model (Model 3), joints at, and just below, the excavation floor influence the floor displacement profile resulting in more equally distributed displacement across the floor. Constraint imposed by sub-vertical jointing results in a lower average displacement across the excavation floor. Vertical stress at the excavation floor remains compressive throughout the model. As shown in Figure 4.35, the magnitude of stress reduction at the excavation floor in response to a 100 m deep excavation, is lower for the variably jointed model (Model 3) than for the bedding only model (Model 2).

Model 2 - Bedding only

Excavation Floor
Highest Magnitude Displacement
at Excavation Centre

Bedding Plane Dilation Greatest
at Excavation Centre

Vertical Floor Displacement (m)

Model 2 (k=0.27)   Model 3(k=0.27)

Model 3 - Variably jointed

Excavation Floor
Displacement Magnitude Lower due to
Influence of Sub-vertical Jointing

Bedding Plane Dilation Influenced by
Sub-vertical Jointing

Figure 4.38: Comparison of excavation floor displacement profile between Model 2 and Model 3 showing the influence of sub-vertical jointing. Central bar chart shows the variation in vertical displacement magnitude along the excavation floor.

Rock mass displacements under high lateral stress are presented as Figure 4.39 and 4.40. Under high lateral stress conditions, the vertical displacement response results in lower magnitude rock mass displacement for all three depths of excavation. At 100 m depth of excavation, and high lateral stress, the maximum vertical displacement is 0.026 m, a decrease of 21% on the low lateral stress response. Lateral displacement towards the open excavation face is comparable to the lateral displacement observed with low lateral stress. This is consistent with results for the bedding only model (Model 2).
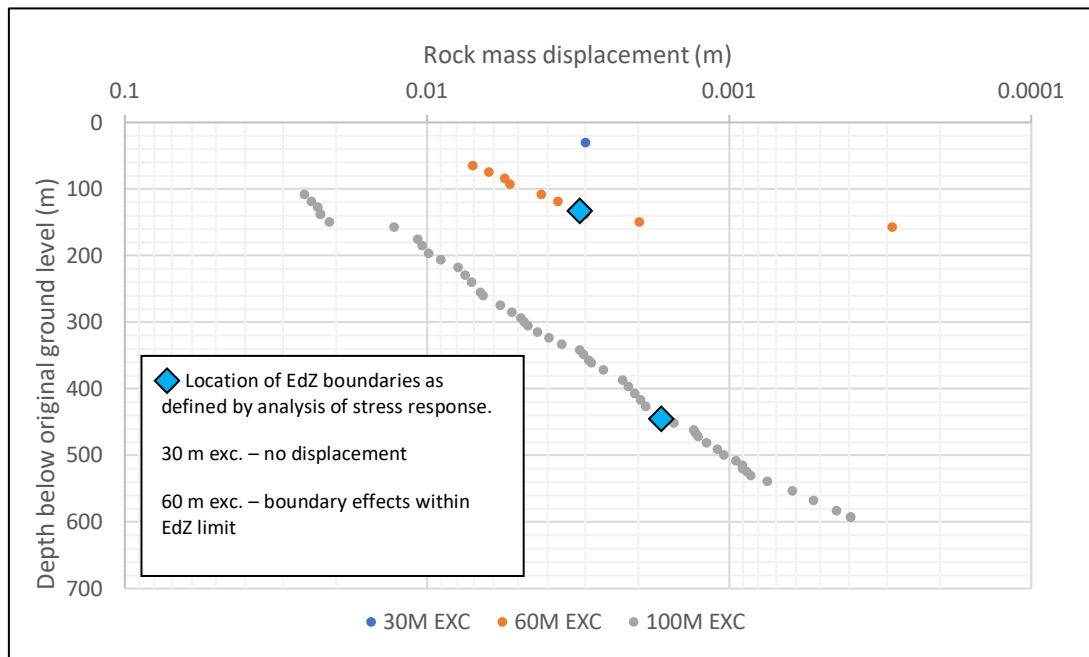
Figure 4.39: Model 3 Vertical rock mass displacement below the excavation floor for excavation depths of 30 m, 60 m and 100 m (k=2.0). Under high lateral stress conditions maximum rock mass vertical displacement is reduced when compared to displacement under low lateral stress conditions (Figure 4.36). For the 30 m deep excavation there is no definable rock mass displacement beyond the excavation face. The potential influence of boundary effects is less well-defined.

Comparison of vertical and horizontal displacement data with calculated EdZ extents for Model 3 indicates that definable vertical displacement occurs over a distance below the excavation floor that exceeds the EdZ extent. The limits of definable horizontal displacement behind the excavation face are consistent with EdZ extents, when potential boundary effects are accounted for.

It is concluded that definable vertical displacement, beyond the limits of the EdZ, represents the influence of model boundary conditions, as discussed in relation to models 1 and 2. The 'no-displacement' lower model boundary at a distance of 500 m below the excavation floor in the 100m deep excavation scenario, introduces definable displacement values on a linear basis between the lower boundary and the limit of the EdZ. Reference to Figures 4.36 and 4.39, confirms a change in the rate of reduction of rock mass displacement (i.e. inflection point on each graph) at the defined EdZ limit. Vertical displacement beyond these points is a consequence of boundary effects and can be ignored.
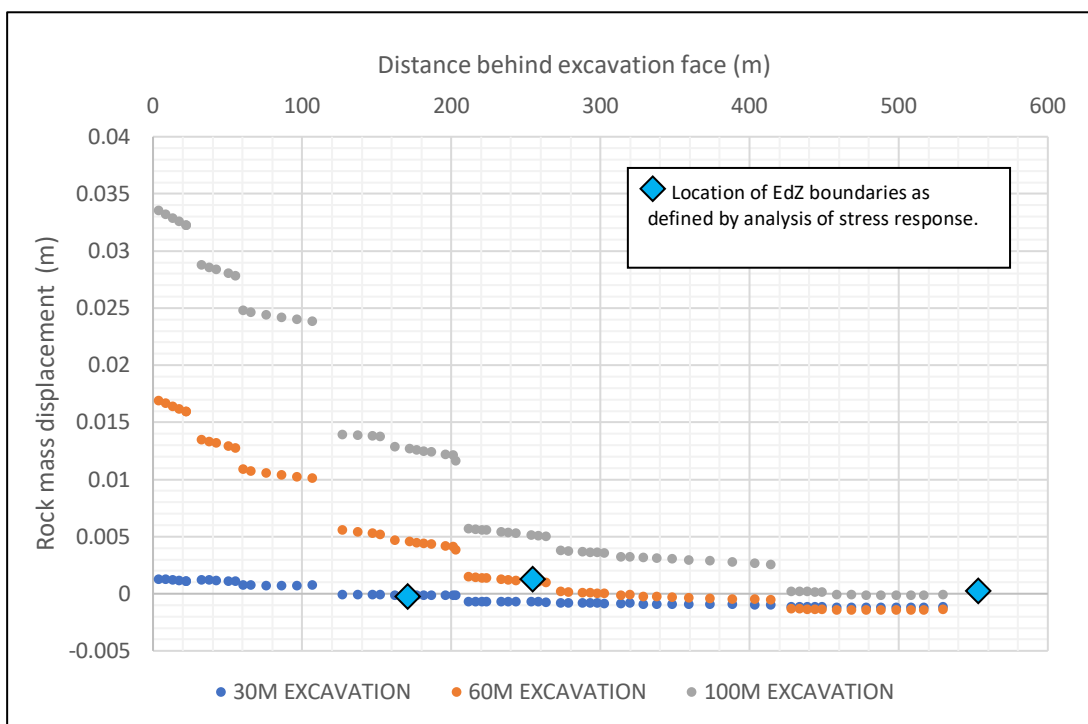
Figure 4.40: Model 3 Horizontal rock mass displacement behind upper excavation face for excavation depths of 30 m, 60 m and 100 m (k=2.0). Maximum lateral displacement magnitudes are comparable to the results for the low lateral stress case.

4.3.3.4   Discontinuity dilation

As the joints included in the model are variably orientated and relatively steeply dipping, there is low potential for normal joint dilation in a vertical direction. The bedding planes included in the model are the same as in the previous bedding plane only model (Model 2). Analysis has therefore been focused on the potential for bedding plane dilation beneath the excavation floor and joint dilation behind the excavation face.
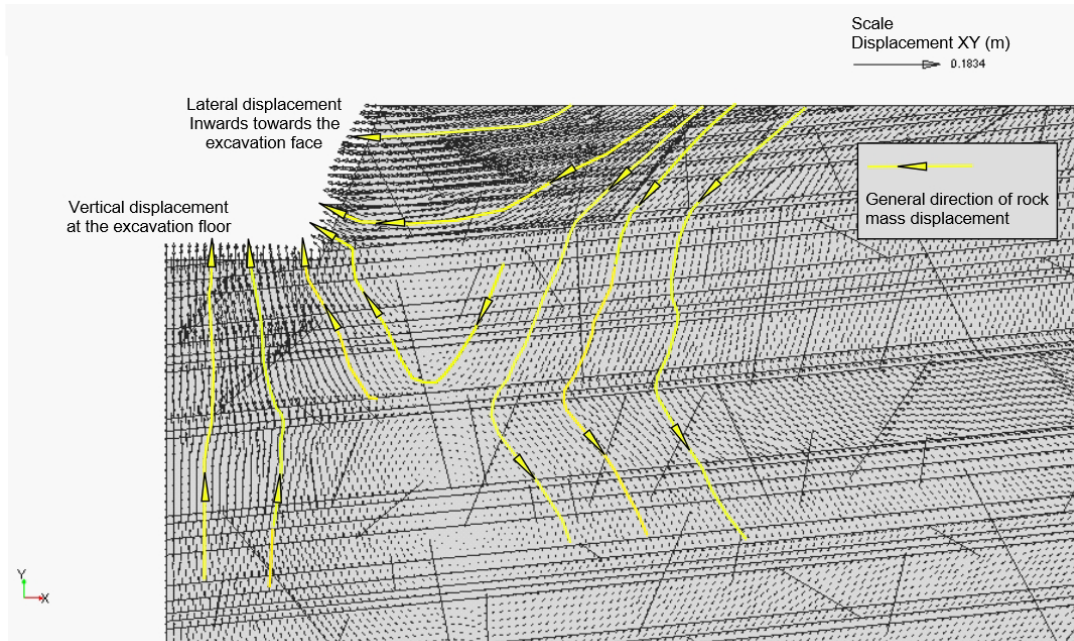
Figure 4.41: Model 3 XY displacement vectors at 100 m depth of excavation under low lateral stress conditions, showing displacement towards the excavation face and vertically at the excavation floor in relation to joint orientation. Yellow lines indicate the general direction of displacement within the rock mass.

In contrast to the bedding planes, the joints included in this model do not extend across the full model domain and therefore joint ends are mostly within intact rock. The joints are therefore constrained and unable to function as sliding surfaces for adjacent rock blocks in the way that bedding planes and fully persistent joints (Model 4) are able to. Two factors are important when considering modelled joint dilation results as follows.

○ Joint orientation
○ Measurement location with respect to joint length

As shown in Figure 4.41, joints are orientated at a range of angles behind the excavation face, although most joints are relatively steeply dipping. Stress response, and hence the potential for joint dilation, is highly sensitive to joint orientation with respect to the principal normal stresses. Figure 4.41 shows the direction and magnitude of displacement in the XY direction for all model nodes, including joint and bedding plane surfaces. It is apparent that discontinuity dilation will be influenced by joint orientation in relation to the displacement direction.

For joints close to the excavation face, displacement is approximately normal to joint surfaces. Further from the face, in those areas where displacement is sub-vertical, there is only a small normal displacement component consistent with low potential for joint dilation.
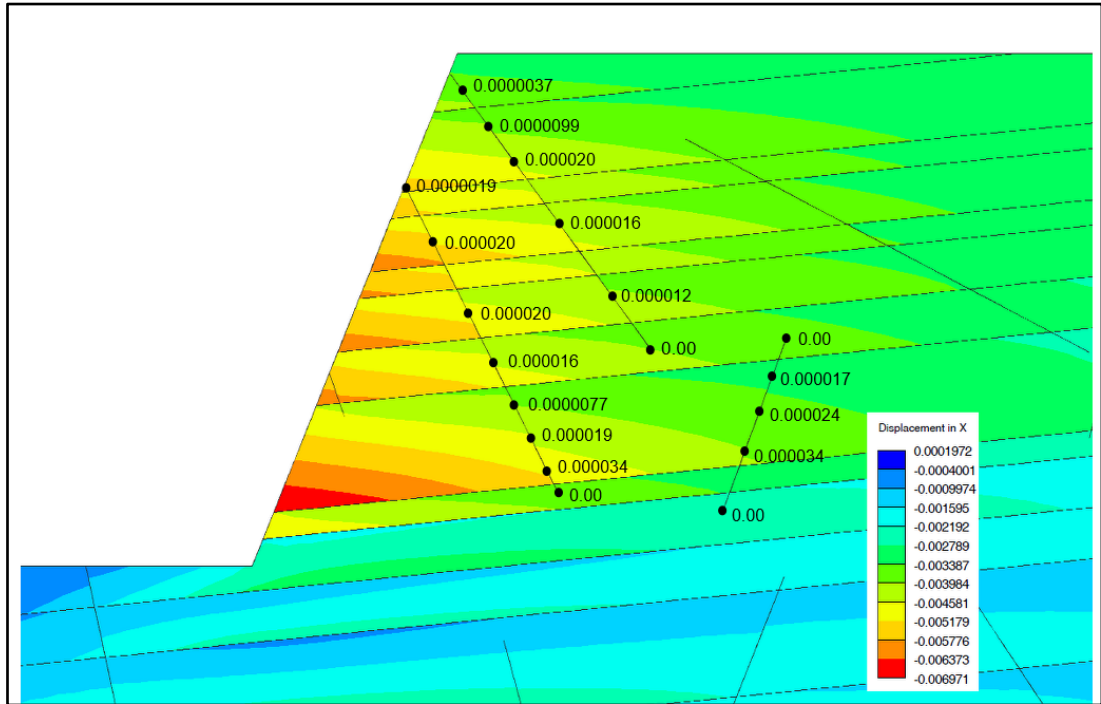
Figure 4.42: Model 3 Variation in normal joint dilation along the joint length (m) showing minimum dilation at constrained joint ends and maximum dilation towards the joint centre.

As the joints included in this model are constrained at either end, joint dilation magnitude varies along the length of each joint with maximum dilation occurring close to the joint mid-point, subject to the influence of connecting discontinuities. Model results have been derived from a mid-distance location along each joint, where possible. The finite element mesh and node locations do not produce mid-point results at all locations, particularly within the thinner lithological units. Figure 4.42 shows an example of variation in joint dilation along the length of specific joints behind a 100m deep excavation face. As shown, joint dilation varies significantly from zero at the constrained end of each joint to a maximum value towards the joint mid-point.

Determination of discontinuity dilation magnitudes is therefore complicated by both joint orientation and measurement location, resulting in more heterogeneity in the results than observed in the bedding only model (Model 2) results. All bedding planes remained in contact throughout all stages of Model 3 development and therefore analysis of variation in penetration values remains a valid approach to vertical dilation of bedding planes, as with previous models. The results for both modelled lateral stress conditions are presented as Figure 4.43 and 4.44.

Under both stress states, discontinuity dilation magnitude in bedding planes below the excavation floor declines from a maximum at the excavation floor to a minimum at the limit of the EdZ. As shown in Figures 4.43 and 4.44, definable dilation extends a short distance beyond the limit of the EdZ at all depths. As with displacement data, this is attributable to model lower boundary effects.

With low lateral stress, the maximum bedding plane dilation, at the first bedding plane below the excavation floor, is 0.41 mm, 0.66 mm and 0.98 mm for excavation depths of 30 m, 60 m and 100 m respectively. These values reduce to 0.22 mm, 0.52 mm and 0.83 mm under high lateral stress conditions.

Bedding plane dilation magnitude below the excavation floor, with the inclusion of sub-vertical jointing (Model 3) is approximately one-third of the observed dilation magnitude for the bedding only model (Model 2). The presence of sub-vertical jointing in Model 3 is therefore resulting in a reduction in the magnitude of both vertical displacement and bedding plane dilation when compared to the bedding only model (Model 2).

The results for normal dilation of joints behind the excavation face are presented for both lateral stress conditions in Figure 4.45 and 4.46. Under low lateral stress conditions there is no discernible dilation of joint surfaces during a 30 m deep excavation. This primarily reflects the location of most joints below the base of strata affected by excavation at this depth.
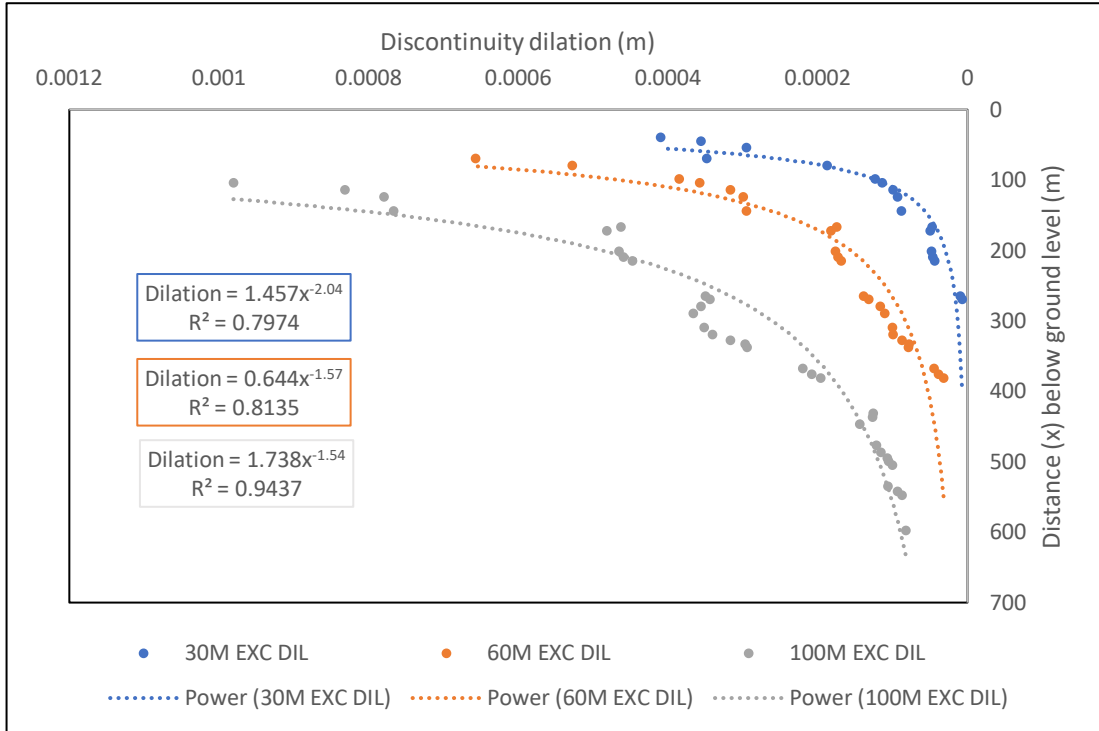
Figure 4.43: Model 3 Discontinuity dilation below excavation floor for excavation depths of 30 m, 60 m and 100 m (k=0.27) with power law fittings.
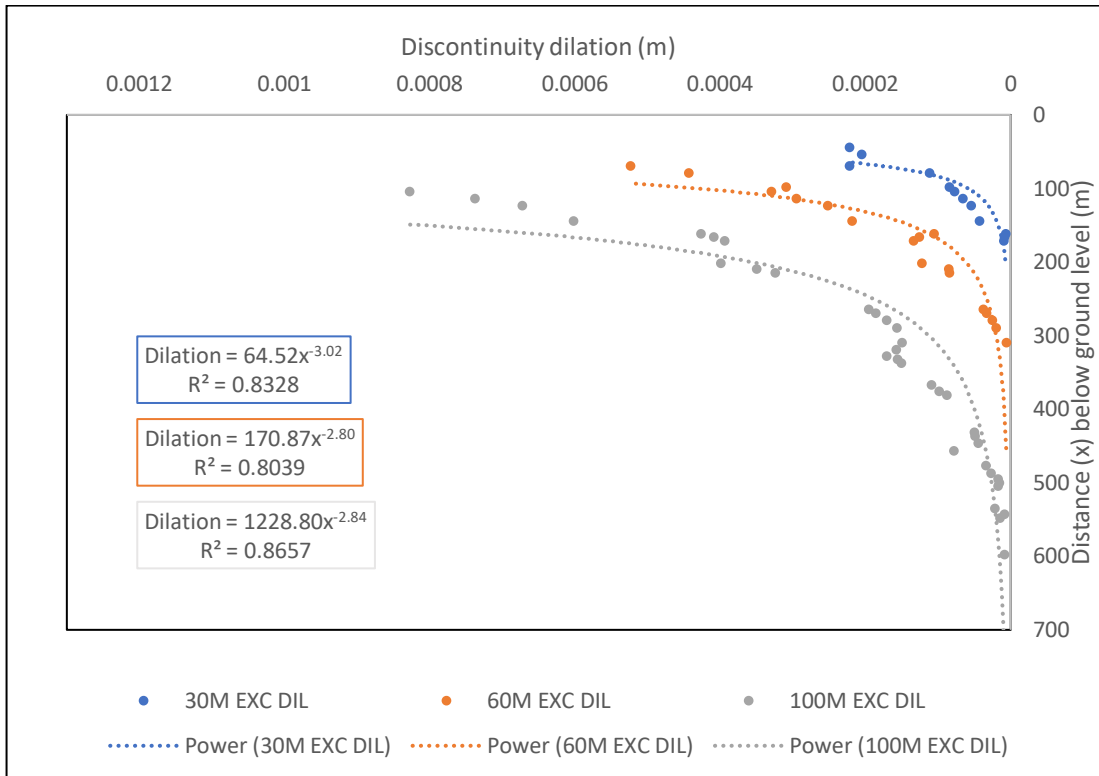
Figure 4.44: Model 3 Discontinuity dilation below excavation floor for excavation depths of 30 m, 60 m and 100 m (k=2.0) with power law fittings.
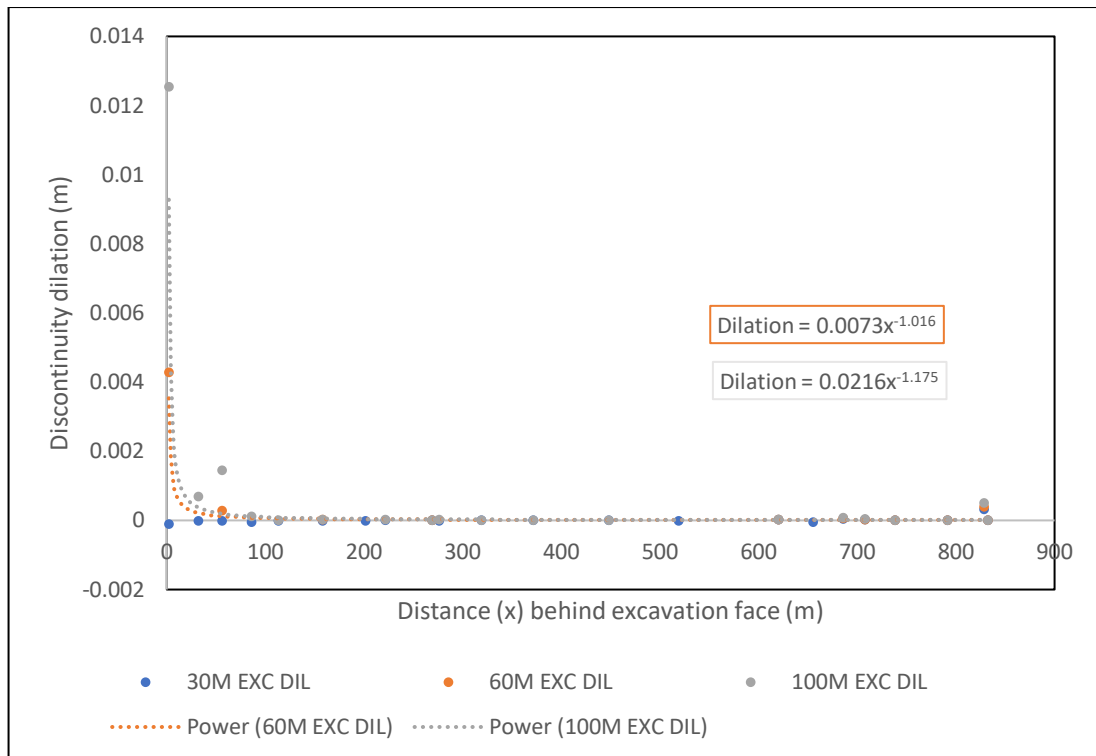
Figure 4.45: Model 3 discontinuity dilation behind the excavation face for excavation depths of 30 m, 60 m and 100 m (k=0.27) with power law fittings. There is no definable joint dilation for the 30 m deep excavation.

Maximum joint dilation, at the first joint behind the excavation face, has a magnitude of 4.28 mm and 12.54 mm for the 60 m and 100 m excavation depths respectively. Under high lateral stress conditions, the maximum dilation at all excavation depths is significantly lower at 0.18 mm and 0.32 mm for the 60 m and 100 m excavation depths respectively. The reduced dilation under high lateral stress is attributable to the greater joint normal stiffness assigned through the non-linear compliance process for sub-vertical joints behind the face.

Under low lateral stress conditions, joint dilation behind the face reduces to zero within a distance of less than 100 m, a significantly shorter distance than the definable displacement zone or the EdZ extents. Under high lateral stress, dilation with distance from the face is more variable with an indication that definable dilation, at lower magnitude, extends further from the face. Dilation variability, influenced by variation in joint orientation, does not fit a power law function or any other easily defined function. Curve fitting may be improved if dilation magnitudes were corrected for joint orientation.
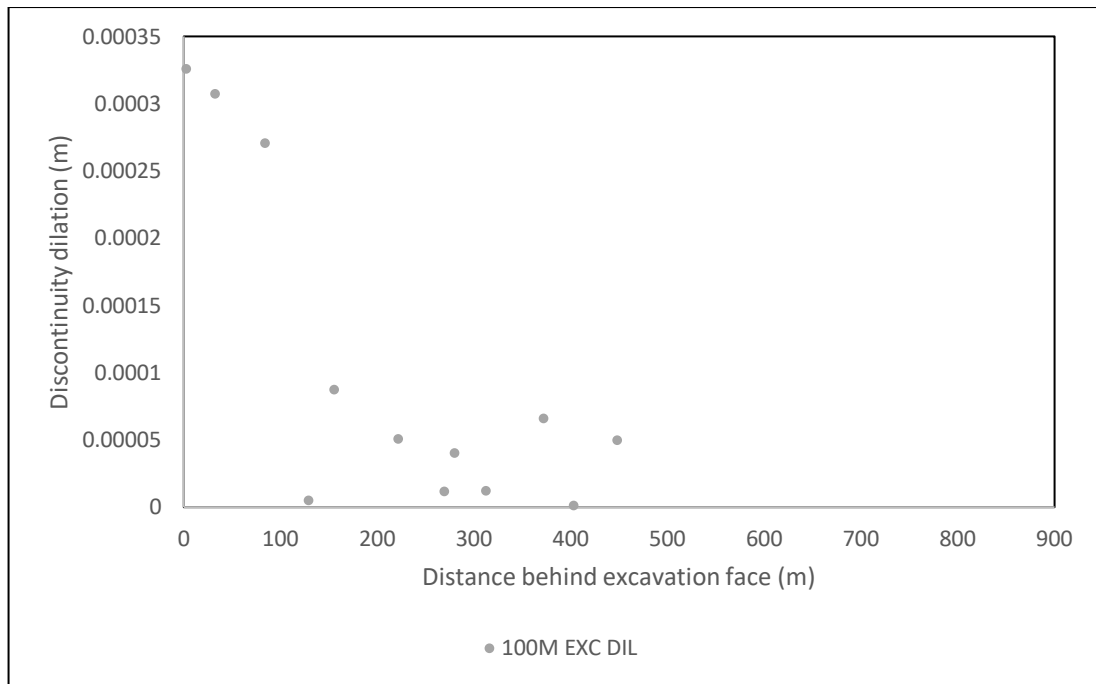
Figure 4.46: Model 3 discontinuity dilation behind the excavation face for excavation depth of 100 m (k=2.0). Dilation magnitude variability is associated with variable joint orientation. All dilation measurements are normal to joint surfaces.

Model 3 dilation/distance relationships for bedding plane dilation beneath the excavation floor and joint dilation behind the excavation face demonstrate that dilation magnitude is approximately proportional to the reciprocal of the distance from the floor or face. As shown on Figures 4.43 to 4.46, dilation/distance relationships can be defined by the power law function at Equation 4.2.

As with the bedding only model (Model 2), the total cumulative magnitude of discontinuity dilation on all discontinuities can be considered in relation to total rock mass displacement, as shown in Table 4.8.

The results in Table 4.8 indicates that, with the inclusion of the variably orientated joints, bedding plane dilation accounts for between 33% and 34% of total vertical displacement, comparable to the bedding only model (Model 2) in which it accounted for approximately 50% of vertical displacement. Cumulative dilation accounts for a higher percentage of horizontal displacement behind the excavation face of between 52% and 58%.

Excavation depth (mbgl)	Modelled displacement (m)	Cumulative dilation (m)	Dilation % displacement
Bedding plane displacement/dilation below excavation floor			
30	0.0084	0.00277	33
60	0.0177	0.00600	34
100	0.0378	0.01264	33
Joint displacement/dilation behind excavation face			
30	0.0013	n/a	n/a
60	0.0230	0.01202	52
100	0.0518	0.02981	58

Table 4.8: Model 3 Discontinuity dilation as a % of total displacement

In a vertical direction, the displacement observed at the excavation floor can be fully accounted for as the combination of rock mass extensional strain and cumulative bedding plane dilation. However, behind the excavation face, the summation of extensional strain and cumulative dilation does not equate to maximum displacement at the face. An additional process is contributing to displacement.

Reference to model results demonstrates that sliding on bedding plane surfaces is contributing to lateral displacement. Analysis of model outputs demonstrates that sliding on discontinuities primarily occurs as elastic shear strain. Sliding distance is determined in Elfen as tangential stress/tangential stiffness. At most locations, elastic shear strain does not lead to failure at the bedding plane as frictional resistance exceeds the critical shear stress. However, in the 100 m deep excavation, model results indicate bedding plane failure for a distance of up to 10 m behind the face at the lowest bedding plane in the face. The sliding distance, excluding the effects of extensional strain and joint dilation, is calculated at the upper model boundary to avoid double accounting of lateral displacement as sliding distance is reported on a cumulative basis. A displacement balance for both vertical and horizontal displacement is presented as Table 4.9.

Excavation depth (mbgl)	Max Modelled displacement (m)	Cumulative dilation (m)	Dilation % displace	Rock mass strain	Bedding sliding % contribution
Bedding plane displacement/dilation below excavation floor					
30	0.0084	0.00277	33	0.00563	0
60	0.0177	0.00600	34	0.01170	0
100	0.0378	0.01264	33	0.02516	0
Joint displacement/dilation behind excavation face					
30	0.0013	n/a	n/a	n/a	0
60	0.0230	0.01202	52	0.00310	34
100	0.0518	0.02981	58	0.00639	30

Table 4.9: Model 3 Displacement balance showing contribution of extensional strain, cumulative discontinuity dilation and bedding plane sliding distance.

Summary findings from the variable joint model (Model 3) are as follows.

o Variably orientated jointing results in a reduction in the vertical and lateral extent of the EdZ;

o Maximum rock mass displacement beneath the excavation floor and behind the excavation face is reduced with the inclusion of variably orientated jointing. Vertical and lateral displacement are both lower than in the bedding only model (Model 2);

o Bedding plane dilation below the excavation floor is reduced to one-third of the value observed in the bedding only model (Model 2). Lateral joint dilation achieves a maximum magnitude of 12 mm for a 100 m deep excavation;

o Discontinuity dilation contributes up to 34% of the total vertical displacement and up to 58% of total lateral displacement. The balance consists of extensional strain and, in the case of lateral displacement, sliding on discontinuity surfaces.

4.3.5 Model 4: Orthogonal jointed model

Model 4 represents a significantly higher degree of DFN connectivity by incorporation of a high-density network of sub-vertical domain-wide joints. The model configuration is intended to replicate the orthogonal jointing systems

frequently observed in bedded sandstone formations across northern England, as discussed in Chapter 3. Joints are included as persistent discontinuities that extend across the full height of the model domain with multiple bedding plane intersections. Multiple joints and bedding planes extend through the simulated excavation face and floor. Vertical joint configuration is loosely based on measurements taken at Blaxter Quarry with jointing at an angle of 85° to the horizontal and a spacing of 10 m. All joints are defined as discontinuities in the model and therefore discontinuity contact properties and controls apply, as detailed at Chapter 3. The orthogonally jointed model configuration is shown in Figure 4.47.
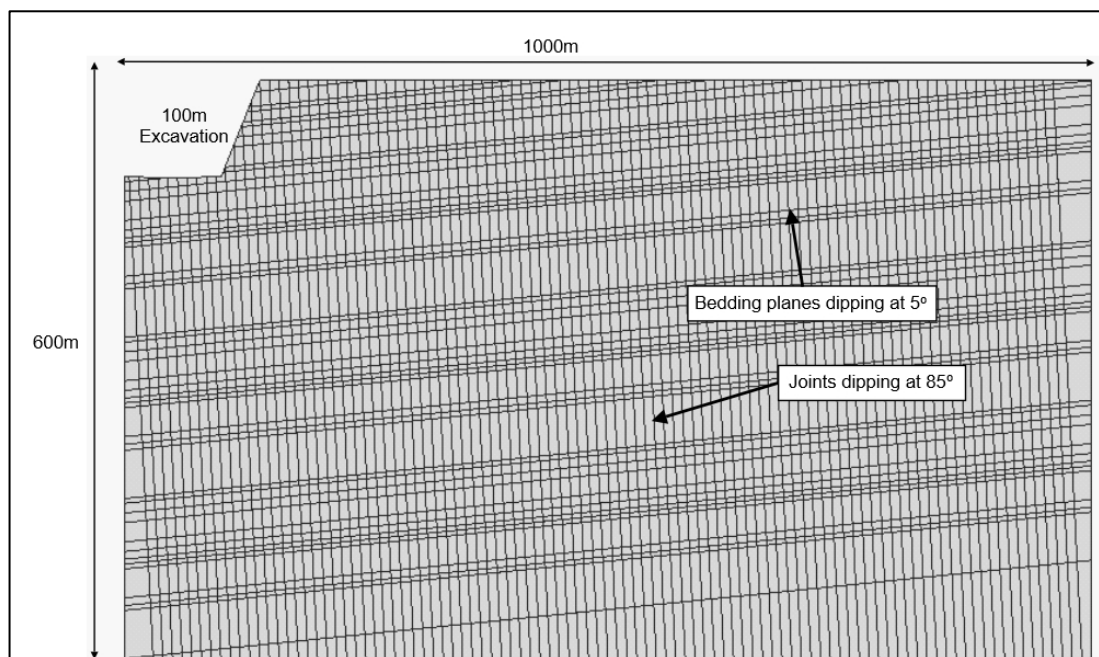
Figure 4.47: Model 4 Orthogonally jointed model configuration showing bedding planes dipping at 5° and joints dipping at 85°. Bedding spacing 10m-40m and joint spacing 10m.

It was anticipated that the introduction of multiple sub-vertical discontinuities would increase the potential for development of increased lateral displacement in response to lithostatic unloading as the discontinuities have lower stiffness than the surrounding rock mass. Although the joint stiffness values assigned through the NLC function are an order of magnitude higher than bedding plane stiffness values. Additionally, where joint cohesion is lost due to vertical loading or unloading the presence of vertical jointing could increase the potential for mobilisation at joint surfaces.

4.3.5.1 Stress response

The observed stress response to progressive excavation in the orthogonally jointed model (Model 4) can be compared to the stress response in the bedding only model (Model 2). With an excavation depth of 100 mbgl and low lateral stress ratio of 0.27, the magnitude of vertical stress reduction at the excavation floor, compared to pre-excavation, is 2.24 MPa which is slightly lower than the reduction of 2.31 MPa in the bedding only model. Variation in reported vertical stress reduction in all models is less than 5% which is considered acceptable given the variation in model geometries. Horizontal stress reduction at the base of the excavation face is 0.613 MPa which is higher than the 0.180 MPa recorded in the bedding only model. The vertical stress distribution around a 100m deep excavation is shown in Figure 4.48. As with the variably jointed model (Model 3), the introduction of sub-vertical joints with a higher stiffness than the bedding planes results in a net reduction in bedding plane deformation potential.
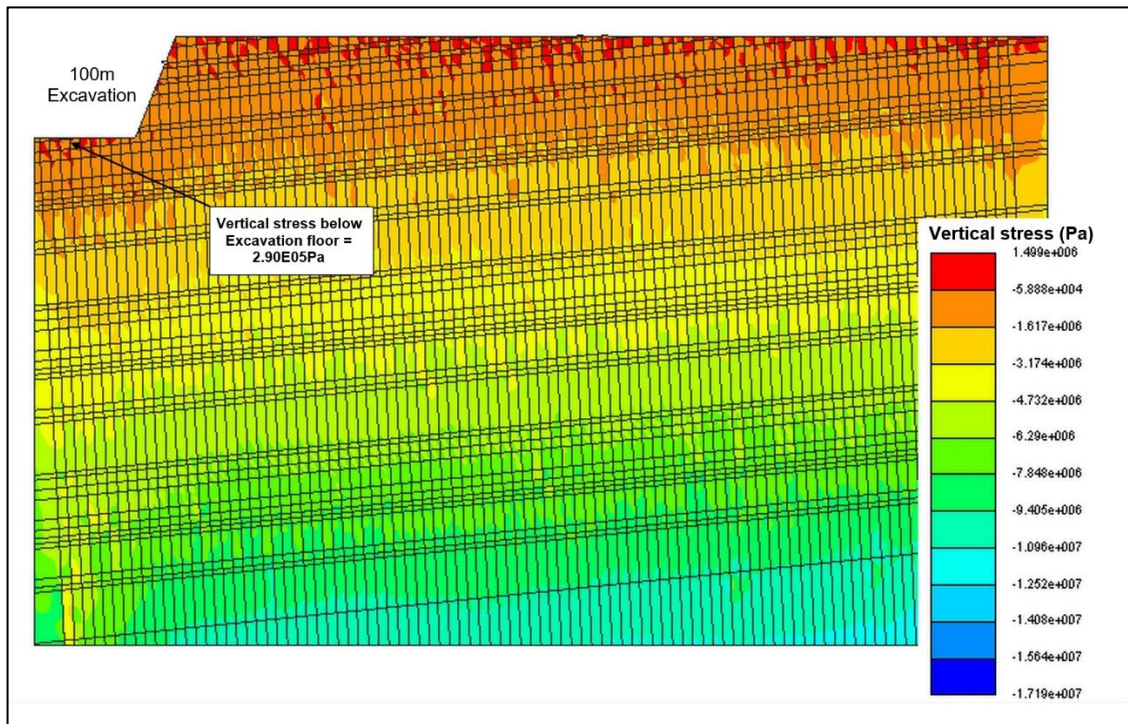
Figure 4.48: Model 4 Vertical stress distribution (Pa) around a 100 m deep excavation under low lateral stress conditions (k=0.27). The figure shows the reduction in vertical stress beneath the excavation floor.

The presence of sub-vertical jointing precludes the development of a continuous lateral tensile stress or extensional strain zone at the excavation floor. However, as shown in Figure 4.49, extensional strain conditions develop locally at discontinuity surfaces behind the excavation face.
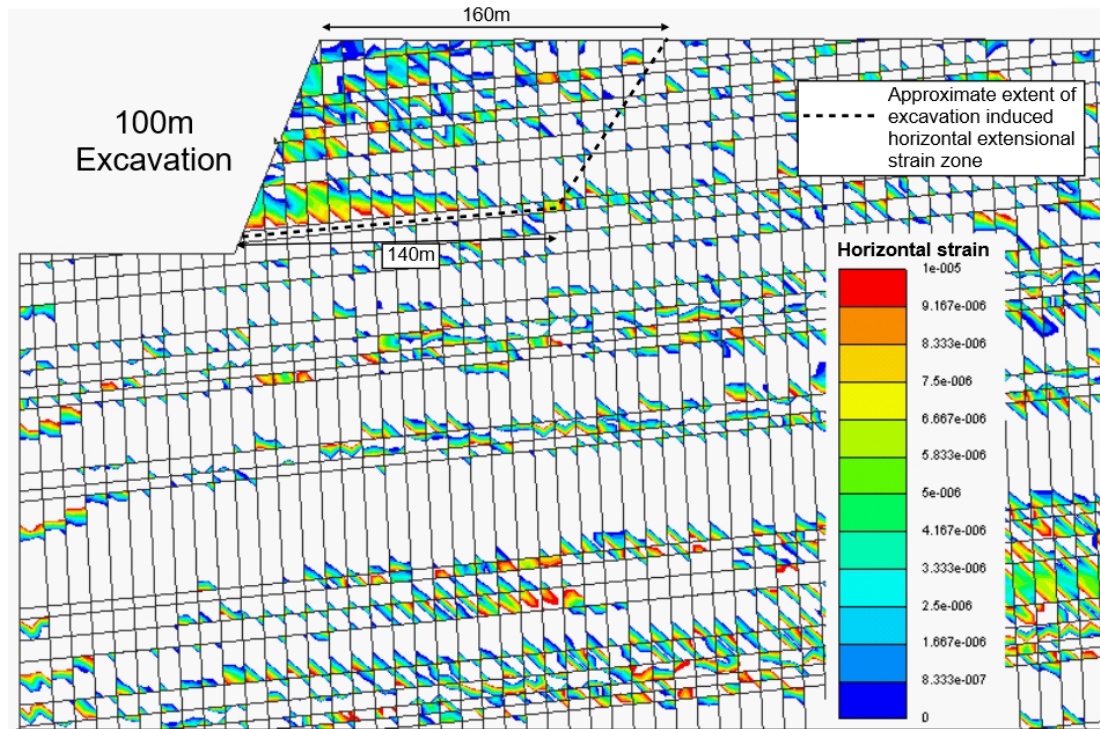
Figure 4.49: Model 4 Lateral extensional strain behind the excavation face showing the influence of discontinuities on extensional strain zone development behind the face. Local extensional strain zones at greater depth developed during the gravitational initialization stage of the model as a consequence of stress adjustment at the intersection of dipping bedding and joint surfaces. Extensional strain behind the face achieves a maximum magnitude of 0.00001. The figure shows part of the full model domain and has dimensions of 500 m x 300 m.

Figure 4.49 shows that extensional strain associated with discontinuity surfaces is developed behind the excavation face and at discontinuity intersections in deeper areas of the model. Extensional strain conditions at depth below the excavation floor develop at the gravitational initialisation stage as a direct consequence of vertical gravitational loading on dipping joints and bedding planes. With a 'no-displacement' left side boundary, extensional strain progresses further to the left down-dip boundary with increasing depth. This effect is entirely separate from the development of extensional strain behind the excavation face which is not present following gravitational initialisation

and does not occur until the excavation exceeds 30 m depth. At a 100 m depth of excavation, the lateral extensional strain zone extends approximately 140 m from the base of the excavation face, comparable to the bedding-only model (Model 2).

4.3.5.2 Excavation disturbed Zone (EdZ) extents

In common with previous models, the limits of the EdZ have been defined by reference to vertical and lateral stress variation in relation to stresses developed during gravitational initialisation. Results are shown in Table 4.10.

Lateral Stress Ratio (k)	Excavation depth (mbgl)	Limit of Vertical EdZ below Exc. Floor (m)	Limit of EdZ Horizontal Upper Face (m)
k=0.27	30	78	106
	60	88	261
	100	128	417
k=2.0	30	119	96
	60	144	246
	100	184	536

Table 4.10: Model 4 EdZ extents in the vertical and horizontal direction for excavation depths of 30 m, 60 m and 100 m under high and low lateral stress conditions.

Under low lateral stress, the vertical extents of the EdZ beneath the excavation floor are significantly lower than with the variably jointed model (Model 3) and the bedding only model (Model 2). The results indicate that inclusion of multiple fully persistent joints increases rock mass mobility, resulting in attenuation of the stress response by reduction in stored elastic strain energy over a shorter distance. Similarly, the lateral extent of the EdZ behind the excavation face is also lower in the orthogonally jointed model (Model 4) than in Models 2 and 3, indicating that the presence of multiple sub-vertical joints results in attenuation of the stress response as multiple joints dilate behind the excavation face.

In common with the variably jointed model (Model 3) in which the presence of internal joints influenced the vertical and horizontal extents of the EdZ, the introduction of fully persistent sub-vertical jointing in Model 4 has a significant effect on EdZ extents which are lower than in all previous models. Under high lateral stress conditions, EdZ extents are increased beneath the excavation floor but generally unchanged behind the excavation face.

4.3.5.3　　　　Rock mass displacement

When compared to other models, the displacement results for Model 4 demonstrate a reduction in the maximum vertical displacement to 0.024 m compared to 0.041 m in the bedding only model (Model 2). Vertical displacement values are shown on Figure 4.50.
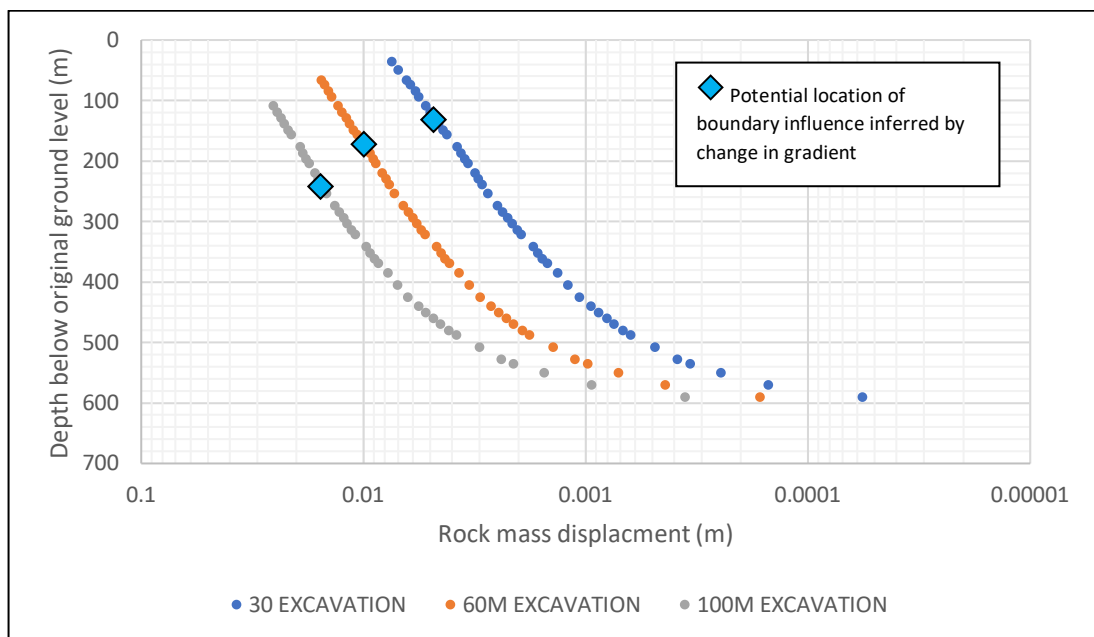
Figure 4.50: Model 4 Vertical rock mass displacement under low lateral stress conditions (k=0.27) for excavation depths of 30 m, 60 m and 100 m. At all excavation depths the potential depth of boundary influences is much greater than EdZ extents defined by analysis of the stress response, suggesting potential underestimate of Model 4 EdZ extents.
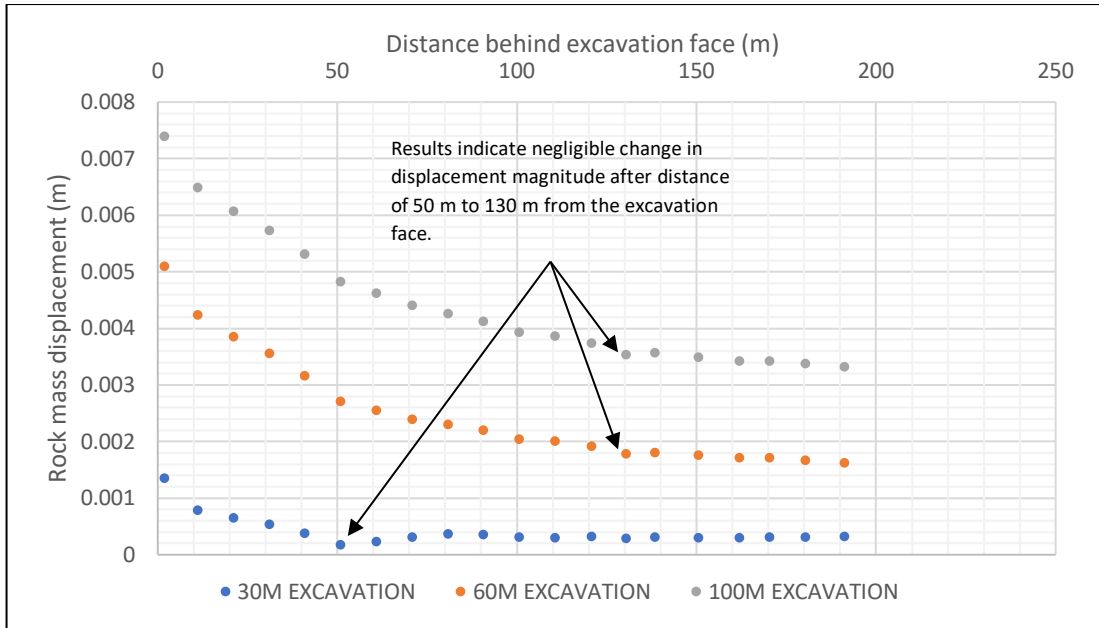
Figure 4.51: Model 4 Lateral rock mass displacement with increasing distance behind the upper excavation face (data extracted from a bedding plane parallel transect which intersects the upper model boundary at 200 m from the face). (k=0.27).
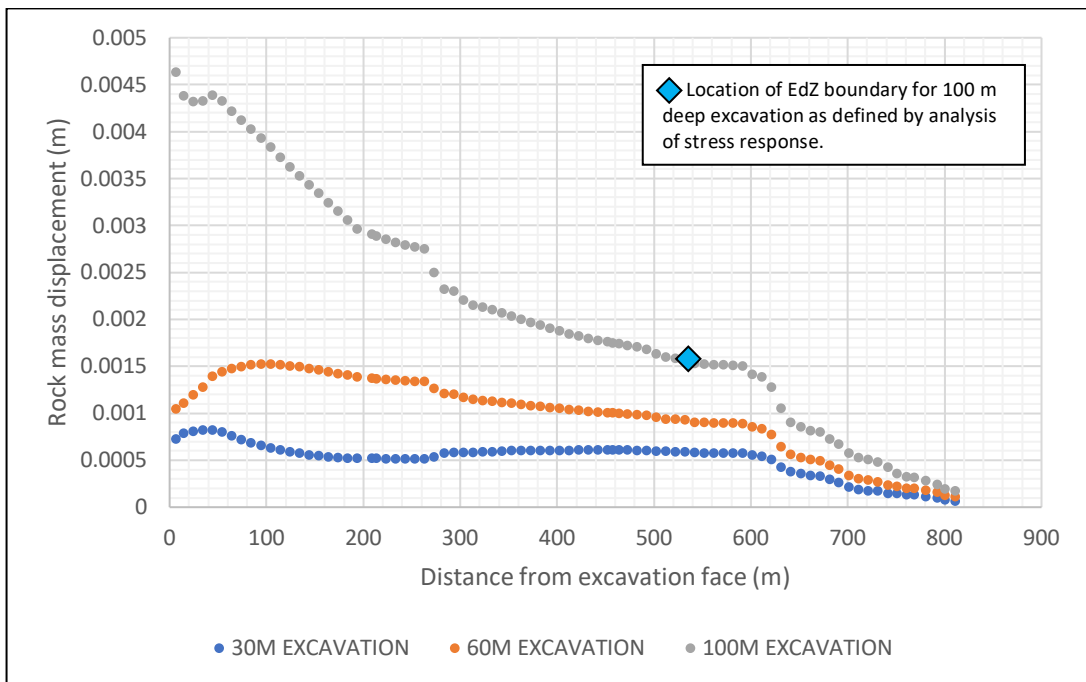
Figure 4.52: Model 4 Lateral rock mass displacement with increasing distance behind the lower excavation face. Results are extracted from a bedding parallel transect at 90 m depth and hence there is relatively small response to 30 m and 60 m deep excavation as shown (k=0.27). Curve step at 610 m is due to step change in horizontal transect elevation to maintain horizontal transect as node locations vary.

Lateral rock mass displacement values behind both the upper and lower excavation faces at low lateral stress are shown in Figures 4.51 and 4.52. Maximum lateral displacement behind the upper face is approximately 0.0072 m compared to 0.0046 m behind the lower face. Lateral displacement values in the orthogonally jointed model (Model 4) are approximately one-quarter of the magnitude of the lateral displacement values in the bedding only model (Model 2) and the variably jointed model (Model 3).

The introduction of multiple persistent orthogonal joints to the model results in a decrease in the maximum vertical displacement at the excavation floor and in the lateral displacement at the excavation face, when compared to the bedding only model (Model 2) and the variably jointed model (Model 3).

4.3.5.4   Discontinuity dilation

Analysis of bedding plane dilation beneath the excavation floor has been undertaken by reference to variation in joint surface penetration rates in response to progressive reduction in lithostatic load. The results are presented in Figure 4.53. Bedding plane dilation trends are comparable to that observed in the bedding only model (Model 2) with the majority of dilation occurring within the first 100 m - 200 m below the excavation floor. Maximum bedding plane dilation at 100 m depth of excavation is 0.26 mm. This compares to maximum dilation in the bedding only model at the same excavation depth of 2.7 mm, which is an order of magnitude higher.

The same analysis has been undertaken to calculate joint dilation behind the upper and lower excavation face. The results for the upper and lower of the excavation face are presented in Figures 4.54 and 4.55. The magnitude of joint dilation behind the excavation face, in response to lithostatic unloading to increasing depth, is relatively small when compared to bedding plane dilation in the bedding only model (Model 2). Joint dilation has been determined at two depths behind the face, (i) at a depth of 20 mbgl behind the 30 m deep excavation and (ii) at a depth of 90 mbgl behind the 100 m deep excavation. It is noted that the lower transect is below the 30 m and 60 m excavation depths and therefore the geomechanical response at these depths is minimal and not included on Figure 4.55
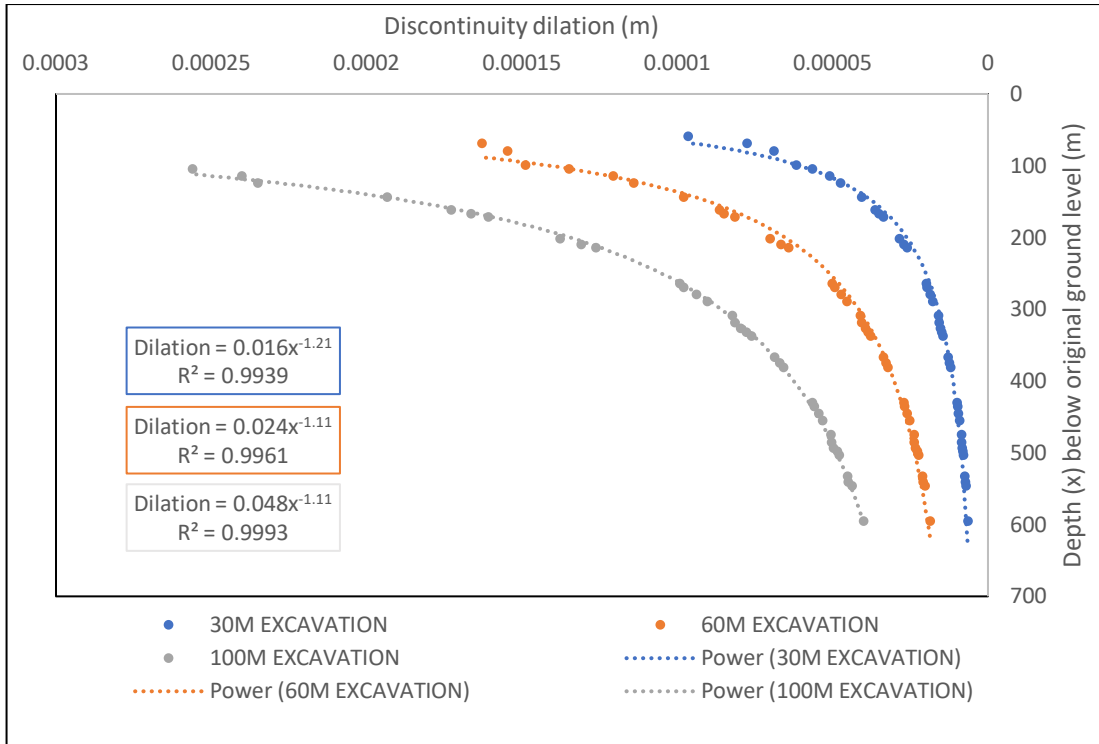
Figure 4.53: Model 4 Vertical discontinuity dilation beneath excavation floor showing reduction in dilation magnitude (m) with increasing distance below the excavation floor under low lateral stress conditions (k=0.27).
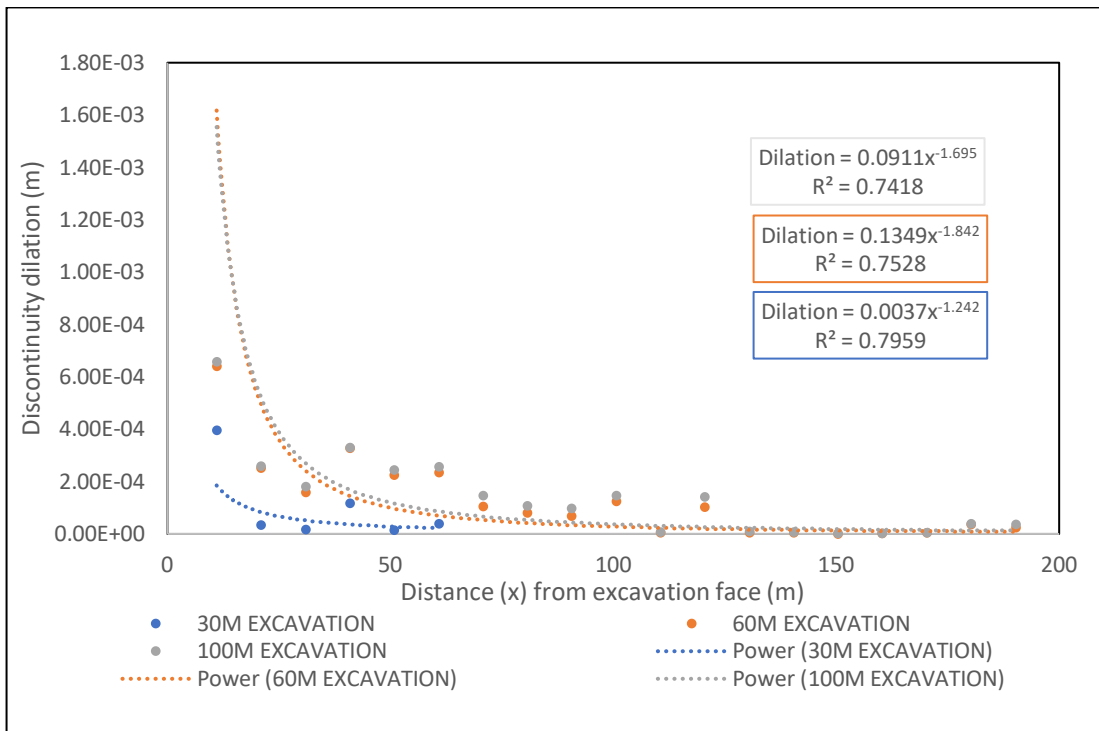
Figure 4.54: Model 4 Discontinuity dilation behind the upper face for excavation depths of 30 m, 60 m amd 100 m showing no signifcant dilation beyond a distance of 130 m from the upper excavation face (k=0.27).

Under low lateral stress conditions, the maximum individual joint dilation in the upper face occurs just behind the excavation face with a magnitude of 0.66 mm. Joint dilation does not occur beyond a distance of approximately 130 m from the upper excavation face. At the lower excavation face, maximum dilation at 100 m depth of excavation is 0.018 mm with negligible dilation beyond 200 m from the face.
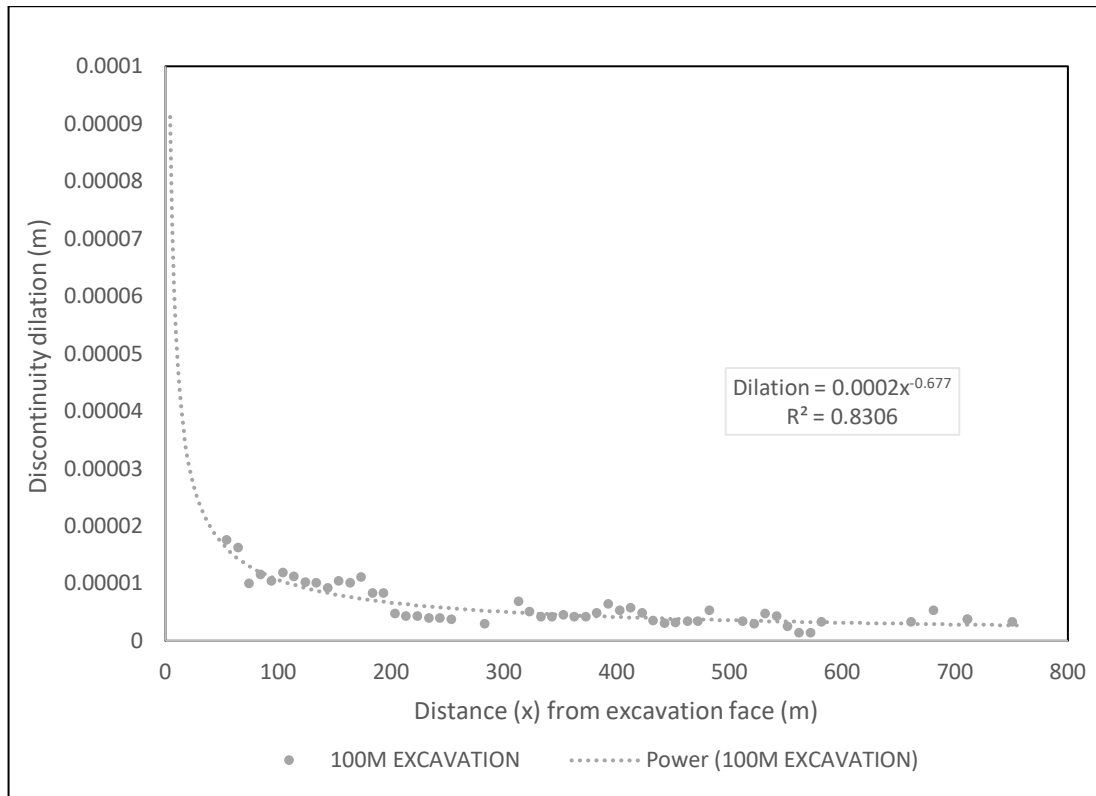
Figure 4.55: Model 4 Joint dilation with increasing distance behind the lower excavation face for an excavation depth of 100 m indicating that negligible dilation occurs beyond a distance of approximately 200 m from the excavation face (k=0.27).

Model 4 dilation/distance relationships for bedding plane dilation beneath the excavation floor and joint dilation behind the excavation face demonstrate that dilation magnitude if approximately proportional to the reciprocal of the distance from the floor or face. As shown on Figures 4.53 to 4.55, dilation/distance relationships can be defined by the power law function at Equation 4.2.

Excavation depth (mbgl)	Modelled displacement (m)	Total dilation (m)	Dilation % displacement
Bedding plane displacement/dilation below excavation floor			
30	0.007004	0.00130	19
60	0.015023	0.00280	19
100	0.024490	0.00365	15
Joint displacement/dilation behind excavation face			
30	0.001348	0.00062	46
60	0.005102	0.00241	47
100	0.007395	0.00269	36

Table 4.11: Model 4 Cumulative joint dilation in relation to maximum displacement for low lateral stress conditions (k=0.27).

Although the magnitude of individual joint dilation is relatively small the stress response in this model is distributed across multiple sub-vertical joints. The model incorporates joints at a spacing of 10 m resulting in a total of 100 sub-vertical joints within the model domain and approximately 20 joints within 200 m of the open excavation face. Cumulative dilation totals in relation to maximum displacement are shown in Table 4.11. On average, joint dilation accounts for approximately 20% of modelled displacement at the excavation floor and approximately 40% of modelled displacement behind the excavation face for all depths of excavation. Residual model displacement is accounted for by a combination of rock mass strain and sliding on discontinuity surfaces, as discussed in relations to Models 2 & 3.

As shown in Figure 4.53, bedding plane dilation reduces rapidly below a depth of 100 m to 200 m below the excavation floor, depending on depth of excavation. As summarised in Table 4.10, the estimated EdZ extent below the excavation floor is comparable to the distance over which dilation occurs. In a lateral direction behind the excavation face the majority of joint dilation occurs within a distance of 200m from the face. This is approximately consistent with the extent of the lateral EdZ behind the upper face.

The above analysis indicates that, for the orthogonally jointed model (Model 4), joint dilation beneath the excavation floor and behind the excavation face extends over a vertical and lateral distance from the excavation floor and face respectively, that is approximately equal to the defined extents of the EdZ.

Discontinuity dilation below the excavation floor with orthogonally orientated joint sets, as shown in Figure 4.53, can be compared to discontinuity dilation below the excavation floor with just bedding planes, as shown in Figure 4.27. The inclusion of orthogonal jointing results in 50% reduction in maximum bedding plane dilation magnitude when compared to the bedding-only model (Model 2). The presence of relatively closely spaced orthogonal joints crossing the bedding planes appears to influence stress redistribution at the excavation floor resulting in a more consistent floor-wide displacement than observed with the bedding-only model. In the bedding-only model the floor displacement at the centre of the excavation (left side model boundary) is approximately 50% greater than at the edges. In the orthogonally jointed model, floor displacement at the centre is only 30% higher than at the edges with lower variance across the floor. The presence of cross-cutting orthogonal jointing therefore appears to increase lateral distribution of stress at the excavation floor resulting in lower uplift with lower magnitude bedding plane dilation.

4.3.6 Summary results for all models

A summary of the key results for all models is presented in Table 4.12 for an excavation depth of 100 m under low lateral stress conditions. The summary results presented in Table 4.12 demonstrate that increasing discontinuity intensity leads to reducing EdZ extents. There is less variance in the vertical displacement results with an indication that increased discontinuity intensity leads to slightly reduced maximum displacement at the excavation floor. Larger differences occur in a lateral direction where maximum displacement in the orthogonally jointed model (Model 4) is much lower than for other models with discontinuities. This result appears to indicate that displacement is accommodated in multiple closely spaced joints resulting in lower maximum displacement at the excavation face. Increasing discontinuity intensity leads to reduced discontinuity dilation contribution to vertical displacement but has

no effect on discontinuity contribution to horizontal displacement. The significance of these results is discussed in detail at Chapter 5.

Parameter	Model 1 No Discontinuity.	Model 2 Bedding only	Model 3 Variably jointed	Model 4 Orthogonally jointed
EdZ Vertical Extent (m)	491	490	362	118
EdZ Horizontal Extent (m)	770	780	530	417
Max. Vertical Displacement (m)	0.020	0.041	0.033	0.024
Max Horizontal Displacement (m)	0.007	0.030	0.034	0.007
% Vertical Dilation Contribution	n/a	50	35	20
% Horizontal Dilation Contribution	n/a	n/a	40	40

Table 4.12: Summary geomechanical response results for all models

4.3.7 Sensitivity analysis

The sensitivity of model results to variation in critical parameters has been investigated to establish an understanding of influences on model outputs and the reliability and applicability of the input data sets. Key considerations include model sensitivity to variation in the following:

- Pre-existing lateral stress
- Discontinuity stiffness
- Rock mass material properties

All models developed in this study have incorporated analysis of two alternative lateral stress conditions intended to be reasonably representative of the likely range of real world in-situ stress conditions at the majority of open pit mineral excavation sites. No further analysis of sensitivity to variation in in-situ stress is therefore considered necessary.

4.3.7.1 Response to discontinuity stiffness variation

All discontinuities included in all models have been assigned variable normal stiffness values through the Elfen non-linear compliance function. As detailed at Chapter 3, a non-linear compliance curve was developed for each set of discontinuities based on the expected stress range and discontinuity average length. Normal stiffness values are calculated by reference to the non-linear compliance curve and the magnitude of joint surface penetration/dilation such that stiffness increases with increasing penetration and reduces with increasing dilation. Elfen does not return results for variable stiffness directly and therefore the values assigned at each stage of modelling have to be calculated using the relationship contact normal stiffness = 0.5 x Normal Contact pressure/Normal penetration.

The derivation of the non-linear compliance curves for bedding planes and the joints is described in Chapter 3. The curves are presented for reference as Figure 4.56 and 4.57.

In general, discontinuity penetration distances are low on all discontinuities and therefore the stiffness values assigned to the discontinuities are also relatively low, reflecting the relatively long length of the features modelled. Application of the non-linear compliance curves in Elfen models allows discontinuity stiffness to vary in relation to joint surface separation as simulated by a reduction in the penetration parameter.
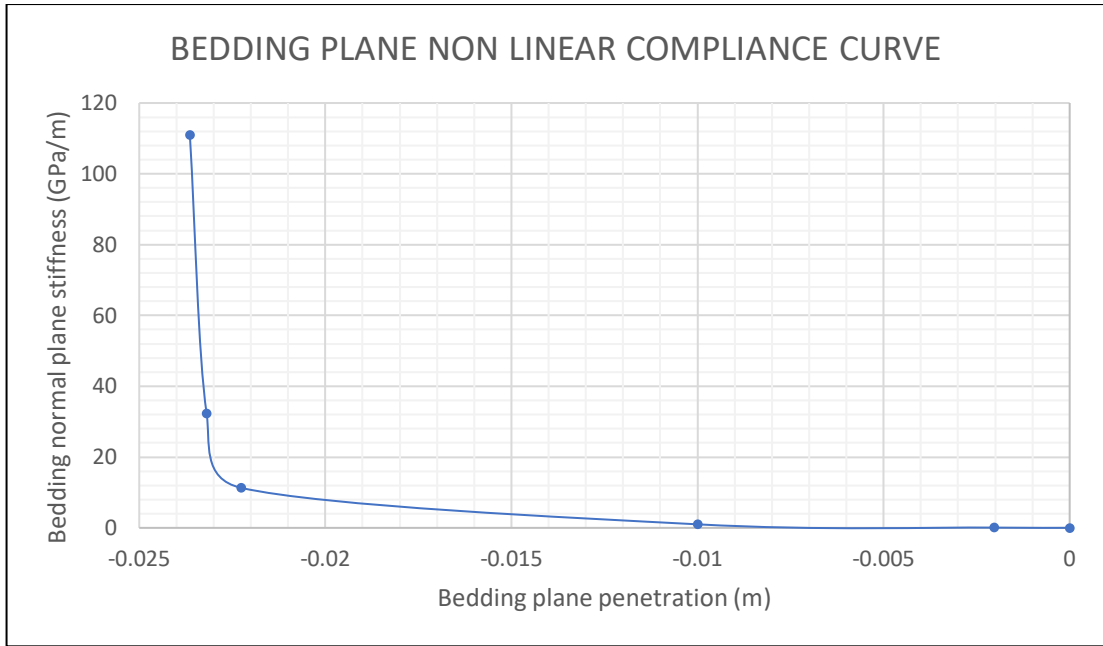
Figure 4.56: Non-linear compliance curves for bedding planes
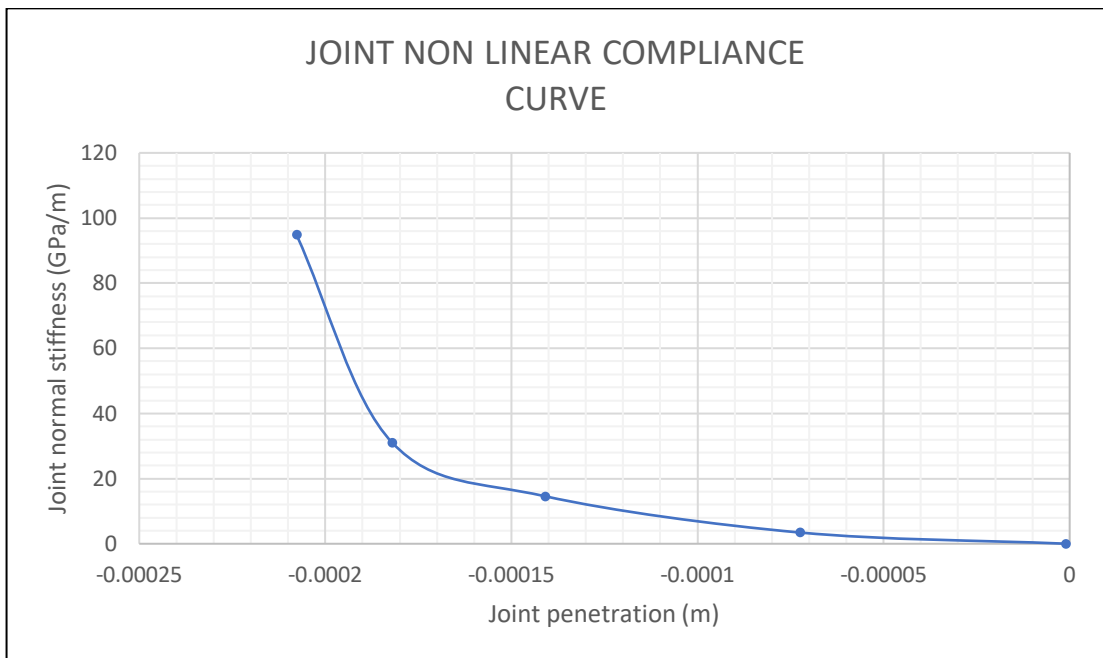
Figure 4.57: Non-linear compliance curve for joints

Stiffness values presented in Figure 4.58 have been extracted from model results using the relationship, contact normal stiffness = 0.5 x normal contact pressure/normal penetration, as discussed above. Example bedding plane and sub-vertical joint stiffness values are shown in Figures 4.58 and 4.59. In the bedding plane model, as shown in Figure 4.58, the data relates to normal stiffness of bedding planes beneath the excavation floor with increasing distance from original ground level for all three phases of excavation. It is

apparent that the assigned bedding plane stiffness values are relatively low, due to the high persistence of bedding planes in the models but are generally consistent with stiffness/length/stress relationships previously reported by other (Morris et al, 2017) as discussed at Chapter 3.
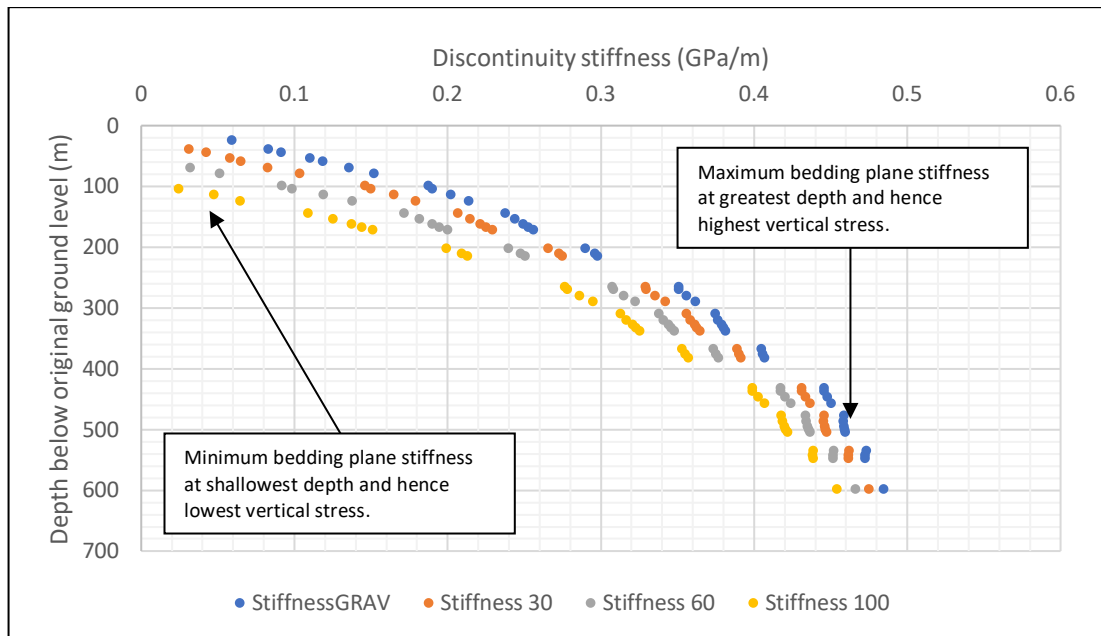
Figure 4.58: Model 2 resultant bedding plane stiffness variation with depth (for excavation depths of 30 m, 60 m and 100 m) after application of the non-linear compliance function relating bedding plane stiffness to bedding plane dilation for each of the four stages of model development. The results show that lowest stiffness values are assigned in response to the deepest excavation as maximum bedding plane dilation is achieved.

As shown in Figure 4.58, at depth, bedding plane stiffness values approach 0.5 GPa which is the default value derived from stress/length analysis. Stiffness values reduce to a minimum of less than 0.1 GPa/m at shallow depth. Joint dilation resulting from excavation unloading leads to reduction in bedding plane stiffness at any specified depth when compared to the pre-excavation gravitational initialisation condition.

Joint stiffness variation behind the excavation face in the orthogonally jointed model is shown in Figure 4.59. Stiffness variation is less consistent due to the location on joints at which the measurement is taken and the variable interaction between intersecting joints and bedding planes. Figure 4.59

demonstrates that there is no significant variation in joint stiffness in a horizontal direction behind the excavation face as stress magnitude variation is low. Joint stiffness reduces with increasing depth of excavation as joints behind the face dilate in response to stress reduction and loss of lateral containment. Assigned joint stiffness values are higher than bedding plane values with initial stiffness of approximately 1.5 GPa/m, reducing to less than 0.5 GPa/m within 50 m of the excavation face for 100 m depth of excavation. Joint stiffness at 30 m depth of excavation remains higher than the pre-excavation value throughout the model domain. Contact property measurement used in the Figure 4.59 analysis are derived from a horizontal transect at the base of the 30 m deep excavation.
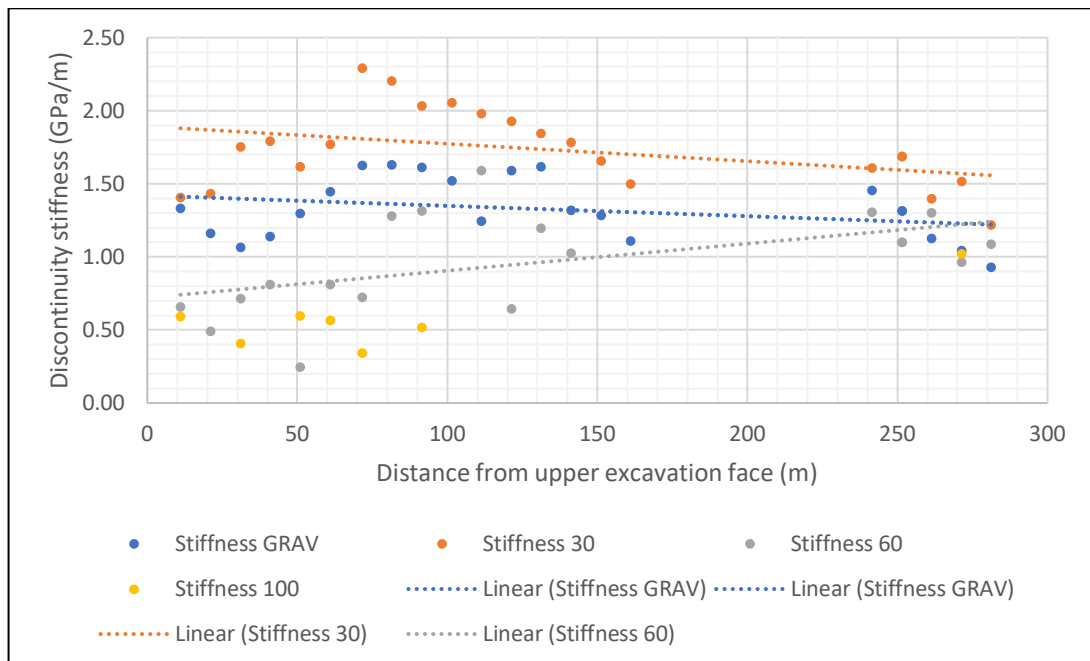
Figure 4.59: Model 4 resultant joint stiffness variation with distance from the excavation face after application of the non-linear compliance function relating joint stiffness to joint dilation for each of the four stages of model development. The results show that, due to low variation in stress magnitude laterally, there is low variation in assigned stiffness values laterally. Linear trend lines indicate a tendency to convergence towards a common joint stiffness value with increasing distance from the excavation face.

All the discontinuities included in the models used in this study exceed several metres in length and hence assigning stiffness values in relation to stress/length relationships inevitably leads to relatively low stiffness

magnitudes. It is acknowledged that smaller scale joints are likely to have a higher stiffness than the values used in this study.

4.3.7.2 Response to material strength variation

Investigation of model response to variation in rock mass material properties was undertaken by variation of properties in the variably jointed model (Model 3). Modelling was undertaken with all model surfaces assigned as sandstone, with associated material properties, and as limestone, with associated material properties. The main variations between the two materials are summarised in Table 4.13. The 'limestone' properties define a higher strength/stiffer material than the 'sandstone' material.

Comparative analysis of vertical displacements and normal bedding plane dilation for the two materials demonstrates the effect of variation in material properties on model results. As shown in Figure 4.60, results for the lower stiffness sandstone material at an excavation depth of 100 m indicate a maximum vertical displacement of 0.054 m. With the higher stiffness limestone material the maximum vertical displacement is 0.027 m, half the sandstone displacement.

Property	Sandstone Materials	Limestone Materials
Young's Modulus (GPa)	32.7	49.0
Poisson's Ratio	0.211	0.20
Shear Modulus (GPa)	13.36	15.00
Density (kg.m^3)	2360	2660
Friction Angle	27.8	42
Tensile Strength (MPa)	6.5	10.6
Cohesion (MPa)	27.2	42

Table 4.13: Material property variations used in analysis of model results sensitivity to variation in material properties.
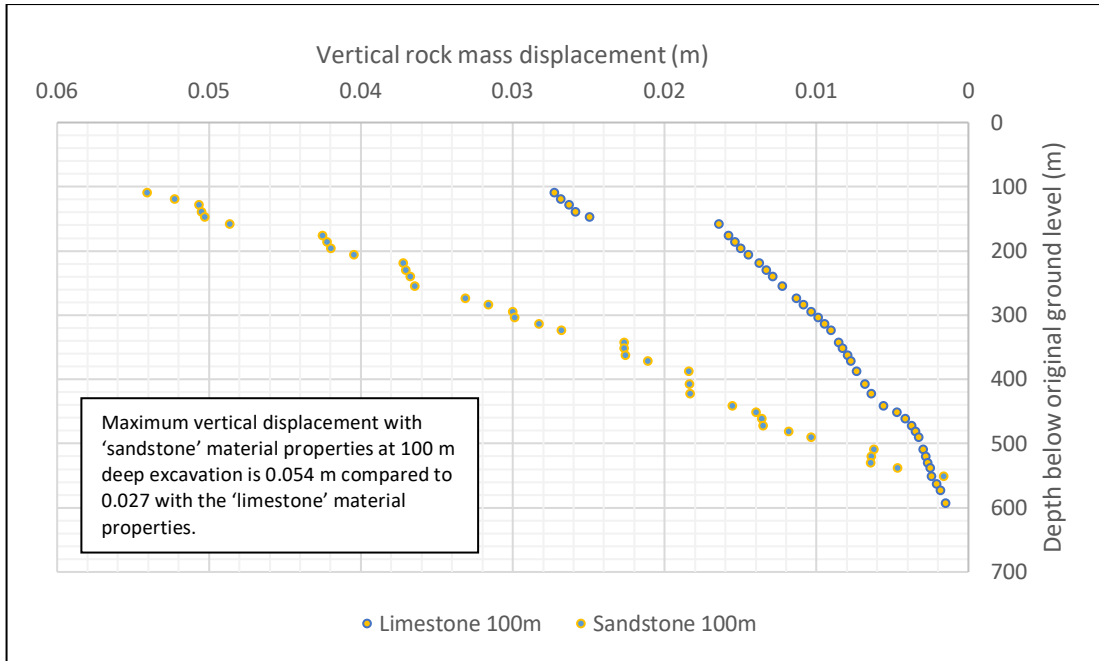
Figure 4.60: Model 3 Variably jointed model – comparison of vertical rock mass displacement below excavation floor at 100 m depth of excavation for models with different material properties, showing greater vertical displacement with the lower stiffness sandstone when compared to the higher stiffness limestone material.
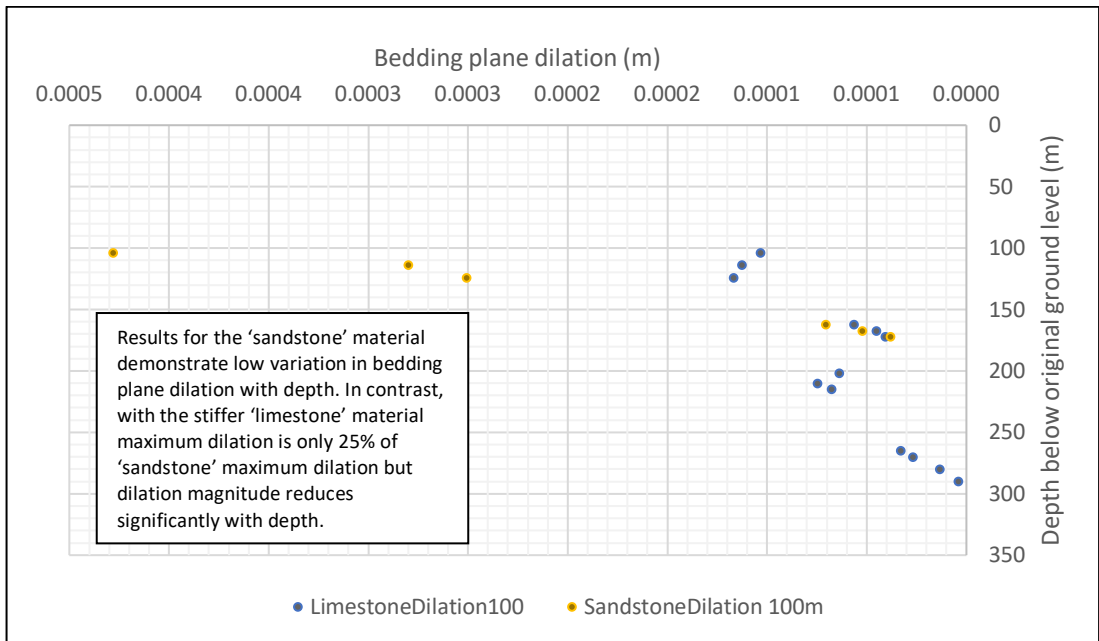
Figure 4.61: Model 3 Variably jointed model – comparison of bedding plane normal dilation below excavation floor at 100m depth of excavation for models with different material properties. Model results indicate that in the higher stiffness material, bedding plane dilations have lower magnitude but extend for greater distance below the excavation floor.

Reference to Figure 4.61, demonstrates that bedding plane normal dilation below the excavation floor for a 100 m deep excavation is significantly greater with the lower stiffness sandstone model than with the limestone model. Maximum sandstone dilation is 0.43 mm compared to a maximum limestone dilation of 0.12 mm. However, it is also apparent that, in the sandstone model, there is no definable bedding plane dilation below a depth of 172 m which equates to 72 m below the floor of the excavation. In the limestone model, definable dilation extends to a depth of 290 m which equates to 190 m below the excavation floor.

The above analysis demonstrates that rock mass material strength/stiffness has a significant effect on the geomechanical response to excavation unloading with lower stiffness materials responding with higher vertical displacement and higher discontinuity dilation magnitude than observed with higher stiffness materials. However, the depth at which definable dilation is observed is lower in lower stiffness materials. The general conclusions are as follows:

(i) Lower stiffness materials – higher discontinuity dilation over a shorter distance

(ii) Higher stiffness materials – lower discontinuity dilation over a larger distance

Comparison of cumulative dilation beneath the excavation floor demonstrates that cumulative dilation in the lower stiffness sandstone at 1.43 mm is approximately twice the cumulative dilation in the higher stiffness limestone at 0.76 mm.

4.3.6.3 Sensitivity summary

Analysis of model response to variations in pre-existing lateral stress, discontinuity stiffness and rock mass material properties has demonstrated that:

(i) In general, the vertical extent of the EdZ below the excavation floor is sensitive to changes in lateral stress but the lateral extent of the EdZ behind the excavation face is relatively insensitive to changes in lateral stress;

(ii) Model discontinuity normal stiffness values have been adjusted within a pre-determined stiffness range through application of the non-linear compliance function in Elfen; and

(iii) Variation in rock mass material properties has a significant effect on rock mass displacement extents and discontinuity dilation magnitude.

The results of the 2D and 3D modelling programme have been presented in this chapter. Results for all models are presented collectively with interpretation and consideration of respective geomechanical processes. The results of the modelling programme are discussed in detail in Chapter 5.

CHAPTER 5 DISCUSSION – GEOMECHANICAL RESPONSE, EXCAVATION DISTURBED ZONE EXTENTS AND DISCONTINUITY DILATION MAGNITUDE

5.1 Introduction

This chapter discusses the collective results of the geomechanical modelling programme, as presented in Chapter 4, with the aim of defining new approaches to the estimation of EdZ extents and advancing understanding of discontinuity displacement -v- dilation relationships around open pit mineral workings.

The geomechanical modelling programme has produced data related to the effects of lithostatic unloading at open pit excavations on the host rock stress response, rock mass displacement and dilation of pre-existing discontinuities. Model results are further discussed in this chapter through combined interpretation and analysis of data from all models and all in-situ stress conditions. Analysis is specifically focussed on the following issues:

1. Development of a generic approach to estimation of EdZ extents;

2. Interpretation of discontinuity dilation contribution to rock mass displacement; and

3. Improved definition of EdZ characteristics related to rock mass displacement and discontinuity dilation.

It is recognised that the geomechanical response of a rock mass to excavation-induced unloading will be highly site-specific. However, with the aim of supporting subsequent evaluation of hydrogeological significance, the methodologies presented in this Chapter should have generic application.

5.2 Review of the stress/strain response to lithostatic unloading

Geomechanical modelling with Elfen has been undertaken to support evaluation of stress response to lithostatic unloading at multiple excavation depths and in-situ stress states. In general, the reduction in load and lateral containment results in an elastic strain response with rock mass displacement arising from a combination of strain, discontinuity dilation and movement on discontinuity surfaces.

Modelling without discontinuities resulted in the development of a lateral tensile stress zone in the excavation floor under low lateral stress conditions and development of a lateral tensile stress zone in the upper excavation face under high lateral stress conditions. This response is consistent with results reported previously by others (Stacey, 2003). In other areas of the model domain, stresses remained compressive but, around the excavation void, were less compressive than prior to excavation. Under both modelled in-situ stress regimes, extensional strain zones were established beneath and behind the excavation floor and face.

Although extensional strain conditions developed in the floor and face, the strain magnitude is generally not high enough to result in the development of new fractures in the rock mass materials specified in the models. Stacey (2003) previously reported that critical extensional strain magnitudes at which fracturing might be expected in intact rock are within the range 0.0001 to 0.0003. Extensional strains developed in the current models are an order of magnitude lower than the levels normally required for fracturing of the rock mass. It is however, acknowledged that new fracturing could be expected in lower strength or weathered materials.

The introduction of sub-horizontal discontinuities to represent bedding planes (Model 2), precludes the development of a lateral tensile stress zone in the excavation floor. Behind the upper excavation face, a significantly reduced lateral tensile stress zone is developed. Lateral tensile stress in the excavation floor, with no discontinuities present, results from the differential uplift that occurs in the floor due to unloading. The presence of sub-horizontal bedding

planes allows lateral sliding on contact surfaces which appears to prevent the establishment of lateral tensile stress beneath the floor. The potential for sliding on contact surfaces also accounts for the reduction in the tensile stress zone behind the excavation face.

With the presence of bedding planes, in common with the no-discontinuity models (Model 1), extensional strain conditions develop vertically below the excavation floor and both laterally and vertically behind the excavation face. In contrast to the no-discontinuity model, there is no lateral extensional strain beneath the excavation floor. Lateral extensional strain developed due to differential uplift in the excavation floor in the no-discontinuity model appears to be accommodated by localised bedding plane contact surface sliding in the bedding only model.

In summary, the introduction of sub-horizontal discontinuities representing bedding planes, results in the following variations from the no-discontinuity model.

o   Absence of lateral tensile stress and lateral extensional strain beneath the excavation floor; and

o   Reduction in the extent of the lateral tensile stress zone behind the excavation face.

Models 3 (variably jointed model) and 4 (orthogonally jointed model) introduce sub-vertical jointing to the model in addition to the sub-horizontal bedding planes. The joints in the variably jointed model are variably distributed and orientated. Discontinuity connectivity is relatively low and joints mostly terminate within the model domain. The orthogonally jointed model incorporates equally spaced sub-vertical jointing that extends across all bedding planes and terminate at the model domain boundaries. Discontinuity connectivity is high.

The introduction of variably orientated sub-vertical jointing (Model 3) has relatively minor effect on the stress response to excavation when compared to the bedding-only model (Model 2). There remains no lateral tensile stress zone

in the excavation floor. Lateral tensile stress behind the excavation face is, however, more variable due to the influence of jointing. As with the no-discontinuity model (Model 1), extensional strain is developed vertically beneath the excavation floor and both vertically and horizontally behind the excavation face. In the orthogonally jointed model (Model 4) there is no development of a continuous tensile stress zone behind the excavation face, although tensile stress conditions develop locally at some joint surfaces. As with Model 3, vertical extensional strain develops beneath the excavation floor and both vertical and horizontal extensional strain zones develop behind the excavation face, although the extent of both is influenced by the presence of joints, with higher extensional strain focussed at discontinuity intersections.

The vertical extent of the extensional strain zone beneath the excavation floor is comparable for all models at 5 m, 15 m and 35 m for excavation depths of 30 m, 60 m and 100 m respectively. Behind the excavation face the horizontal extensional strain zone extent reduces with increasing discontinuity intensity or connectivity, with the smallest extensional strain zone arising from the orthogonally jointed model. In the bedding only model the extensional strain zone is influenced by the location and orientation of bedding planes and, for an excavation depth of 100 m, extends to a distance of up to 410 m from the face. The horizontal extensional strain zone behind the face is reduced to 320 m in the variably jointed model (Model 3) due to the introduction of sub-vertical jointing. In the orthogonally jointed model the horizontal extensional strain zone is limited to approximately 140 m from the excavation face for the same 100 m depth of excavation.

The primary conclusions regarding the role of discontinuities in the stress/strain response to lithostatic unloading are as follows:

o The presence of sub-horizontal bedding planes appear to prevent the formation of lateral tensile stress and lateral extensional strain conditions in the excavation floor;

o Vertical extensional strain conditions beneath the excavation floor are relatively insensitive to the presence of discontinuities; and

o Extensional strain extents behind the excavation face reduce with increasing discontinuity intensity/connectivity.

In general, model results demonstrate collectively that the presence of discontinuities in the host rock has a significant influence on the stress/strain response to excavation unloading, with consequent influence on the development of the EdZ and the displacement of discontinuous strata around the excavated void.

5.3 Excavation disturbed zone (EdZ) extents and configuration

Three-dimensional model results have demonstrated that the lateral extent of the disturbed zone (EdZ) around non-circular open pit excavations is not the same at all locations around the excavation perimeter. Where excavation faces are bounded by intersecting faces, as is the case in most excavations, the absence of a free face at the intersection restricts lateral displacement and reduces the lateral extent of the EdZ. As shown at Figure 4.8, in three-dimensions, the EdZ extends the furthest from the excavation face at the centre of the face and reduces to approximately 50% of this extent at the face boundaries. EdZ extents are therefore not represented by concentric circles around an excavation but by a series of connecting arcs with maximum radius at the centre of the face. In all 2D models, plane strain conditions are assumed. Such conditions are representative of the centre of an excavation face in the corresponding 3D models, where there is minimum confining from intersecting boundary faces. On this basis, the EdZ extents derived from 2D modelling can be considered to represent the maximum extent of the EdZ around an open pit excavation.

Excavation disturbed zone vertical extents beneath the excavation floor are well-defined for all models. The use of stress change, when compared to pre-excavation stress distribution, to define vertical EdZ boundaries during excavation unloading is comparable to the Boussinesq approach to determination of ground stresses below surface loading (Craig, 1987). The disturbed area within which stresses are reduced due to excavation unloading has a configuration comparable to the Boussinesq 'stress bulb' below a

surface load. This is shown clearly in vector displacement plots at Figures 4.2, 4.3 and 4.4 that provide an indication of EdZ boundaries.
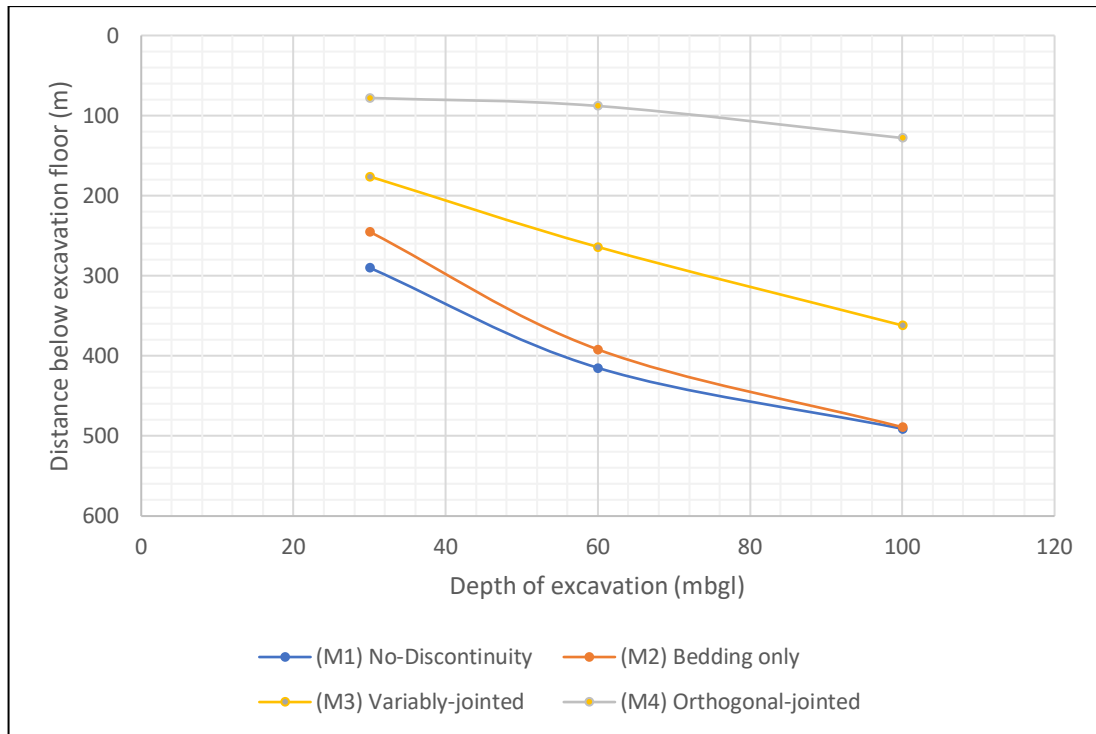
Figure 5.1: Vertical EdZ extents for all models at lateral stress ratio of 0.27. Combined results show increasing vertical EdZ extents with increasing depth for all models and reduction in EdZ extents with increasing discontinuity intensity.

As shown on the composite graphs at Figures 5.1 and 5.2, the depth of the EdZ beneath an excavation floor increases with increasing depth of excavation. As this is primarily an elastic response, increasing EdZ depth with increasing magnitude of unloading is consistent with expectations. For shallow excavations of 30 m depth under low lateral confining stress, the disturbed zone beneath the floor extends for 80 m - 290 m, depending on the presence and configuration of discontinuities. As shown in Figure 5.2, under higher lateral confining stress conditions, where there is increased lateral compression, the disturbed zone extends over a shorter range of distances below the excavation floor for all modelled excavation depths.
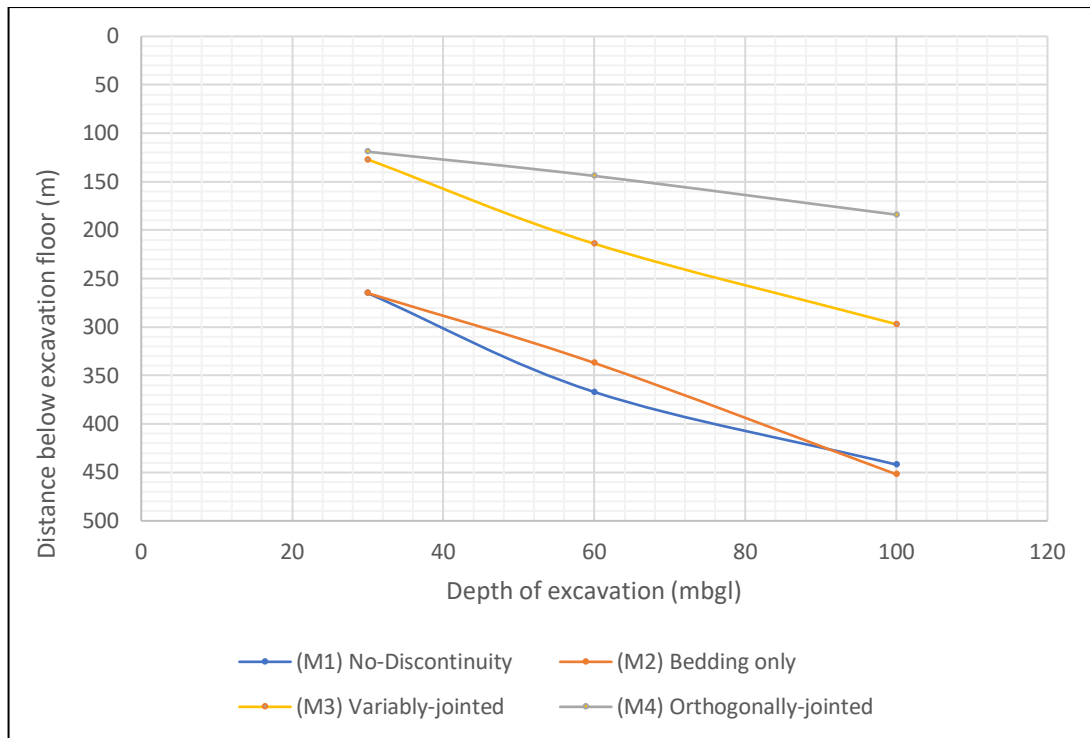
Figure 5.2: Vertical EdZ extents for all models at lateral stress ratio of 2.0. Combined results show increasing vertical EdZ extents with increasing depth for all models and reduction in EdZ extents with increasing discontinuity intensity. With higher lateral confining stress, EdZ extents for all excavation depths are defined by a smaller range of values when compared to the low lateral confining stress results.

Excavation disturbed zone vertical extents can be normalised in relation to excavation depth and width. Excavation depths of 30 m, 60 m and 100 m have been modelled with equivalent excavation floor widths of 256 m, 232 m, and 200 m, respectively (twice the model floor dimensions as excavations are modelled on a half space basis), defined in the models as a consequence of the fixed 70° face angle. Analysis of EdZ extents in relation to excavation configuration indicates that vertical EdZ extents are influenced by both the magnitude of load reduction and the length (2D) or area (3D) over which load reduction is applied. With an angled face, load reduction occurs at both the floor and the face and therefore normalisation has incorporated reference to unloading on all surfaces. In effect, it is the areal (2D) or volumetric (3D) unloading over the unloading surface (2D) or area (3D) that determines EdZ extents and configuration.

As excavation faces are sloping at a steep angle the unloading surface can be approximated as the width of the floor plus twice the excavation depth, as shown in Figure 5.3 (with a face angle of 70° the vertical depth of excavation equates to 94% of the length of the face. At steeper angles the excavation depth would equate to a higher percentage of the face length), which simplifies the application of this approach. Normalisation of vertical EdZ results has therefore been undertaken through application of the following formula.

Normalised EdZ$_v$ (n$_v$) = $\dfrac{(EdZ_v \times \text{unloading surface length})}{(\text{Excavation depth} \times \text{Excavation width})}$ [5.1]
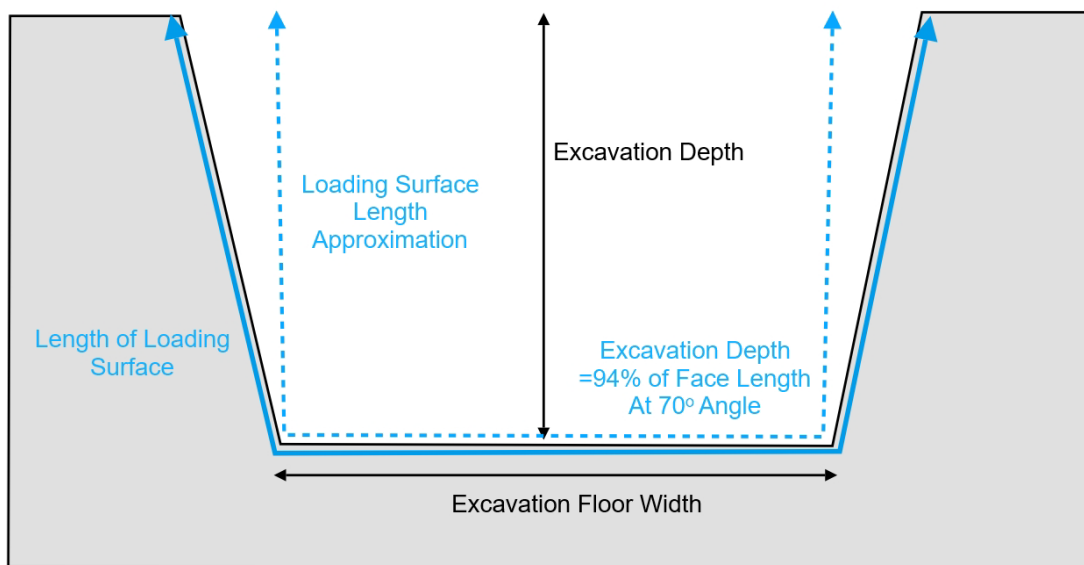
Figure 5.3: Schematic representation of dimensions used in normalisation of vertical EdZ extents with respect to excavation configuration. With sub-vertical excavation faces, the length of the unloading surface can be approximated as excavation floor width plus 2 x excavation depth as shown.

The normalised value (n$_v$) is dimensionless. The location of respective dimensions used in the normalisation process is shown schematically in Figure 5.3. Normalisation coefficients for the low lateral stress models are presented in Table 5.1. Due to the different response to unloading for respective discontinuity configurations it is not appropriate to approximate a single normalised coefficient for application to all models. Normalisation coefficients (n$_v$) defined by Equation 5.1 do not vary significantly with depth of excavation and mean values across all excavation depths are therefore considered to be representative.

Exc. depth (m)	Exc. width (m)	Unloading surface length (m)	Model 1 No discon.	Model 2 Bedding	Model 3 Variably jointed	Model 4 Orthogonal jointed
30	256	316	13.4	10.3	7.4	3.3
60	232	352	12.4	10.2	6.9	2.3
100	200	400	12.4	10.3	7.6	2.5
Mean normalisation coefficient (n_v)			**12.7**	**10.2**	**7.3**	**2.7**

Table 5.1. Normalised vertical EdZ extent coefficients (n_v).

Table 5.1 demonstrates that whilst normalisation coefficients are not depth sensitive, they vary in relation to discontinuity intensity. Using these values an estimate of potential vertical EdZ extent would be determined as follows.

$$EdZ_v = n_v \times (depth \times width)/(width + 2 \times depth) \qquad [5.2]$$

Examples of the application of this procedure are included below.

Example 1: excavation 30 m deep and 100 m wide with variably jointed strata
EdZ_v = 7.3 x (30 x 100)/(100 + 60)
= 136 m

Example 2: excavation 70 m deep and 200 m wide in bedded strata
EdZ_v = 10.2 x (70 x 200)/(200 + 140)
= 420 m

Although the above analysis is based on the range of model depths and widths included in this study, the principle of EdZ extent normalisation based on open pit geometry should remain applicable to other geometries, where a rock mass

can be defined by a large enough representative elementary volume (REV) to capture discontinuity spacing.

5.3.1 Comparison to Boussinesq analysis

With a constant excavation depth across the excavation floor, as configured in all models in this study, lithostatic unloading results in homogeneous reduction in stress across the floor. Model results can therefore be considered in relation to Boussinesq analysis for a uniform load on a 2D strip with infinite length. For vertical stress below the strip foundation, the relevant equation is Equation 2.7 with geometrical configuration as shown in Figure 3.7.

Boussinesq analysis indicates that, for an elastic half-space, below a linear strip subject to uniform load/unload the subsurface stress can be related to the width of the unloaded surface with residual stress equal to approximately 20% of the applied load at a depth of approximately 3 times the width of loading (Craig, 1987). For an unloading situation this would translate to an expectation that subsurface stress would equate to 80% of the pre-unloading stress at a depth of 3 times the width of the excavation. Hencher (2016) refers to stress beneath foundations and suggests that in practice, vertical stress is reduced by about 90% of the surface load at a depth of approximately 1.5 x foundation width.

Excavation depth (m)	Excavation width (m)	EdZ extent K=0.27 (m)	EdZ (0.27)/width	EdZ extent K=2.0 (m)	EdZ (2.0)/width
30	256	290	1.13	265	1.04
60	232	415	1.79	366	1.58
100	200	491	2.46	440	2.20

Table 5.2: Excavation width multipliers to define vertical EdZ extent in rock mass without discontinuities for lateral confining stress ratios of 0.27 and 2.0.

Excavation disturbed zone extents have been defined in this study as approximately 95% of the pre-unloading stress. Although the modelled excavations constitute a half-space excavation, vertical stress measurements have been taken at the left-side model boundary equating to the centre of the excavation and therefore consistent with stress measurements beneath the centre of a strip foundation. As shown in Table 5.2, calculation of vertical EdZ extents for a range of excavation widths indicates that, for a rock mass with no discontinuities, the 95% stress magnitude is achieved at depths between 1.04 and 2.46 times the width of the unloaded area.

It is apparent therefore that vertical EdZ extents defined from model results for rock without discontinuities are reasonably consistent with analytical results based on application of Boussinesq analysis and representative of the 'stress bulb' for uniform unloading. Table 5.2 indicates that width multipliers decrease with increasing lateral confining stress as vertical EdZ extents are reduced.

5.3.2 Effect of pre-existing discontinuities on EdZ development

Reference to Figure 5.1 and 5.2 shows the effect of discontinuities on the modelled vertical extent of the EdZ. In general, the results demonstrate that the vertical extent of the EdZ decreases with increasing discontinuity intensity/connectivity. The decrease is less significant under high lateral stress conditions where, due to effective increase in discontinuity stiffness, the modelled response is closer to the no-discontinuity model, with the exception of the most mobile orthogonal model which retains much shallower vertical EdZ extents. Decrease in vertical EdZ extents is attributable to the presence of discontinuities (bedding planes in Model 2) with a lower stiffness than the host rock, and increased rock mass mobility due to the presence of sub-vertical jointing (Models 3 and 4). The elastic response to lithostatic unloading is dissipated over a shorter distance beneath the excavation floor when discontinuities are present.

For the maximum modelled excavation depth of 100 mbgl, EdZ vertical extents range from 120 m below the excavation floor to 490 m below the excavation floor. Under high lateral stress conditions the vertical EdZ extents vary slightly

for the same excavation depth within a narrower range of 184 m to 450 m below the excavation floor.

Whilst the vertical response to lithostatic unloading occurs primarily as an elastic response to stress reduction, under low lateral confining stress, the lateral response behind an excavation face occurs in response to a loss of lateral containment, leading to development of an unconstrained free surface at the excavation face, and both a lateral elastic response and unconstrained displacement. The response is critically influenced by the presence and configuration of discontinuities in the rock mass.
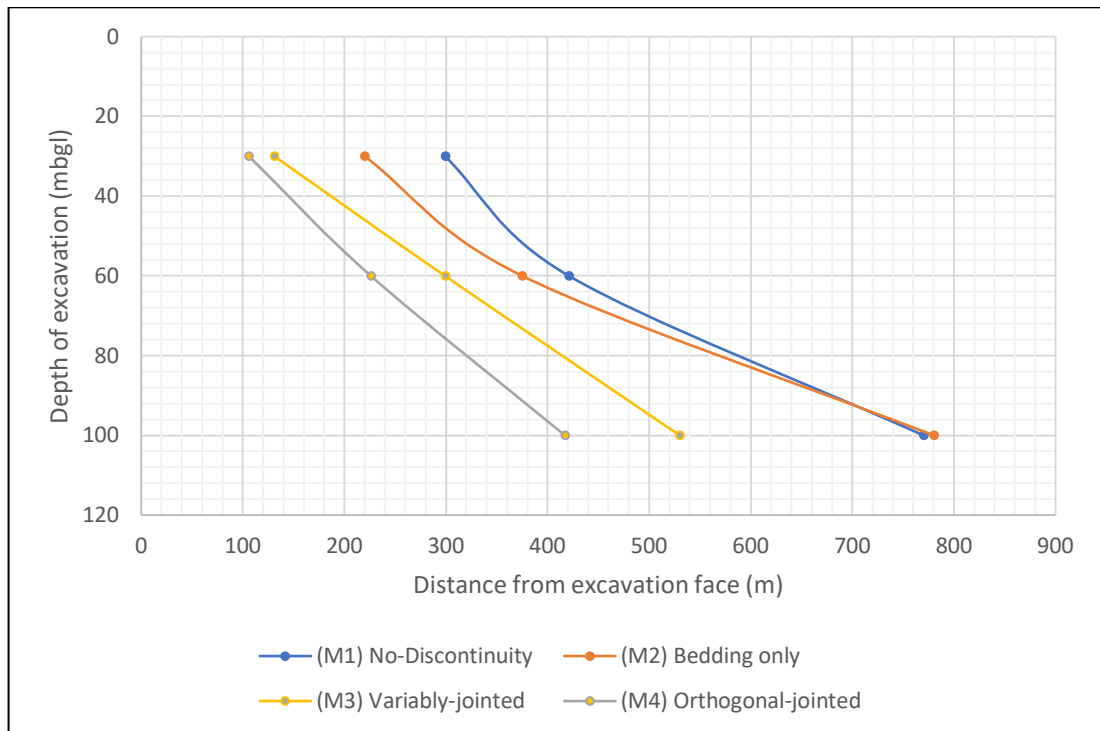
Figure 5.4: Lateral EdZ extents behind the upper excavation face for all models at low lateral confining stress. The results show progressive reduction in the horizontal distance of the EdZ behind the excavation face with increasing discontinuity intensity.

Modelled outputs for the lateral extent of the EdZ behind the excavation face are shown in Figures 5.4 and 5.5. As discussed at Section 4.3.1.3, under low lateral stress conditions there is no lateral displacement inward towards the excavation face for the model without discontinuities, however, the stress response allows definition of EdZ extents. Figures 5.4 and 5.5 show the EdZ extents for the no-discontinuity model and the three discontinuity models. The

figures present data for a horizontal transect at the base of the upper 30 m deep excavation and therefore represent conditions in the upper excavation face.

Lateral EdZ extents in all models increase significantly with increasing depth of excavation. At 30 m depth of excavation, the minimum EdZ extents occur in the jointed models within a range of 106 m – 220 m behind the excavation face. At 100 m depth of excavation this increases to almost 800 m behind the upper excavation face in the bedding-only model. Under high lateral stress conditions the lateral EdZ extents increase slightly with the response for the bedding-only model (Model 2) being comparable to the no-discontinuity model (Model 1).
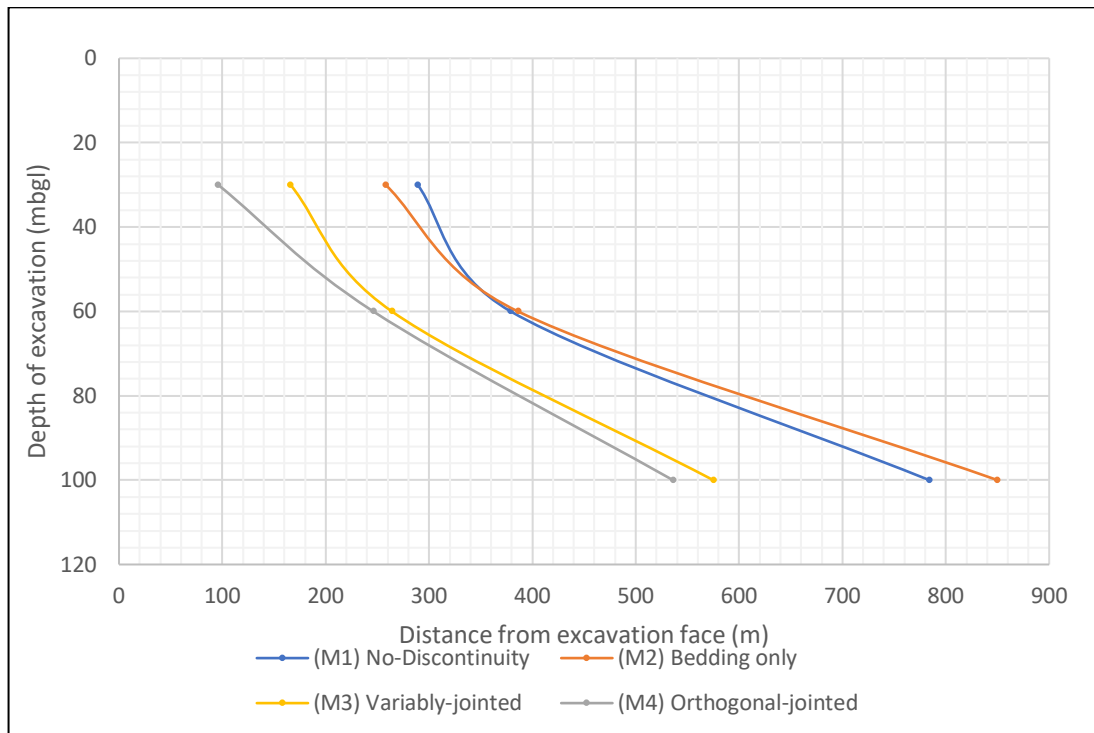
Figure 5.5: Lateral EdZ extents behind the upper excavation face for all models at high lateral confining stress. The results demonstrate that the effect of discontinuities on reducing the extent of the EdZ behind the face is reduced when compared to results under low lateral confining stress (see Figure 5.4).

Model results demonstrate that under low lateral stress conditions, the introduction of sub-vertical jointing, either variably orientated or orthogonally orientated, results in a decrease in the lateral extent of the EdZ, when

compared to the no-discontinuity model. This is attributed to dissipation of elastic strain over a shorter distance due to the presence of discontinuities with a stiffness that is lower than rock mass stiffness. The lateral EdZ extents associated with the bedding-only model are the largest of all the models although similar to the no-discontinuity model (Model 1). This effect occurs as a consequence of the dip of the bedding planes. The EdZ boundary coincides with the point at which the bedding planes intersects either the upper or the right-side model boundaries. With potential for displacement by sliding on bedding planes that intersect the excavation face, resulting in both shear failure near the face and elastic shear deformation further from the face, there is a definable stress response along the full bedding plane length.

The observed lateral response to unloading, with reducing EdZ extent in response to the presence of discontinuities, is consistent with the observed results for the vertical extents of the EdZ which show the same trend.

Under high lateral stress conditions there is an increase in the lateral extent of the EdZ in all models. This is contrary to the model results for the EdZ in the vertical direction where EdZ extents reduce under high lateral stress conditions. In a horizontal direction the high lateral stress acts to increase discontinuity stiffness such that the presence of discontinuities has a reduced impact on rock mass stiffness and the stress response that defines the EdZ boundaries is closer to the response for the bedding-only model (Model 2).

Lateral EdZ extents are not influenced by excavation width as width variation has no influence on the height or angle of the free face. Lateral EdZ extents can therefore be normalised in relation to excavation depth alone by applying Equation 5.3. The results are presented in Table 5.3 for the low lateral stress condition. The use of Equation 5.3 results in little variation in the multiplier with depth but captures the impact of variation in discontinuity intensity. As with vertical EdZ extents, normalisation coefficients decrease with increasing DFN intensity.

Excavation depth (m)	No discon.	Bedding	Stochastic	Orthogonal
Lateral EdZ extent depth multiplier				
30	9.97	7.33	4.36	3.53
60	7.02	6.25	4.98	3.77
100	7.70	7.80	5.30	4.17
Mean Values (n_h)	**8.23**	**7.13**	**4.88**	**3.82**

Table 5.3. Normalised horizontal EdZ extents

Lateral EdZ_h extent can be estimated by reference to excavation depth as:

$$EdZ_h \text{ (m)} = n_h \times depth, \qquad\qquad\qquad [5.3]$$

where n_h = a normalisation coefficient as detailed in Table 5.2

In summary, EdZ vertical and horizontal extents for excavations in host rock with and without discontinuities can be estimated by use of Equations 5.2 and 5.3.

On this basis an open pit excavation 60 m deep and 200 m wide in orthogonally jointed fractured hard rock might be expected to generate an EdZ that extends 100 m below the base of the excavation floor and 230 m behind the excavation face.

5.4 Rock mass displacement and the effect of pre-existing discontinuities

Rock mass displacement magnitude around an open pit excavation of increasing depth has been determined for each of the four models under two lateral stress regimes. Displacements are shown at locations with increasing distance from the excavation floor or face. The results for all models are presented collectively in Figures 5.6 and 5.7 for each lateral stress condition.
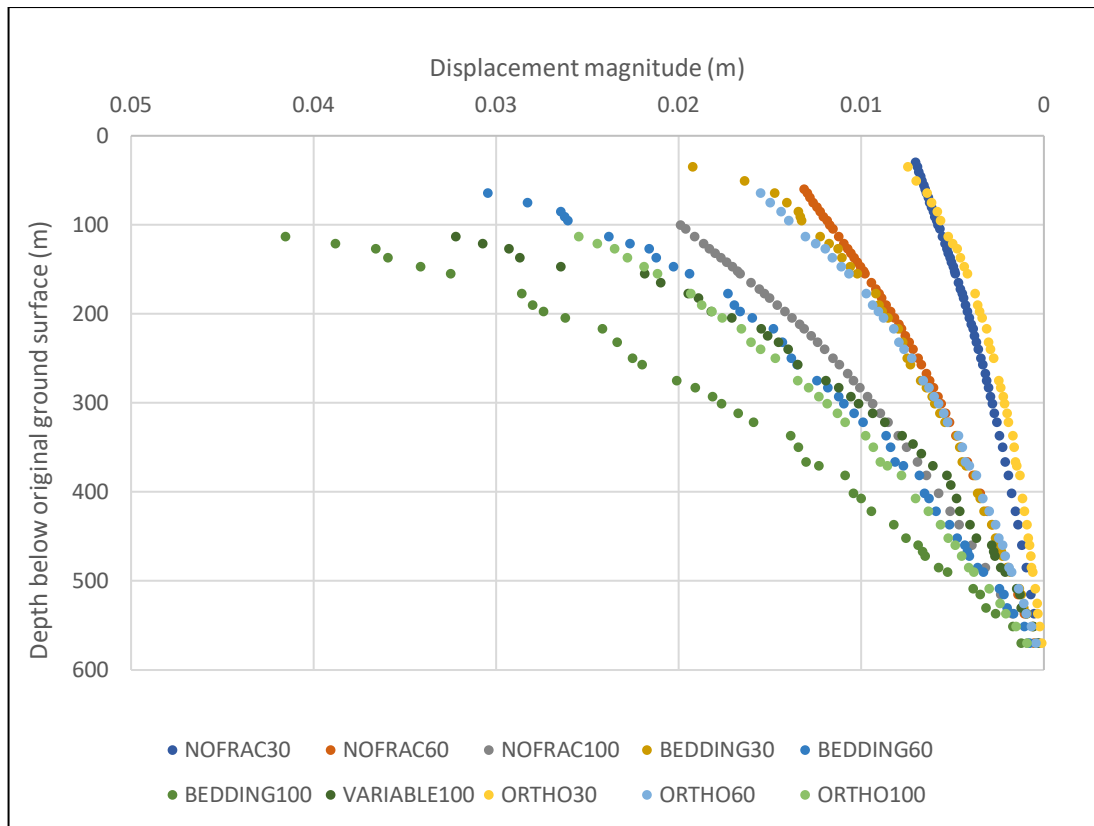
Figure 5.6: Vertical rock mass displacement beneath the excavation floor under low lateral stress conditions. All plotted displacement curves follow a similar trend with displacement magnitude declining with depth. Maximum vertical displacement magnitude at the excavation floor ranges from 0.75 cm for a 30 m deep excavation without discontinuities to 4.15 cm for a 100 m deep excavation with bedding planes only [NOFRA = Model 1, BEDDING = Model 2, Variable = Model 3, ORTHO = Model 4].

Collective results demonstrate that, under a low lateral stress regime, maximum rock mass displacement occurs at the excavation floor and reduces progressively with increasing depth below the excavation floor for all models. Maximum vertical displacement magnitude is 4.15 cm observed in the bedding-only model (Model 2) at 100 m depth of excavation. As shown in Figure 5.7, under high lateral stress conditions there is a general increase in maximum vertical displacement magnitude, when compared to the low lateral stress case, for all models with the maximum modelled displacement of 4.9 cm at the excavation floor for a 100 m deep excavation in the orthogonally jointed model.

Order of increasing displacement	Low lateral stress (k=0.27)	Max. Disp. at Exc. Floor (cm)	High lateral stress (k=2.00)	Max. Disp. at Exc. Floor (cm)
1	Orthogonally-jointed (30m)	0.75	No-discontinuity (30m)	0.68
2	No-discontinuity (30m)	0.70	No-discontinuity (60m)	1.18
3	No-discontinuity (60m)	1.28	Bedding-only (30m)	1.81
4	Bedding-only (30m)	1.92	No-discontinuity (100m)	1.71
5	Orthogonally-jointed (60m)	1.50	Variably-jointed (100m)	2.53
6	No-discontinuity (100m)	1.96	Bedding-only (60)	3.13
7	Bedding-only (60m)	2.83	Bedding-only (100m)	4.22
8	Variably-jointed (100m)	3.07	Orthogonally-jointed (30m)	4.15
9	Orthogonally-jointed (100m)	2.54	Orthogonally-jointed (60m)	4.32
10	Bedding-only (100m)	4.15	Orthogonally-jointed (100m)	4.91

Table 5.4: Showing the sequential position of the vertical displacement curve in Figure 5.6 and Figure 5.7 for each model in relation to vertical rock mass displacement and the magnitude of maximum vertical displacement at the excavation floor. The table demonstrates that vertical displacements are higher under high lateral stress conditions and that the presence of discontinuities has less of an effect on vertical displacement magnitude at low lateral stress than under high lateral stress conditions.

The data presented in Table 5.4 indicates that under low lateral stress conditions, the presence of discontinuities has less impact on rock mass displacement magnitude at shallow excavation depth than is observed at greater depth.
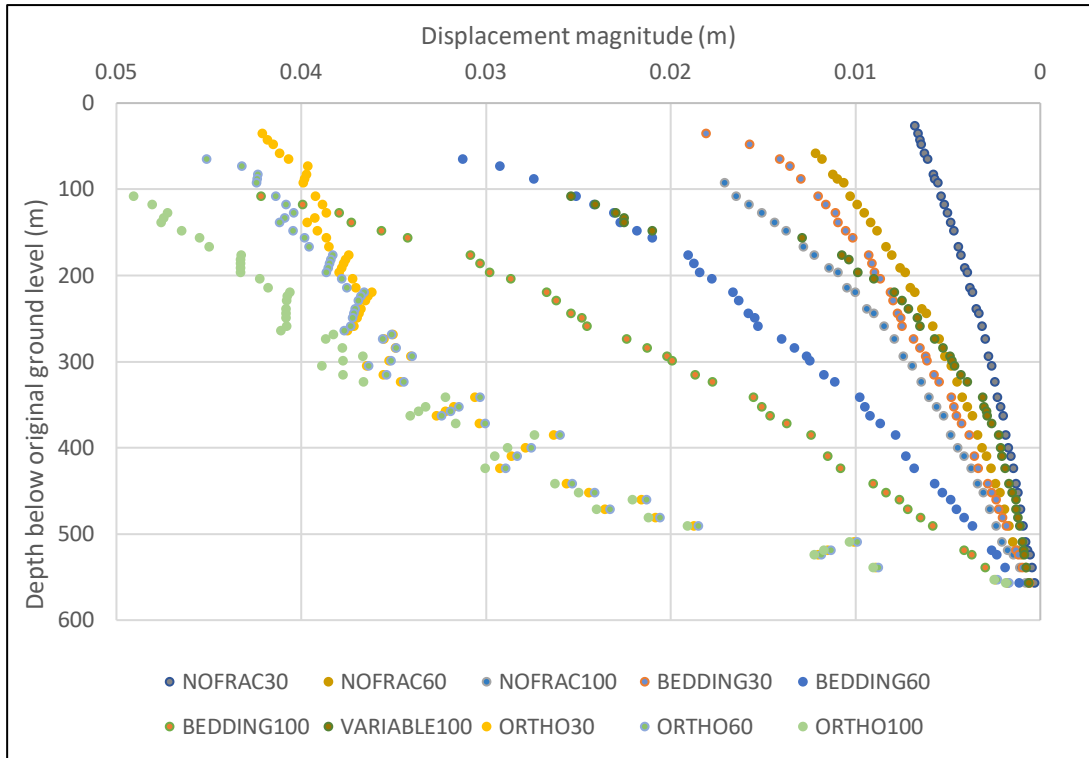
Figure 5.7: Vertical rock mass displacement beneath the excavation floor under high lateral stress conditions. When compared to displacement variation under low lateral stress conditions (Figure 5.6) vertical displacement magnitudes at shallow depth are increased and, for the orthogonally jointed models, vertical displacement reduces at a lower rate with increasing depth below the excavation floor. The stepped profile in the orthogonally jointed model plots reflect variation in delineation of the vertical data transect in relation to model node locations. [NOFRA = Model 1, BEDDING = Model 2, Variable = Model 3, ORTHO = Model 4].

Under higher lateral stress conditions, as shown in Figure 5.7 and Table 5.4, there is evidence to demonstrate that vertical displacement magnitude increases with increasing discontinuity intensity and that displacement magnitude is greatest for the more intensely jointed models although it is notable that the displacement magnitudes for models with discontinuities occur within a narrower range and with lower variation with depth when compared to the low lateral stress case, indicating that whilst the presence of discontinuities sub-parallel to the displacement direction has an influence on displacement magnitude, the configuration of such discontinuities is of lower significance under high lateral stress conditions.

Combined model results for lateral displacement behind the excavation face are presented in Figures 5.8 and 5.9 for the two lateral stress conditions. Under low lateral stress, maximum lateral displacement magnitude is 3.4 cm inwards towards the upper excavation face for the variably jointed model. Lowest lateral displacement is observed in the no-discontinuity models. The response for the bedding-only models and the variably jointed models are comparable. For the majority of models there is no significant horizontal displacement beyond a distance of 500 m from the excavation face. The exception is the no-discontinuity model for all depths of excavation where definable displacement occurs at a distance in excess of 700 m from the excavation face.
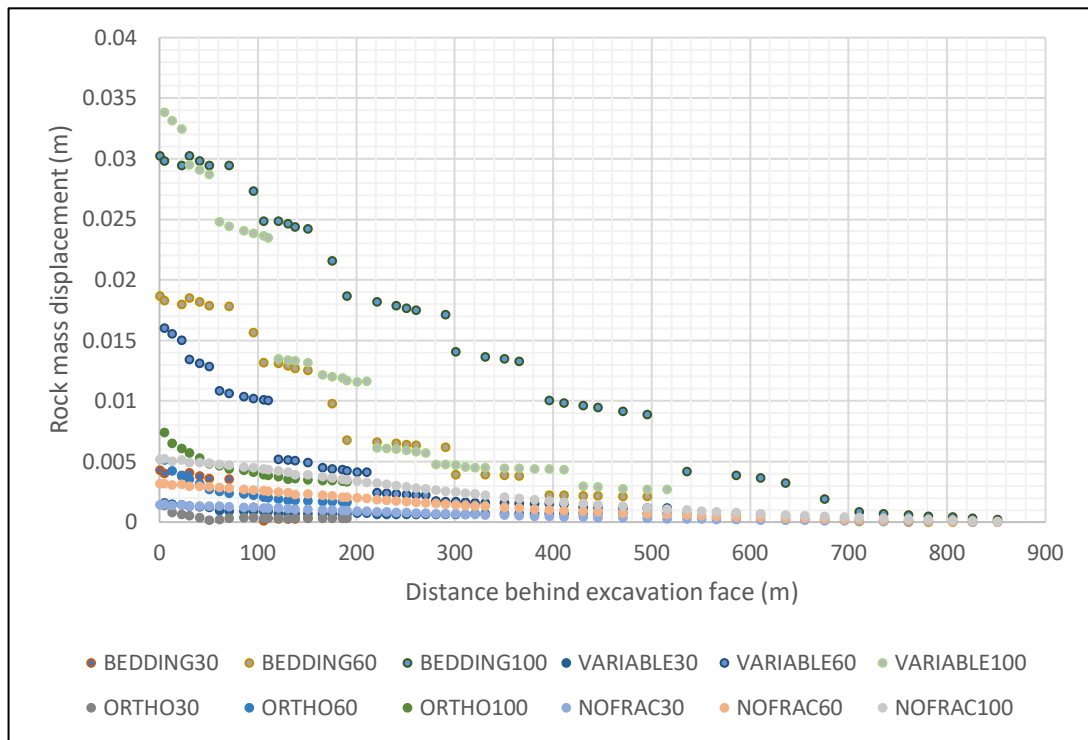
Figure 5.8: Horizontal rock mass displacement behind the upper excavation face under low lateral stress conditions. The results demonstrate that the majority of horizontal displacement towards the excavation face occurs within a distance of 500 m from the face and that the presence of discontinuities increases both the magnitude and extent of horizontal displacement behind the face. [NOFRA = Model 1, BEDDING = Model 2, Variable = Model 3, ORTHO = Model 4].

Under high lateral stress conditions there is a significant change in model response for all model configurations. As shown in Figure 5.9, with the exception of the bedding only model at 100 m depth of excavation, model

results demonstrate lower lateral displacement magnitudes than the equivalent low lateral stress model, with the model response at 30 m and 60 m depth of excavation showing maximum displacements of less than 1cm at the excavation face. It is also apparent that, with the exception of the bedding only model at 100 m depth of excavation, the high lateral stress results demonstrate that rock mass displacements reduce to close to zero over a shorter distance than was observed with the low lateral stress model. For the bedding only model at 100 m depth of excavation, lateral displacement over a greater distance occurs due to the effect of sliding on bedding planes, uninterrupted by sub-vertical joints.
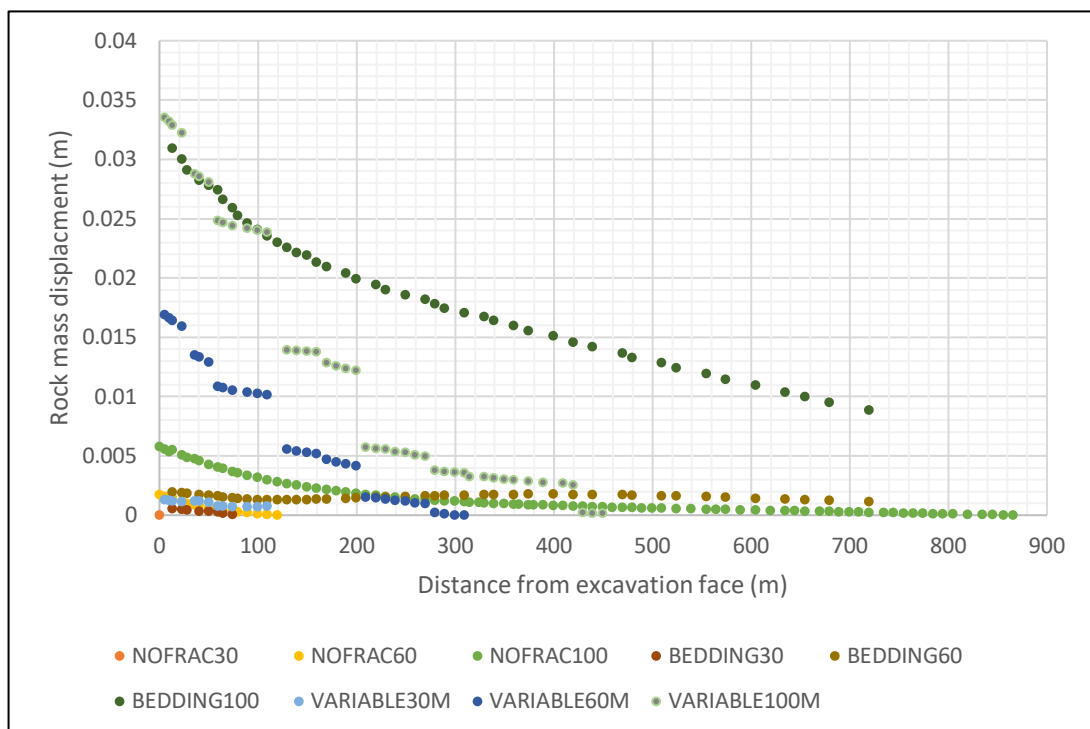
Figure 5.9: Horizontal rock mass displacement behind upper excavation face with high lateral stress conditions. When compared to the low lateral stress results (Figure 5.8), the results for most models demonstrate lower displacement magnitude and reduction to no definable displacement over a shorter distance. [NOFRA = Model 1, BEDDING = Model 2, Variable = Model 3, ORTHO = Model 4].

Reduction in displacement magnitude over a shorter distance under high lateral stress conditions can be compared to the results for EdZ lateral extents derived from analysis of stress variation. Under high lateral stress conditions the lateral EdZ is shown to extend a longer distance into the rock mass behind the excavation face when there are no sub-vertical joints e.g. the no-

discontinuity model (Model 1) and the bedding-only model (Model 2), but a shorter distance where joints are present e.g. the variably jointed model (Model 3) and the orthogonally jointed model (Model 4). Displacement analysis indicates that under high lateral stress conditions the majority of the rock mass displacement takes place over a shorter distance than is observed under low lateral stress conditions. This is attributed to the increased sub-vertical discontinuity stiffness that results from increased lateral stress.

5.5 Discontinuity response

In relation to potential hydrological significance in fractured hard rock environments, it is the effect of lithostatic unloading on individual discontinuity systems, rather than the rock mass, that is most relevant. Discontinuity dilation results for each model have been presented in Chapter 4. Dilation data is more specific to individual discontinuities and discontinuity systems and is influenced by discontinuity-specific parameters such as orientation, stiffness, persistence and intensity. Collective comparison of dilation data for multiple models therefore needs to be carefully undertaken.

It is important to restate that, although dilation results are recorded along a vertical and horizontal transect in each model, the results represent normal dilation at each discontinuity surface and have not been adjusted for discontinuity orientation. Key data derived from the discontinuity dilation analysis are as follows:

- Dilation magnitude;
- Dilation magnitude variation with distance; and
- Dilation contribution to displacement.

In all models the maximum discontinuity dilation occurs at the excavation face or floor. Maximum dilation magnitude for each model is summarised in Table 5.5. With the exception of dilation at a joint daylighting in the excavation face in the variably jointed model (Model 3), the highest magnitude dilations occurred in the bedding planes beneath the excavation floor under both lateral stress conditions with a maximum dilation of 2.7 mm. The introduction of sub-

vertical jointing in both the variably jointed and the orthogonally jointed models results in a reduction in the maximum bedding plane dilation magnitude. With joints present, the largest dilations occur in the bedding planes beneath the excavation floor with a maximum value of 0.98 mm and 0.26 mm for the variably jointed (Model 3) and orthogonal models (Model 4), respectively.

Direction/	k = 0.27			k = 2.0		
Depth	Bedding	Variable	Orthog.	Bedding	Variable	Orthog.
Vertical						
30m	1.400	0.303	0.078	1.300	0.222	0.167
60m	1.900	0.657	0.152	1.700	0.524	0.303
100m	2.700	0.981	0.257	2.300	0.829	0.397
Horizontal						
30m	-	See note1	0.397	-	See note1	0.319
60m	-	4.28 (0.280)	0.641	-	0.180	0.375
100m	-	12.54 (0.690)	0.657	-	0.320	0.444

Table 5.5: Maximum normal dilation magnitude (mm) comparison for all models with discontinuities. The results represent dilation magnitude at the first discontinuity encountered beneath the excavation floor (vertical) or behind the excavation face (horizontal). The high joint horizontal dilation values for the variably jointed model (Model 3) represent a joint that intersects the 60 m deep excavation face and joint dilation magnitude represents joint opening at the face. As this is not representative of dilation trends behind the face, the dilation magnitude at the next joint from the face is included in red. There are no joints behind the face in the bedding-only model (Model 2) and therefore no data for the horizontal transect. [note 1 – in the variably jointed model the first joint behind a 30 m excavation face is too far from the face to show any dilation].

Under high lateral stress conditions, dilation magnitudes for all discontinuities in the bedding-only (Model 2) and variably jointed (Model 3) models are

reduced when compared to the results for low lateral stress conditions. In the orthogonally jointed model, maximum dilation magnitude is increased under high lateral stress conditions. This result is consistent with the analysis of rock mass displacement response where high lateral stress resulted in an increase in horizontal displacement towards the face, compared to displacement under low lateral stress conditions, whilst for other models there was a decrease.

Within the discontinuity models (Models 2, 3 and 4), the shorter sub-vertical joints are assigned a higher stiffness than the more persistent bedding planes. Joint tangential stiffness exceeds bedding plane normal stiffness and consequently the inclusion of sub-vertical joints appears to increase resistance to sub-vertical dilation at bedding planes. This is reflected in the reducing bedding plane dilation magnitude with increasing joint intensity, as indicated in Table 5.5 and shown schematically in Figure 5.10. As discussed at Section 4.3.3.3, assignment of discontinuity normal stiffness through the non-linear compliance function in Elfen results in increased stiffness at bedding/joint intersections in the variably jointed model (Model 3) due to higher penetration in response to higher stress. Increased bedding plane stiffness may account for reduced bedding plane dilation in Model 3. This effect may be an artefact of the model and not representative of real environments where it is difficult to conceive of a situation where the introduction of joints would stiffen the rock mass.

The observed increased in the magnitude of horizontal displacement towards the excavation face and maximum sub-vertical joint dilation magnitude behind the excavation face in the orthogonally jointed model (Model 4), under high lateral stress conditions, when compared to the response under low lateral stress conditions, is related to the orientation of joints sub-normal to the direction of increased lateral stress. Increased normal dilation results in increased horizontal displacement. In the variably jointed model, the joints behind the face are orientated at angles of between 30° and 70° to the horizontal and therefore an increase in lateral confining stress has less effect on joint normal dilation and horizontal rock mass displacement.
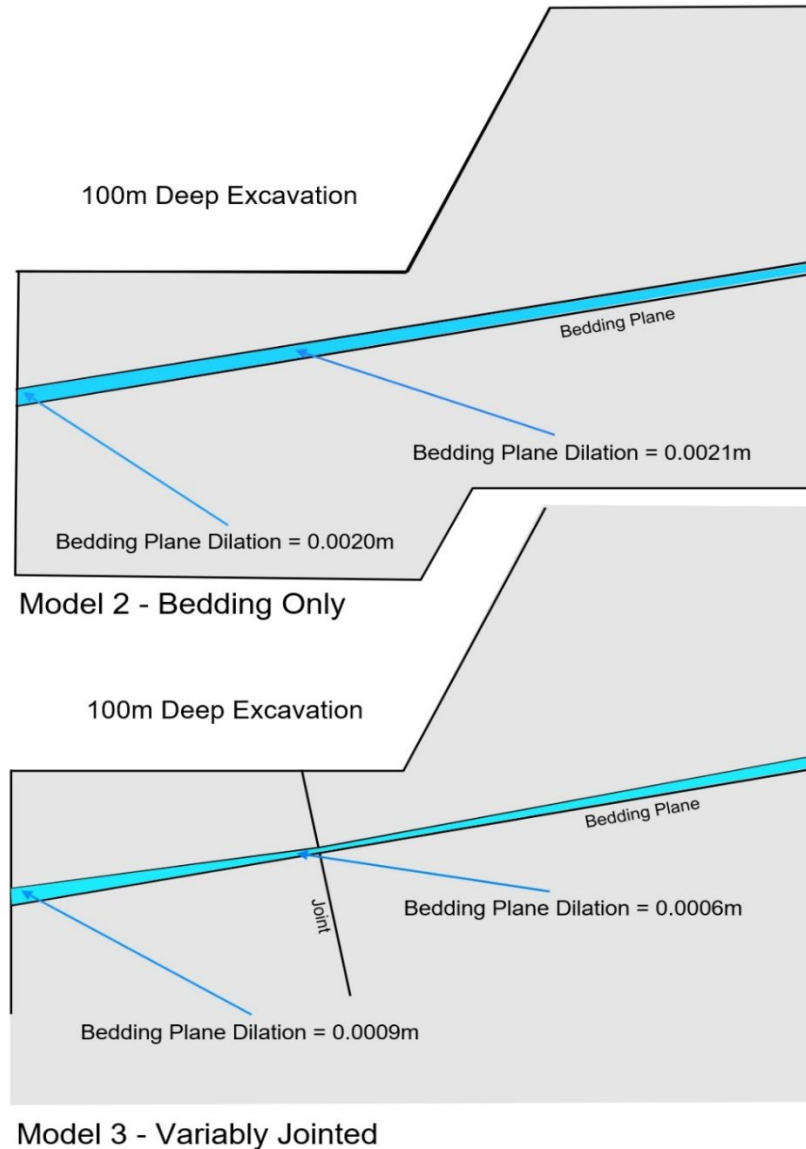
Figure 5.10: Comparative representation of bedding plane dilation in bedding only and variably jointed models at 100m depth of excavation demonstrating the effect of sub-vertical jointing on dilation magnitude and variation (k=0.27). In the bedding-only model bedding plane dilation below the excavation floor has a consistent magnitude. In the variably jointed model, normal bedding plane dilation is constrained at the joint intersection resulting in differential dilation along the bedding plane with reduced dilation magnitude.

Maximum discontinuity dilation data, as summarised in Table 5.5, demonstrates that, dilation magnitudes in bedding planes beneath the excavation floor can be relatively high, and may, therefore, be hydrologically significant. Dilation magnitudes in strata behind the excavation face are lower

than bedding plane dilation below the excavation floor, but with dilation magnitudes of up to 0.7 mm, may still have hydrological significance, particularly where there are multiple joints with high connectively as simulated in the orthogonally jointed model (Model 4).

In all models, discontinuity dilation magnitude reduces with increasing distance from the excavation face or floor. The rate of reduction has been established for each model. Comparative analysis of discontinuity dilation rates and rock mass displacement rates is presented in the following Figures 5.11 to 5.15.
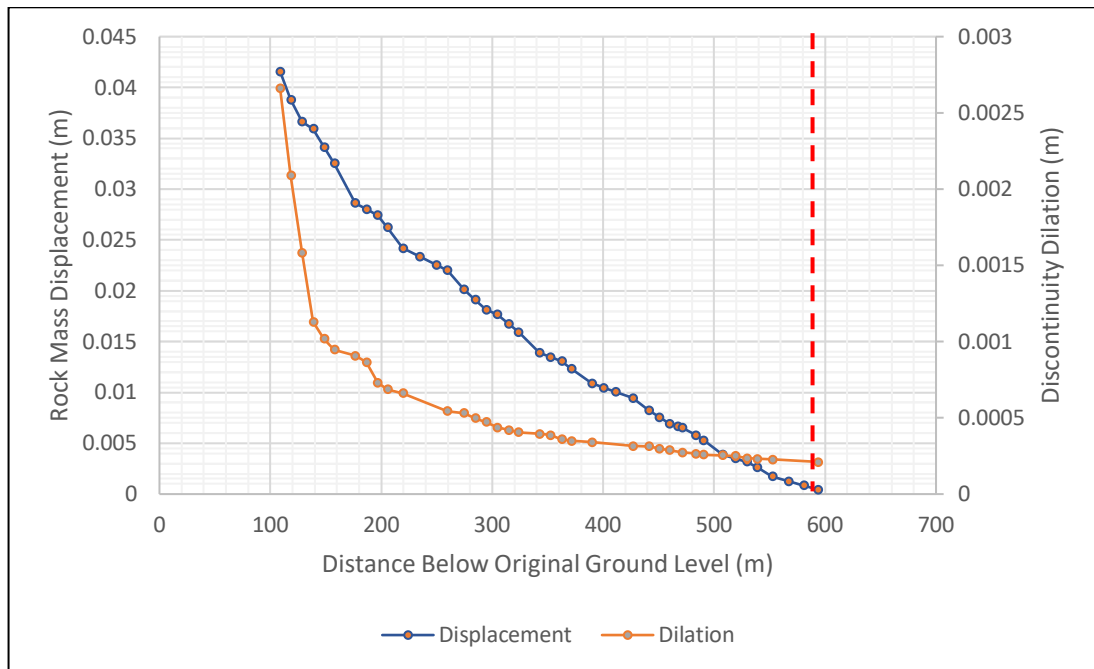
Figure 5.11: Comparison of vertical displacement and dilation limits for 100 m excavation in bedding only model (Model 2). The figure shows that whilst the magnitude of rock mass displacement reduces steadily over the full model depth, the magnitude of bedding plane dilation reduces rapidly to a depth of approximately 60 m below floor level before further reduction at a slower rate to the base of the model. (k=0.27). EdZ extent indicated by red vertical dashed line.

Figure 5.11 shows the modelled reduction in bedding plane dilation with depth for a 100 m deep excavation in comparison to the variation in rock mass displacement for the same depth of excavation. Whilst the rate of reduction of rock mass displacement magnitude decreases steadily towards the lower

model boundary, discontinuity dilation magnitude decreases more rapidly with approximately 70% reduction during the first 60m below the excavation floor. At a depth of 100 m below the excavation floor the rock mass vertical displacement magnitude is reduced by approximately 40% from the maximum value at the excavation floor. At the same depth, bedding plane dilation magnitude is reduced by approximately 75% of the maximum dilation below the excavation floor. In this model (Model 2) it is apparent that the majority of bedding plane normal dilation occurs over a shorter distance beneath the excavation floor than the distance over which rock mass vertical displacement is observed. As shown on Figure 5.11, the limit of the EdZ in this model has been defined as 490m below the excavation floor (590 m below original ground level).
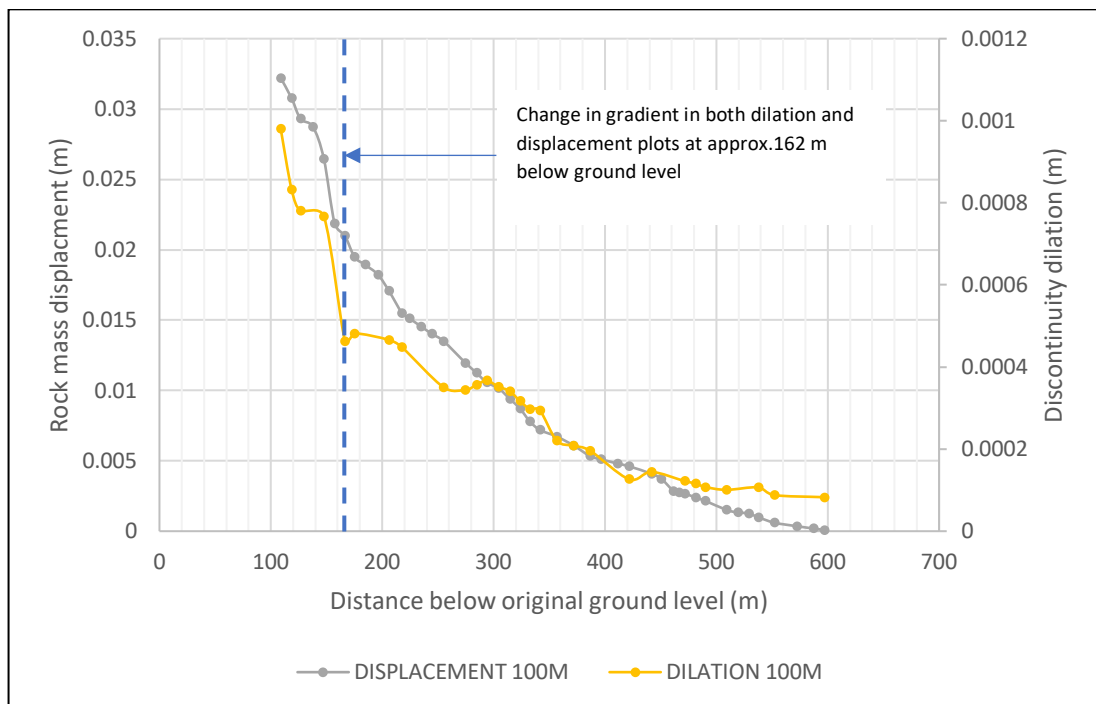
Figure 5.12: Comparison of vertical displacement and dilation limits for 100 m deep excavation in variably jointed model (Model 3) showing higher rate of reduction in discontinuity dilation magnitude over the first 60 m beneath the excavation floor, when compared to the rate of reduction of rock mass vertical displacement over the same distance. (k=0.27).

The same trend is observed in the variably jointed model (Model 3) for the same depth of excavation, although the variation in the rate of change of displacement and dilation magnitude is smaller than with the bedding only

model (Model 2). As shown in Figure 5.12, dilation magnitude is reduced by approximately 50% of the maximum magnitude over a distance of 60 m below the excavation floor. Over the same distance, displacement magnitude is reduced by 35%. Figure 5.12 indicates that beneath a depth of approximately 200 m below the excavation floor, the rate of reduction of rock mass displacement and discontinuity dilation is comparable.

It is noted that in both the bedding-only model (Model 2) and the variably jointed model (Model 3) the rate of dilation reduction is related to the rate of displacement reduction, suggesting that dilation magnitude may be approximated as the first derivative of rock mass displacement.
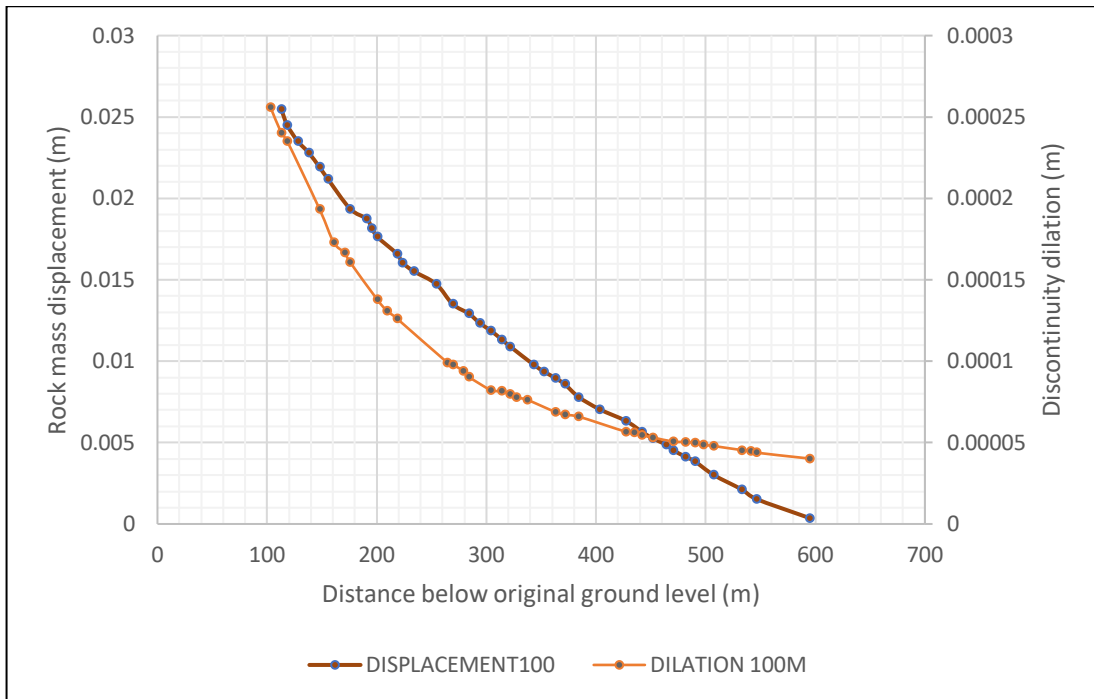
Figure 5.13: Comparison of vertical displacement and dilation limits for 100 m excavation in the orthogonal model (Model 4). The results demonstrate a higher rate of reduction in discontinuity dilation magnitude than the rate of reduction in rock mass vertical displacement magnitude over the first 200 m below the excavation floor. (k=0.27)

The results for the orthogonally jointed model (Model 4) are comparable to the results for the bedding only model (Model 2) with discontinuity dilation magnitude reducing at a higher rate than rock mass displacement magnitude

over a distance of approximately 200 m below the excavation floor. The results are shown in Figure 5.13. In Model 4, the vertical EdZ extents have been estimated to be 128 m below the excavation floor (e.g. 228 m below original ground level). In this case, as shown in Figure 5.13, both the displacement and the dilation magnitude reduce gradually with distance with no clearly defined threshold at which the rate of dilation changes.

Model results indicate that where there is low vertical connectivity in the discontinuity network, dilation of bedding planes or sub-horizontal jointing below the excavation floor occurs over a much shorter depth than the distance over which definable rock mass displacement occurs. However, when vertical connectivity is higher e.g. the orthogonally jointed model (Model 4), definable bedding plane dilation may extend to greater distance.
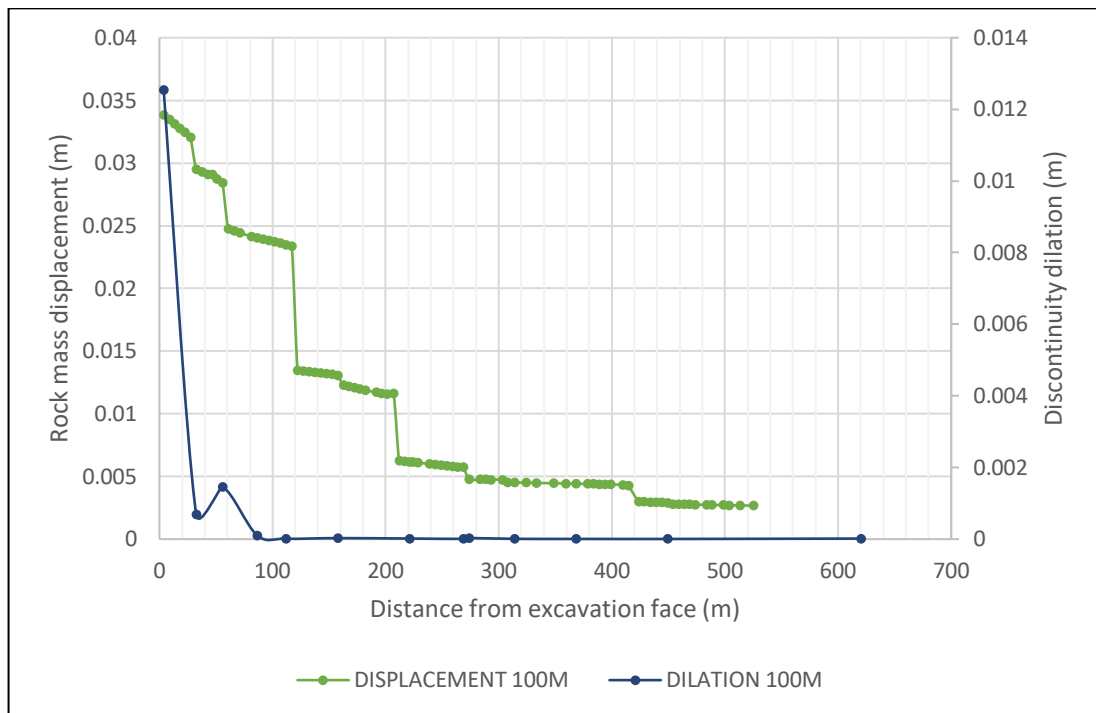
Figure 5.14: Comparison of horizontal displacement and dilation limits for 100 m excavation in variably jointed model (Model 3) showing dilation magnitude close to zero at a distance of 86 m from the excavation face. (k=0.27)

The same comparative analysis has been undertaken with regard to dilation of sub-vertical jointing behind the excavation face. As there is no sub-vertical jointing in the bedding only model, the results are restricted to the variably

jointed (Model 3) and the orthogonally jointed model (Model 4). Figure 5.14 shows the results for the variably jointed model. Allowing for dilation magnitude variations that are associated with variable joint orientation, the general trend indicates that dilation magnitudes reduce to around zero at a distance of approximately 86 m from the excavation face, whilst rock mass displacement remains at over 2 mm at a distance of 500 m from the excavation face.

As with the vertical dilation/displacement comparison shown in Figures 5.11 and 5.12, there is evidence in Figure 5.14 to suggest that dilation can be approximated as a first derivative of displacement.
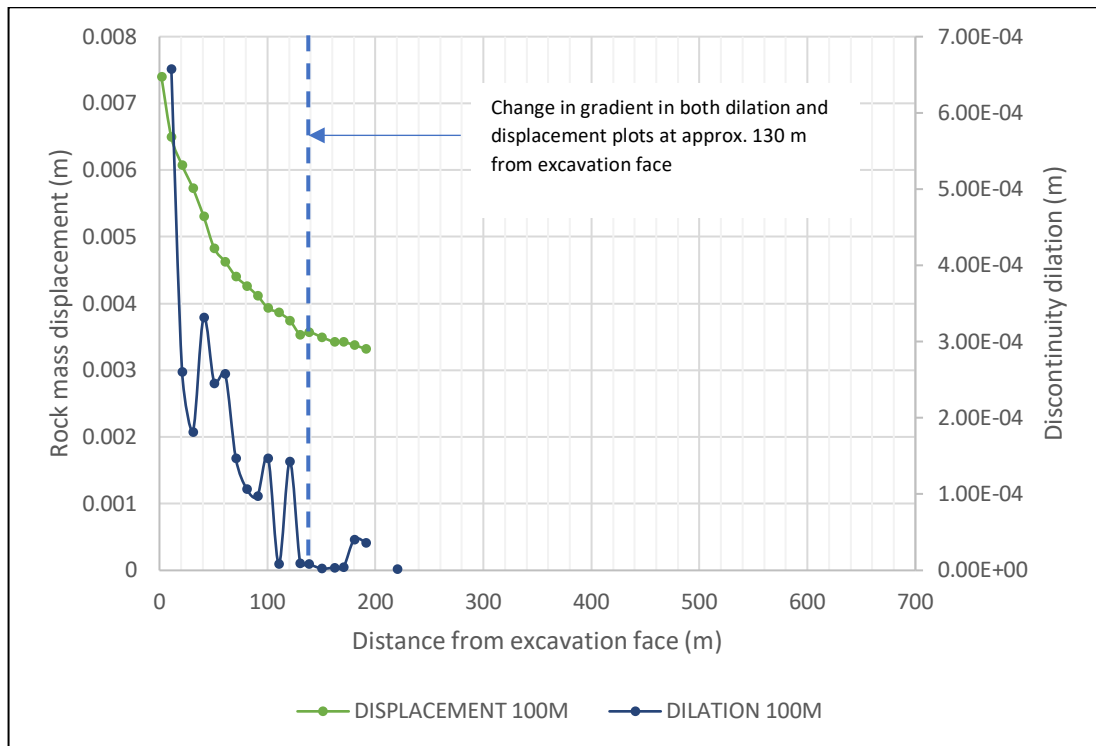
Figure 5.15: Comparison of horizontal displacement and dilation limits for 100 m excavation in orthogonal model (Model 4) showing no significant joint dilation beyond 130 m from the excavation face. (k=0.27).

Comparative results for normal joint dilation and rock mass displacement in the orthogonally jointed model (Model 4) are presented in Figure 5.15. The results indicate the same trend as demonstrated for the variably jointed model (Model 3) as joint dilation magnitude reduces at a higher rate over the first 30

m from the excavation face and then at a lower rate for a further 190 m. Joint dilation ceases to occur within 130 m of the excavation face.

Joint dilation magnitudes in the orthogonal model (Model 4) are significantly lower than in the variably jointed model (Model 3). In the orthogonally jointed model, maximum joint normal dilation is 0.66 mm compared to 12.5 mm in the variably jointed model. However, the first joint in the variably jointed model intersects the excavation face and therefore registers dilation at the free surface which is not representative of joint dilation behind the face. The next joint behind the face registers a joint normal dilation of 0.70 mm at a distance of 30 m from the face. At the same distance from the face the joint normal dilation in the orthogonally jointed model is 0.2 mm.

The orthogonally jointed model incorporates a minimum of 86 subvertical joints behind the excavation face. The variably jointed model includes 22 variably orientated joints behind the excavation face. As detailed at Chapter 4, the total cumulative lateral dilation in the variably jointed and the orthogonally jointed models is 3.0 cm (58% of total displacement) and 2.7 cm (36% of total displacement), respectively. Cumulative lateral dilation in both models is similar in magnitude although the contribution to total lateral displacement is greater in the variably jointed model (Model 3).

Although not fully consistent in all data sets, a general conceptual understanding of the geomechanical response behind the excavation floor and face, to open pit excavation, is indicated in Figure 5.16.

For fractured hard rock formations where groundwater flow primarily occurs via discontinuity based secondary porosity systems, it is the 'zone of joint dilation' that is of primary interest and where change in the hydraulic characteristics of the groundwater drainage system is most likely to occur. For the purpose of this study this zone is referred to as the Hydrologically Significant Excavation disturbed Zone (HS-EdZ) to differentiate from less hydrologically significant disturbance.
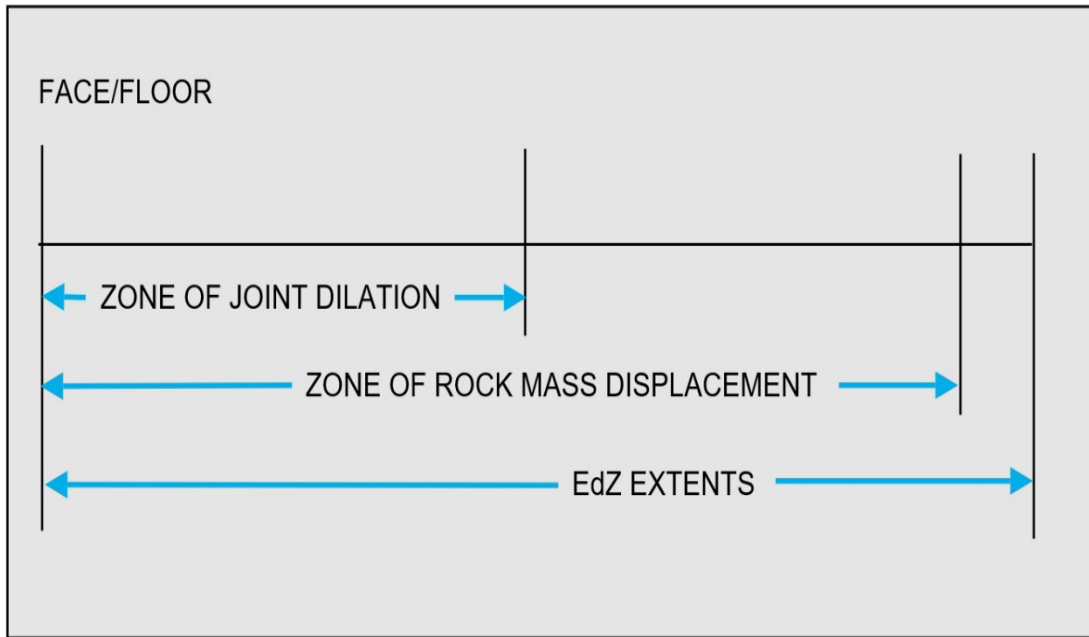
Figure 5.16: General configuration of dilation, displacement and disturbed zones beneath an excavation floor and behind an excavation face. In general, model results demonstrate that the 'zone of dilation' occurs within the 'zone of rock mass displacement' which extends to a shorter distance from the excavation floor and face than the limit of the EdZ defined by change in stress.

To further support consideration of hydrological significance it is necessary to better define the potential range of dilation magnitudes and dilation extents by comparative analysis of results for all models. Figure 5.17 shows a comparison of bedding plane vertical dilation magnitude and distances for all discontinuity models. As discussed above, it is apparent that within the first 200m below original ground level the presence of sub-vertical jointing (variably jointed and orthogonal models) significantly reduces modelled bedding plane dilation when compared to the bedding-only model (Model 2). At greater depth, the presence of jointing has much lower effect on bedding plane vertical dilation magnitude.

Comparative analysis of sub-vertical joint dilation in a horizontal direction behind the excavation face is less conclusive as only two models include sub-vertical jointing. The results are shown in Figure 5.18. As discussed above, dilation magnitude in the orthogonal joints reduces significantly over a distance of 130 m from the excavation face and no joint dilation occurs beyond 200 m from the face. The variably jointed model demonstrates higher magnitude

dilation, the majority of which occurs within 100 m of the excavation face. Model results indicate higher magnitude dilation in the variably jointed model (Model 3) as the displacement response is distributed over fewer joints.
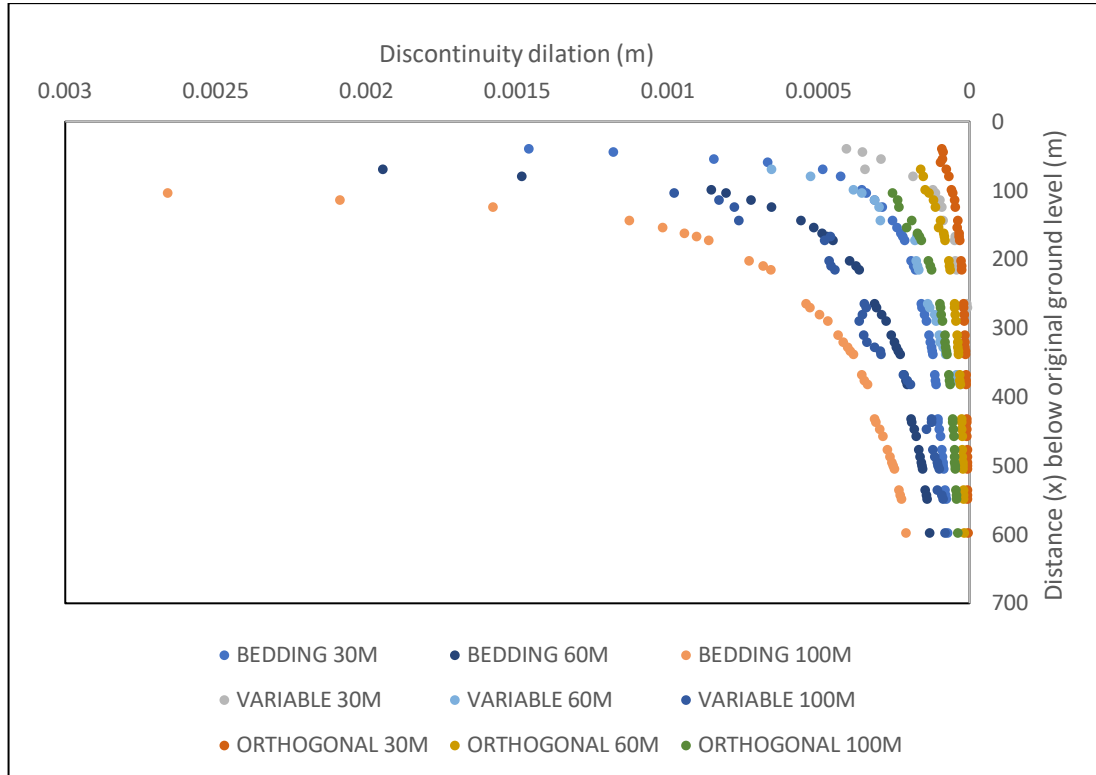
Figure 5.17: Comparison of vertical discontinuity dilation trends for all models at excavation depths of 30 m, 60 m and 100 m showing reduction in dilation magnitude with increasing discontinuity intensity within the first 200 m below the upper model boundary. Maximum vertical dilation of 2.7 mm is achieved in the bedding only model (Model 2) for an excavation depth of 100 m. All results represent the low lateral confining stress case (k=0.27).

Cumulative discontinuity dilation totals can be compared to maximum rock mass displacement values to provide an indication of dilation contribution to displacement. The results are presented in Table 5.6. The results demonstrate that discontinuity dilation constitutes between 15% and 54% of vertical displacement beneath the excavation floor.
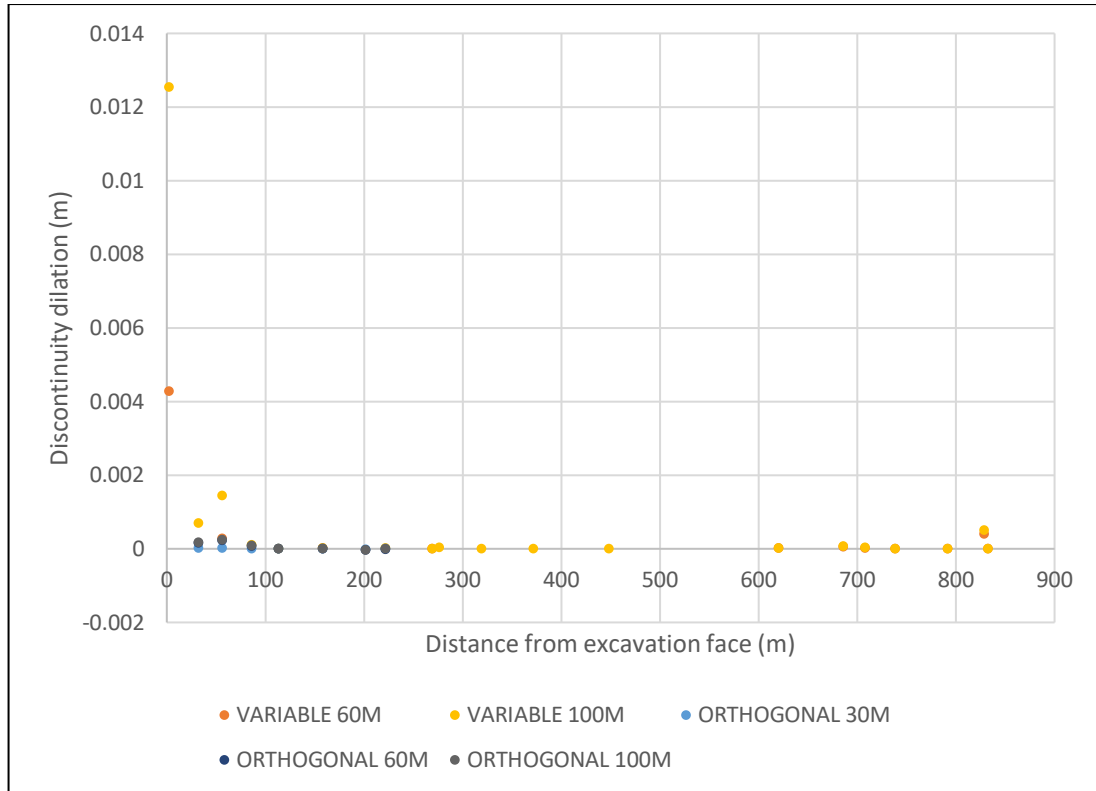
Figure 5.18: Lateral discontinuity dilation trends for variably jointed (Model 3) and orthogonally jointed (Model 4) models at excavation depths of 30 m, 60 m and 100 m, showing that in both models the majority of joint dilation occurs within a distance of 100 m from the excavation face. All results represent the low lateral confining stress case (k=0.27).

Model	Depth of excavation (mbgl)	Max Displacement (m)	Cumulative dilation (m)	Dilation % of Displacement
Vertical below excavation floor				
Bedding	30	0.0192	0.0067	35
	60	0.0283	0.0153	54
	100	0.0415	0.0218	53
Variably jointed	30	0.0084	0.0028	33
	60	0.0177	0.0060	34
	100	0.0378	0.0126	33
Orthogonal	30	0.0070	0.0013	19

	60	0.0150	0.0028	19
	100	0.0245	0.0037	15
Horizontal behind excavation face				
Bedding	30	0.0036	n/a	n/a
	60	0.0187	n/a	n/a
	100	0.0298	n/a	n/a
Variably jointed	30	0.0013	n/a	n/a
	60	0.0230	0.0120	52
	100	0.0518	0.0298	58
Orthogonal	30	0.0013	0.0006	46
	60	0.0051	0.0024	47
	100	0.0074	0.0027	36

Table 5.6: Cumulative discontinuity dilation as a percentage of maximum displacement below the excavation floor and behind the excavation face for all models at excavation depths of 30 m, 60 m and 100 m. All results relate to low lateral confining stress (k=0.27). [n/a – no sub-vertical jointing in the model or no dilation recorded].

In a lateral direction behind the excavation face, model results are less variable with a cumulative dilation contribution within the range of 36% to 58% of total displacement (excluding the low displacement contribution at 30 m depth of excavation in the orthogonal model (Model 4).

In a vertical direction, maximum displacement at the excavation floor is fully accounted for by a combination of rock mass extensional strain and cumulative bedding plane dilation. Detail for the variably jointed model (Model 3) are presented in Table 4.10 in Chapter 4. In a lateral direction, maximum displacement at the excavation face is not fully accounted for by a combination of rock mass extensional strain and cumulative joint dilation. In the jointed models rock block sliding on discontinuity surfaces, as shown on Figure 4.50 in Chapter 4, also contributes to total displacement at the excavation face.

It is acknowledged that in all models developed during this study, the discontinuity spacing has been fixed within each model. Results sensitivity to variation in discontinuity spacing has not been directly investigated. However, whilst bedding plane spacing has remained consistent in all discontinuity models, the spacing of sub-vertical joints in Model 3 is generally much greater than in Model 4. Average joint spacing in Model 3 is typically 15 m to 40 m whilst in Model 4 the joint spacing is a consistent 10m. Reference to Table 5.6 demonstrates that with larger joint spacing (Model 3 – variably jointed) cumulative joint dilation magnitude is significantly greater than with the more closely spaced jointing in Model 4 (orthogonal). Dilation of more widely spaced joints also contributes a higher percentage of the maximum displacement at the excavation floor and face.

5.6 Basis for consideration of hydrogeological significance

Subsequent analysis of the potential hydrogeological significance of the geomechanical response to lithostatic unloading around open pit excavations requires input data in relation to the following:

1. The vertical and lateral extent of the excavation disturbed zone (EdZ) and the discontinuity dilation characteristics within the hydrologically significant zone (HS-EdZ); and

2. Discontinuity dilation magnitude and magnitude variation with distance from the excavation floor and face.

Data is required to represent three generic modelled discontinuity configurations applicable to hard rock mineral extraction as follows:

1. Bedded sedimentary deposits with limited jointing (e.g. Coal Measures Strata – mudstone with subordinate sandstone)

2. Bedded sedimentary or igneous deposits with variably orientated jointing (e.g. Limestones, granites, basalts)

3. Bedded sedimentary deposits with high intensity orthogonal jointing (e.g. Sandstones)

Whilst EdZ extents are inevitably site-specific and dependant on open pit configuration, at the level of significance assessment, it has been possible to generalise by normalisation of results with regard to open pit depth and width. EdZ extents for use in hydrological assessment can be defined by application of Equations 5.2 and 5.3.

The magnitude and extent of discontinuity dilation varies significantly in relation to DFN configuration and therefore must be specified separately for each of the three discontinuity models. Dilation/distance equations have been developed for each of the three models with discontinuities using a power law function as defined at Equation 4.2. The power value (b) in Equation 4.2 is different for each excavation depth and discontinuity configuration. This variability makes application of dilation/distance relationships overly complex. Analysis of power magnitude for all model results is presented in Table 5.7.

Power magnitude (b)			
Vertical			
M2 (0.27)	-0.986	-1.156	-1.314
M2 (2.0)	-1.095	-1.040	-1.180
M3 (0.27)	-2.040	-1.570	-1.540
M3 (2.0)	-3.020	-2.800	-2.840
M4 (0.27)	-1.210	-1.110	-1.110
M4 (2.0)	-2.540	-2.520	-3.340
Horizontal			
M2 (0.27)	n/a	n/a	n/a
M2 (2.0)	n/a	n/a	n/a
M3 (0.27)	n/d	-1.016	-1.175
M3 (2.0)	n/d	-1.000	-0.672
M4 (0.27)	-1.695	-1.842	-1.242

M4 (2.0)	n/d	-0.863	-1.072
All results – Geometric mean -1.44, SD 0.73			
Vertical results only – Geometric mean – 1.64, SD 0.78			
Horizontal results only – Geometric mean – 1.12, SD 0.36			
All results excluding M3 – Geometric mean – 1.28, SD 0.62			

Table 5.7: Variation in power magnitude (b) in Equation 4.2 for all model dilation/distance fittings (n/a – no joints in the model, n/d – no dilation determined).

Reference to Table 5.7 demonstrates that the value of b varies above and below -1. The geometric mean for all results is -1.44 with a standard deviation of 0.73. As discussed at Section 5.5, the dilation response in the variably jointed model (Model 3) may be constrained by the approach in Elfen to stress allocation at joint endings in non-persistent joints. The dilation response in Model 3 may therefore be underestimated. Removal of Model 3 power magnitude values from the data set in Table 5.7 results in a geometric mean of 1.28 with a standard deviation of 0.62.

On the basis of the above analysis, and to facilitate effective application of dilation/distance relationship functions to real world environments, as presented in Chapter 6, all dilation/distance power law functions have been adjusted to fit a power magnitude of -1. In the majority of cases the adjustment is minimal with no significant change in residual values.

Dilation/distance relationships are defined by Equation 4.2. Coefficient (c) for use in Equation 4.2 in the form Dilation (D) = c x^{-1}, are presented in Table 5.8.

Model 2 – Bedding-only model			
Excavation Depth (m)	Coefficient (c)		
	Bedding (0.27)	Joint (0.27)	Joint (2.00)	Bedding (2.00)
30m	0.037	n/a	n/a	0.037
60m	0.080	n/a	n/a	0.080
100m	0.150	n/a	n/a	0.150
Model 3 – Variably jointed model			

Excavation Depth (m)	Coefficient (c)			
	Bedding (0.27)	Joint (0.27)	Joint (2.00)	Bedding (2.00)
30m	0.012	n/d*	0.0001	0.011
60m	0.030	0.010	0.0005	0.029
100m	0.090	0.030	0.0007	0.075
Model 4 – Orthogonally jointed model				
Excavation Depth (m)	Coefficient (c)			
	Bedding (0.27)	Joint (0.27)	Joint (2.00)	Bedding (2.00)
30m	0.005	0.002	n/d*	0.005
60m	0.014	0.007	0.001	0.020
100m	0.026	0.011	0.001	0.050

Table 5.8: Discontinuity dilation/distance equation coefficients for models with discontinuities for excavation depths of 30 m, 60 m and 100 m and lateral stress ratios of 0.27 and 2.0. Bedding results define coefficients related to normal dilation of sub-horizontal bedding planes beneath the excavation floor. Joint results define coefficients related to normal dilation of joints behind the excavation face. (n/a – no joints in the model, n/d – no dilation determined).

5.7 Summary and conclusions

The primary conclusions from the interpretation and analysis of the geomechanical modelling programme results are as follows.

Estimation of EdZ extents

Normalisation of vertical and horizontal EdZ extent results from all models has resulted in the development of new equations for the estimation of EdZ extents for any open pit configuration. The equations take account of variation in discontinuity configuration.

Compatibility with Boussinesq analysis

Comparative analysis of vertical EdZ extents defined through geomechanical modelling and residual stress magnitude beneath an unloaded strip as calculated by the Boussinesq approach (Equation 2.7) has demonstrated reasonable consistency of results between the two methods.

Discontinuity dilation -v- distance relationships

Analysis of all model results has demonstrated that, in general discontinuity dilation magnitude, below an excavation floor and behind an excavation face, decreases with increasing distance from the floor/face in accordance with a reciprocal power law function. Dilation -v- distance relationships have been defined by the formula Dilation (D) = $c\, x^{-1}$, where x is the distance below the excavation floor (m) and c is a coefficient related to depth of excavation.

EdZ zonation and the Hydrogeological Significant Zone (HS-EdZ)

Analysis of discontinuity dilation distances in relation to rock mass displacement characteristics and stress based EdZ extents for all models has revealed zonation within the EdZ around open pit mineral workings. Model results demonstrate that the zone of discontinuity dilation (defined as the HS-EdZ due to its hydrogeological significance) extends over a shorter distance from the excavation floor/face than the extent of definable rock mass displacement. The zone of displacement does not typically extend to the full EdZ boundary.

CHAPTER 6: EVALUATION OF HYDROGEOLOGICAL SIGNIFICANCE

6.1 Introduction

In this chapter the results of the geomechanical modelling programme are translated to hydrological parameters to support analysis of the potential hydrogeological significance of the geomechanical response to lithostatic unloading at open pit mineral sites. The key outputs from the geomechanical modelling programme are:

- o The extent of the Hydrologically Significant Excavation disturbed Zone (HS-EdZ)

- o Discontinuity dilation magnitude with increasing distance from excavation face and floor

Whilst it is recognised that the hydrogeological effects of lithostatic unloading will be highly site-specific, evaluation of 'hydrogeological significance' has been based on analysis of the potential effects for a range of geological environments, discontinuity configurations and hydraulic characteristics, with the aim of establishing an improved understanding of the range of conditions under which pre-excavation hydrogeological conditions may be subject to change during mineral extraction.

It is apparent that 'significance' is also related to the hydrological sensitivity of the local environment and the type of extractive, and subsequent restoration, operations undertaken. In low sensitivity environments, changes to the hydrological characteristics of the host rock around an excavation may have low significance, regardless of magnitude. Conversely, in sensitive locations, or where open pit restoration proposals may incorporate use of non-inert materials, small changes in hydrological characteristics may have high hydrological significance.

Whilst many deeper mineral excavations extend below the groundwater table and therefore involve progressive dewatering of saturated formations, shallower excavations may remain above groundwater elevation. Changes in hydraulic characteristics resulting from lithostatic unloading have the potential to influence groundwater flow in saturated strata (phreatic zone) and unsaturated zone (vadose zone) drainage.

In all cases, the primary effect of discontinuity dilation within the disturbed zone will be to change discontinuity hydraulic conductivity and, potentially, to change DFN connectivity. Both effects would manifest as a change in the bulk transmissivity or equivalent hydraulic conductivity of the host rock around a mineral excavation. In the phreatic zone, changes to hydraulic conductivity would tend to influence the following:

o Groundwater flow rates
o Hydraulic gradients
o Area influenced by excavation dewatering
o Contaminant attenuation processes

In general, an increase in hydraulic conductivity would tend to reduce hydraulic gradients and increase the area of influence around an excavation. Groundwater flow rates towards an open excavation would tend to increase, resulting in higher magnitude inflow and hence, increased dewatering requirement. More rapid flow through the DFN would tend to reduce the effectiveness of time-dependent natural contaminant attenuation processes but attenuation resulting from dilution and diffusion processes may be enhanced.

In the vadose zone, open pit excavation tends to change unsaturated zone drainage characteristics as new excavation faces provide a free outfall for water percolating through unsaturated strata. An increase in vadose zone hydraulic conductivity could therefore result in increased surface recharge and soil drainage rates with associated reduction in temporary vadose zone storage capacity. Conversely, enhanced vadose zone hydraulic conductivity could increase the rate of fluid migration from flooded or infilled mineral

excavations, reducing the flow and contaminant transport attenuating capacity of the zone.

Investigation of the potential hydrogeological significance of lithostatic unloading around open-pit mineral workings has been focused on internal excavation effects such as groundwater inflow or recharge rates and external effects on peripheral groundwater levels, flow directions, soil drainage and contaminant attenuation capacity. The results of the assessment are intended to support development of guidance on the range of geological conditions and hydrological environments in which consideration of the effects of lithostatic unloading should form part of the hydrogeological impact assessment process.

6.2   Approach to assessment of hydrological significance

Investigation of the potential hydrological significance of lithostatic unloading at open-pit mineral sites has been undertaken by reference to multiple case study examples, real and idealized, intended to be reasonably representative of hydrological conditions relevant to mineral excavations with a maximum depth of up to 100mbgl. Hydrological and hydrogeological models have been developed and adapted to incorporate hydraulic conductivity changes associated with unloading, as defined at Chapter 5. Due to the various processes under investigation and the alternative modelling approaches available, the assessment has been undertaken in three parts as follows.

Hydraulic gradients, area of influence and groundwater flow;

Contaminant migration and environmental risk; and

Vadose zone drainage, recharge and soil zone.

Investigation of potential effects on groundwater flow, hydraulic gradients and area of influence has been undertaken through the adaptation of existing groundwater flow models using the MODFLOW 3D finite difference modelling

system. A pre-existing model of the groundwater system around Appleton Quarry in West Yorkshire, UK, has been used as the basis for investigation of DFN dilation effects for a range of original hydraulic conductivity values. Appleton Quarry is established in orthogonally jointed Lower Coal Measures sandstone. Further investigation has been based on analysis of hydraulic conductivity variation at a second site, Copley Lane Quarry, Sherburn in Elmet, North Yorkshire, UK, which is established in the Upper Magnesian Limestone with a more variably jointed discontinuity configuration.

In both case studies, the bulk hydraulic conductivity values applied in the pre-existing models have been translated into a fracture aperture magnitude for each discontinuity set. Aperture values have then been amended in accordance with the dilation/distance relationships established in Chapter 5 to produce new hydraulic conductivity values for models re-run to investigate changes in the predicted groundwater regime.

Simple 3D MODFLOW models allow visual representation of groundwater levels and flow rates at all model locations and hence support investigation of changes in groundwater levels, hydraulic gradients, flow rate at all modelled receptors and the areal extent of dewatering effects. Whether effects are considered to be significant is highly site-specific, but attempts have been made to identify impact thresholds beyond which impacts could be considered significant.

Hard rock mineral excavations are rarely at risk of contamination due to inflowing groundwater or vadose zone drainage. Issues related to contaminant migration are usually associated with pathways out of the excavation to surrounding receptors. Although extractive operations can generate potential contaminants in the form of fine particulate matter or hydrocarbon compounds used in plant and machinery, water quality issues are primarily related to after use of the excavation void. Whether flooded to form a water body or backfilled with waste materials there is potential for generation of new contaminant source-pathway-receptor linkages.

Investigation of the effect of lithostatic unloading on contaminant migration risk has been undertaken by use of several pre-existing models of mineral

excavations that have been backfilled with a range of waste types from inert waste materials to non-hazardous waste. Assessment has been based on use of statistical risk models using the LandSim modelling system developed by Golder Associates for the UK Environment Agency. LandSim is a probabilistic model which uses the Monte Carlo simulation technique to select randomly from a pre-defined range of possible input values to create parameters for use in model calculations (Environment Agency, 2005). The model uses vadose and phreatic zone hydraulic conductivity value distributions in the assessment of contaminant attenuation processes, leading to predicted contaminant concentration at defined receptors. Change in hydraulic conductivity has the potential to influence attenuation processes.

Analysis of potential hydrogeological significance has been undertaken by comparison of predicted contaminant concentration with distance for a range of amended hydraulic conductivity values derived from application of the DFN dilation/distance relationships presented at Chapter 5. Due to the general requirement for waste deposition above the water table in most excavation locations, analysis using LandSim modelling takes account of both vertical unsaturated and lateral saturated flow in each model.

Geomechanical modelling has demonstrated the potential for dilation of sub-vertical discontinuities behind an excavation face, with particular impact in the upper 30m of the face. With regard to external effects, such changes have the potential to change surface infiltration or shallow sub-surface percolation capacity as a consequence of joint dilation near surface. Hydrological aspects of vertical drainage through the vadose zone with a range of discontinuity hydraulic conductivity variations has been reviewed.

The use of several modeling systems and approaches allows analysis of the potential for significant hydrological effects to occur in relation to key hydrological processes associated with open pit mineral excavation. The specific approach and outputs from each of the three types of assessment are presented in the following sections, concluding with discussion and general conclusions.

6.3 Hydraulic gradients, area of influence and groundwater flow

The potential impact of a variation in discontinuity network hydraulic conductivity, due to discontinuity dilation, on groundwater flow characteristics around open pit excavations has been undertaken through investigation using groundwater models from case study examples. Initial analysis is based on a pre-existing model of the groundwater flow regime around Appleton Quarry in West Yorkshire. Appleton Quarry is working orthogonally jointed Lower Coal Measures Sandstone with excavations extending below the local groundwater table. The existing groundwater model has been simplified to allow investigation of hydraulic conductivity variation over several orders of magnitude.

Further investigation of alternative hydrogeological environments has been undertaken through use of a second case study based on Copley Lane Quarry which is established in the Upper Magnesian Limestone. Details of both case studies are presented below.

6.3.1 Appleton Quarry case study

6.3.1.1 Site description and hydrogeological context

Appleton Quarry is located in Upper Cumberworth, near Huddersfield, West Yorkshire and is developed to work sandstones of the Lower Coal Measures. More specifically stone is extracted from the Grenoside Rock and the underlying Greenmoor Rock. The two sandstone formations are separated by a mudstone, coal and associated seatearth. A number of exploratory boreholes have been constructed at the site. Information obtained from such boreholes has been used to establish a local stratigraphic dip of approximately 4° to the south east. Several faults are present to the north and east of the quarry. Of particular significance is a major south east north west trending fault that has resulted in stratigraphic downthrown to the north east. The fault runs approximately 500 m north east of Appleton Quarry. According to British Geological Survey (BGS) mapping, the eastern side of the quarry is directly

underlain by the Grenoside Rock. The sequence extends south and east to underlie land between the quarry and the River Dearne. A 13 m thick sequence of mudstones and shales separates the Grenoside Rock from the underlying Greenmoor Rock which outcrops to the north west of the quarry and extends beneath the mudstone to the south east. The location of the site in relation to local geology is shown on Figure 6.1.

The Grenoside and Greenmoor Rocks, are both water bearing with the capacity for groundwater conveyance although the majority of groundwater encountered within workings at Appleton Quarry is derived from the Greenmoor Rock with perched water present in the Grenoside Rock. The large number of springs and issues in the area provide a further source of data indicating potential minimum groundwater levels associated with water bearing strata. The elevation of water bodies in Appleton Quarry is considered to be representative of groundwater in the Greenmoor Rock. The location and elevation of springs and water bodies is shown on Figure 6.1.

Movement of groundwater through the Grenoside and Greenmoor Rock is naturally controlled and influenced by the geological structure of the area, topographic variation and the influence of surface emissions in the form of springs and issues. Groundwater movement in the Grenoside Rock and the Greenmoor Rock can be considered separately. The Grenoside rock outcrops close to surface over a relatively large area to the south east of Appleton Quarry and groundwater movement is likely to be influenced by the surface water system related to the River Dearne and its tributaries. Discharges from the Grenoside Rock in the vicinity of the Appleton Quarry occur as springs/issues on the northern side of the A635 Barnsley Road and around the confluence of Park Dyke and River Dearne.
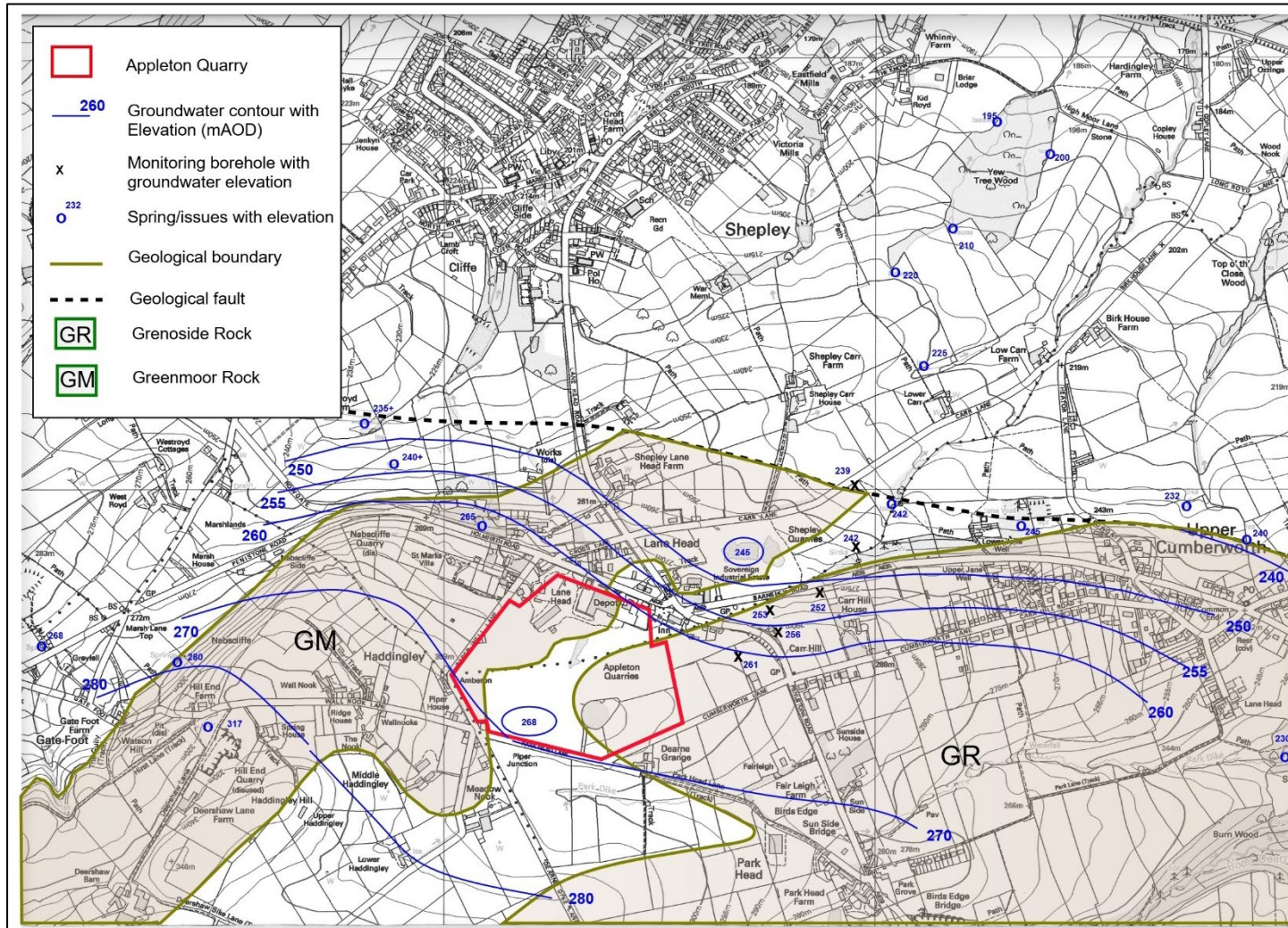
Figure 6.1: Plan showing the location of Appleton Quarry, Upper Cumberworth, West Yorkshire, UK in relation to local geology and natural spring elevations. Inferred groundwater contours developed from local groundwater monitoring boreholes and spring elevations.

The Greenmoor Rock outcrops in the north western part of Appleton Quarry and land to the west of the site. The Greenmoor Rock aquifer is confined beneath mudstones and the overlying Grenoside Rock beneath land to the south and east. Due to the south easterly stratigraphic dip there is no natural discharge from the Greenmoor Rock in a down-dip direction. As a consequence groundwater in the Greenmoor Rock tends to discharge at surface around outcrop through a series of springs and issues that are generally associated with the geological structure of the area and the main east west trending fault in particular. Geological strata are downthrown to the north with both the presence of low hydraulic conductivity formations and the disturbance associated with faulting contributing to the development of an effective barrier to groundwater flow. The numerous springs that occur on the southern side of the fault line is evidence of the hydraulic restriction imposed by the fault. Dewatering at Appleton Quarry has resulted in a localised reduction in groundwater levels by up to 10 m.

Coal Measures Sandstones typically form dual porosity aquifer systems with the potential for groundwater movement through intrinsic permeability and through higher permeability fracture systems. Small scale hydraulic conductivity tests on rock samples are of limited value when attempting to quantify groundwater systems based on fracture flow networks. There is a limited amount of published data regarding the hydraulic properties of Coal Measures sandstones. The most relevant data is included in the BGS technical report WD/00/04 'The physical properties of minor aquifers in England and Wales' (Jones et al, 2000) in which the range of observed permeability values for Lower Coal Measures sandstone is 2.1×10^{-5} m/day to 0.019 m/day with a mean of 6.3 m/d $\times 10^{-3}$ m/d. These values are derived from core samples and do not take account of fracture-based flow systems.

Transmissivity values for Coal Measures sandstones in the east Pennines derived from pumping test data are reported to be in the range 0.4 m^2/day to 413 m^2/day reflecting the high variability of hydraulic properties in Coal Measures strata. The arithmetic average value is 46 m^2/day. Given that Coal Measures sandstones tend to range in thickness from 5 m to 20 m it is clear that the effect of fracturing on secondary porosity has a major impact on the potential to store and transmit groundwater.

A local value for the hydraulic conductivity of the Greenmoor Rock can be estimated from the impact of Appleton Quarry dewatering on groundwater levels. In the immediate vicinity of the quarry the Greenmoor Rock can be considered largely unconfined. Groundwater monitoring data suggests that dewatering activity at the quarry has influenced groundwater levels within a radius of approximately 250 m from the quarry face. The volume of water pumped from the quarry averages approximately 2000 m^3/day from an open face of up to 200 m long. The reduction in groundwater level is assumed to be 10 m. Using the standard form of the Dupuit Forscheimer equation an average 'bulk' hydraulic conductivity can be calculated as follows:

$$q = K/2x \ (h_1^2 - h^2) \hspace{3cm} [6.1]$$

Where,

q = inflow per metre of open face (m^2/d)

K = hydraulic conductivity (m/d)

x = radius of influence (m)

h_1 = head at limit of influence (m)

h = head at quarry face (m)

On this basis the bulk hydraulic conductivity is calculated to be 17 m/d which for a saturated thickness of 10 m to 15 m would result in a transmissivity of between 170 m^2/day and 255 m^2/day. This range of values is within, but towards the upper end of, the range of values considered to be representative of Coal Measures sandstones.

6.3.1.2 MODFLOW groundwater model development and calibration

A MODFLOW groundwater flow model of Appleton Quarry was developed in 2009 by reference to detailed geological, hydrological and hydrogeological information for the quarry and surrounding area. The primary objective of the original modelling study was to investigate the groundwater regime in the Greenmoor Rock and the potential impact of further quarry development. Over

the majority of the area around Appleton Quarry groundwater in the Greenmoor Rock is confined by overlying shales which form a low permeability cover. To the east and south east the Greenmoor Rock is progressively overlain by the Grenoside Rock and subsequently the Penistone Flags, each with intervening shales. Recharge to the Greenmoor Rock is controlled by the presence of overlying formations, and therefore it was necessary to include additional layers in the model to simulate groundwater conditions in both the Grenoside Rock and the Penistone Flags plus the intervening shales. The model therefore consists of five separate layers stacked one above the other with lateral dimensions equivalent to the respective area of outcrop of each formation. The local outcrop of the Greenmoor Rock and the Grenoside Rock is shown on Figure 6.1.

The model covers an area of approximately 20 km^2 extending 5 km in a north west – south east direction and 4 km south west – north east. Careful consideration has been given to the definition of model boundaries. The downstream boundary has been established to coincide with the location of the northern fault which forms a hydraulic barrier to northerly groundwater movement to the immediate north of Appleton Quarry. This boundary has been specified as a horizontal flow barrier. The western boundary has been configured to represent the limit of the Greenmoor Rock outcrop in the vicinity of Gatefoot. The eastern boundary has been configured to represent both the perceived groundwater divide in the upper aquifers at the River Dearne valley and the estimated groundwater elevation at a suitable distance remote from Appleton Quarry. Outcrop and catchment boundaries have been set as no-flow boundaries. The southern model boundary has been set as a constant head boundary to represent the estimated rest groundwater level in the Greenmoor Rock three kilometres to the south - south west of Appleton Quarry. The elevation of the top and bottom of all five model layers have been configure by reference to published geological maps and geological cross-sections derived from local site investigation boreholes.

Hydraulic data for the three aquifers and the intervening shales has been based on published hydrogeological data sources (Jones et all, 2000) and the results of previous hydrogeological studies at Appleton Quarry (S M Foster Associates Limited, 2007). Data used in the model is summarised in Table 6.1.

Model layer	Greenmoor Rock	Shale	Grenoside Rock	Shale	Penistone Flags
Parameter					
Horizontal hydraulic conductivity (m/s)	2×10^{-4}	1×10^{-9}	2×10^{-4}	1×10^{-9}	2×10^{-4}
Vertical hydraulic conductivity (m/s)	2×10^{-5}	1×10^{-9}	2×10^{-5}	1×10^{-9}	2×10^{-5}
Effective porosity (%)	0.25	0.1	0.25	0.1	0.25
Thickness (m)	15	15	5	10	5

Table 6.1: Original Appleton Quarry MODFLOW groundwater model hydraulic properties.

Southern boundary constant head values were set at 275 mAOD to 280 mAOD by reference to the groundwater contour plan and the elevation of local spring issues from the Greenmoor Rock, as shown on Figure 6.1. Initial heads in the Greenmoor Rock were set at 270mAOD which represents an average value across the modelled area. In the absence of any quarry abstraction, the primary discharge points from the Greenmoor Rock are the series of springs that occur at the fault junction modelled as the northern model boundary. Springs were represented in the model as constant head cells at which outflow is dependent on the differential head between the spring and the surrounding groundwater level. Spring fixed heads were set at the relevant spring elevations as defined on Ordnance Survey mapping and included on the groundwater contour map, as shown on Figure 6.1.

Model calibration was achieved by minor adjustment of boundary conditions, recharge inputs and aquifer hydraulic conductivity values in relation to observed groundwater levels as defined at monitoring boreholes at Appleton Quarry plus the elevation and location of surface issues from the Greenmoor Rock. Due to the relatively small number of groundwater monitoring locations,

and intermittent monitoring record, calibration was also referenced to the previously defined groundwater contour plan and knowledge of groundwater level variations over several years.

For the existing level of development at the quarry the model produced a net groundwater inflow to the excavation of 2056 m³/day which is comparable to the estimated daily dewatering rate of 2000 m³/day. Model output in the form of groundwater contours for the quarry at current development is shown in Figure 6.2.
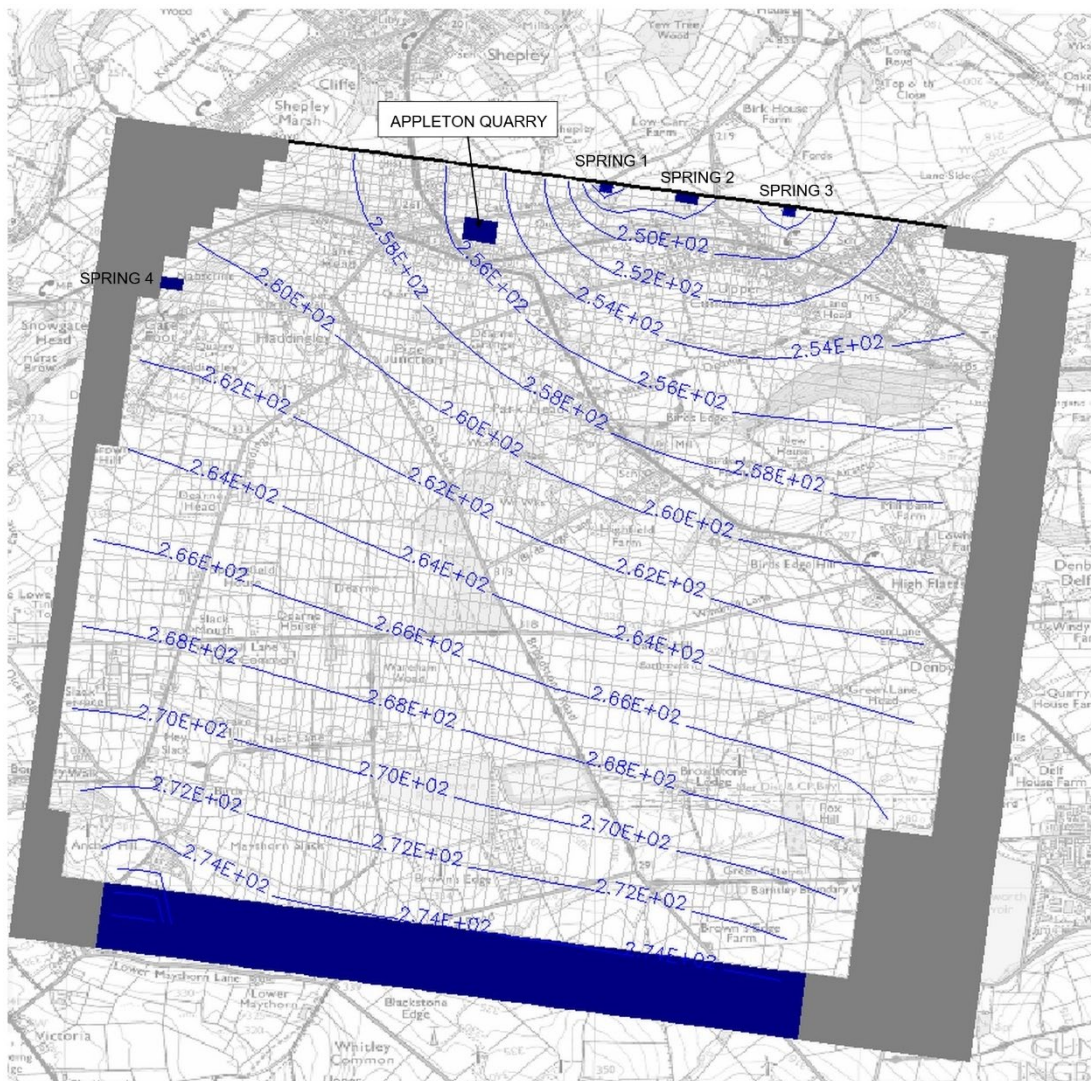
Figure 6.2: Modelled groundwater levels in the Greenmoor Rock (mAOD) from the original model showing groundwater levels in response to dewatering at Appleton Quarry and spring discharge at the northern model boundary.

6.3.1.3 Fracture flow analysis

The groundwater flow model is based on a bulk hydraulic conductivity value for the Greenmoor Rock derived from inflow analysis. Although it is recognized that the majority of groundwater flow occurs via joints and bedding planes, there is no explicit account of discontinuity hydraulic conductivity. To allow comparative assessment of model results in relation to discontinuity dilation, further analysis has been undertaken to estimate Greenmoor Rock discontinuity aperture dimensions based on observed groundwater flow conditions.

The Greenmoor Rock contains two distinct discontinuity sets in the form of well-defined bedding planes and sub-vertical jointing that extends through the full stratigraphic depth. The cubic law has therefore been applied in the following form (Bear, 1993).

$$Q = \rho g/12\mu \; [\Sigma b_i^3 + \Sigma b_j^3] \; . \; dh/dx \qquad\qquad [6.2]$$

Where,

ρ = fluid density (kg/m^3)

g = gravitational acceleration (m/s^2)

Q = flow (m^3/s)

μ = dynamic viscosity (p.s)

b_i = joint aperture normal dimension (m)

b_j = bedding plane aperture normal dimension (m)

dh/dx = hydraulic gradient

Equivalent aperture dimensions have been calculated from the baseline model results. It is assumed that groundwater flow occurs through the full 200 m long up-gradient excavation face. Bedding plane separation is approximately 3 m and joint spacing is approximately 3 m. Assuming that all bedding plane apertures are homogeneous and that all joint apertures are homogeneous, for an inflow of 2000 m^3/day and a hydraulic gradient into the quarry of 0.05

estimated from local groundwater monitoring data, the following equation applies:

$$0.023 = 9810/0.0156 \, [70b_i{}^3 + 3b_j{}^3] \, . \, 0.05$$

$$7.31 \times 10^{-7} = 70b_i{}^3 + 3b_j{}^3$$

There are an infinite number of solutions to the above equation. However, on-site observation has established that average bedding plane aperture is approximately 5 mm. On this basis the equation can be constrained to allow calculation of average joint aperture. The calculated joint aperture is 1.72 mm. Cubic law calculation therefore results in a requirement for the following discontinuity aperture dimensions to produce the modelled groundwater discharge to the quarry excavation.

Joint aperture – 1.72 mm

Bedding plane aperture – 5 mm

As the above analysis is related to the modelled discharge rate it is apparent that the calculated DFN dimensions relate only to hydraulically connected discontinuity networks. This approach therefore inherently takes account of DFN connectivity.

The baseline bulk hydraulic conductivity is related to baseline discontinuity aperture dimensions through the following equation (Bear, 1993):

$$K = \rho g/12\mu A \, . \, [\Sigma b_i{}^3 + \Sigma b_j{}^3], \, = Q/A(dh/dx), \qquad\qquad [6.3]$$

where,

A = the cross-sectional area perpendicular to the groundwater flow path (m^2)

Application of the above analysis for a cross-section flow area of 2100 m^2 (210 m x 10 m) results in a calculated K of 2.19 x 10^{-4} m/s which compares to the previous estimate of 1.96 x 10^{-4} m/s derived from manual inflow analysis and

the value of 2×10^{-4} m/s used in model calibration. Re-running the baseline groundwater flow model with Greenmoor Rock horizontal hydraulic conductivity increased from 2×10^{-4} m/s to 2.19×10^{-4} m/s results in a predicted quarry inflow of 2290 m^3/s.

6.3.1.4 Simulating lithostatic unloading effects

The original groundwater model of Appleton Quarry was further developed to investigate potential quarry inflow and external hydrogeological effects associated with quarry development to full lateral and depth extents. Development would involve deepening the quarry by a further 4m, with associated increase in required groundwater drawdown, and extending the southern quarry face to 300m wide. The full development model has been re-run during this study with a global horizontal hydraulic conductivity value of 2.19×10^{-4} m^3/s in the Greenmoor Rock to allow subsequent comparative analysis of lithostatic unloading effects. Modelled inflow/discharge rates at full development are presented in Table 6.2.

Location	Discharge elevation (mAOD)	Modelled discharge rate (m^3/s)	Modelled discharge rate (m^3/d)
Appleton Quarry	251	0.073	6,300
Spring 1	242	0.079	6,826
Spring 2	246	0.025	2,160
Spring 3	245	0.038	3,715
Spring 4	280	0.002	173

Table 6.2: Modelled discharge to the quarry excavation and natural springs from the original model of Appleton Quarry as extended. Spring locations as shown on Figure 6.2.

Geomechanical modelling has provided the basis to define potential discontinuity dilation magnitude and extents behind the quarry face. The Greenmoor Rock at Appleton Quarry can be considered an orthogonally

jointed formation and therefore discontinuity dilation relationships from the orthogonally jointed geomechanical model are applicable. However, on-site survey has indicated that groundwater flow occurs predominantly through bedding planes and therefore the bedding-plane only dilation/distance relationship equation has been applied to bedding plane dilation estimation. The relevant distance/dilation equations for this site are therefore as follows.

Horizontal dilation of sub-vertical joints - $Dilation_h = 0.002x^{-1}$

Vertical dilation of bedding planes - $Dilation_v = 0.037x^{-1}$

Horizontal hydraulic conductivity values in the original model have been varied through application of both vertical and horizontal discontinuity dilation adjustment. Vertical hydraulic conductivity values have been varied through application of just vertical discontinuity apertures.

The distance over which discontinuity dilation occurs is defined by the equation for horizontal EdZ extent behind the excavation face, as developed in Chapter 5.

$EdZ_h = n_h \times depth,$

For an orthogonally jointed discontinuity configuration $n_h = 3.82$. For an average excavation depth of 30 m, the $EdZ_h = 115$ m from the excavation face.

To simulate the effects of lithostatic unloading, the baseline joint and bedding plane aperture dimensions of 1.72 mm and 5.00 mm respectively, have been adjusted in accordance with the above distance/dilation equations over a distance of approximately 115 m from the excavation face. The adjustment process and results are shown in Table 6.3.

The previously calculated joint and bedding plane aperture dimensions of 1.72 mm and 5.00 mm respectively, represent discontinuity aperture dimensions

after mineral extraction has taken place. However, as the baseline hydraulic conductivity value of 2.19 x 10^{-4} m/s has been applied throughout the model, for the purpose of this study the calculated discontinuity apertures are assumed to represent pre-development conditions. Investigation of the effect of mineral extraction on groundwater flow has therefore been undertaken by adding calculated discontinuity dilation magnitudes from baseline discontinuity aperture dimensions to produce a higher hydraulic conductivity, representative of the effect of excavation induced unloading.

Pre-excavation discontinuity aperture dimensions have been calculated by increase of the calculated joint and bedding plane aperture dimensions at 50m intervals behind the excavation face and floor in accordance with the above dilation/distance relationships. Bedding plane dilation has only been applied to the quarry floor area and surrounding 50 m zone.

The analysis summarised in Table 6.4 demonstrates a calculated increase in horizontal hydraulic conductivity from 2.19 x 10^{-4} m^3/s to 4.70 x 10^{-4} m^3/s in the first 50 m behind the excavation face, with 2.67 x 10^{-4} m^3/s and 2.35 x 10^{-4} m^3/s in successive 50 m distances behind the face. These adjustments have been applied to the groundwater flow model with model inflow/discharge results as summarised in Table 6.3.

Location	Discharge elevation (mAOD)	Modelled discharge rate (m^3/s) Pre excavation	Modelled discharge rate (m^3/s) Post extraction
Appleton Quarry	251	0.073	0.087
Spring 1	242	0.079	0.078
Spring 2	246	0.025	0.024
Spring 3	245	0.038	0.037
Spring 4	280	0.002	0.005

Table 6.3: Modelled discharge to quarry excavation and natural springs – comparison of pre and post-discontinuity dilation results.

Distance (D) from excavation face (m)	Joint Dilation (Dil$_{gJ}$) from geotech model equation(m)	Mean Joint dilation (m)	Original joint aperture of 1.72 mm adjusted for dilation (m)	Bedding dilation (Dil$_{gb}$) from geotech model equation (m)	Mean bedding dilation (m)	Original bedding aperture of 5.00 mm adjusted for dilation (m)	New horizontal K calculated from cubic law (m/s)
Formula	0.002*(D^-1)		0.00172+ Mean Dil$_{gJ}$	0.037*(D^-1)		0.005+Mean Dil$_{gb}$	$\rho g/(12*\mu*2100) = 300$ 300[70(b$_i$^3) + 3(b$_j$^3)] =21000(b$_i$^3) + 900(b$_j$^3)
10	0.000200			0.003700			
		0.000120	0.001840		0.002220	0.007220	0.000470
50	0.000040			0.000740			
		0.000030	0.001750		0.000555	0.005555	0.000267
100	0.000020			0.000370			
		0.000017	0.001737		0.000185	0.005185	0.000235
150	0.000013						
		0.000007	0.001727			0.005000	0.000221
200							
			0.001720			0.005000	0.000219
250							
			0.001720			0.005000	0.000219
300							
			0.001720			0.005000	0.000219
350							
			0.001720			0.005000	0.000219

Table 6.4: Discontinuity dilation adjustment and calculation of adjusted horizontal hydraulic conductivity. Hydraulic conductivity calculated using formula K = 21000*(adjusted joint aperture^3) +900*(adjusted bedding aperture^3).

Model results demonstrate that with excavation induced discontinuity dilation the predicted excavation inflow would be approximately 19% higher than if unloading effects were not accounted for. The analysis indicates that the increased groundwater flow to the quarry excavation following discontinuity dilation would lead to relatively minor reduction in flow to Springs 1, 2 and 3.
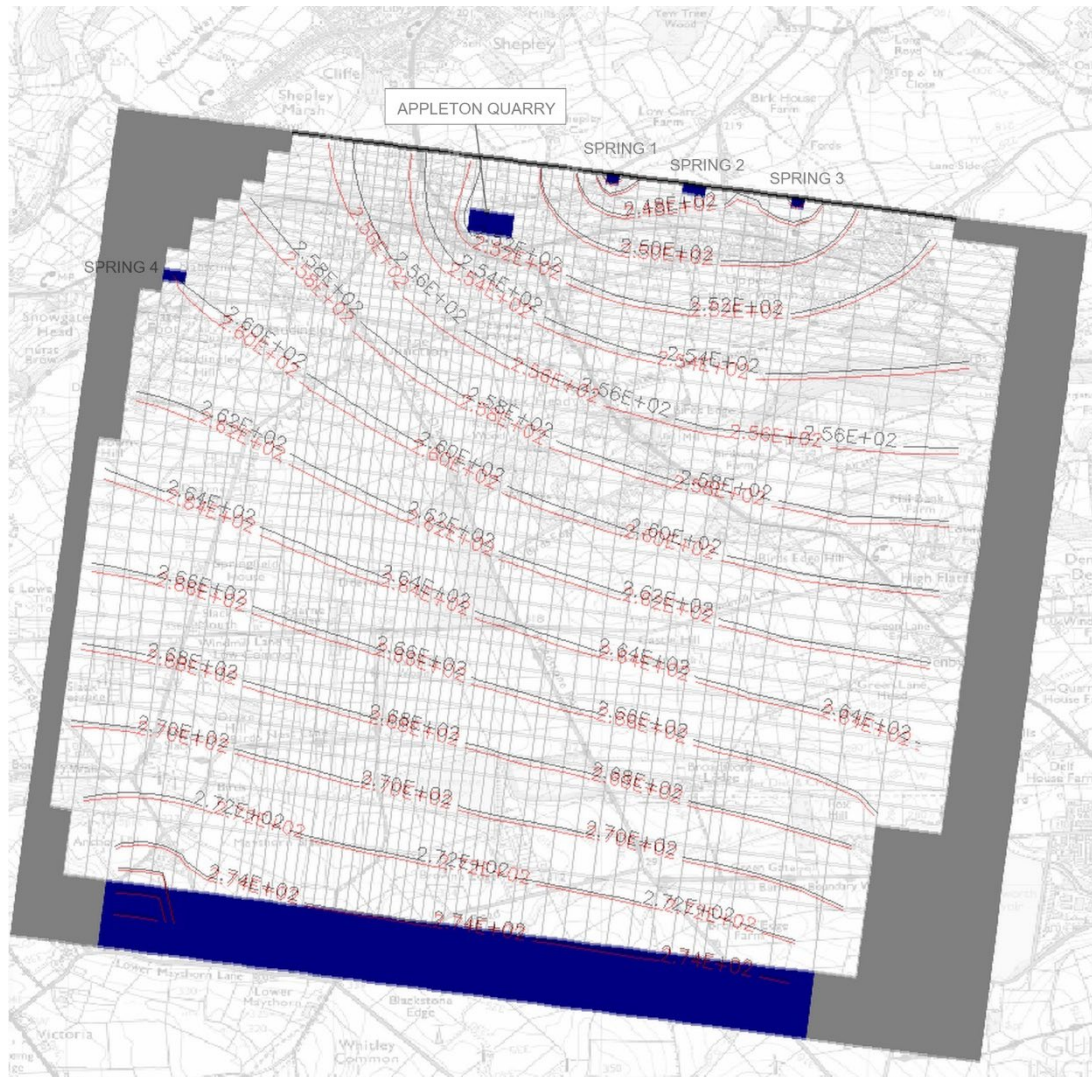
Figure 6.3: Modelled groundwater levels in the Greenmoor Rock (mAOD) for models with (red lines) and without discontinuity dilation (black lines). Results show a reduction in groundwater elevation around the quarry excavation with groundwater levels reduced over a distance of approximately 2 km from the excavation.

Groundwater level contours with and without discontinuity dilation are shown on Figure 6.3. Model results demonstrate that the inclusion of discontinuity dilation has an effect on groundwater levels for a distance of up to approximately 2 km from the quarry excavation. However, the reduction in

groundwater level is approximately 1 m at a distance of 50 m from the excavation and reduces to less than 0.5 m at a distance of approximately 1 km from the excavation.

In this case study, the consequence of including allowance for excavation induced discontinuity dilation is relatively minor with changes to groundwater levels and flow unlikely to have any significant external hydrogeological impact or internal operational impact.

The above analysis has been undertaken by reference to the calibrated bulk hydraulic conductivity value of 2 x10^{-4} m/s. This is a relatively high bulk hydraulic conductivity for hard rock formations. The same model has therefore been used to investigate the potential significance of lithostatic unloading in lower hydraulic conductivity formations. Generic bulk hydraulic conductivity values for less permeable hard rock formations have been derived from standard texts (Todd, 2005). Within the group of sandstone, limestone and fractured igneous or metamorphic rocks reference hydraulic conductivity values have a range of 1 x 10^{-10} m/s to 1 x 10^{-3} m/s. Reference to pumping test data for Coal Measures Sandstones (Jones et al, 2000), as described above, indicates transmissivity values in the range 0.4 m^2/d to 400m^2/d. Assuming a 5 m average thickness such values can be translated to hydraulic conductivity values within the range 9.3 x 10^{-7} m/s to 9.3 x 10^{-4} m/s.

Additional groundwater model simulations have therefore been undertaken with the base bedding and joint aperture dimensions reduced to result in a hydraulic conductivity value at 2.7 x 10^{-5} m/s. Discontinuity aperture dimensions have been recalculated for each hydraulic conductivity value through application of the cubic law, and pre-lithostatic unloading hydraulic conductivity values have been calculated, taking account of discontinuity dilation, through application of the process defined at Table 6.4.

Assuming that, in a lower hydraulic conductivity environment, post excavation bedding plane aperture would be 3 mm and applying the cubic law in the form defined above, post unloading joint aperture dimension has been calculated as follows:

Bulk hydraulic conductivity – 2.7 x 10^{-5} m/s

Joint aperture = 0.37 mm

Bedding aperture = 3.0 mm

Excavation induced discontinuity dilation adjustments have been calculated using the same dilation/distance equations and EdZ extents that were applied to the higher hydraulic conductivity case. The analysis results in a pre-excavation hydraulic conductivity of 1.13 x 10^{-4} m/s at the excavation face increasing to 4.4 x 10^{-5} m/s and 3.2 x 10^{-5} m/s at further 50 m intervals from the face. Re-running the groundwater flow model with higher hydraulic conductivity values results in a change in excavation inflow and spring discharge data as summarized in Table 6.5.

Location	Discharge elevation (mAOD)	Modelled discharge rate (m^3/s) Pre excavation	Modelled discharge rate (m^3/s) Post excavation
Appleton Quarry	251	0.0109	0.0130
Spring 1	242	0.0104	0.0102
Spring 2	246	0.0039	0.0038
Spring 3	245	0.0060	0.0059
Spring 4	280	0.0004	0.0003

Table 6.5: Comparison of excavation inflow and spring discharge rates pre and post-excavation.

Groundwater model results demonstrate that, in a lower hydraulic conductivity environment, the impact of discontinuity dilation may be greater as prediction dilation magnitudes are a higher percentage of original discontinuity aperture. Model results also show a 19% increase in predicted inflow to the excavation if discontinuity dilation is accounted for. There are associated reductions in predicted spring flow. It is however, noted that the inflow rates are relatively

low at 940 m³/d without discontinuity dilation and 1123 m³/d following inclusion of discontinuity dilation.

The effect of discontinuity dilation on groundwater levels and flow direction is shown on Figure 6.4 which includes model results with and without inclusion of dilation allowance.
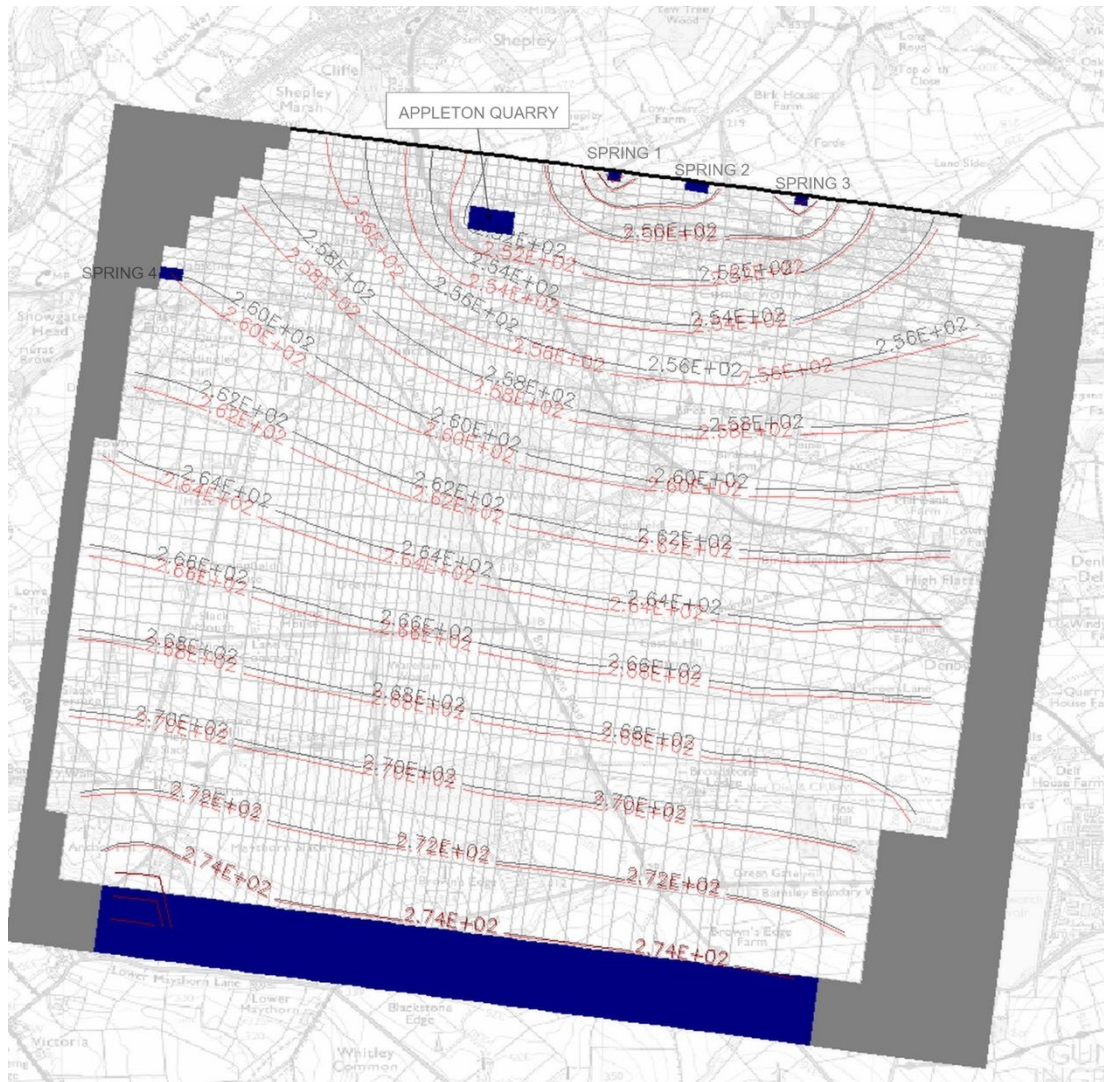
Figure 6.4: Groundwater contour plot showing predicted groundwater elevations (mAOD) around quarry excavation in simulated lower hydraulic conductivity environment. Groundwater contours show elevations without discontinuity dilation (black lines) and with discontinuity dilation (red lines) indicating approximate 2 m difference in groundwater levels within 100 m of the excavation face.

Groundwater level contour plots, as shown in Figure 6.4, demonstrate that in a lower hydraulic conductivity environment, with all other parameters e.g. material properties, boundary conditions, etc., remaining the same, excavation induced discontinuity dilation has greater impact on local groundwater levels around the excavation area. Model results suggest that groundwater levels with discontinuity dilation included would be at least 1 m lower than levels predicted without account for discontinuity dilation, for a distance of up to 3 km from the excavation face.

The above analyses have been based on mineral extraction to a depth of 30mbgl. This is the minimum depth for which discontinuity dilation data was reported during the geomechanical modelling programme. As discussed in Chapter 5, discontinuity dilation magnitude increases with increasing depth of excavation. The case study analysis reported here is therefore likely to be representative of hydrogeological effects at the lower end of the range of potential effects. For deeper or larger excavations, or less intensively jointed environments, potential discontinuity dilation magnitudes and extents are expected to be larger, resulting in potentially higher magnitude impact on groundwater levels and flow.

6.3.2 Copley Lane Quarry case study

The second groundwater flow case study is based on application of an existing MODFLOW 3D groundwater flow model of Copley Lane Quarry, Sherburn in Elmet, North Yorkshire. The quarry is established in the Permian Upper Magnesian Limestone and is best represented by the variably jointed models developed through the geomechanical modelling programme.

6.3.2.1 Site description and hydrological context

Copley Lane Quarry is located in Sherburn in Elmet, Tadcaster, Yorkshire, LS25 6BJ. The centre of the site is at National Grid Reference 4483 4350. The site covers an area of some 7 hectares (Ha). The main surface water feature in the vicinity of the site is a small ephemeral stream known locally as Stream Dike which flows west to east approximately 200 m to the south of the

southern quarry face. The stream drains a catchment area of 11.6 km^2 which extends from Sherburn in the east to Old Micklefield in the west. In the vicinity of the quarry the stream flows on relatively low hydraulic conductivity calcareous mudstone of the Middle Permian Marl.

The Permian deposits dip to the east at a gradient of 1:50 and rest unconformably on a weathered surface of Carboniferous strata. The geological succession at the site is described below.

Brotherton Formation (Upper Magnesian Limestone- UML). These limestones are 20 m – 24 m thick, and are thinly bedded, grey to buff, occasionally white to yellow, flaggy, sometimes oolitic. There are occasional soft, earthy, marly beds and partings. The quarrying operation within the site exploited the lower 20 m of these limestones and dolomites.

Edlington and Hayton (Anhydrite) Formations (Middle Permian Marl - MPM) comprise 20 m of red and green calcareous clays with increasing amounts of gypsum and anhydrite towards to base. From the nature of the strata, the marl/clay formations are considered likely to have a very low permeability. The gypsum and anhydrite lenses may be subject to solution by groundwater.

Cadeby Formation (Lower Magnesian Limestone - LML) comprises 24 m -34 m of limestones. The upper subsection comprises yellow and cream dolomitic limestones, sometimes oolitic, often wedge bedded. The lower subsection comprises calcareous clays and clayey limestones.

Available geological data for the centre of the site indicates that the base of the UML is approximately 17 mAOD. As the stratigraphic dip is to the north east it is probable that the base of the UML is below 17 mAOD around the north and east of the site and slightly higher than 17 mAOD to the south and west.

Groundwater level monitoring has been undertaken continuously since 2007. Data indicates that, throughout the monitoring period, water levels in each

UML monitoring borehole have remained at around the base of the UML. On the basis that the MPM is likely to have particularly low vertical hydraulic conductivity it can be concluded that the observed water levels reflect groundwater heads in the UML. Groundwater contour plans for the UML demonstrate a consistent groundwater flow direction to the east and south east, along strike, with a hydraulic gradient of approximately 0.025. Groundwater levels at the site and surrounding area are shown on Figure 6.5.
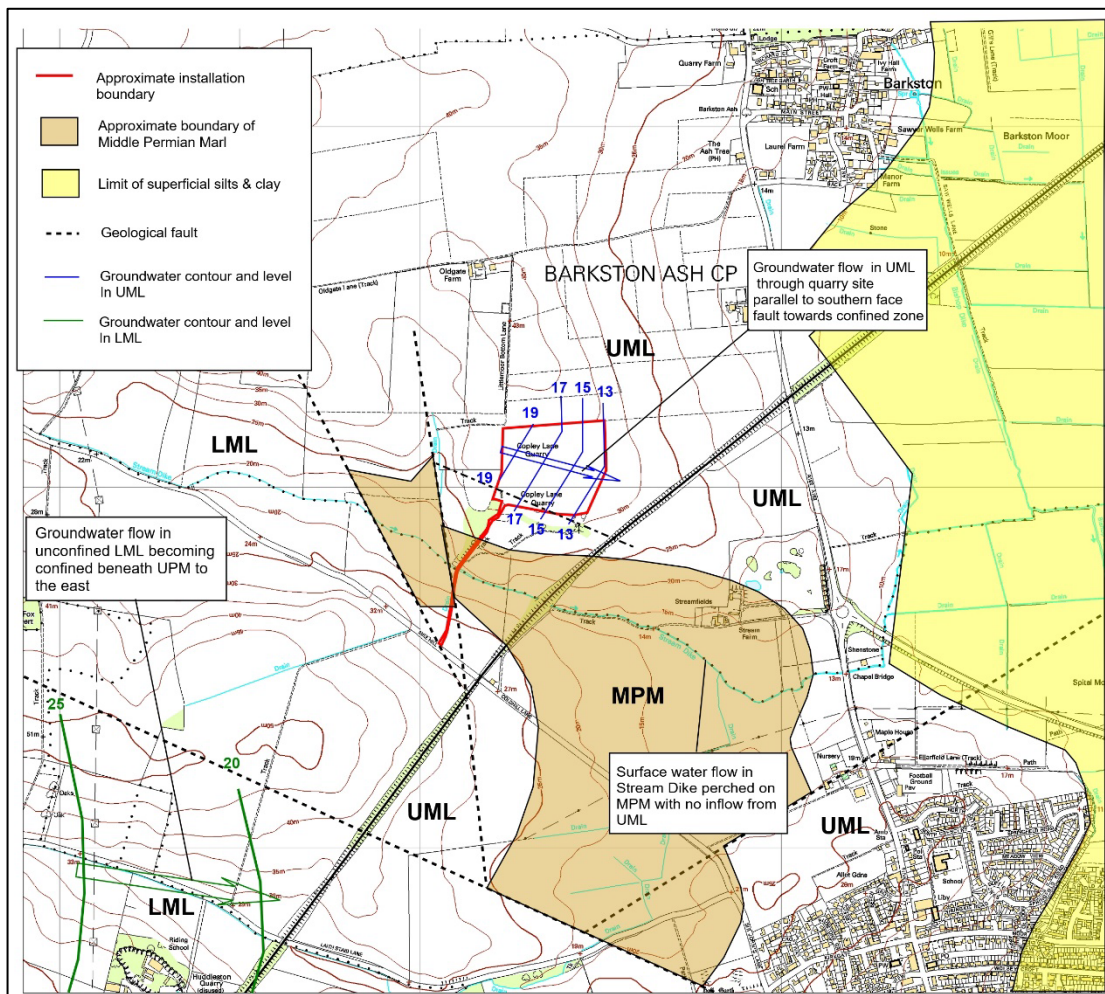
Figure 6.5: Conceptual hydrogeological model showing inferred groundwater flow direction and elevations (mAOD) in the UML and LML in the vicinity of Copley Lane Quarry.

It is considered likely that any groundwater present in the UML in the vicinity of the site drains in an east and south-easterly direction, as indicated by groundwater monitoring, towards the confined section of the aquifer beneath the Triassic sandstones north of Sherburn in Elmet. Monitoring data suggests

that groundwater levels in the UML to the east of the site are too low to allow discharge of groundwater at surface.

6.3.3.2 MODFLOW groundwater model development and calibration

A 3D MODFLOW model of Copley Lane Quarry was developed in 2013 to investigate groundwater flow through and beneath the quarry and the fate of selected contaminants associated with non-hazardous landfilling at the site. The model covers an area of 2 km x 2 km centred on Copley Lane Quarry. The model constitutes a single layer representing the UML. The southern and western boundaries are formed by the MPM and the faulted boundary with the LML. The northern boundary, parallel to the regional groundwater flow direction, is defined as a no-flow boundary and fixed head boundaries are specified at the north western and eastern boundaries.

The quarry site has been represented as a single excavation with dimensions of 300 m x 200 m through the full height of the model layer. A clay liner associated with landfilling at the quarry is represented as a vertical 1 m thick low hydraulic conductivity layer around all four excavation sides. The base of the model layer is impermeable. The liner is represented as a horizontal flow barrier around all four sides of the cell. Model parameters are summarised below.

Flow model input data

Upstream fixed head boundary – 18 mAOD

Downstream fixed head boundary – 0 mAOD

Horizontal hydraulic conductivity Limestone – 0.0002 m/sec

Horizontal hydraulic conductivity Clay liner – 1 x 10^{-9} m/sec

Effective porosity – 0.20

Recharge – 250 mm/year

The model geometrical configuration is shown in Figure 6.6.
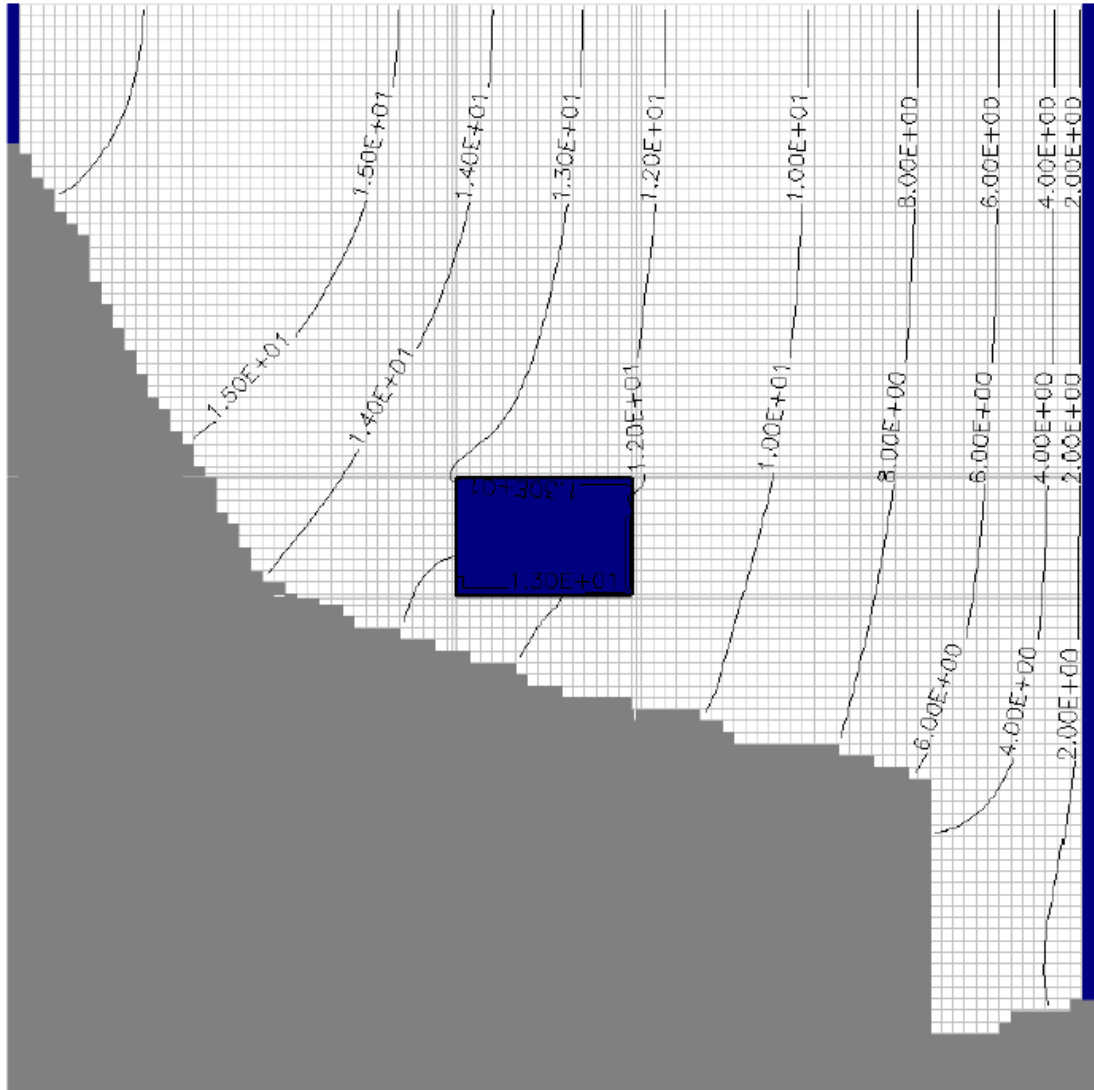
Figure 6.6: Copley Lane MODFLOW model configuration showing quarry excavation as rectangular cell. Grey area represents the outcrop of the MPM. Blue boundaries are fixed head boundaries. Contours represent groundwater elevation (mAOD) showing flow from north west to south east. Scale – quarry excavation width = 300 m.

As indicated in Figure 6.6, groundwater flows north west to south east through the model domain from a maximum elevation of 16 mAOD in the north west to a minimum elevation of 2 mAOD in the south east.

6.3.3.3 Fracture flow analysis

The UML at Copley Lane Quarry is thinly bedded and variably jointed. An average saturated thickness of 5m is assumed in this analysis. With a base hydraulic conductivity of 2×10^{-4} m/s and a local hydraulic gradient of 0.007 the average flow rate through the 300 m wide excavation is estimated to be approximately 180 m^3/d. Site survey has demonstrated that bedding plane spacing is approximately 1m and that joint spacing, although variable is approximately 0.5 m. Assuming that post extraction bedding plane aperture is a nominal 3 mm, joint aperture can be estimated through application of the cubic law, as applied in case study 1, resulting in an estimated joint aperture width of 0.80 mm.

6.3.3.4 Simulating lithostatic unloading effects

The relevant dilation/distance equations for this model are as follows.

Horizontal dilation of sub-vertical joints - Dilation = $0.01x^{-1}$

Vertical dilation of bedding planes - Dilation = $0.037x^{-1}$

Horizontal hydraulic conductivity values in the original model have been varied through application of both vertical and horizontal discontinuity dilation adjustment. Vertical hydraulic conductivity values have been varied through application of just vertical discontinuity apertures.

The distance over which discontinuity dilation occurs is defined by the equation for horizontal EdZ extent behind the excavation face, as developed in Chapter 5.

$EdZ_h = n_h \times$ depth,

For a variably jointed discontinuity configuration $n_h = 4.88$. For an average excavation depth of 30 m, the $EdZ_h = 146$ m from the excavation face.

To simulate the effects of lithostatic unloading, the baseline joint and bedding plane aperture dimensions of 0.80 mm and 3.00 mm respectively, have been adjusted in accordance with the above distance/dilation equations over a distance of approximately 150 m from the excavation face. The adjustment process and results are shown in Table 6.6.

In this case study the baseline horizontal hydraulic conductivity has been assigned by reference to literature values and has not been calibrated from quarry abstraction data. Assessment of the potential effect of excavation induced discontinuity dilation has therefore been undertaken by increasing discontinuity aperture around the excavation in accordance with the above criteria.

As shown in Table 6.6, adjustment for discontinuity dilation results in a hydraulic conductivity of 1.034×10^{-3} m/s at the excavation face, reducing to 2.18×10^{-4} m/s at a distance of 150 m from the face. This adjusted hydraulic conductivity distribution has been added to the MODFLOW model to investigate the impact on both groundwater flow and selected contaminant transport. Comparative groundwater contour plots are presented as Figure 6.7.

Increased hydraulic conductivity around the excavation due to excavation induced discontinuity dilation results in a reduction in groundwater elevation up-gradient of the quarry site. There is negligible effect down-gradient of the site. A reduction in up-gradient groundwater level by approximately 0.5m when compared to the original model is unlikely to be hydrogeologically significant. In this case study, such a change would not affect downstream receptors or groundwater conditions within the UML.

Distance (D) from excavation face (m)	Joint Dilation (Dil$_{gJ}$) from geotech model equation(m)	Mean Joint dilation (m)	Original joint aperture of 0.83 mm adjusted for dilation (m)	Bedding dilation (Dil$_{gb}$) from geotech model equation (m)	Mean bedding dilation (m)	Original bedding aperture of 3.00 mm adjusted for dilation (m)	New horizontal K calculated from cubic law (m/s)
Formula	0.01*(D^-1)		0.00083+ Mean Dil$_{gJ}$	0.037*(D^-1)		0.003+Mean Dil$_{gb}$	ρg/(12*μ*1500) = 420 420[600(b$_i$^3) + 5(b$_j$^3)] =251538(b$_i$^3) + 2097(b$_j$^3)
10	0.001000			0.003700			
		0.000600	0.001430		0.002220	0.005220	0.001034
50	0.000200			0.000740			
		0.000150	0.000980		0.000555	0.003555	0.000331
100	0.000100			0.000370			
		0.000083	0.000913		0.000185	0.003185	0.000259
150	0.000067						
		0.000033	0.000863			0.003000	0.000218
200							
			0.000830			0.003000	0.000200
250							
			0.000830			0.003000	0.000200
300							
			0.000830			0.003000	0.000200
350							
			0.000830			0.003000	0.000200

Table 6.6: Discontinuity dilation adjustment and calculation of adjusted horizontal hydraulic conductivity. Hydraulic conductivity calculated using formula k = 251538*(adjusted joint aperture³) +2096*(adjusted bedding aperture³).
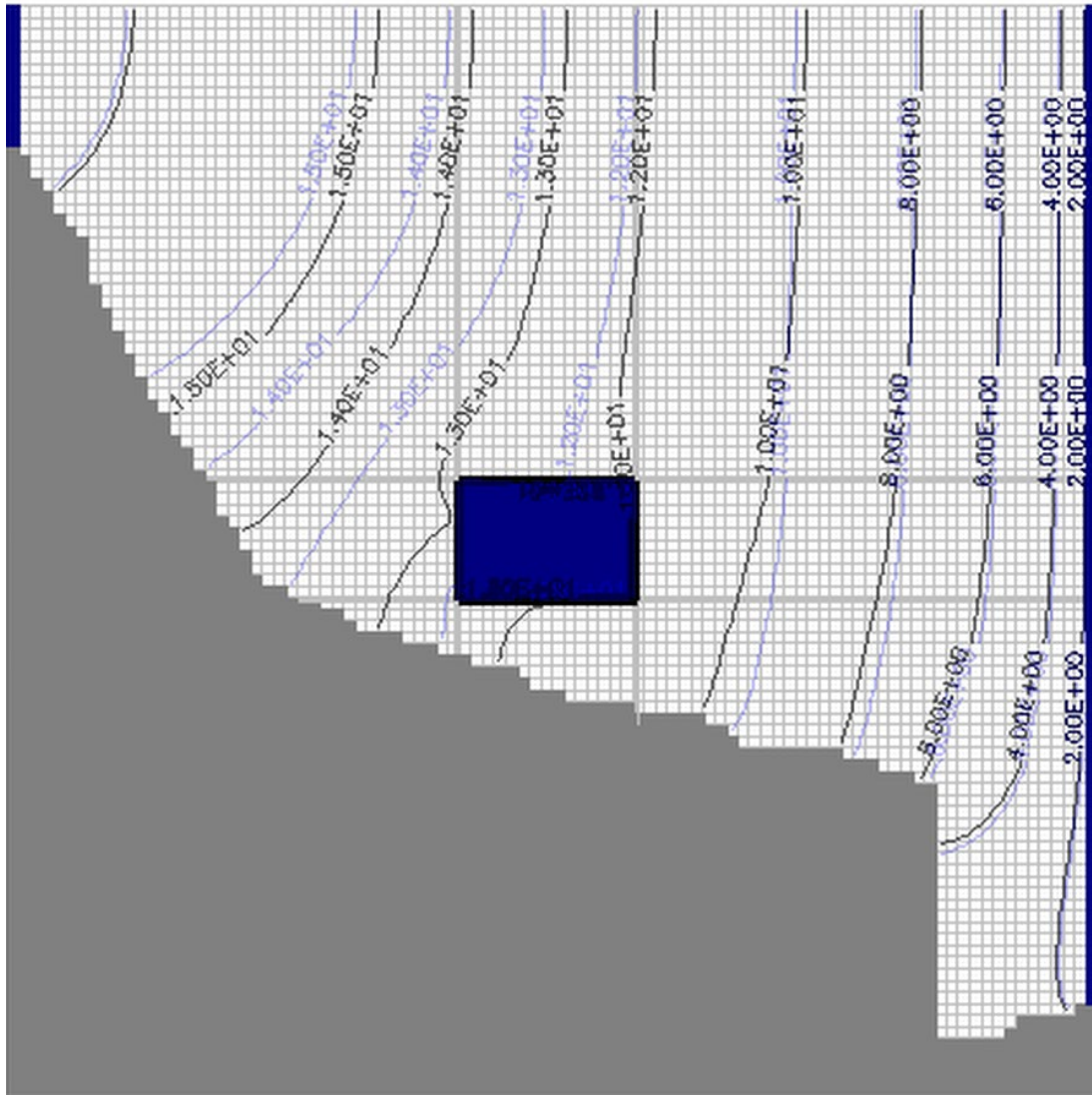
Figure 6.7: Groundwater contour plan showing groundwater elevations (mAOD) with (blue lines) and without (black lines) discontinuity dilation. Results show reduction in groundwater levels by approximately 0.5 m upstream of the quarry when discontinuity dilation is accounted for.

6.4 Contaminant transport and environmental risk

Investigation into the potential effect of changes to fracture flow characteristics in hard rock formations around open pit mineral workings on the fate of contaminants in both the vadose and phreatic zones has been undertaken by reference to three case study examples. Case studies have been selected to represent a range of geological environments and potential contaminant types. Summary details are provided below.

Copley Lane Quarry Landfill: a MT3D model of hazardous and non-hazardous contaminant lateral migration through Upper Magnesian Limestone based on the MODFLOW groundwater flow model discussed in Section 6.3

Tong Quarry: a LandSim contaminant migration risk-based model of non-hazardous contaminant vertical and lateral migration through Coal Measures mudstone and sandstone

Farley Quarry: a LandSim contaminant migration risk-based model of non-hazardous contaminant vertical and lateral migration through Wenlock Limestone.

All analyses in this section are based on amendments to existing contaminant transport models to represent physical changes to saturated and unsaturated zone hydraulic conductivity associated with excavation induced discontinuity dilation. Model results with and without inclusion of the effects of excavation unloading are compared to evaluate the significance of unloading effects on the fate of contaminants. As it is the comparative analysis that is the basis of this section, only brief details of each case study site and the original models are presented here.

Details presented in this section are indicative only, as it is recognized that the use of equivalent hydraulic conductivity values to represent fracture flow systems does not fully account for variation in contaminant attenuation

characteristics. However, as the objective is to investigate potential hydrogeological significance this approach is considered to be informative.

6.4.1 Copley Lane Quarry Landfill case study

The hydrogeology of Copley Lane Quarry is described in Section 6.3. The quarry is partly restored by importation of non-hazardous waste materials that are deposited in lined cells within the quarry excavation. Leachate quality monitoring over several years demonstrated the presence of hazardous and non-hazardous substances in waste leachate. A conceptual hydrogeological model of the site identified two potential contaminant migration pathways from the site, as indicated schematically in Figure 6.8.

Upper Magnesian Limestone
Horizontal Hydraulic conductivity - 2×10^{-4} m/s
Porosity - 0.2

Copley Lane Quarry Landfill

UML

1m Thick compacted clay barrier and
Bentomat sealing liner

Accumulated leachate   PATHWAY 1

Groundwater level in UML

MPM   PATHWAY 2

Unsaturated zone in MPM

Piezometric head in LML

Middle Permian Marl
Hydraulic conductivity - 1×10^{-5} m/s
Porosity - 0.24

LML

Lower Magnesian Limestone
Hydraulic conductivity - 1×10^{-6} m/s - 4×10^{-5} m/s
Porosity - 0.16

Figure 6.8: Schematic illustration of potential contaminant migration pathways from Copley Lane Quarry Landfill. Pathway 1 – lateral flow through the UML. Pathway 2 – vertical flow through the MPM followed by lateral flow in the LML.

Assessment of potential lateral contaminant migration to the UML was undertaken by addition of an MT3D contaminant transport model to the existing MODFLOW groundwater flow model. Assessment of vertical leakage to the LML was undertaken by development of a LandSim risk based model. The potential effect of lithostatic unloading on groundwater flow in the UML has been established through adjustment to the groundwater flow model as described in Section 6.3. The MT3D contaminant transport model has been re-run by linkage to the amended groundwater flow model. No other changes were made to the original MT3D model. On the basis that dilation of bedding planes below the excavation floor would have minimal impact on vertical hydraulic conductivity in the MPM, changes to Pathway 2 are represented by bedding plane dilation in the lateral pathway in the LML. The effect of discontinuity dilation along Pathway 2 has been simulated in LandSim by variation in the hydraulic conductivity of the lateral pathway in the LML.

The original MT3D model incorporated simulation of the fate of ammoniacal nitrogen, chloride and cadmium in the UML. Model parameters are summarized as:

Initial Amm-N concentration in waste – 600 mg/l

Initial Chloride concentration in waste – 1,075 mg/l

Initial Cadmium concentration – 0.0012 mg/l

Longitudinal dispersivity – 10

Horizontal transverse dispersivity – 1

Vertical transverse dispersivity – 0.1

Amm-N retardation coef. – 0.002 m^3/kg

Cadmium retardation coef. – 0.75 m^3/kg

Amm-N biodegradation half-life – 5 years

Chloride and Cadmium no biodegradation

Results are reported as contaminant concentration against time at down-gradient monitoring boreholes.
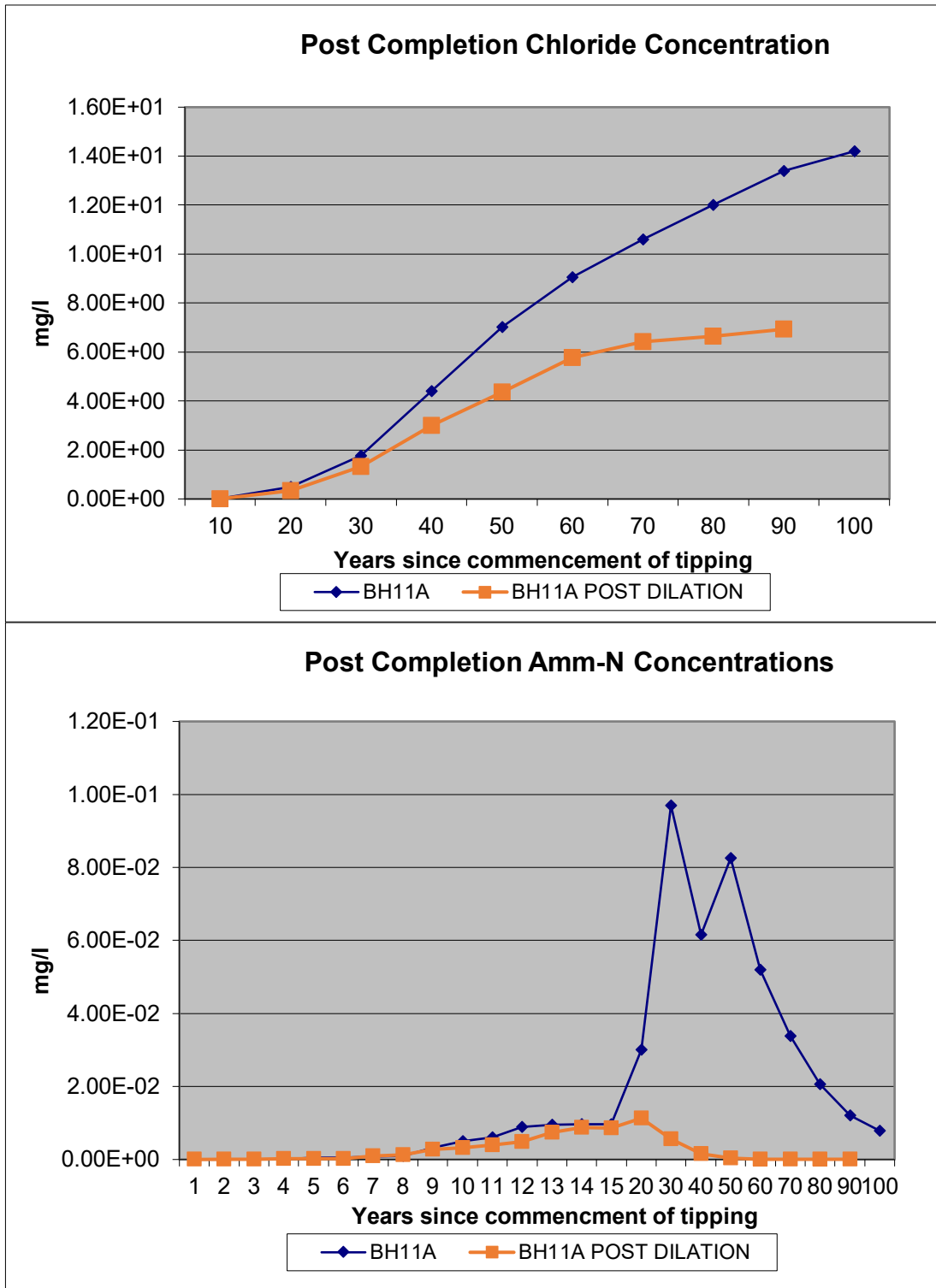
Figure 6.9: Modelled concentration of chloride and ammoniacal nitrogen at monitoring BH11A down-gradient of Copley Lane Quarry Landfill with (brown line) and without (blue line) the inclusion of discontinuity dilation.

Discontinuity dilation analysis has been based on the dilation/distance relationship for a variably jointed formation within an HS-EdZ extent of

approximately 150 m from the excavation face. The results of this approach are presented in Section 6.3 for the groundwater flow model. A comparison of contaminant concentrations at the downstream receptor with and without discontinuity dilation is presented as Figure 6.9.

The MT3D model results suggest that the increase in limestone hydraulic conductivity in response to lithostatic unloading could have a significant effect on the fate of contaminants in groundwater. Figure 6.9 shows that, under increased hydraulic conductivity conditions, the peak concentration of both modelled substances is significantly reduced at the down-gradient monitoring borehole. In the case of chloride, which is treated as a conservative substance with no retardation or biodegradation, reduced down-gradient concentration occurs as a consequence of increased dilution in the aquifer. Although ammoniacal-nitrogen is modelled with both retardation and biodegradation, increased dilution has a greater effect on down-gradient concentration than reduction in time-related attenuation processes, resulting in a lower peak concentration.

Analysis of the fate of potential contaminants in the LML via pathway 2 through the MPM was simulated through development of a LandSim model. The model has been amended to increase the LML horizontal hydraulic conductivity in accordance with the changes developed for the MODFLOW groundwater flow model due to discontinuity dilation. On this basis the LML hydraulic conductivity has been increased from a range of 1×10^{-6} m/s – 4×10^{-5} m/s to a range of 1.9×10^{-4} m/s – 7.6×10^{-4} m/s. A comparison of the results with and without discontinuity dilation is shown in Figures 6.10 and 6.11.
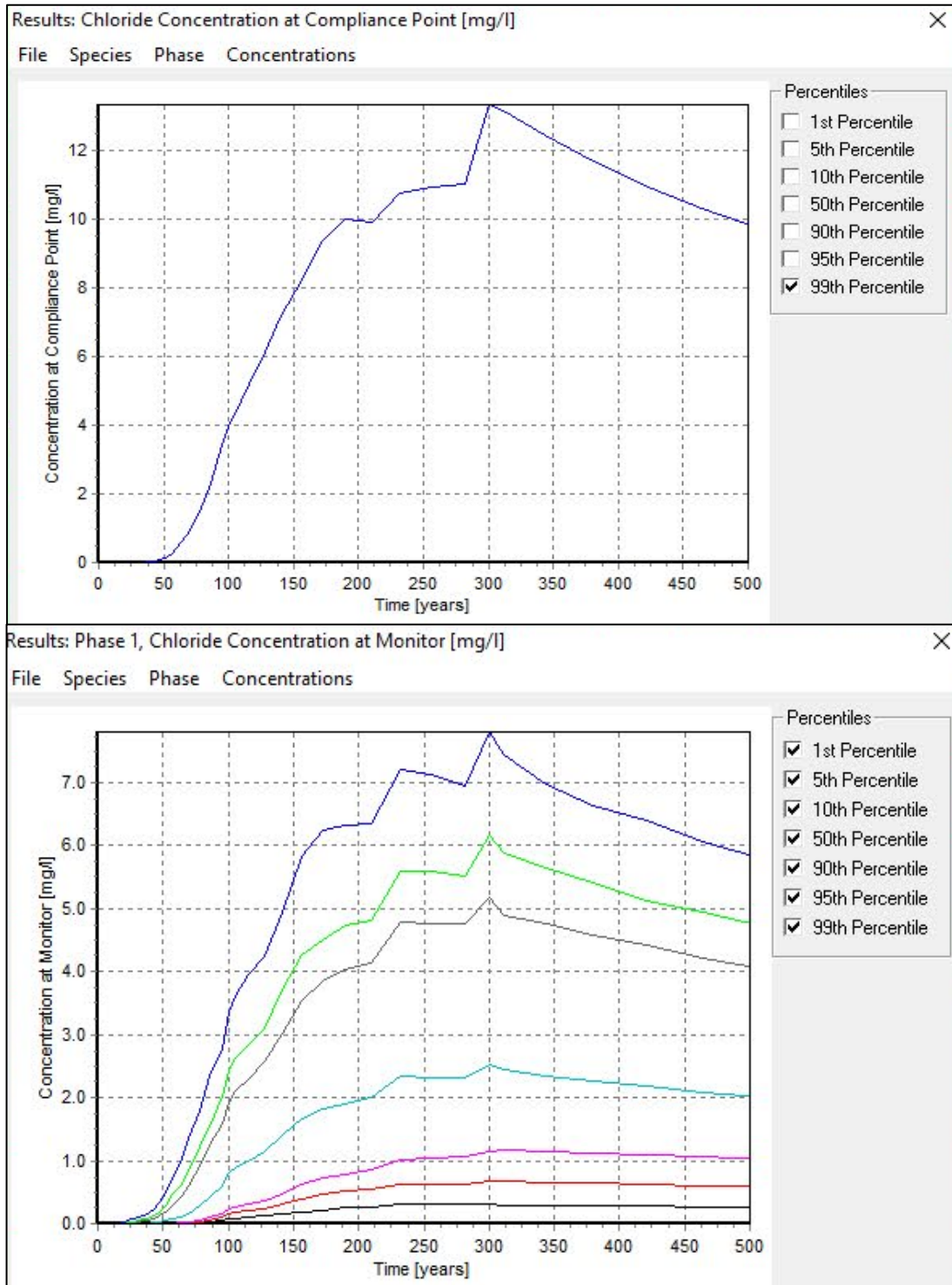
Figure 6.10: Predicted chloride concentration at down-gradient monitoring location. Upper diagram shows chloride concentration at 99th percentile with original model LML hydraulic conductivity. Lower diagram shows predicted chloride concentrations with LML hydraulic conductivity increased in response to excavation induced discontinuity dilation.
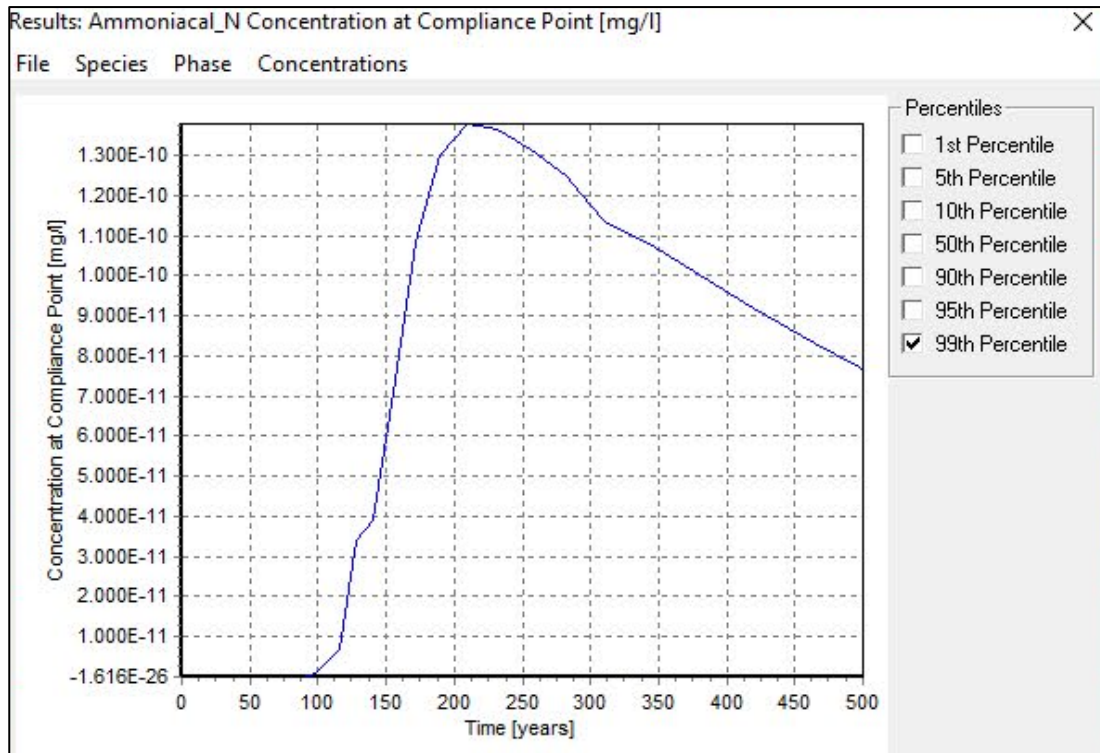
Figure 6.11: Predicted ammoniacal-nitrogen concentration at down-gradient monitoring location. Diagram shows concentration from original model without adjustment for lithostatic unloading. When LML hydraulic conductivity is increased in response to excavation induced discontinuity dilation there is no discernible concentration of ammoniacal-nitrogen at the monitoring location.

The results in Figures 6.10 and 6.11 demonstrate that increasing the hydraulic conductivity of the LML beneath Copley Lane Quarry Landfill results in a reduction in the concentration of both modelled substances when compared to the original model predictions.

6.4.2 Tong Quarry Landfill case study

Tong Quarry is located near Rochdale in Lancashire, UK. The quarry is established in the Lower Coal Measures strata and has been worked for the extraction of sandstone, coal and brick clay. Quarry restoration is being achieved through importation of inert waste. As part of a Hydrogeological Risk Assessment (HRA) a LandSim model of the site and surrounding area was developed in 2019. The site is underlain by coal measures mudstone beneath which is the Woodhead Hill Rock (WHR), a locally important aquifer. A

conceptual model showing potential contaminant migration routes from the site is shown in Figure 6.12.
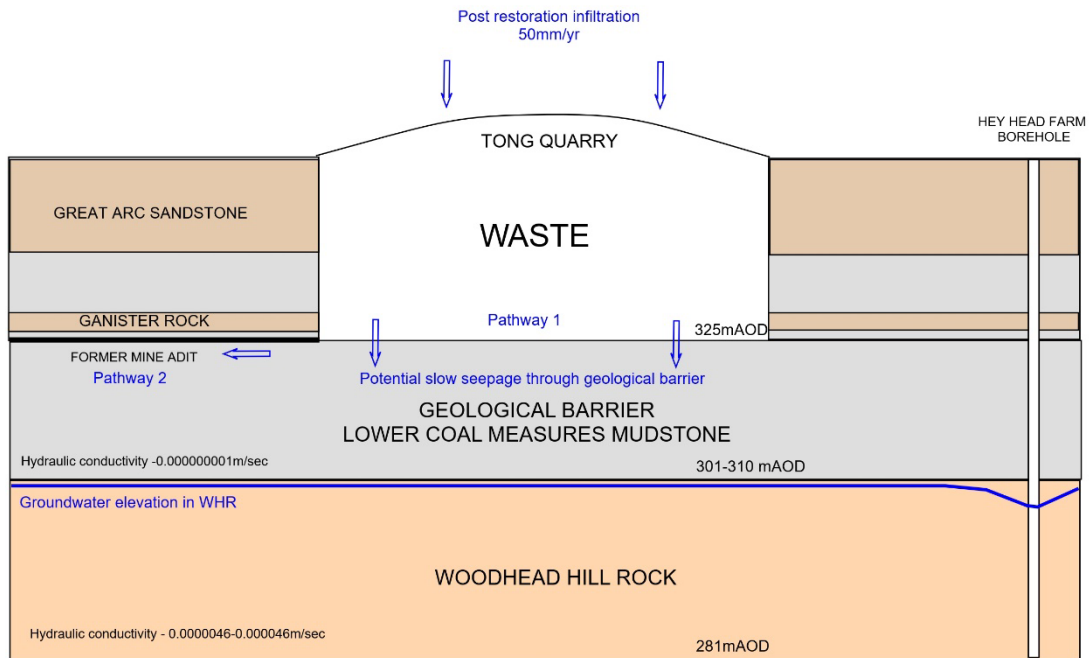
Figure 6.12: Schematic conceptual model of potential contaminant migration pathways from Tong Quarry Landfill.

Considering the effects of excavation induced unloading, the primary impact at the site would be dilation of bedding planes in the coal measures mudstone and the WHR. Although dilation of mudstone bedding planes could introduce new lateral flow paths through the mudstone, for the purpose of this analysis only changes to the WHR sandstone aquifer have been considered. The existing LandSim model, representing vertical drainage through the mudstone followed by lateral drainage through the sandstone, includes a sandstone horizontal hydraulic conductivity of 4.6×10^{-5} m/s to 4.6×10^{-6} m/s. The top of the WHR occurs within a depth of approximately 20m below the base of the quarry excavation.

Tong Quarry is approximately 200 m wide and 30 m deep. Results from the bedding-only geomechanical model (Model 2) therefore indicate a vertical EdZ extent of up to 235 m below the excavation floor, with the majority of the bedding plane dilation occurring within 40 m of the excavation floor. The base of the WHR is approximately 40 m below the quarry floor and therefore within the HS-EdZ. Potential bedding plane dilation magnitude has been determined

at 10 m intervals below the floor using the approach developed in Chapter 5 and applying the bedding-only model dilation/distance equation in the form,

Dilation = 0.037 x^{-1}, where x is vertical distance from the excavation floor.

Existing model hydraulic conductivity for a flow path area of 200 m x 20 m and bedding plane spacing of 1 m has been related to bedding plane aperture dimensions by application of the cubic law for a single set of discontinuities. The analysis indicates a bedding plane aperture of 2.5 mm would equate to the existing model hydraulic conductivity. Hydraulic conductivity values adjusted for excavation induced bedding plane dilation are summarised in Table 6.7.

Distance from excavation floor (m)	Bedding dilation from geotech model (m)	Mean bedding dilation (m)	Bedding aperture adjusted for dilation (m)	New horizontal K with base k=0.000046 (m/s)
10	0.003700			
		0.002775	0.005275	0.000461
20	0.001850			
		0.001542	0.004042	0.000207
30	0.001233			
		0.001079	0.003579	0.000144
40	0.000925			
		0.000833	0.003333	0.000116
50	0.000740			

Table 6.7: Table shows horizontal hydraulic conductivity estimates for the WHR following excavation induced bedding plane dilation in accordance with the dilation/distance relationship defined in Chapter 5 for a 30 m deep excavation

On the basis of the analysis in Table 6.7 the WHR hydraulic conductivity has been adjusted to the range 1.44×10^{-4} m/s – 2.07×10^{-4} m/s. No other changes were made to the LandSim model. The original Tong Quarry model included analysis of the fate of 12 substances that were identified as present in waste leachate at concentrations in excess of relevant environmental assessment levels (EAL's). Comparative analysis of the fate of two substances has been considered in this study. Chloride is included as a conservative substance

unlikely to be affected by subsurface attenuation processes. Naphthalene is included as an example of a substance for which both mudstone retardation and biodegradation processes have a role in down-gradient contaminant concentrations. Substance concentrations are evaluated at a down-gradient compliance point approximately 100m down-gradient of the site. Results are presented in Figures 6.13 and 6.14.
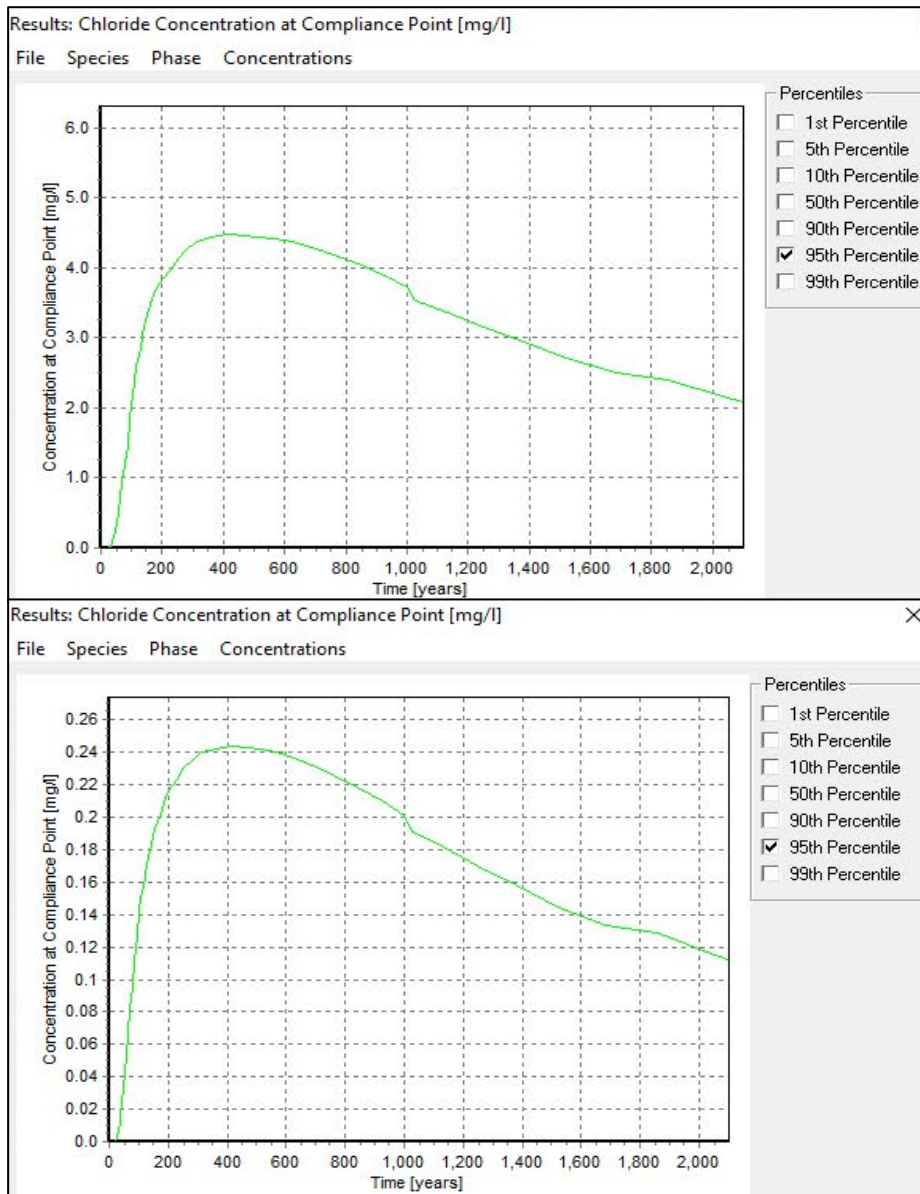
Figure 6.13: Predicted chloride concentration 100 m down-gradient of Tong Quarry Landfill. Upper diagram shows chloride concentration with no allowance for excavation induced bedding plane dilation in WHR. Lower diagram shows chloride concentration with dilation based increase in WHR hydraulic conductivity. Note difference in vertical scales.
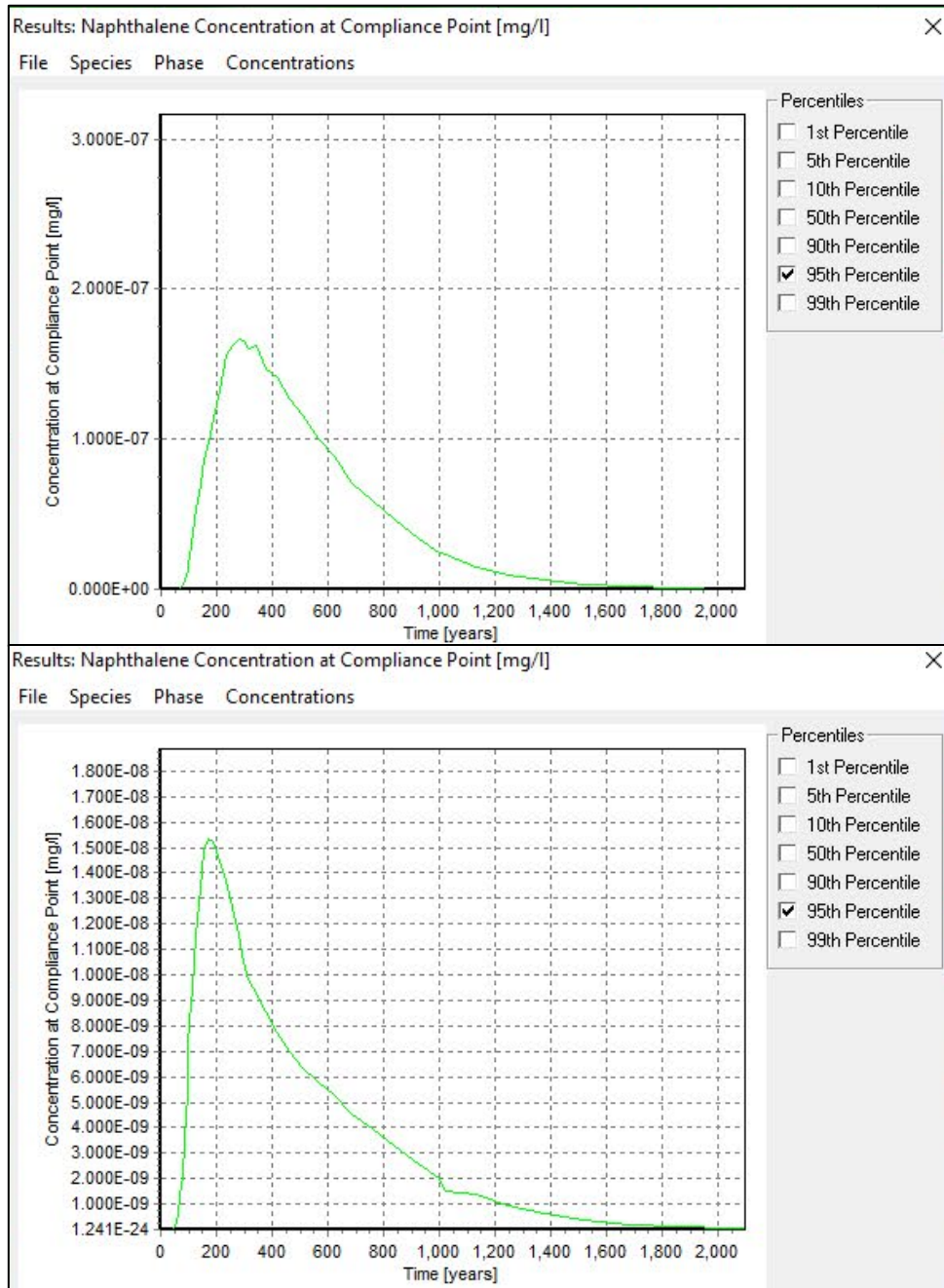
Figure 6.14: Predicted naphthalene concentration 100 m down-gradient of Tong Quarry Landfill. Upper diagram shows chloride concentration with no allowance for excavation induced bedding plane dilation in WHR. Lower diagram shows chloride concentration with dilation-based increase in WHR hydraulic conductivity. Note difference in vertical scales.

Figure 13 demonstrates that, whilst the time to peak chloride concentration is unaffected by increased horizontal hydraulic conductivity in the WHR, the predicted peak concentration is reduced from 4.3 mg/l to 0.24 mg/l. Although both concentrations are low when compared to an EAL of 250 mg/l, the

variation demonstrates significant reduction in the peak concentration of a conservative substance as a consequence of increased dilution in the aquifer. Figure 6.14 shows that, post bedding plane dilation, both the time to peak and the peak concentration of naphthalene are reduced. The time to peak is shortened from approximately 275 years post completion of waste disposal to approximately 175 years from completion of waste disposal. The predicted peak naphthalene concentration is reduced from 1.6×10^{-7} mg/l to 1.5×10^{-8} mg/l.

6.4.3 Farley Quarry case study

Farley Quarry is located near Wenlock in Shropshire and consists of a relatively shallow mineral excavation in Silurian limestone at the western side of Wenlock Edge. Hydrogeological risk assessment was undertaken at the site in 2019 to investigate the potential hydrogeological implications of filling the excavation void with inert waste materials. A LandSim model of the site and surrounding area was developed to support assessment of potential contaminant migration risk. A simple conceptual model of potential contaminant migration pathways at Farley Quarry is presented as Figure 6.15.
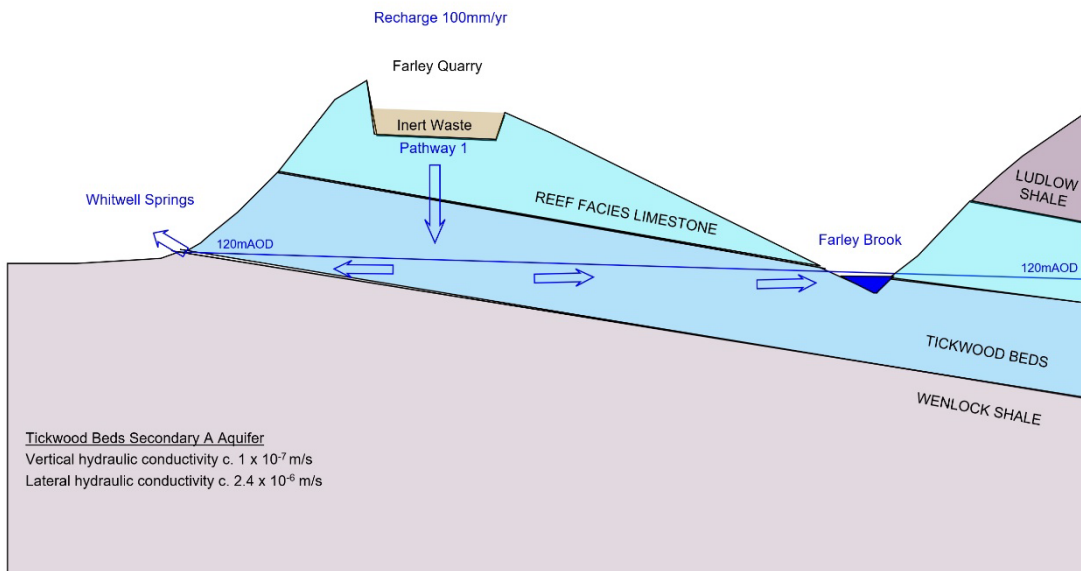
Figure 6.15: Schematic illustration of potential contaminant migration pathways from Farley Quarry showing vertical unsaturated flow through reef limestone followed by lateral flow through Tickhill Beds.

At Farley Quarry the Wenlock Limestone is thinly bedded and variably jointed. Excavation induced unloading has the potential to affect both the vertical unsaturated pathway through the reef facies limestone due to variably orientated joint dilation and the lateral pathway through the Tickhill Beds due to bedding plane dilation. The existing LandSim contaminant fate model for Farley Quarry assigns hydraulic conductivities as follows.

Vertical pathway through reef facies limestone – 9.87×10^{-7} m/s

Lateral pathway through Tickhill Beds – 2×10^{-6} m/s

The specified hydraulic conductivities have been related to discontinuity aperture dimensions using the approach set out in Chapter 5 for a vertical flow path area of 20 000 m^2 (area of the base of the excavation) and joint spacing of 1m and a lateral flow path cross sectional area of 2000 m^2 and bedding plane spacing of 1 m. It has been assumed that only one joint set is active in each limestone formation. The analysis results in an estimated joint aperture size of 0.68 mm and an estimated bedding aperture size of 0.86 mm. Variable jointing in the reef facies limestone at Farley Quarry is shown in Figure 6.16.

Figure 6.16: Variably orientated jointing and bedding in the reef facies limestone at Farley Quarry.

The potential effects of lithostatic unloading have been defined by application of dilation/distance equations for a variably jointed formation, as set out at Chapter 5, as follows,

Joint dilation = $0.010 \, x^{-1}$

Bedding dilation = $0.012 \, x^{-1}$, where x = distance from excavation floor

Adjusted hydraulic conductivity for the vertical unsaturated flow path is within the range 1×10^{-6} m/s – 7×10^{-6} m/s. For the lateral flow path the adjusted hydraulic conductivity values are within the range 2×10^{-6} m/s – 1.2×10^{-5} m/s. The original LandSim model was adjusted to incorporate these hydraulic conductivity ranges and re-run to investigate the impact on contaminant fate. The results are presented in Table 6.8.

Substance	Original model time to peak (yrs)	Time to peak with adjusted K (yrs)	Peak concentration (mg/l)	Peak concentration with adjusted K (mg/l)	EAL (mg/l)
Arsenic	20,000	20,000	0.006	0.0042	0.005
Chloride	25	15	52	35	250
Lead	20,000	20,000	0.00038	0.0001	0.0002
Sulphate	25	15	280	175	250

Table 6.8: Comparison of time to peak and peak concentration of substances at down-gradient receptor 300 m from Farley Quarry with and without inclusion of the effects of lithostatic unloading. EAL – Environmental Assessment Levels based on UK Drinking Water Standards for non-hazardous substances and minimum reporting values for hazardous substances.

Table 6.8 demonstrates that with higher hydraulic conductivity flow paths there is a reduction in the time to reach peak concentration at the down-gradient receptor and, on average, a 30-40% reduction in peak concentration (the 20 000 year time period is the model upper limit which may be shorter than the

actual time to peak). It is noted that for three of the modelled substances (arsenic, lead and sulphate) inclusion of the effects of excavation induced discontinuity dilation has the effect of bringing predicted substance concentrations below the relevant EAL which could be significant in relation to evaluation of environmental risk and regulatory acceptance.

6.5   Unsaturated zone drainage

Dilation of sub-vertical discontinuities within the vadose zone behind an excavation face has the potential to influence unsaturated drainage characteristics. Although any effects are likely to be highly site-specific, a basic review of critical processes has been undertaken to establish an understanding of the potential hydrogeological significance of lithostatic unloading effects in the vadose zone.

The infiltration capacity of a fractured hard rock formation depends on the rate at which water can percolate via connected fracture systems with outlet to the water table or the open excavation face. Where soil and overburden are present above the fractured bedrock, infiltration capacity may be regulated by the infiltration capacity of the overlying deposits. In such conditions, bedrock drainage capacity could influence soil or overburden drainage characteristics. In many open pit mineral locations in the UK superficial geological deposits are often absent and soil cover may be thin with limited capacity to regulate infiltration to underlying bedrock.

Detailed investigation into the effects of lithostatic unloading on vadose zone drainage is beyond the scope of this study. However, it is useful to recognize the potential hydrological implications of an increase in bedrock infiltration capacity that could occur in response to sub-vertical discontinuity dilation behind an open pit face. Geomechanical modelling studies, as detailed in Chapters 4 and 5, have demonstrated that joints present behind an excavation face may dilate in response to excavation induced unloading for distances of around 100 m from the face. Dilation magnitudes range up to several millimetres, resulting in the potential for 'order of magnitude' increases in vertical hydraulic conductivity.

Unsaturated zone drainage can be described by Darcy's Law in the form,

$$q = -K(\theta) \, dh/dx, \qquad\qquad\qquad\qquad [6.4]$$

where q = volumetric flux, $K(\theta)$ = unsaturated hydraulic conductivity, dh/dx = hydraulic gradient.

If it is assumed that the hydraulic gradient and the unsaturated water content remain unchanged, the unsaturated hydraulic conductivity can be considered proportional to the saturated hydraulic conductivity. Joint dilation analyses referenced earlier in this chapter have demonstrated joint system hydraulic conductivity change from 10^{-5} m/s to 10^{-4} m/s. With unlimited water supply, the corresponding unsaturated zone vertical drainage rate could increase by a factor of 10.

Changes to the rate of drainage through the unsaturated zone may have implications for the following,

o   Drainage of overlying soils and superficial deposits;
o   Timing of groundwater recharge; and
o   Recharge water quality.

Enhanced bedrock infiltration capacity can result in enhanced underdrainage of overlying materials. In locations where soil water content is important i.e. where required to support vegetation or other water dependent features, increased soil drainage may have an adverse impact. As summarised at Chapter 2, there are examples of such effects leading to deterioration in vegetation growth around hard rock mineral workings.

As discussed at Chapter 2, the role of the unsaturated zone in the temporary storage of recharge water and slow release to the phreatic zone has long been recognised. Enhanced vadose zone hydraulic conductivity may result in more rapid drainage to the phreatic zone with a tendency to increase groundwater recharge during wetter months and decrease recharge during drier summer

months. This effect has been identified as a consequence of limestone quarrying in the Mendip Hills where seasonal spring flows have been affected.

As discussed at Chapter 2, the unsaturated zone provides a water quality control function as infiltrating rainwater is subject to filtration and retardation processes. More rapid transmission through the unsaturated zone may reduce water quality improvement potential. Such effects may be particularly important where recharge water is subject to contamination i.e. by agricultural practices or urban development.

Although unquantified in this study, potential changes to unsaturated zone drainage characteristics are defined as a potentially significant consequence of excavation induced discontinuity dilation. However, geomechanical modelling studies, detailed at Chapters 4 and 5, indicate that such effects are likely to be relatively localised and restricted to a distance of approximately 100 m from an excavation boundary for excavations with a depth of up to 100 m.

6.6   Discussion – hydrological significance

The objective of Chapter 6 is to investigate the potential hydrogeological significance of excavation induced geomechanical change to fractured bedrock formations. The approach and methodologies developed in Chapter 5, for determination of EdZ/HS-EdZ extents and dilation/distance relationships for several generic discontinuity configurations, have been applied to several case studies to investigate potential impacts on groundwater flow and groundwater quality. Although only a small number of case studies have been tested, there is a basis to draw generic conclusions regarding hydrogeological significance.

Evaluation of hydrogeological significance will always be highly site-specific and dependent on both the operational circumstances of individual open pit mineral workings and the sensitivity of local hydrological receptors. Formal quantification of hydrogeological significance does not form part of this study but it is instructive to reference the usual approach to defining impact significance when applied to environmental impact assessment. The approach

is based on definition of low, medium or high effect significance on the basis of potential effect magnitude and receptor sensitivity as indicated in Table 6.9.

Sensitivity	Examples of receptor response
High	The receptor/resource has little ability to absorb change without fundamentally altering its present character, or is of international or national importance
Moderate	The receptor/resource has moderate capacity to absorb change without significantly altering its present character, or is of high importance
Low	The receptor/resource is tolerant of change without detriment to its character, is of low or local importance
Magnitude of impact	**Criteria for assessing impact**
Major	Total loss or major/substantial alteration to key elements/features of the baseline (pre-development) conditions such that the post development character/composition/attributes will be fundamentally changed
Moderate	Loss or alteration to one or more key elements/features of the baseline conditions such that post development character/composition/attributes of the baseline will be materially changed
Minor	A minor shift away from baseline conditions. Change arising from the loss/alteration will be discernible/detectable but not material. The underlying character/composition/attributes of the baseline condition will be similar to the pre-development circumstances/situation
Negligible	Very little change from baseline conditions. Change barely distinguishable, approximating to a 'no change' situation

EFFECT SIGNIFICANCE			
Sensitivity			
Magnitude	**High**	**Moderate**	**Low**
Major	High	High-Medium	Medium-Low
Moderate	High-Medium	Medium-Low	Low
Minor	Medium-Low	Low	Low-Very Low
Negligible	Very Low	Very Low	Very Low

Table 6.9: Indicative approach to evaluation of environmental significance by relating potential effect magnitude to receptor sensitivity.

Table 6.9 indicates a widely applied approach to evaluation of the significance of external environmental impacts. Effects rated medium or high would normally be considered significant enough to require mitigation.

In addition to external impacts, hydrogeological effects associated with lithostatic unloading, as defined in this study, also have the potential to impact open pit design and operation. Changes to the hydraulic conductivity of fracture flow networks around open pit workings may result in lowered groundwater levels and increased groundwater inflow. Contaminant migration risk variation due to the effects of lithostatic unloading may influence regulatory acceptability of post-extraction restoration options.

The two case studies aimed at investigating the effect of excavation induced discontinuity dilation on groundwater levels and flow both demonstrated that, on the basis of dilation/distance relationships developed in this study, the consequent increase in fracture network bulk hydraulic conductivity would have relatively minor effect on local groundwater levels and hydraulic gradients around excavation areas. Analyses demonstrated a reduction in groundwater elevation of between 0.5 m and 1.0 m within a distance of up to 100m from the excavation boundary. At greater distance the additional drawdown was less than 0.5 m. Such changes are unlikely to be significant with regard to effects on external receptors unless small change in groundwater elevation is critical.

Groundwater flow model results for the two case studies indicate that changes to groundwater inflow rates to open pit excavations as a consequence of excavation induced discontinuity dilation are likely to be relatively low. In the two case study examples, the increased in hydraulic conductivity resulted in a 20% increase in groundwater inflow when compared to the model results without allowance for discontinuity dilation. For lower hydraulic conductivity formations, analytical results indicated a potential 20% increase in groundwater inflow rate, but the increase applied to low rates of inflow. From an operational perspective, relatively low increase in the rate of groundwater inflow to open pit excavations would normally be accommodated through increased storage and pumping capacity without significant impact on site operations.

Three case study examples have been used to investigate the potential impact of excavation induced discontinuity dilation on the fate of contaminants that may be present within mineral workings. The analyses included in this study are indicative only as all processes in the contaminant migration pathway are not fully considered. However, case study results suggest that changes to discontinuity networks following lithostatic unloading may have a more significant effect on contaminant migration risk than on groundwater flow rates.

Case study models, based on adjustment of flow path hydraulic conductivity values, have primarily demonstrated the effect of changes to physical parameters, such as contaminant dilution and travel time, but have not accounted for change in other biochemical attenuation processes such as ion exchange or biodegradation. However, for the case studies considered, increased hydraulic conductivity along the migration pathway resulted in a reduction in contaminant concentration at down-gradient receptors and, in some cases, a reduction in the time to achieve peak concentration. In some examples the predicted contaminant concentration reduction was potentially significant when referenced to relevant environmental quality standards.

Review of potential excavation induced change to unsaturated zone drainage characteristics identified potential impacts on soil zone drainage, groundwater recharge rate attenuation and recharge water quality. Where soil saturation levels are ecologically critical, increased soil drainage due to enhanced infiltration capacity in the underlying bedrock could have a significant external impact. However, where soil or overburden infiltration capacity is lower than the underlying bedrock, soil drainage rates may not be significantly influenced by enhanced bedrock infiltration capacity.

Geomechanical modelling has demonstrated that the HS-EdZ is relatively localised, extending approximately 100m from excavations up to 100 m deep. Unsaturated zone storage and recharge changes within 100 m of mineral workings are unlikely to have a significant effect on water resources at a more regional scale unless directly linked to sensitive receptors e.g. local springs. However, the potential development of higher hydraulic conductivity flow paths through the unsaturated zone could increase risk of contaminant migration from surface or near-surface sources to groundwater. In areas where surface

contamination is present e.g. high nitrate concentration associated with use of fertilizers in agricultural areas or ground contamination due to past industrial activity, the increased risk of contaminant migration to groundwater resources could be considered significant.

In summary, the assessment of the hydrogeological significance of the effects of lithostatic unloading at open pit excavations has concluded that;

1. Impacts on groundwater flow rates, groundwater elevations and hydraulic gradients around open pit mineral workings are unlikely to have significant effect on open pit design, operation or external impact;

2. Changes in hydraulic conductivity of fracture flow systems in response to excavation induced discontinuity dilation around open pit mineral workings could have a significant impact on the fate of contaminants, with implications for both environmental risk and regulatory compliance; and

3. Changes to the drainage characteristics of the unsaturated zone around open pit mineral workings as a consequence of excavation induced discontinuity dilation could have a significant effect on soil drainage rates and dependent ecosystems at locations where unsaturated zone infiltration capacity is a critical control on soil water retention rates.

This study has considered mineral workings to a maximum depth of 100 mbgl and typical basal floor width of 200 m, although all the case study examples presented in this chapter are much shallower at approximately 30 m deep. It is recognized that for larger or deeper excavations the extent or magnitude of potential hydrological effects identified in this study are likely to be proportionately larger. Excavations that extend much further below the rest groundwater elevation than observed at the two case study examples are likely to have greater impact on groundwater levels and flow as a consequence of the effects of lithostatic unloading. Whether such effects become hydrologically significant is therefore also related to development scale.

CHAPTER 7: CONCLUSIONS AND RECOMMENDATIONS

7.1 Introduction

The primary aim of this research study has been to investigate the hydrogeological significance of the effects of lithostatic unloading at open pit mineral workings. Following the acquisition of field data from UK mineral sites, hydrogeological significance has been evaluated by analysis of the results of a programme of geomechanical and hydrogeological modelling and cross-reference to several case study examples of open pit mineral site development. This chapter provides a summary of the main conclusions of the study and identifies areas in which further research may enhance understanding of critical processes.

7.2 Conclusions

Review and discussion of the results of the geomechanical modelling programme is included at Chapter 5 and discussion regarding hydrogeological significance is included at Chapter 6. Considering the outcomes of both geomechanical and hydrogeological investigation, the principal conclusions from this study are presented below.

7.2.1 Excavation Disturbed Zone (EdZ)

Geomechanical modelling has demonstrated that an excavation disturbed zone (EdZ), defined as the zone in which post-excavation vertical and lateral stress magnitude is less than 95% of the pre-excavation magnitude, develops vertically and laterally beneath an excavation floor and behind an excavation face, respectively. As reported by previous researchers, modelling results reconfirm that tensile stress and extensional strain zones are developed in the excavation floor and face, dependent on in-situ stress conditions. In the models developed during this study, tensile stress and extensional strain magnitudes where not large enough to promote new fracturing of intact rock.

Three-dimensional modelling results show that, in non-circular excavations, the extent of the EdZ, both laterally and vertically, is not a consistent distance around the full perimeter of the excavation. The constraining effect of perpendicular excavation faces at the end of each face acts to reduce EdZ development at excavation corners. EdZ extents are greatest at the centre of each open face.

In general, the introduction of sub-vertical discontinuities to the rock mass resulted in a reduction in the vertical and lateral extents of the EdZ, with the greatest reduction occurring in models with the highest discontinuity intensity. Reduction in EdZ extent with increasing joint intensity is attributed to distribution of elastic strain over a shorter distance as the stress response is attenuated by discontinuities with lower stiffness than the rock mass.

Modelling results demonstrate that, for a 100 m deep and 200 m wide excavation, the EdZ extends for a distance of between 128 m to 490 m below the excavation floor and between 417 m to 850 m behind the excavation face, depending on discontinuity configuration and in-situ stress state. Model results demonstrate that at the higher lateral confining stress ratio (k=2.0), the vertical EdZ extent is reduced and the lateral EdZ is increased, when compared to results for the lower lateral confining stress ratio (k=0.27).

Modelled EdZ extents below the excavation floor compare well with rates of stress reduction calculated by application of the Boussinesq approach to 2D analysis of ground stress below a loaded/unloaded strip.

Vertical and lateral EdZ extents can be normalised with respect to functions of excavation width and depth, or only depth, respectively. This approach allows estimation of maximum EdZ extents for all four modelled discontinuity configurations based on excavation dimensions. In practice, the formulae can be applied to open pit excavations of any depth and width produce estimates of potential EdZ extents.

7.2.2 Stress Response, Rock Mass Displacement and Discontinuity Dilation.

Geomechanical modelling results have demonstrated that, for all models, displacement of the rock mass below the excavation floor and behind the excavation face occurs in response to reduction in stress as a consequence of lithostatic unloading. Three displacment mechanisms have been recognised in model outputs, as follows:

(i) Rock mass strain;
(ii) Discontinuity dilation; and
(iii) Rock block sliding on discontinuity surfaces.

The magnitude of discontinuity dilation is dominantly influenced by discontinuity normal stiffness, discontinuity orientation with respect to the direction of stress reduction and connectivity with other discontinuties. Rock block sliding on discontinuity surfaces primarilly occurs where discontinuities i.e. bedding planes and/or sub-vertical joints, daylight in the excavation face or floor.

Analysis of results for all models indicates that significant rock mass displacment does not extend to the full boundary of the EdZ. Similarly, discontinuity dilation does not occur over the full distance of rock mass displacement. These conclusions suggest that the EdZ can be sub-divided, resulting in a hierarchical relationship between discontinuity dilation, rock mass displacement and stress response. This arrangement is illustrated in Figure 7.1 (based on Figure 5.16). When considering hydrogeological systems in fractured rocks, it is the potential for groundwater flow through the discontinuity network that is of greatest interest. The zone in which discontinuity dilation occurs could therefore be defined as the zone that has greatest hydrogeological significance. In this study the discontinuity dilation zone has been defined as the Hydrologically Significant Excavation disturbed Zone (HS-EdZ).
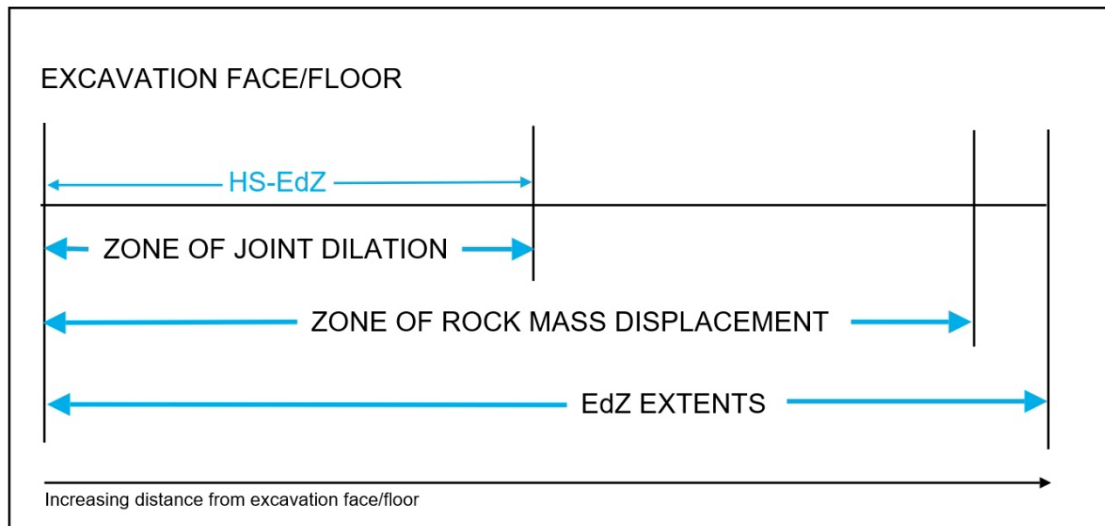
Figure 7.1: Schematic illustration to show the definition of the Hydrologically Significant Excavation disturbed Zone (HS-EdZ).

Results for all four models, under two alternative in-situ stress conditions, indicate that cumulative discontinuity dilation contributes between approximately 20% to 60% of total rock mass displacement with a tendency for lower contribution to be associated with higher discontinuity intensity. Total displacement magnitude is also lower for models with higher discontinuity intensity as discontinuity dilation, rock mass displacement and stress reduction occurs over a shorter distance from the excavation face and floor.

Variation in discontinuity dilation with increasing distance from the excavation face and floor can be defined by a power law relationship. Dilation -v- distance relationships have been defined for all models in the form,

Dilation (D) = cx^{-1}, where D=normal dilation (m), c=coeffient (m^2) related to excavation depth and disocntinuity configuration, and x=distance (m) from the excavation face or floor.

A table of coeffcents for each of the three models with discontinuties, for all excavation depths and in-situ stress conditions, is presented as Table 5.6. in Chapter 5.

7.2.3 Hydrogeological Significance

Evaluation of the potential hydrological significance of discontinuity dilation within the HS-EdZ has been undertaken by adjustment of hydraulic conductivity parameters in several pre-existing groundwater flow and contaminant transport models. Discontinuity dilation -v- distance relationships within the HS-EdZ have been translated to equivalent porous media (EPM) hydraulic conductivity values through application of the cubic law based on estimated discontinuity aperture dimensions for each of the case study sites. Models have been re-run to investigate the effect of variation in hydraulic conductivity, as a consequence of lithostatic unloading, on groundwater flow rates, groundwater levels and contaminant transport processes.

Case study analysis indicated that the impact of increased hydraulic conductivity, due to the effects of lithostatic unloading, on groundwater flow rates, groundwater heads and hydraulic gradients around open pit mineral workings are unlikely to have significant effect on open pit design, operation or external impact for the range of lithological types and open pit dimensions investigated. However, the case studies used in this study all represent relatively shallow excavation in relatively high permeability strata. For deeper excavations, the change in hydraulic conductivity due to lithostatic unloading would be higher with potentially greater effect on groundwater levels and flow. The low hydraulic conductivity example included in Chapter 6 demonstrates that in low permeability strata the change in groundwater flow rate due to lithostatic unloading around an excavation could be significant.

Hydrogeological modelling results indicate that changes in hydraulic conductivity of fracture flow systems, in response to excavation induced discontinuity dilation around open pit mineral workings, could have a significant impact on the fate of contaminants, with implications for both environmental risk and regulatory compliance. Model results indicate that the effect of increased dilution and dispersion in an enhanced hydraulic conductivity fracture flow system would have greater effect on contaminant concentration than reduction in chemical or biological attenuation processes, resulting in reduced contaminant concentration at down-gradient receptors. Case study models suggest that change in contaminant concentration could be several orders of magnitude.

Analysis of variation in vertical hydraulic conductivity values suggests that changes to the drainage characteristics of the unsaturated zone around open pit mineral workings, as a consequence of excavation induced discontinuity dilation, could have a significant effect on soil drainage rates and dependent ecosystems at locations where unsaturated zone infiltration capacity is a critical control on soil water retention rates.

This study has considered mineral workings to a maximum depth of 100 mbgl and typical basal floor width of 200 m. It is recognized that for larger or deeper excavations the extent or magnitude of potential hydrogeological effects identified in this study are likely to be proportionately larger. Excavations that extend much further below the rest groundwater elevation than observed at the case study examples are likely to have greater impact on groundwater levels and flow as a consequence of the effects of lithostatic unloading. Whether such effects become hydrogeologically significant is therefore also related to development scale.

7.3 Recommendations

This study has been aimed at assessment of the effects of lithostatic unloading at the level of determining hydrogeological significance. Key geomechanical and hydrogeological processes have been incorporated into the modelling programme. However, as summarised in Chapter 3, the scope of this research does not extend to investigation of all processes that could influence the geomechanical and hydrogeological response to lithostatic unloading. There is scope to undertake further research to improve understanding of the sensitivity of the results of this study to other geomechanical and hydrogeological variables.

7.3.1 Further Research

Further research in the following areas would complement work undertaken in this study and improve understanding of uncertainties and sensitivities in the application of research results to mineral development projects.

7.3.1.1 Representation of Shear Dilation

Geomechanical modelling undertaken as part of this study has incorporated simulation of discontinuity normal dilation but the potential for dilation during shearing has not been represented. There is currently no capability within Elfen to simulate shear dilation. Shear dilation of discontinuities under loading or unloading conditions could have a significant impact on discontinuity dilation magnitude, particularly for discontinuities orientated at low angle to the principal direction of stress reduction. Where discontinuities are orientated at high angle to the principal direction of stress reduction, normal dilation may reduce the potential for significant dilation due to shear. Development of procedures for representation of both normal and shear dilation in DFN models would advance the validity of model outputs and improve prediction of discontinuity dilation magnitude and extents.

7.3.1.2 Groundwater Drainage and Effective Stress

Pore pressure has not been included in the geomechanical models developed through this research study. This is justified on the basis that the effects of lithostatic unloading are considered to far outweigh the effects of any change in pore pressure due to fracture network hydraulic conductivity change. However, for excavations that extend a significant distance below the rest groundwater elevation, increased discontinuity network drainage due to enhanced hydraulic conductivity may influence groundwater diffusion rates between the rock matrix and the discontinuity network where matrix porosity is significant. Further research into rock mass/fracture network drainage rates, based on the dilation -v- distance relationships developed through this study, would improve understanding of the potential beneficial effect of enhanced groundwater drainage on rock mass pore pressures with implications for excavation design.

7.3.1.3 DFN Storage and Transient Groundwater Response

Assessment of hydrogeological significance in this research study has been based on steady-state hydrogeological modelling that incorporates hydraulic

conductivity change but does not include any allowance for change in DFN storage capacity; no change in storage is usually a key assumption in steady-state modelling. However, under transient conditions, DFN storage variation due to fracture network dilation, may influence the timing and magnitude of groundwater drainage, particularly in the vadose zone. Transient groundwater flow and contaminant transport modelling, using DFN dilation outputs from this study, would provide a wider basis for consideration of hydrogeological significance.

7.3.2 Application of Research Results

This research study has resulted in the development of a new EdZ extent estimation methodology and formula for the estimation of discontinuity dilation -v- distance relationships around open pit mineral workings. These procedures are directly applicable to real world mineral design and development projects. In addition to publication of study results in relevant academic journals, it is proposed that study outputs are communicated to the minerals industry through the development of guidance to support consideration of the potential effects of lithostatic unloading in environmental impact assessment for new mineral development projects.

Bibliography

ALEJANO, L. A., E 2005. Considerations of the dilatancy angle in rocks and rock masses. *International Journal of Rock Mechanics and Mining Sciences,* 42**,** 481-507.

ALLEN, D., BREWERTON, L., COLEBY, L., GIBBS, B., LEWIS, M., MACDONALD, A., WAGSTAFF, S. & WILLIAMS, A. 1997. *The physical properties of major aquifers in England and Wales*.

ALTINORS, A. O., H 2008. A double-porosity model for a fractured aquifer with non-darcian flow in fractures. *Hydrological Sciences Journal,* 53**,** 868-882.

AOYAGI, K., TSUSAKA, K., KONDO, K. & INAGAKI, D. 2014. Quantitative assessment of an excavation damaged zone from variations in seismic velocity and fracture distribution around a gallery in the Horonobe Underground Research Laboratory. *In:* ALEJANO, P., OLALLA & JIMENEZ (ed.) *Rock Engineering and Rock Mechanics: Structures in and on rock masses.* London: Taylor & Francis Group.

AUTIO, J. H., T; SIITARI-KAUPPI, M 2003. Porosity, Diffusivity and Permeability of EDZ in Crystalline Rock and Effect on the Migration in a KBS-3 Type Repository. *In:* DAVIES, C. B., F (ed.). European Commission.

BAI, M. & ELSWORTH, D. 1994. Modelling of subsidence and stress-dependent hydraulic conductivity for intact and fractured porous media. *Rock Mechanics and Rock Engineering,* 27**,** 209-234.

BANDIS, S. C., LUMSDEN, A. C. & BARTON, N. R. 1983. Fundamentals of rock joint deformation. *International Journal of Rock Mechanics, Mining Science and Geomechanics,* 20**,** 249-268.

BARTON, N. & SHEN, B. 2017. Extension failure mechanisms explain failure initiation in deep tunnels and critical heights of cliff faces and near vertical mountain walls. *ARMA 51st US Rock Mechanics Symposium.* San Francisco: ARMA.

BEALE, G. & READ, J. 2014. *Guidelines for evaluating water in pit slope stability*. CRC

BEAR, J. T., C F; DE MARSILY, G 1993. *Flow and Contaminant Transport in Fractured Rock*, Elsevier.

BELL, F. G. 1978. PHYSICAL AND MECHANICAL-PROPERTIES OF FELL SANDSTONES, NORTHUMBERLAND, ENGLAND. *Engineering Geology,* 12**,** 1-29.

BISDOM, K. B., G; NICK, H. M. 2016. The impact of in-situ stress and outcrop-based fracture geometry on hydraulic aperture and upscaled permeability in fractured reservoirs. *Techtonophysics,* 690**,** 63-75.

BISDOM, K. N., H. M; BERTOTTI, G. 2017. An integrated workflow for stress and flow modelling using outcrop-derived discrete fracture networks. *Computers & Geosciences,* 103**,** 21-35.

BLACK, J. & BARKER, J. 2018. Analternative approach to understanding groundwater flow in sparse channel networks supported by evidence from 'background' fractured crystalline rocks. *Hydrogeology Journal,* 26**,** 27072723.

BLACK, J. W., ND, BARKER, JA 2017. Groundwater flow into underground openings in fractured crystalline rocks: an interpretation based on long channels. *Hydrogeology Journal,* 25**,** 445-463.

BROWN, E. T. H., E. 1978. Trends in Relationships between Measured *In-Situ* Stresses and Depth. *International Journal of Rock Mechanics and Mining Sciences & Geomechanics Abstracts,* 15**,** 211-215.

BUCKLEY, R. 1991. Auditing the precision and accuracy of environmental impact predictions in Australia. *Environmental Monitoring and Assessment,* 18**,** 1-23.

CRAIG, F. E. 1987. *Soil Mechanics,* London, Chapman Hall.

CRAWFORD, B. R., HOMBURG, J. M., FERNANDEZ-IBANEZ, F., MYERS, R. & GAO, B. 2018. Predicting pore volume and transmissivity multipliers for simulating geomechanical effects in naturally fractured reservoirs. *DFNE18.* Seattle, USA: ARMA.

DIGGES LA TOUCHE, G. & COTTRELL, M. The application of discrete fracture network models to mine groundwater studies. *In:* WOLKERSDORFER, C. S., L; SILLANPAA, M; HAKKINEN, A, ed. Mine Water and Circular Economy, 2017 Lappeenranta, Finland. IMWA, 548-555.

DUDGEON, C. Effects of non-Darcy flow and partial penetration on water levels near open-pit excavations. Congress of the International Association of Hydrogeologists, 18, 1985a. IAH, 122-32.

DUDGEON, C. R. 1985b. *Non-Darcy flow of groundwater, 2. Inflows and water levels for de-watered circular pits in unconfined aquifers*.

ELMO, D. R., S; STEAD, D; EBERHARDT, E 2014. Discrete fracture network approach to characterise rock mass fragmentation and implications for geomechancial upscaling. *Mining Technology,* 123**,** 149-161.

ENVIRONMENT AGENCY 2005. LandSim: Landfill Performance Simulation by Monte Carlo Method.

FOSTER, S. M. 1998. *Mining and Environmental Management,* London, Financial Times Business Limited.

FOSTER, S M ASSOCIATES LIMITED 2007. Appleton Quarry, Shepley, West Yorkshire: Proposed Extension - Hydrogeological Risk Assessment.

GOODMAN, R. E. 1989. *Introduction to Rock Mechanics*, Wiley.

GROSS, M. R. & ENGELDER, T. 1991. A case for neotectonic joints along the Niagara Escarpment. *Tectonics,* 10**,** 631-641.

HAAGENSON, R. R., H; KARRA, S; ALLEN, J 2018. Modelling non-linear diffusion in fractured rock with deformable fractures and applications to injection induced seismicity. *ARMA DFNE18.* Seattle: ARMA.

HAWKINS, A. M., BJ 1991. Influence of Geology on Geomechanical Properties of Sandstones. *International Society of Rock Mechanics 1991.* ISRM.

HEDAYAT, A. W., J 2019. The Elasto-Plastic Response of Deep Tunnels with Damaged Zone and Gravity Effects. *Rock Mechanics and Rock Engineering,* 52**,** 5123-5135.

HENCHER, S. 2015. *Practical Rock Mechanics*, CRC Press.

HILLIS, R. R. 1998. The influence of fracture stiffness and the *in situ* stress field on the closure of natural fractures. *Petroleum Geoscience,* 4**,** 57-65.

HOBDAY, C. W. M. H. 2012. Field measurements of normal and shear fracture compliance. *Geophysical Prospecting,* 60**,** 488-499.

HOMBURG, J. M., CRAWFORD, B. R., FERNANDEZ-IBANEZ, F., FREYSTEINSON, J. A. & REECE, W. C. 2018. Model for fracture stiffness incorporating surface roughness effects based on testing of naturally cemented fractures. *DFNE18.* Seattle, USA.

INDRARATNA, B., RAMBANDA, P. & SINGH, R. H. Numerical analysis of water inflows to underground excavations - current status and future trends. *In:* REDDISH, D. J., ed. 5th International Mine Water Congress, September 1994 1994 Nottingham, UK. IMWA, 339-354.

JAEGER, J. C., COOK, N. G. & ZIMMERMAN, R. 2007. *Fundamentals of rock mechanics*, John Wiley & Sons.

JIANG, X.-W. W., L; WANG, X; LIANG, S; HU, B. X. 2009. Estimation of fracture normal stiffness using a transmissivity-depth correlation. *International Journal of Rock Mechanics and Mining Sciences,* 46**,** 51-58.

JONES, H., MORRIS, B., CHENEY, C., BREWERTON, L., MERRIN, P., LEWIS, M., MACDONALD, A., COLEBY, L., TALBOT, J. & MCKENZIE, A. 2000. The physical properties of minor aquifers in England and Wales.

KALKANI, E. C. 1977. Excavation unloading effect in rock wedge stability analysis. *Canadian Geotechnical Journal,* 14**,** 259-262.

KELSELL, P. C., CASE, J. B. & CHABANNES, C. R. 1984. Evaluation of excavation-induced changes in rock permeability. *International Journal of Rock Mechanics, Mining Sciences and Geomechanics,* 21**,** 123-135.

LEE, C. 1978. Stress relief and cliff stability at a power station near Niagara Falls. *Engineering Geology,* 12**,** 193-204.

LEI, Q. H., LATHAM, J. P. & TSANG, C. F. 2017. The use of discrete fracture networks for modelling coupled geomechanical and hydrological behaviour of fractured rocks. *Computers and Geotechnics,* 85**,** 151-176.

LEUNG, C. T. O. Z., R. W. 2012. Estimating the Hydraulic Conductivity of Two-Dimensional Fracture Networks Using Network Geometric Properties. *Transp Porous Media,* 93**,** 777-797.

LI, Y. O., J;MITRA, R;HEBBLEWHITE, B 2014. A study of a joint model incorporating excavation-induced opening effect. *In:* ALEJANO, P., OLALLA & JIMENEZ (ed.) *Rock Engineering and Rock Mechanics: Structures in and on rock masses.* London: Taylor & Francis Group.

LIANG, R. X., T; HUANG, M; LIN, C 2017. Simplified analytical method for evaluating the effects of adjacent excavation on shield tunnel

considering the shearing effect. *Computers and geotechnics,* 81**,** 167-187.

LISJAK, A. G., G 2014. A review of discrete modelling techniques for fracturing processes in discontinuous rock masses. *Journal of Rock Mechanics and Geotechnical Engineering,* 6**,** 301-314.

LIU, H. H. & LIU, H. H. 2017. *Generalization of Darcy's Law: Non-Darcian Liquid Flow in Low-Permeability Media*.

LONG, J. C. S. R., J. S; WILSON, C. R; WITHERSPOON, P. A. 1982. Porous Media Equivilents for Networks of Discontinuous Fractures. *Water Resources Research,* 18**,** 645-658.

LUI, J. W., Z; QIAO, L; LI, W; YANG, J 2021. Transition from linear to nonlinear flow in single rough fractures: effect of fracture roughness. *Hydrogeology Journal,* 29**,** 1343-1353.

MA, F. L., KP; ZHAO, H; GUO, J 2013. Water seepage characterisitcs caused by rock mass deformation in a mine. *In:* QI, W. (ed.) *Global View of Engineering Geology and the Environment.* London: Taylor & Francis Group.

MARCHAND, G., WATERHOUSE, J. & CHRISOSTOMO, J. 2010. Mudstone depressurisation behaviour in an open pit coal mine, indonesia. *In:* FREUND, W. (ed.) *IMWA Minewater and innovative thinking.* Sydney: IMWA.

MCEWEN, T. Review of the conclusions of previous EDZ workshops. *In:* DAVIES, C. B., F, ed. Impact of the excavation disturbed or damaged zone (EDZ) on the performance of radioactive waste geological repositories, 2003 Luxembourg. European Commission, 77-89.

MORRIS, J. P., JOCKER, J. & PRIOUL, R. 2017. Numerical investigation of alternative fracture stiffness measures and their respective scaling behaviours. *Geophysical Prospecting,* 65**,** 791-807.

NICHOLS, T. C. 1980. Rebound, its nature and effect on engineering works. *Quarterly Journal of Engineering Geology and Hydrogeology,* 13**,** 133-152.

NIE, L. L., Z; ZHANG, M; XU, L 2015. Deformation charateristics and mechanism of the landslide in West Open-Pit Mine, Fushun, China. *Arabian Journal of Geosciences,* 8**,** 4457-4468.

OBEYSEKARA, A., LEI, Q., SALINAS, P., PAVLIDIS, D., XIANG, J., LATHAM, J.-P. & PAIN, C. 2017. Modelling the evolution of a fracture network under excavation-induced unloading and seepage effects based on a fully coupled fluid-solid simulation. *ARMA 51st US Rock Mechanics Symposium.* San Francisco: ARMA.

PERRAS, M. A. & DIEDERICHS, M. S. 2016. Predicting excavation damage zone depths in brittle rocks. *Journal of Rock Mechanics and Geotechnical Engineering,* 8**,** 60-74.

PHAM, H. V. P., R; SUND, N; POHLMANN, K 2021. Determination of fracture apertures via calibration of three-dimensional discrete-fracture-network models: application to Pahute Mesa, Nevada, National Security Site, USA. *Hydrogeology Journal,* 29**,** 841-857.

PINE, R. C., JS; FLYNN, ZN; ELMO, D 2006. The development of a new numerical modelling approach for naturally fractured rock masses. *Rock Mechanics and Rock Engineering,* 39**,** 395-419.

PRICE, J. 2016. Implications of groundwater behaviour on the geomechanics of rock slope stability. *APSSIM 2016.* Brisbane, Australia: Australian Centre for Geomechanics.

PYRAK-NOLTE, L. J. & NOLTE, D. D. 2016. Approaching a universal scaling relationship between fracture stiffness and fluid flow. *Nature Communications*.

PYRAK-NOLTE, L. J. M., J. P. 2000. Single fractures under normal stress: The relationship between fracture stiffness and fluid flow. *International Journal of Rock Mechanics and Mining Sciences,* 37**,** 245-262.

READ, J. S., P (EDS) 2009. *Guidelines for Open Pit Slope Design*, CSIRO.

ROCKFIELD-INTERNATIONAL 2017. Elfen Interface Laws. *In:* ROCKFIELD-INTERNATIONAL (ed.) *Elfen Help System.*

ROCKFIELD-INTERNATIONAL 2019. Elfen Training Notes: Using the Explicit Dynamic Solution Method. *Elfen Training Notes.* Swansea, UK.

ROGERS, S. E., D; DERSHOWITZ, WS 2011. Understanding hydraulic fracture geometry and interactions in pre-conditioning through DFN and numerical modelling. *ARMA 45th US Rock Mechanics Symposium.* San Francisco: ARMA.

SEAGER, J. 1963. Pre-mining lateral pressures. *International Journal of Rock Mechanics and Mining Sciences,* 1**,** 413-419.

SINGHAL, B. B. S. G., R. P 2010. *Applied Hydrogeology of Fractured Rocks*, Springer.

SIREN, T. K., P.; RINNE, M. 2015. Considerations and observations of stress-induced and construction induced excavation damage zone in crystalline rock. *International Journal of Rock Mechanics and Mining Sciences,* 73**,** 165-174.

SOLEXPERTS 2022. Hydraulic Fracturing Stress Measurements in Borehole 34_BH01.

STACEY, T. 1973. A three-dimensional consideration of the stresses surrounding open pit mine slopes. *International Journal of Rock Mechanics and Mining Sciences,* 10**,** 523-533.

STACEY, T. 1981. A Simple Extension Strain Criterion for Fracture of Brittle Rock. *International Journal of Rock Mechanics and Mining Sciences & Geomechanics Abstracts,* 18**,** 469-474.

STACEY, T., XIANBIN, Y., ARMSTRONG, R. & KEYTER, G. 2003. New slope stability considerations for deep open pit mines. *Journal of the South African Institute of Mining and Metallurgy,* 103**,** 373-389.

TERZAGHI, K. P., R. B 1948. *Soil Mechanics in Engineering Practice*, Wiley.

TODD, D. K., MAYS, L.W 2005. Groundwater Hydrology. 3rd Edition. Wiley.

TSANG, C., BERNIER, F. & DAVIES, C. 2005. Geohydromechanical processes in the excavation damaged zone in crystalline rock, rock salt, and indurated and plastic clays - in the context of radiative waste disposal. *Rock Mechanics and Mining Sciences,* 42**,** 109-125.

TSANG, C. F. Definitions of Excavation Disturbed Zone and Excavation Damaged Zone. *In:* DAVIES, C. B., F, ed. Impact of the excavation disturbed or damaged zone (EDZ) on the performance of radioactive waste geological repositories, 2003 Luxembourg. European Commission, 7-8.

WHITTAKER, B. S., RN; NEATE, CJ 1992. Effect of longwall mining on ground permeability and subsurface drainage. *Investigation and Evaluation of Surface and Subsurface Drainage.* Nottingham: University of Nottingham.

WU, F. D., Y.; WU, J.; LI, B.; SHA, P.; GUAN, S.; ZHANG, K.; HE, K. 2020. Stress-strain relationship in elastic stage of fractured rock mass. *Engineering Geology,* 268.

ZAREIDARMIYAN, A. P., F; MAKHNENKO, R; SALARIRAD, H; VILARRASA, V. 2021. How Equivalent are Equivalent Porous Media. *Geophysical Research Letters,* 48.

ZHANG, Q. Z., Y 2014. Effect of loading rate on fracture behaviour of rock materials. *In:* ALEJANO, P., OLALLA & JIMENEZ (ed.) *Rock Engineering and Rock Mechanics: Structures in and on rock masses.* London: Taylor & Francis Group.

ZHOU, J. H., S.; FANG, S.; CHEN, Y.; ZHOU, C. 2015. Nonlinear flow behaviour at low Reynolds numbers through rough-walled fractures subjected to normal compressive loading. *International Journal of Rock Mechanics and Mining Sciences,* 80**,** 202-218.

ZOORABADI, M. S., S.; TIMMS, W.; HEBBLEWHITE, B. 2022. Analytical methods to estimate the hydraulic conductivity of jointed rock. *Hydrogeology Journal,* 30**,** 111-119.

APPENDIX A

LIST OF MODELS DEVELOPED AND APPLIED DURING THIS STUDY

Model Type	Filename	Description
Elfen	baselinenofrac0502201	2D No discontinuity model with k=0.27
	baselinenofrac0502201	2D No discontinuity model with k=2.0
	beddingonlynew250521	2D Bedding only model with k=0.27
	beddingonlynew250521K2	2D Bedding only model with k=2.0
	stochastic0720K-027plusfinalsandstonenlc#2	2D Variably jointed model with k=0.27
	stochastic0720K-027plusfinalsandstonenlc#2K2	2D Variably jointed model with k=2.0
	Model-2-orthogonal-K27	2D orthogonally jointed model with k=0.27
	Model-2-orthogonal-K2	2D orthogonally jointed model with k=2.0
	hydroresponse3d-03122020_ver2	3D No discontinuity enclosed excavation model with k=0.27
	hydroresponse3d-03122020_ver2opencut	3D No discontinuity open cut excavation model with k=0.27
MODFLOW	Appleton model 1.pm5	3D Groundwater flow model
	Copley hra4.pm5	3D Groundwater flow and contaminant transport model with MT3D addition
LandSim	Copley HRA Finalbase 3phase	Probabilistic contaminant fate risk model – lateral flow
	Tong Quarry Baseline 2017 extension 2019	Probabilistic contaminant fate risk model – lateral flow
	Farley Quarry HRA	Probabilistic contaminant fate risk model – vertical and lateral flow

APPENDIX B

DISCONTINUITY LOG

BOREHOLE 2

## BLAXTER QUARRY, NORTHUMBERLAND, UK

EUROPEAN GEOPHYSICAL SERVICES LTD

Client:	**SM Foster**
Borehole:	**BH2**

Log Type: **Image**

Location: **Blaxter Quarry**	Area: **Northumberland**	Grid Ref:	Elevation:

Drilled Depth: (m)			Date:	**29.11.16**
Logged Depth: (m)	**26.0**		Recorded By:	**R. Powell**
Logging Datum:	**Ground Level**		Remarks:	
Logged Interval: (m)	**1.5 - 26.0**			
Fluid Level: (m)	**14.9**		**Ref:**	

BOREHOLE RECORD

Bit: (mm)	From: (m)	To: (m)

CASING RECORD

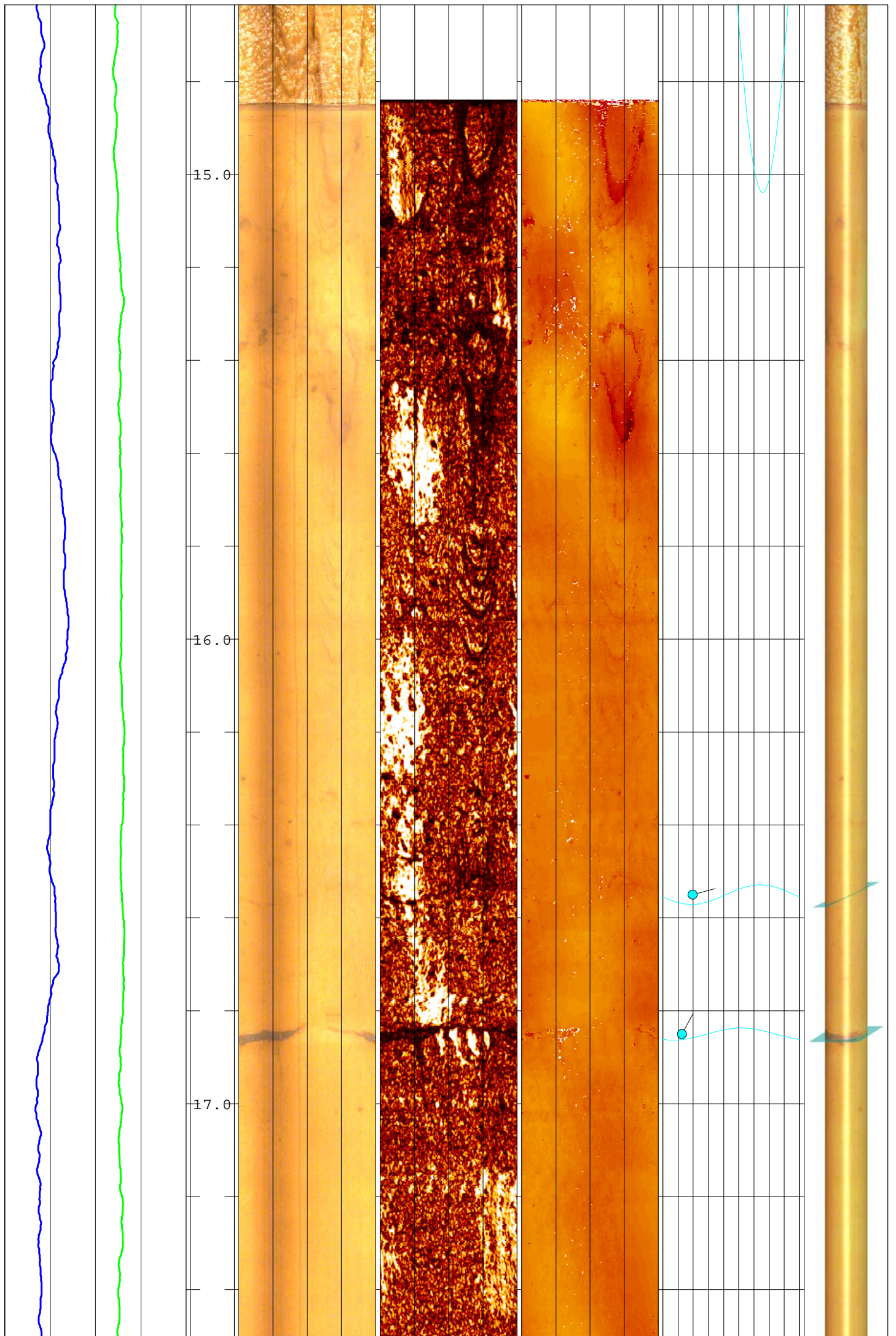| Type	Size: (mm)	From: (m)	To: (m)
None			
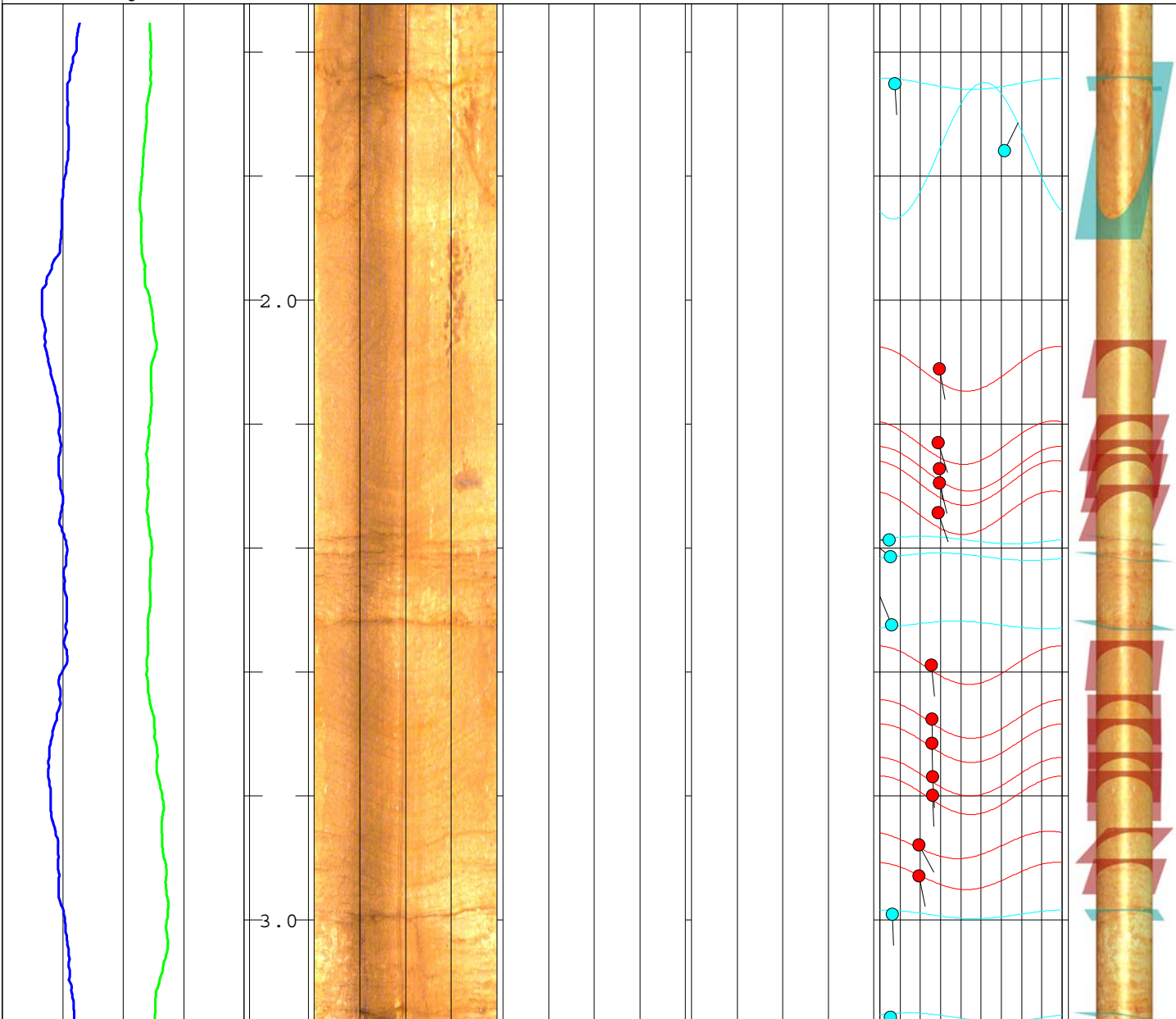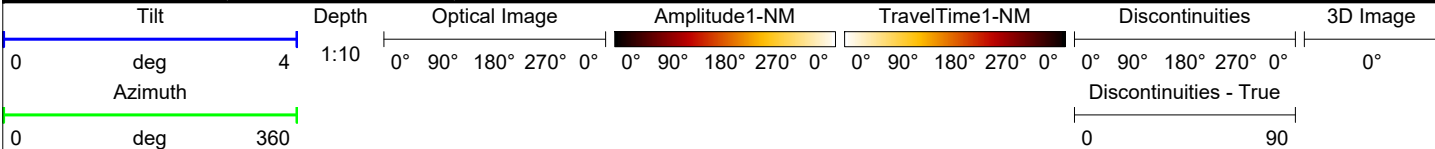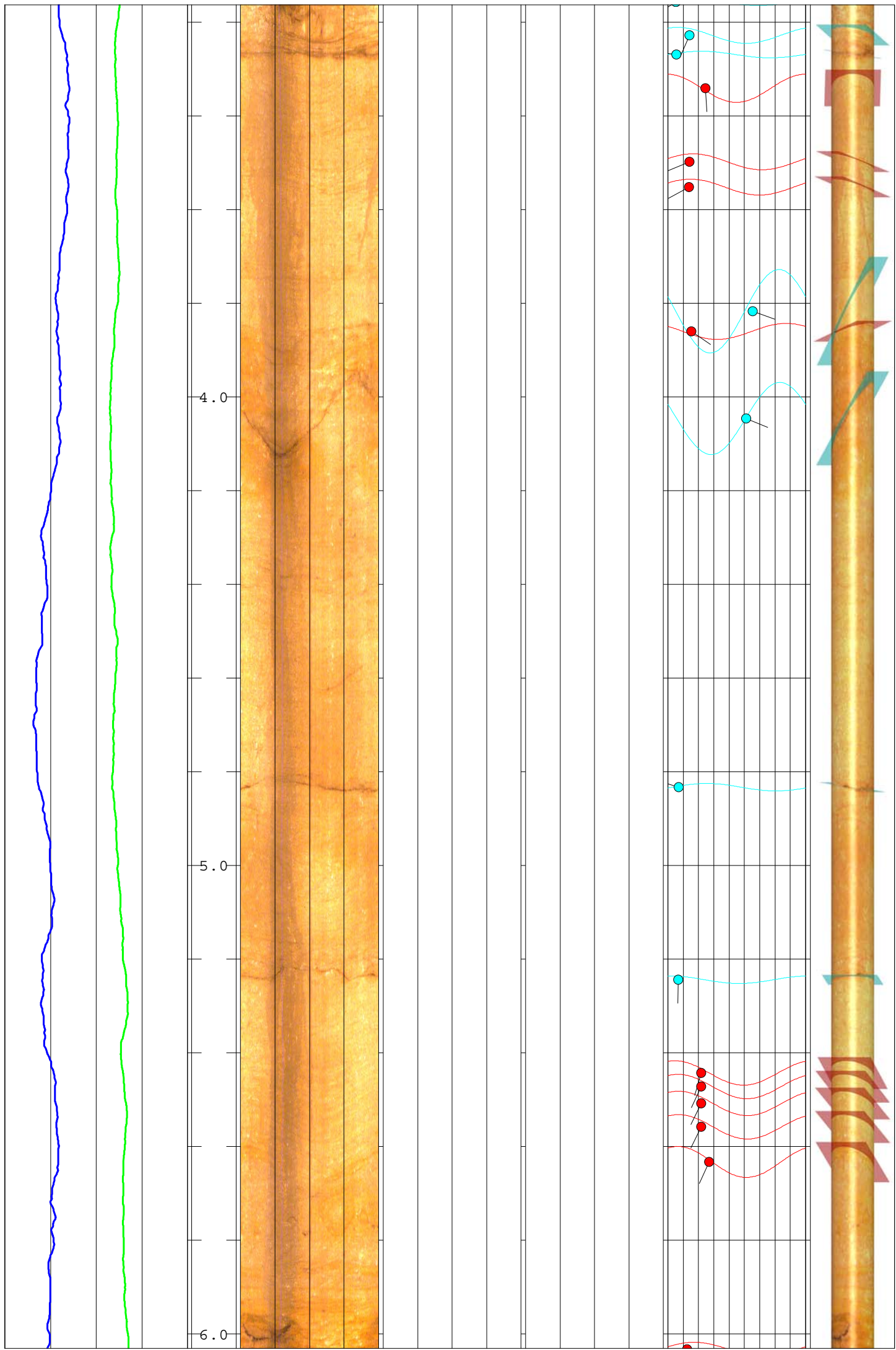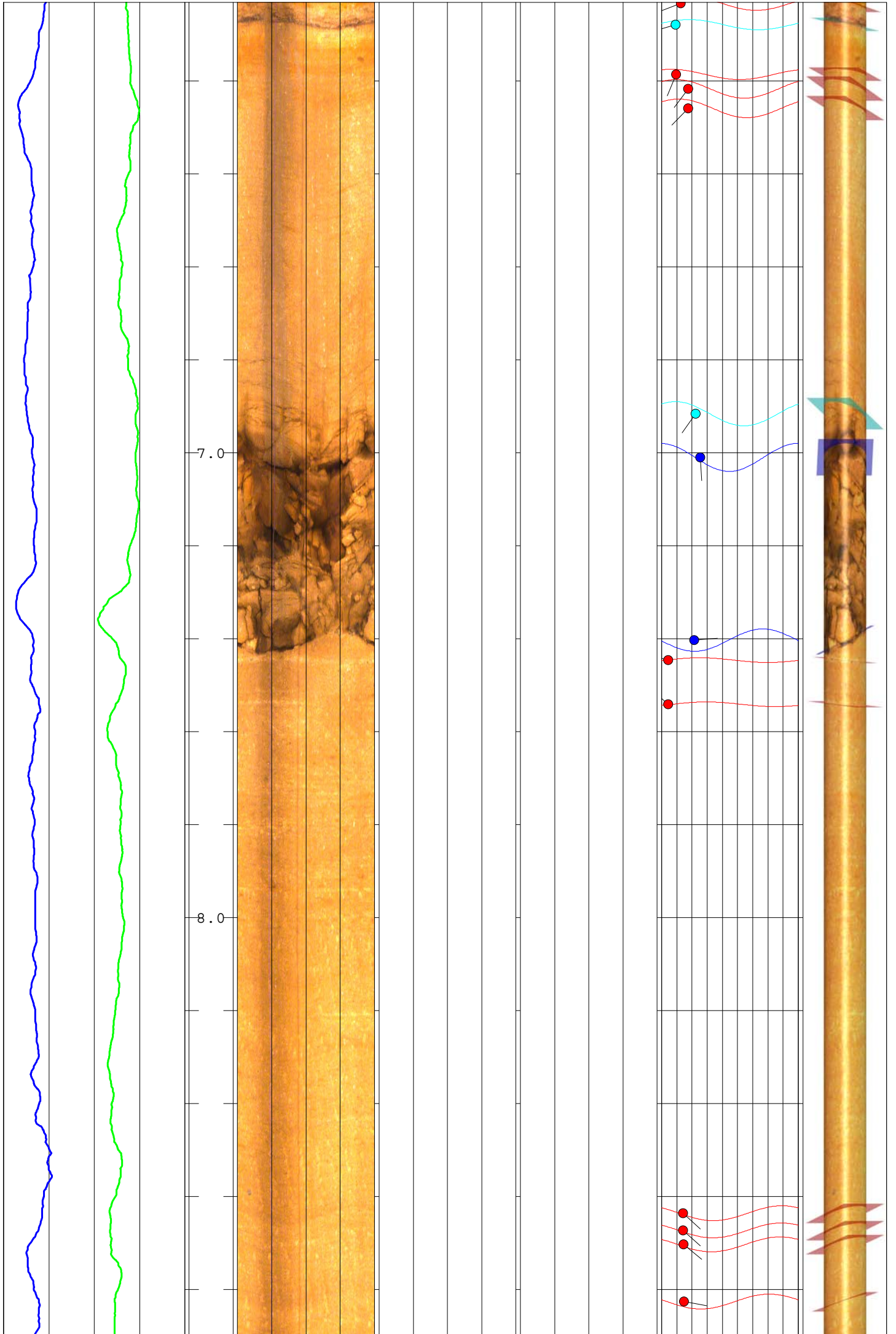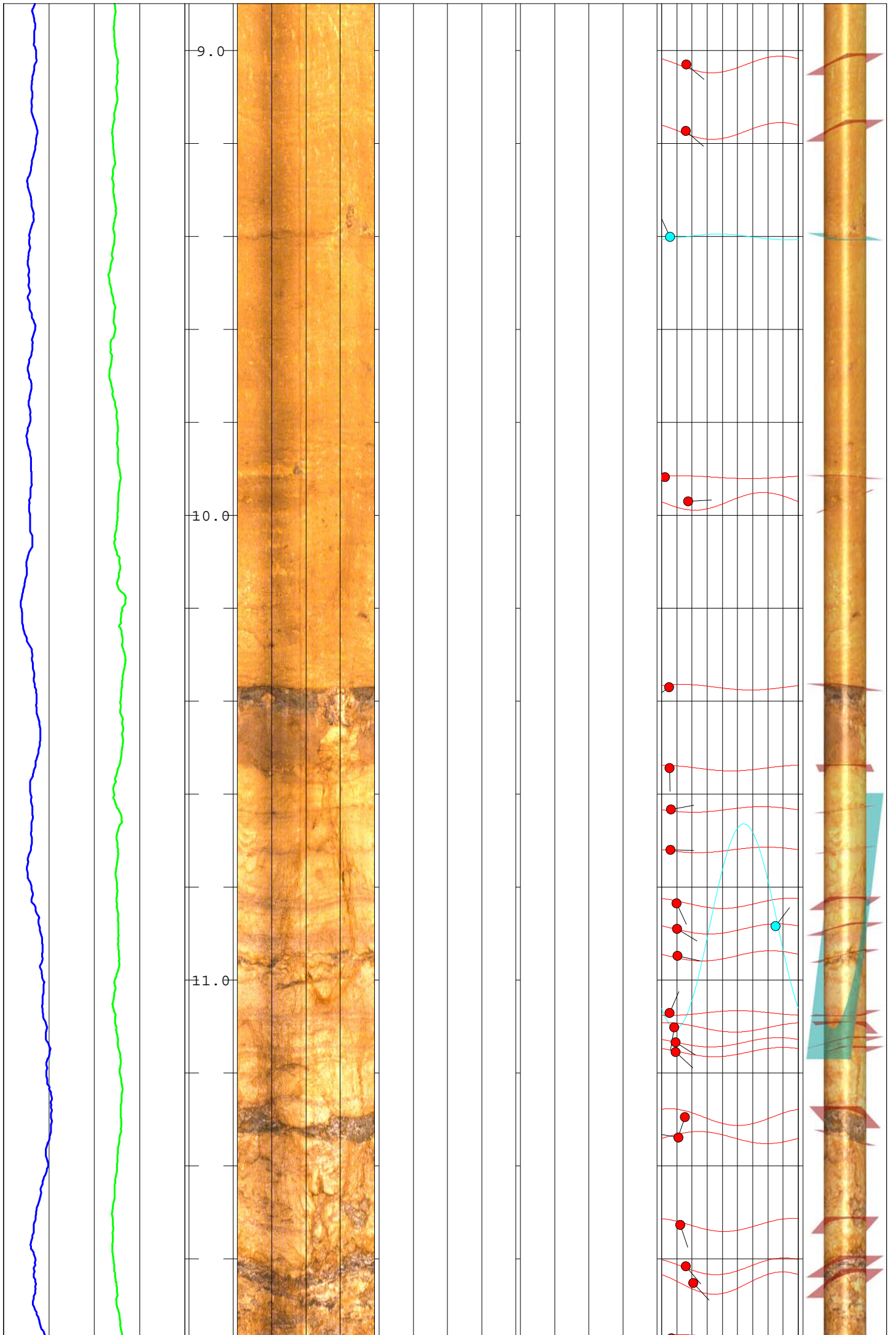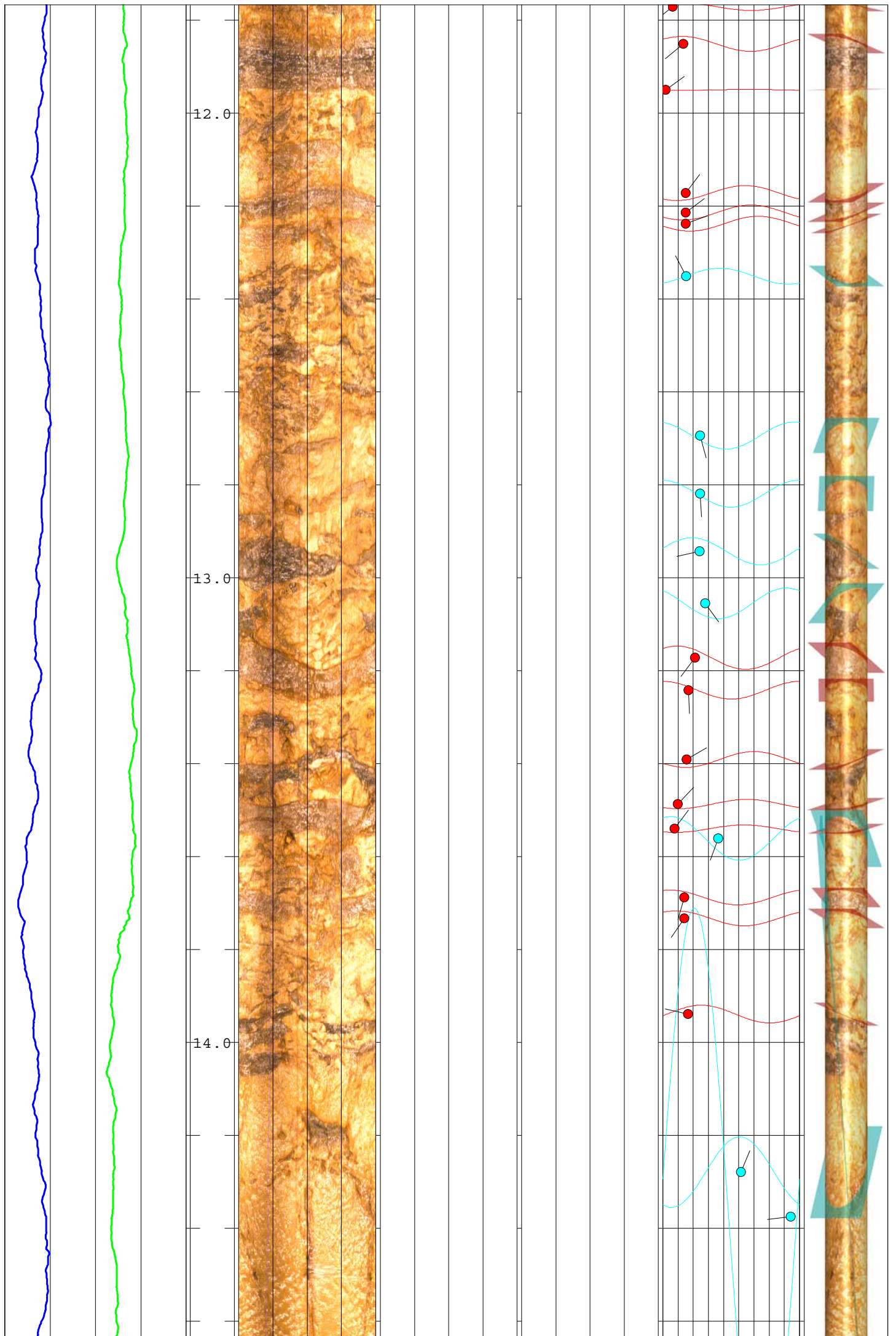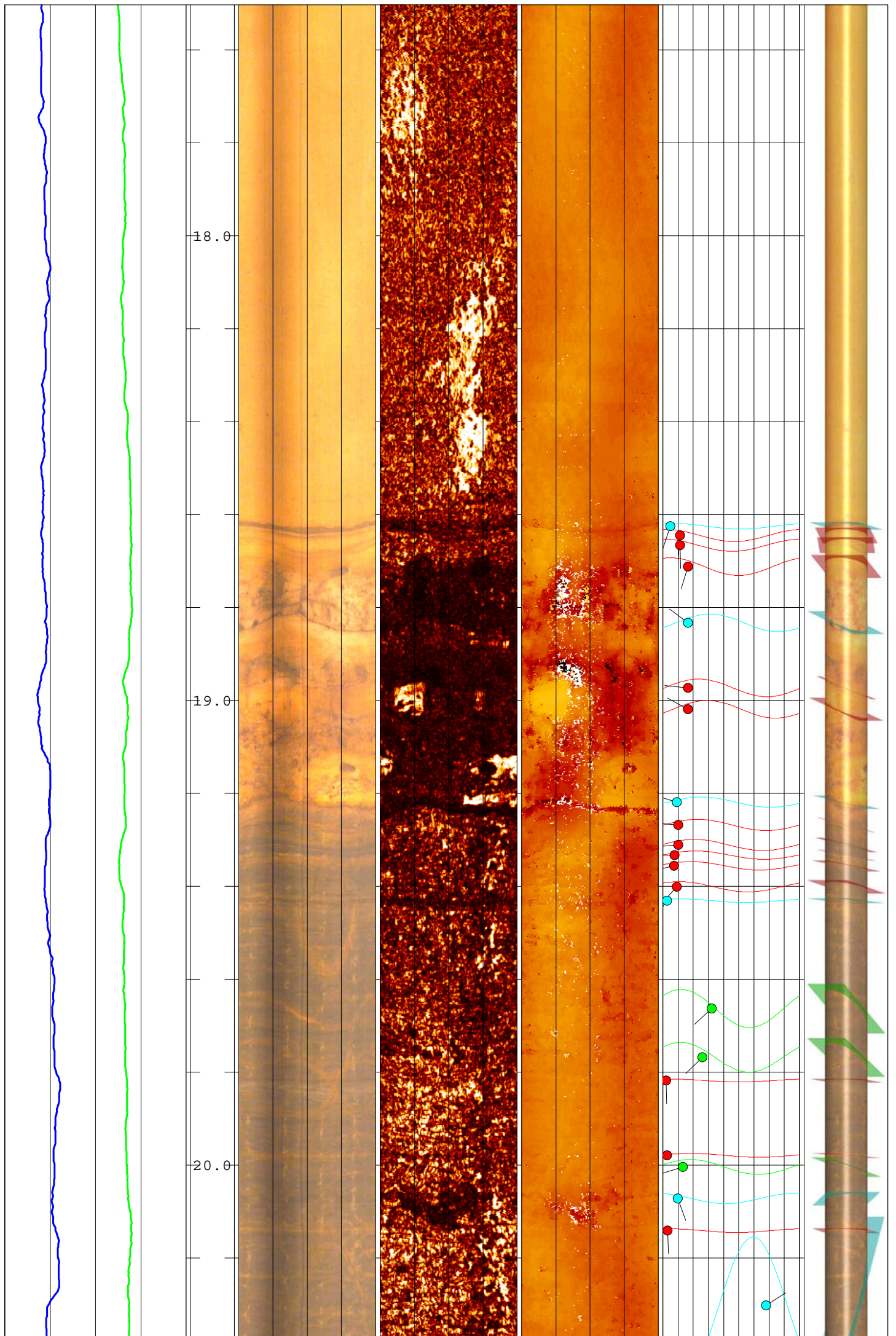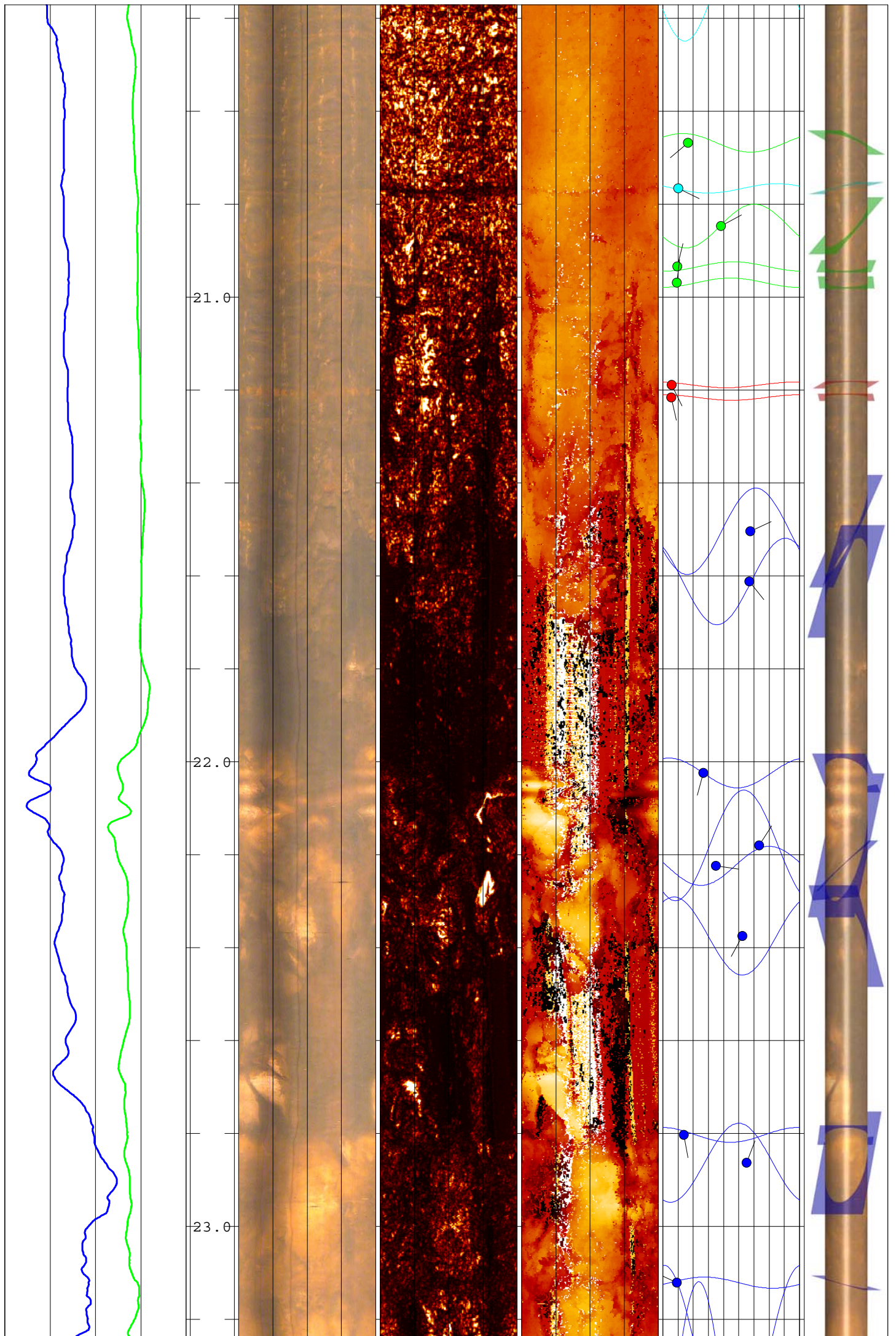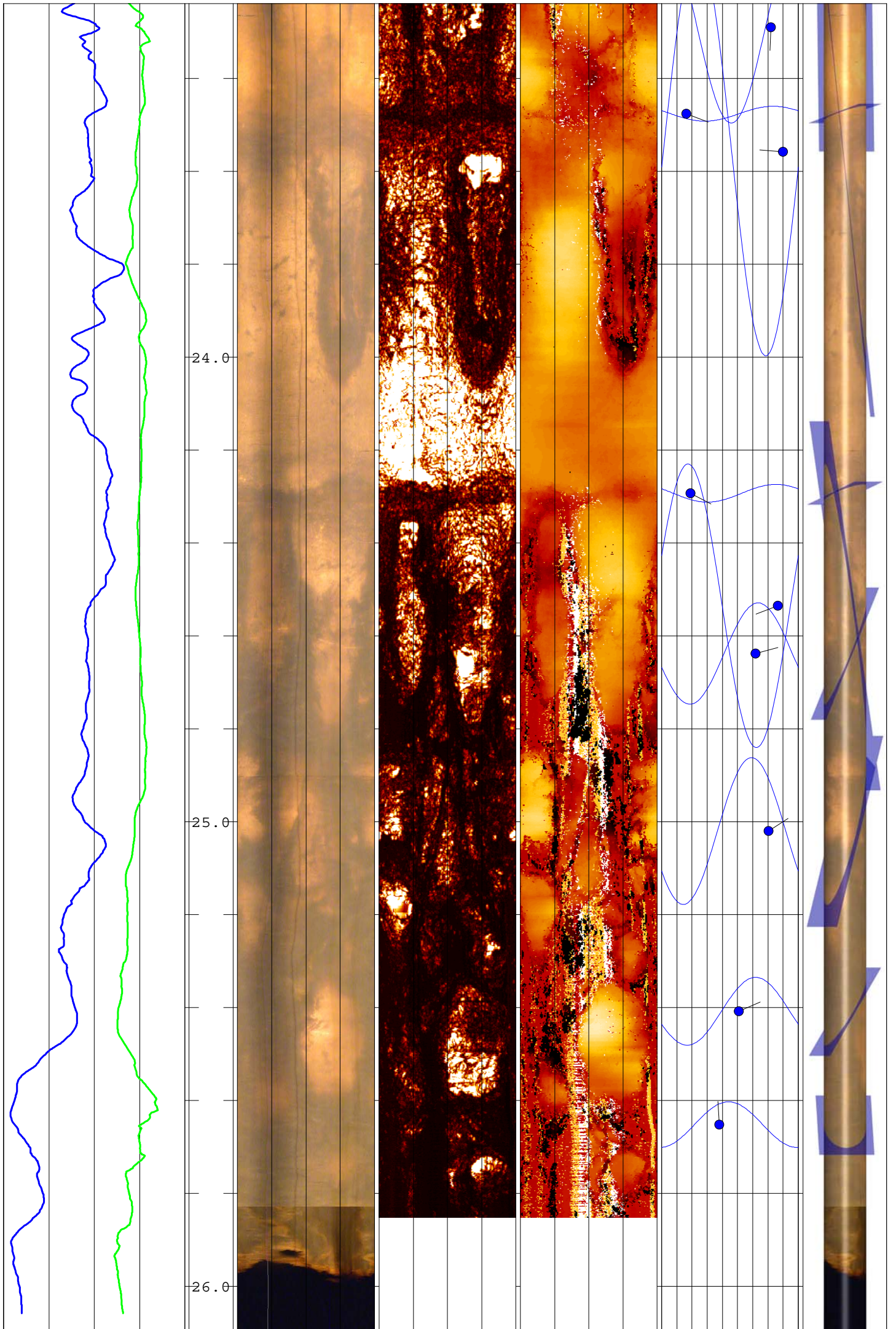
Appendix 1

Discontinuity Classification.

Discontinuity	Colour	Classification Parameters
Major Fracture or Fissure	Blue	An open break in the formation, that is **continuous** across the entire image.
Minor Fracture or Fissure	Turquoise	A thin or closed break in the formation, that is **continuous or discontinuous** across the image.
Vein	Green	That may be **continuous or discontinuous** across the entire image.
Fabric	Red	Defines a feature generally metamorphic, igneous or sedimentary in origin that may be **continuous or discontinuous** across the image, such as bedding and cross-bedding, schistosity or gneissosity.
Intrusions	Purple	Intrusive features such as dykes and sills, generally **continuous** across the image
Unknown	Black	Faint features which **can not** be classified.

APPENDIX C - CONCEPTUAL MODELS FOR GEOMECHANICAL MODELLING

C1   Conceptual model development

Prior to numerical model development, a conceptual geomechanical model was developed for each modelling option. The objective of conceptual model development was to support definition of key parameters and processes associated with unloading and to improve understanding of parameter interaction or interdependence. Conceptual models were developed on the basis of field observation and measurement at several mineral extraction sites in northern England.

C1.1 Model 1 – No-discontinuities

The no-discontinuities model was developed to test the geomechanical response of the bulk rock mass to unloading without the presence of bedding, joints or fractures. The primary objective was to ensure that the model was responding appropriately with regard to stress redistribution and rock mass displacements. The 2D no-discontinuity model also allowed comparison with 3D modelling results which were also based on a no-discontinuity model. Model domain and excavation area dimensions were consistent with all other 2D models.

C1.2 Model 2 – Bedding only model

Model 2 includes the addition of sub-horizontal bedding planes. Geotechnical data used in the development of the model was derived from survey of Blaxter Quarry. Bedding plane spacings and persistence were derived from measured spacings and persistence at the quarry. The model incorporates two separate lithological units that form part of the Tyne Limestone Formation. They are the massive sandstone unit worked at the quarry and the underlying interbedded limestone formations. Bedding planes dip at an angle of 5º to the horizontal. The simulated excavation included in the model extends through both

sandstone and limestone units. The configuration of bedding planes and lithological variation is shown in Figure C1.
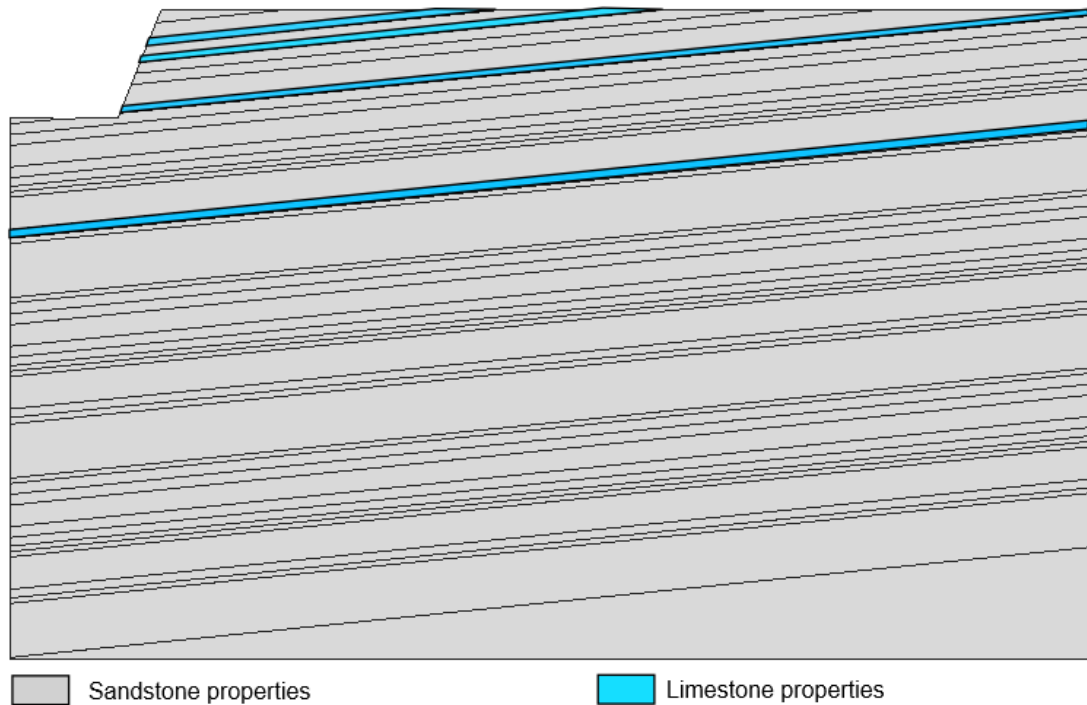

Figure C1: Configuration of bedding planes and lithological variation in the bedding only model (Model 2). Bedding planes dip at 5° to the horizontal with stochastically generated bedding spacings.

Rock mass and discontinuity properties applied in Model 2 are listed at Table 3.3 in Chapter 3. Bedding spacing that becomes more variable with increasing depth reflects the variation in thickness in deeper formations within the Tyne Limestone Formation beneath Blaxter Quarry. Bedding spacings are stochastically generated from Blaxter Quarry based input data to a 3D Fracman model. The same bedding dip and spacings are retained in all subsequent 2D models.

C1.3 Model 3 – Variably jointed model

Model 3 is designed to support investigation of unloading effects with a less regular pre-existing discontinuity network, typical of jointed and fractured carbonate or crystalline geological formations. The geological model has been developed to represent a formation with both regular, variably spaced bedding

planes, and heterogeneously configured jointing. As other models, this model incorporates the same multi-lithology configuration. Examples of less regular discontinuity networks are shown in Figures C2 and C3 which show limestone quarry faces from Yorkshire and Shropshire. Both examples include variably spaced sub-horizonal bedding and jointing at a range of scales and orientations.

The discontinuity distribution in the variably jointed model was initially generated stochastically by application of FracMan software (Golder Associates Ltd). FracMan was used to generate a 3D block model of bedding plane and joint distribution based on input parameters derived from field observation of fractured carbonate formations. To support 2D application a 2D plane was abstracted from the 3D model and translated into input discontinuity configuration for Elfen. This approach introduces stochastically generated heterogeneity into the discontinuity distribution, including persistent cross-bedding joints, strata-bound joints and intra-strata joints, as a contrast to the highly regulated discontinuity configuration in the orthogonally jointed model. Material properties used in the variably jointed model are derived from field observation and literature sources as summarized in Table 3.3 in Chapter 3.

Figure C2: Heterogeneous jointing in a Magnesian Limestone quarry face at Newthorpe Quarry, Sherburn in Elmet, North Yorkshire.

Figure C3: Bedding and variably orientated jointing in the Wenlock Limestone, Farley Quarry, Shropshire, UK.

Discontinuities are present at a range of orientations to test the effect of orientation on discontinuity response. Increase in discontinuity intensity also results in a progressive increase in discontinuity connectivity. The location and orientation of joints included in Model 3 is shown in Figure C4.
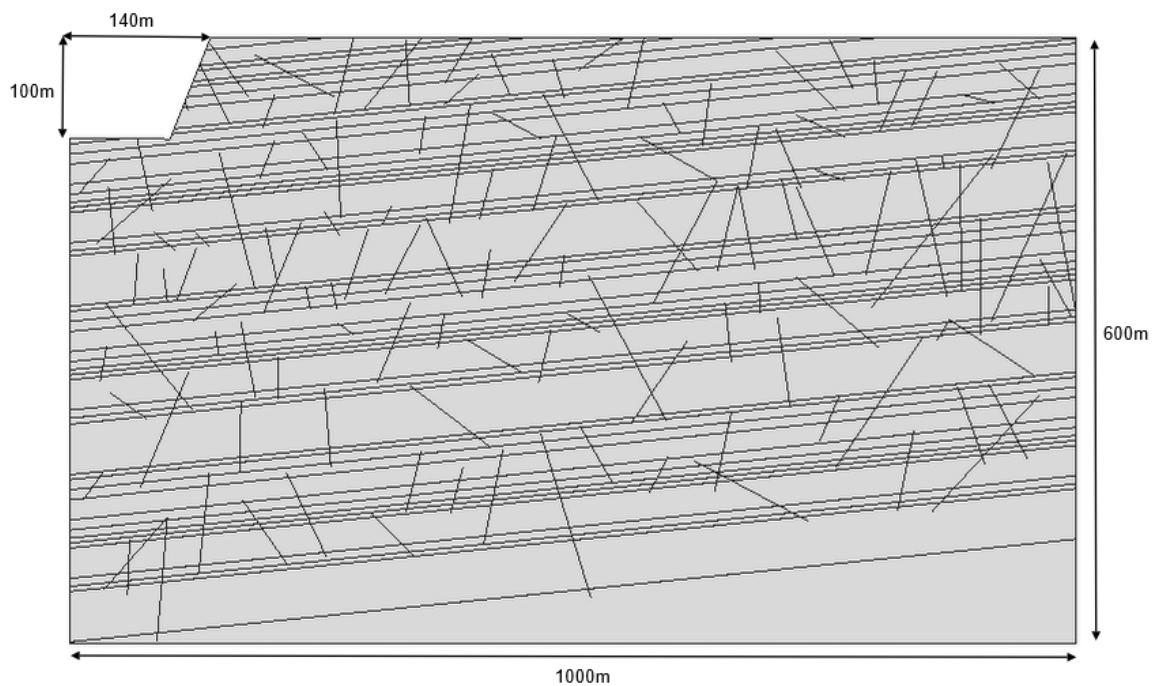

Figure C4: Variably jointed model geometry and discontinuity configuration. Bedding plane configuration and lithological variation remains as defined in Model 2.

The joint configuration included in Model 3 was derived from a FracMan stochastically generated joint distribution designed to produce a joint set of variable orientation and persistence.

C1.4 Model 4 - Orthogonally jointed model

This model represents the highest intensity discontinuity configuration included in this study. The model incorporates orthogonally orientated joints and sub-horizontal bedding planes. This configuration of discontinuities is representative of hard rock mineral workings for both aggregate and dimension stone across the north of England. Three photographic examples are provided as Figures C5, C6 and C7.

Figure C5: View of orthogonally jointed sandstone beds at Scout Moor Quarry, Ramsbottom, Lancashire

At most locations, sub-horizontal bedding planes are well-developed and persist over significant distances throughout the geological formations under consideration. Orthogonal jointing is typically sub-vertical and pervasive, crossing multiple bedding planes. Subordinate jointing is typically strata-bound. With principal joint sets orientated approximately perpendicularly, the configuration is ideally suited to 2D 'plain strain' modelling approaches.

Figure C6: Orthogonal jointing in massive bedded Guiseley Grit sandstone at New Stones Quarry, Hebden Bridge, West Yorkshire, UK

Figure C7: Orthogonal jointing in massive bedded sandstone of the Tyne Limestone Formation, Blaxter Quarry, Northumberland

The combination of orthogonally orientated bedding planes and joint systems results in a 'sugar cube' type discontinuity geometry with the host rock defined as a series of 'blocks' separated by discontinuities. This arrangement results in a relatively high degree of geometrical flexibility and mobility as rock block movement is regulated by discontinuity contact properties rather than host rock geomechanical properties which assume lower significance.

Discussion of modelling results in Chapters 4 and 5 demonstrate the significance of bedding plane orientation in relation to gravity loading and development of in-situ stress conditions. With vertical loading on a horizontal upper model surface, stresses transferred to dipping bedding planes results in the accumulation of lateral stresses, and associated displacements, towards or away from excavations, depending on bedding plane orientation.
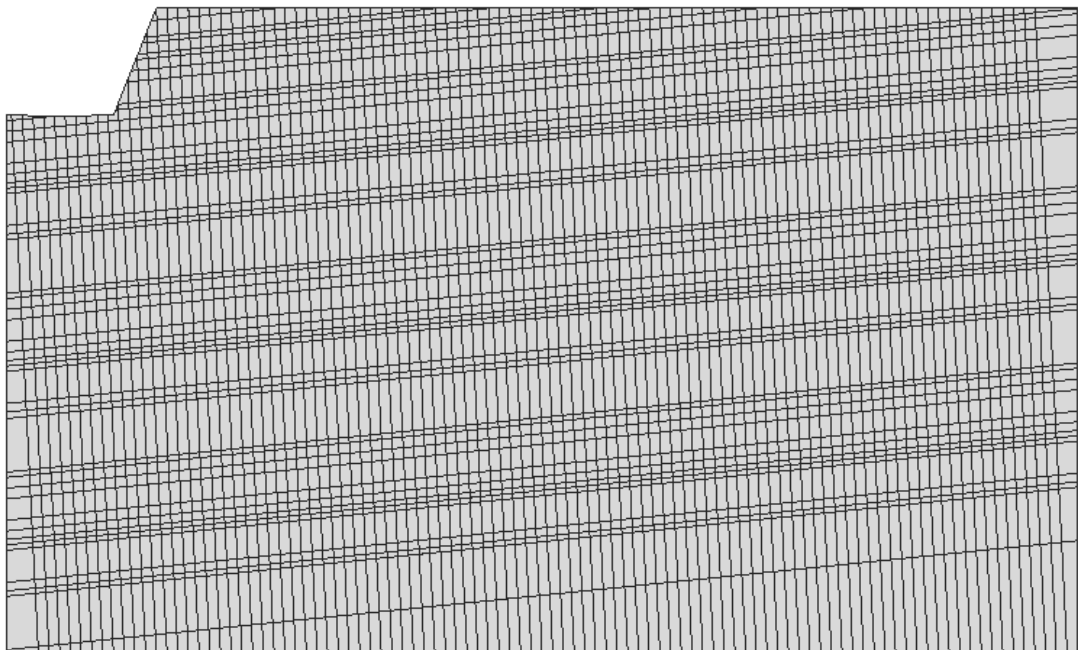

Figure C8: Model 4 – Orthogonally jointed model discontinuity configuration with 100m deep excavation. Joints dip at 85° to the horizontal and daylight in the excavation face.

Discontinuities are represented by bedding planes and joints. The bedding plane configuration is consistent with Models 2 and 3. The main joint sets dip at an angle of 85° to the horizontal resulting in sub-vertical features. Joints are included in the model at 10m intervals and 100% persistence throughout the

model. As shown in Figure C8, the bedding planes intercept the excavation face and floor at shallow angle whilst joint surfaces intersect the floor and face at steep angle.

Elfen requires definition of geomechanical parameters for both the rock mass and the discrete discontinuities. Geomechanical parameters applied to the sandstone and limestone units in the model were derived from analysis of the properties of the Tyne Limestone Group strata within which the sandstones and limestones of the sequence at Blaxter Quarry occur. Additional source data regarding geomechanical properties of both the intact rock and discontinuities was derived from the literature as listed in Table 3.3 in Chapter 3. The intact rock material properties for sandstone and limestone were applied throughout the modelling programme.